Identification of Deubiquitylases Involved in Parkin-mediated Mitophagy

Jin Rui Liang

Thesis submitted in accordance with the requirements of the University of Liverpool for the Degree of Doctor in Philosophy

September 2014

Identification of Deubiquitylases Involved in Parkin-mediated Mitophagy

Jin Rui Liang

Abstract

Ubiquitylation is a post-translational modification of proteins with a broad range of downstream effects, ranging from protein turnover to transcriptional regulation, membrane trafficking and DNA damage repair. The conjugation of ubiquitin to its substrate is a sequential process mediated by three enzymes, termed the E1 ubiquitin-activating enzyme, the E2 ubiquitin-conjugating enzyme and the E3 ubiquitin ligase. Conversely, the removal of ubiquitin is mediated by deubiquitylases (DUBs). My project aims to identify DUBs that are involved in the selective removal of mitochondria via autophagy (mitophagy), a process that is regulated by a serine/threonine kinase, PINK1, and an E3 ligase, Parkin. Loss-of-function mutations in both PINK1 and Parkin have been reported to cause autosomal recessive-juvenile Parkinsonism (AR-JP), a form of early onset Parkinson's Disease (PD).

During mitochondrial depolarisation, PINK1 is stabilized at the outer mitochondrial membrane (OMM) where it recruits and activates Parkin. Subsequently, Parkin ubiquitylates a range of OMM proteins either for their proteasomal degradation or for the recruitment of the autophagic machinery. I first characterised this process in two different cell lines expressing either low endogenous levels of Parkin (SH-SY5Y neuroblastoma cells) or high exogenous levels of YFP-Parkin (hTERT-RPE1-YFP-Parkin, retinal pigment epithelial cells). I developed two different assays to assess Parkin-mediated mitophagy: (1) real time monitoring of YFP-Parkin by live-cell imaging (only in hTERT-RPE1-YFP-Parkin cells), and (2) western blot analysis of the cleavage, ubiquitylation and loss of proteins during mitophagy (in both hTERT-RPE1-YFP-Parkin and SH-SY5Y cells). I used these two assays to perform siRNA screens to identify DUBs, for which depletion resulted in altered Parkin recruitment and/or ubiquitylation and degradation of Parkin

substrates. I identified several DUBs, including USP10, USP30, USP38, USP42, USP43, USP49, BAP1, OTUD4 and TRABID, for which siRNA depletion resulted in delayed Parkin recruitment to the mitochondria. Further characterisation of the effects of USP42 and USP43 siRNA depletions suggests that the loss of these DUBs could either desensitize the cells or affect the cellular response towards mitochondrial depolarisation. Depletion of another DUB, USP31, partially inhibited the later stages of mitophagy, i.e. the degradation of mitochondria via the lysosomal pathway.

I discovered by chance that high expression levels of Parkin resulted in a small percentage of mitophagic cell death that was dependent on both PINK1 and Parkin. This cell death was prevented or delayed by inhibiting the proteasome. Interestingly, depletion of USP30 exacerbated this mitophagic cell death. This effect of USP30 depletion is of particular interest as USP30 is the only mitochondria-localised DUB. Further characterisation revealed that USP30 opposes TOM20 ubiquitylation and degradation, a previously described Parkin substrate. I speculate that USP30 counteracts disproportionate Parkin-dependent ubiquitylation and proteasomal degradation of outer mitochondrial membrane proteins, and its depletion enhances apoptosis by promoting Cytochome-C release from damaged mitochondria. Importantly, USP30 depletion also enhances apoptosis induced by BH3-mimetics ABT-737 and ABT-263, suggesting a more general role for USP30 in determining the threshold for mitochondrial cell death.

As USP30 depletion enhances the degradation of Parkin substrate and sensitize cells to apoptosis, this data suggest that USP30 is a potential drug target not only in Parkinson’s Disease but also in cancer.

Table of Contents

List of Figures

List of Tables

Appendices

Supplementary video 1 – PINK1 depletion inhibits CCCP-induced cell death.

Supplementary video 2 – Z-VAD-FMK treatment inhibits CCCP-induced cell death.

Supplementary video 3 – USP30 depletion enhances CCCP-induced cell death.

Supplementary video 4 – USP30 depletion enhances ABT263-induced cell death.

Supplementary video 5 – USP30 depletion enhances ABT-737-induced cell death.

Abbreviations

AAA-ATPase	Associated With Diverse Cellular Activities
ACN	Acetonitrile
AD	Alzheimer's Disease
AGR2	Anterior Gradient Protein 2 Homolog
AMPK	AMP-Activated Protein Kinase
APAF-1	Apoptotic Protease-Activating Factor 1
ATG	Autophagy-Related Genes
ATP	Adenosine Triphosphate
BCL2	B-Cell Lymphoma 2
BH	Block Homology
BH3	BCL2 Homology 3
C-terminus	Carboxyl-Terminus
Casp	Caspase
CCCP	Carbonyl Cyanide M-Chlorophenylhydrazone
CHIP	Carboxyl Terminus of the Hsc70-Interacting Protein
CIMPR	Cation-Independent Mannose 6-Phosphate Receptor
CMA	Chaperone-Mediated Autophagy
CRISPR	Clustered Regularly Interspaced Short Palindromic Repeats
Cyt-C	Cytochrome-C
DAVID	Database For Annotation, Visualization And Integrated Discovery
DISC	Death-Inducing Signaling Complex
DMEM	Dulbecco's Modified Eagle's Medium
DMEM/F12	Dulbecco's Modified Eagle's Medium/Nutrient Mixture F-12 Ham
DTT	Dithiothreitol
DUB	Deubiquitylating Enzyme/ Deubiquitylase
ECAR	Extracellular Acidification Rate
EDTA	Ethylenediaminetetraacetic Acid
EGF	Epidermal Growth Factor
ER	Endoplasmic Reticulum
ESCRT	Endosomal Sorting Complex Required For Transport
ETC	Elecron Transport Chain
FACS	Fluorescence-Activated Cell Sorting
FADD	Fas-Associated Death Domain
FAND2	Fanconi Anemia Group D2 Protein
FBS	Foetal Bovine Serum
FKBP12	FK506-Binding Protein of 12kda
FYVE	Fab1, YOTB, Vac1 And EEA1 Zinc Finger Domain
GBP	GFP-Binding Protein
GFP	Green Fluorescent Protein
GO	Gene Ontology
HBM	HCF-1 Binding Motif
HCF-1	Host Cell Factor-1
HECT	Homologous To E6-AP Carboxy Terminus

HGF	Hepatocyte Growth Factor
hTERT-RPE1	Human Telomerase Reverse Transcriptase-Immortalized Retinal Pigment Epithelial Cells
IAP	Inhibitors of Apoptosis
IBR	In-Between-RING
IMM	Inner Mitochondria Membrane
IMS	Intermembrane Space
IRS	Insulin Receptor Substrate
ISG15	Interferon Stimulated Gene 15
JAMM	JAB1/MPN/Mov4 Metalloenymes
JNK	C0jun N-Terminal Kinase
KRAB	Kruppel-Associated Box Domain
LB	Lewy Bodies
LB	Lysogeny Broth
LBK1	Liver Kinase B1
LC-MS/MS	Liquid Chromatography-Tandem Mass Spectrometry
LIR	LC3-Interacting Region
LUBAC	Linear Ubiquitin Chain Assembly Complex
MARCHV	Membrane-Associated RING-CH V
MAVS	Mitochondrial Antiviral Signaling
MEFs	Mouse Embryonic Fibroblasts
MES	2-(N-Morpholino)Ethanesulfonic Acid
MF	Nitochondria Enriched Fraction
MJD	Machado-Joseph Disease
mLST8/GβL	Mammalian Lethal With SEC13 Protein 8
MOMP	Mitochondria Outer Membrane Permeabilisation
MOPS	3-(N-Morpholino)Propanesulfonic Acid
MRP	Multidrug Resistance-Associated Protein
MS	Mass Spectrometry
mSIN1/MAPKAP1	Mammalian Stress-Activated Map Kinase-Interacting Protein 1
mTOR	Mammalian Target of Rapamycin
MTS	Mitochondrial-Targeting Signal
N-terminus	Amino-Terminus
NEAA	Non-Essential Amino Acids
NEDD4	Neural Precursor Cell Expressed Developmentally Down Regulated Protein 4
NEDD8	Neural Precursor Cell Expressed Developmentally Down Regulated Protein 8
NEMO	Nfκb Essential Modulator
NF-κB	Nuclear Factor-Kappa-B
NGF	Nerve Growth Factor
NMR	Nuclear Magnetic Resonance
NP-40	Nonidet P-40
NZF	Nuclear Pore Localisation 4(Npl4) Zinc Finger
O+A	Oligomycin A And Antimycin A Co-Treatment

OCR	Oxygen Consumption Rate
OGT	*O*-Linked *N*-Acetylglucosamine Transferase
Omi/htrA2	High-Temperature Requirement
OMM	Outer Mitochondria Membrane
OPA1	Optic Atrophy 1
OXPHOS	Oxidative Phosphorylation
PARP	Poly (ADP-Ribose) Polymerase
PARP-p85	Poly(ADP-Ribose) Polymerase (PARP)-P85 Fragment
PAS	Pre-Autophagosomal Membrane
PBS	Phosphate-Buffered Saline
PCD	Programmed Cell Death
PCNA	Proliferating Cell Nuclear Antigen
PD	Parkinson's Disease
PDK1	Phosphoinositide-Dependent Kinase-1
PE	Phosphatidylethanolamide
PFA	Paraformaldehyde
PGC-1α	Peroxisome Proliferator-Activated Receptor Gamma Coactivator 1-Alpha
PI	Phosphatidylinositol
PI3P	Phosphatidylinositol,3-Phosphate
PINK1	PTEN-Induced Putative Kinase-1
PMS	Post-Mitochondrial Supernatant
PNS	Post-Nuclear Supernatant
PRAS40/AKT1S1	40kda Pro-Rich Akt Substrate
PRC1-dRAF complex	Polycomb Repressive Complex I – Dring-Associated Factor
PROTOR1/2	Protein Observed With RICTOR 1/2
PS	Phosphatidylserine
PTEN	Phosphatase And Tensin Homolog
PX	Phox Homology
qRT-PCR	Quantitative Reverse Transcription-Polymerase Chain Reaction
RAG	Ras-Related GTPase
RAPTOR	Regulatory-Associated Protein of MTOR
RBR	RING-Between-RING
REP	Repressor Element of Parkin
REPTOR	REP Domain-Containing Mtor-Interacting Protein
RHEB	Ras Homolog Enriched In Brain
RICTOR	Rapamycin-Insensitve Companion of Mtor
RING	Really Interesting New Gene
RIP1	Receptor-Interacting Protein 1
RIPA	Radioimmunoprecipitation Assay
ROS	Reactive Oxygen Species
Rot	Rotenone
S.O.C	Super Optimal Borth With Catabolite Repression
SDS-PAGE	Sodium Dodecyl Sulfate Polyacrylamide Electrophoresis

SERCA	Sarco/Endoplasmic Reticulum Ca^{2+} -ATPase
SILAC	Stable Isotope Labeling By Amino Acids In Cell Culture
siRNA	Small Interfering RNA
Smac/DIABLO	Second Mitochondrial Activator of Caspases
SUMO	Small Ubiquitin-like Modifier
TAB	Mitogen-Activated Protein Kinase Kinase Kinase 7 Interacting Protein 1
TAK1	Mitogen-Activated Protein Kinase Kinase Kinase 7
TFA	Trifluoroacetic Acid
TIM	Translocase of Inner Mitochondrial Membrane
TM	Transmembrane
TNF	Tumour Necrosis Factor
TNFR	TNF-Alpha Receptor
TOM	Translocase of Outer Mitochondrial Membrane
TRAIL	TNF-Related Apoptosis-Inducing Ligand
UBA	Ubiquitin-Associated Domain
UBD	Ubiquitin Binding Domain
UBL	Ubiquitin-Like Domain
UBZ	Ubiquitin-Binding Zinc Finger
UCH	Ubiquitin C-Terminal Hydrolase
UIM	Ubiquitin-Interacting Motif
UPR	Unfolded Protein Response
USP	Ubiquitin-Specific Protease
UV	Ultraviolet
UVRAG	Ultraviolet Irradiation Resistance-Associated Gene
WIPI1	WD Repeat Domain Phosphoinositide-Interacting Protein 1
YFP	Yellow Fluorescent Protein
Z-VAD.FMK	Benzyloxycarbonyl-Val-Ala-Asp Fluoromethyl Ketone
ZnF-UBP	Zinc-Finger Domain Found In USPs

Acknowledgement

First and foremost, I would like to express my gratitude to my supervisors, Sylvie Urbé and Michael Clague for their patience, guidance and willingness to share their knowledge with me in the past three years. It has been an invaluable experience for me. I would also like to thank the Wellcome Trust for funding me and giving me this great opportunity to carry out my work.

Thanks go to Judy Coulson, Ian Prior, Igor Barsukov, Jon Lane, Pascal Meier, Gerry Cohen and Shankar Varadarajan for your help and inputs throughout my project. I would like to thank my PhD mentor, David Criddle for his advices. A big thank you goes to Han Liu and Claire Heride for all the help and support, and for setting good examples in the laboratory. Many thanks to all the past and present members of the laboratory, in no particular order, Ewan MacDonald, Craig Mageean, Aitor Martinez, Alice Howarth, Fiona Hood, Emma Rusilowicz, Dora Pedrosa, Anna Newlaczyl, Arnaud Selvais, Viktor Malec, Dean Hammond, Rebecca Eccles, Veronica Aran, Monica Faronato, Yasminka Omerovic, Jenny Martin, Joseph Sacco, Sarah Darling, Jenna Kenyani, Matthew Concannon, Rachel Carter, Alison Beckett and Simon Oliver for all the help and for making the lab such an enjoyable place to work in.

I would also like to extend my gratitude to Jia Lih Wong for inspiring me to do a PhD in the first place, and for all the help extended from the moment I arrived in UK. Many thanks to all my friends all over UK, Chloe Tan, Yvonne Tang, Yi Cheng, Yuan Yuan, Rui Ying, Lih Tyng, Ramsah, Kevin, Bonnie and Cara for all the joy and memories throughout these years. Special thanks to Taylan for being a constant source of support and for the words of encouragement.

Last but not least, I would like to dedicate this thesis to my amazing family for I am who I am because of your unconditional love. Thank you very much mom and dad for all the sacrifices you made to provide me with the best in life. To my two dearest sisters, thank you for always being supportive through the ups and downs in life!

Chapter 1: Introduction

1.1 Intracellular protein degradation

Nowadays, it is a fundamental understanding in cell biology that proteins are selectively targeted for degradation. This process ensures that damaged proteins are not only cleared away but also spatially and temporally regulated for different cellular functions. However, back-track to the early 20th century and intracellular proteins were thought to be long-lived, static constituents of the body whereas the fuel for energy was thought to be derived from dietary sources. It was not until 1939 that Rudolf Schoenheimer and his colleagues challenged this paradigm. With the use of heavy isotope labeling, they discovered that rats fed with ^{15}N-labelled tyrosine only excreted 50% of the isotopic amino acids in their urine while the remainder was incorporated into tissue proteins (Schoenheimer et al. 1939). This provided the first evidence that intracellular proteins exist in a dynamic equilibrium of synthesis and degradation.

In the mid 1950s, Christian de Duve and his colleagues pioneered the technique of differential centrifugation for cell fractionation and serendipitously identified a single membrane-bound vesicle that encloses acid phosphatase and other hydrolases in rat liver (Duve et al. 1953, De Duve and Wattiaux 1966). The term lysosome was chosen to describe these relatively fragile vesicles that engulf macromolecules, endocytosed membrane proteins, worn-out organelles and certain cytosolic proteins for degradation (Pillay et al. 2002). This discovery provided the first insight into the cellular proteolytic machinery.

1.2 Discovery of the proteasomal degradation system

It soon became apparent that lysosomal degradation does not account for all protein degradation. Firstly, while the inhibition of the lysosomal hydrolases (using weak bases) prevented the degradation of extracellular proteins, the

degradation of most intracellular proteins was unaffected (Poole et al. 1977). Secondly, it was reported that the degradation of haemoglobin occurs in immature rabbit reticulocytes that do not contain lysosomes (Rabinovitz and Fisher 1964). Etlinger and Goldberg further demonstrated, using lysates from the immature rabbit reticulocytes, that the degradation of abnormal haemoglobin is ATP-dependent and occurs at neutral rather than acidic pH, strongly indicating the existence of an alternative non-lysosomal degradation pathway (Etlinger and Goldberg 1977, Ciechanover 2005).

Around the same time, Ciechanover and Hershko discovered that ATP is required for the covalent conjugation of a low molecular weight protein to proteins that were subsequently degraded by an unknown ATP-dependent proteolytic machinery in reticulocyte lysates (Hershko et al. 1979, Ciechanover et al. 2012). This protein was appropriately named ATP-dependent proteolysis factor 1 (APF-1).

Independent of their discovery, Goldstein and colleagues discovered a small molecular weight protein that is universally expressed and highly conserved (Schlesinger and Goldstein 1975, Schlesinger et al. 1975, Goldstein et al. 1975). This protein was named ‘ubiquitin’ owing to its ubiquitous expression in cells. Ubiquitin was reported as a DNA-associated protein that was joined through its C-terminus to an internal lysine of histone H2A (Goldknopf and Busch 1977, Goldknopf et al. 1975, Hunt and Dayhoff 1977). Whilst the physiological context of APF-1 and ubiquitin conjugations appeared to be different, the strikingly similar fashion in which the two were conjugated to target substrates raised the interest of Wilkinson and colleagues, who then showed by sequence analysis that the two are indeed the same protein (Wilkinson et al. 1980).

1.2.1 Discovery of the ubiquitin proteasome system (UPS)

Based on the work by Tanaka and colleagues in reticulocyte lysates, it was known that while the presence of ubiquitin and ATP promoted protein degradation, selective removal of ubiquitin by ion exchange chromatography from the lysates did not fully prevent ATP-dependent protein degradation although it slowed down the process. This indicated that there are two ATP-requiring steps in ubiquitin-mediated proteolysis (Tanaka et al. 1983). An important breakthrough was made when Hough and colleagues purified a high-molecular-mass proteolytic complex that degraded ubiquitylated lysozyme in an ATP-dependent manner, which they termed the proteasome (Hough et al. 1986, Hough and Rechsteiner 1986).

The proteasome is a 2.5MDa multicomponent protease that consists of two sub-complexes: the 20S proteolytic core particle (~700kDa) and the 19S regulatory particle (~900kDa) (Figure 1.1A) (Groll and Clausen 2003, Pickart and Cohen 2004, Goldberg 2012). The core particle consists of 2 copies each of 7 different α- and β-subunits (α1-7 and β1-7), which are arranged into four seven-membered rings (2 α- and 2 β-rings) with the two α-rings sandwiching the two β-rings, forming a barrel-like structure (reviewed in (Voges et al. 1999). The two middle β-rings contain three proteolytic subunits each (2 copies each of β1, 2 and 5), forming the catalytic chamber where the degradation of proteins occurs (Figure 1.1B). The α-rings serve as a narrow gate to regulate the translocation of substrates into and out of the proteasome. The inner compartment of the 20S core particle is only a few nanometers in diameter (Groll et al. 2000, Whitby et al. 2000). Therefore, access into the catalytic sites is restricted to unfolded proteins only, preventing non-specific degradation of cytosolic proteins (reviewed in (Voges et al. 1999). The ability of the proteasome to recognise, unfold and translocate targeted proteins into the 20S core particle lies in the 19S regulatory particle, which caps either one or both ends of the 20S core particle (Peters et al. 1993).

The 19S regulatory particle is made up of 19 subunits, including six AAA-ATPases (ATPases associated with a variety of cellular activities; Rpt1-6) and 13 non-ATPase subunits (Rpn1-3, Rpn5-13 and Rpn15). Two of the non-ATPase subunits, Rpn10 (also known as PSME4/S5A/MCB1) and Rpn13 (also known as ADRM1) have been shown to bind polyubiquitin chains (van Nocker et al. 1996, Husnjak et al. 2008, Sledz et al. 2013b, Sledz et al. 2013a). In addition, three so-called 'shuttle' proteins that are not integral subunits of the proteasome, Rad23, Dsk2 and Ddi1 bind and recruit polyubiquitylated proteins to the proteasome (Zhang et al. 2009, Elsasser et al. 2004, Verma et al. 2004, Finley 2009, Schauber et al. 1998, Chen and Madura 2002). Importantly, three deubiquitylating enzymes (DUBs; enzymes that cleave ubiquitin either from ubiquitin chains or from target substrates, discussed in section 1.4), Rpn11 and Ubp6 (POH1/PSMD14, and USP14, as well as a third activity, UCH37/UCHL5 in human) are also associated with the proteasome. Rpn11/POH1 is an integral subunit of the regulatory particle and removes whole ubiquitin chains at once from substrates prior to their degradation (Yao and Cohen 2002). In contrast to Rpn11, Uch37 and Ubp6/USP14 bind to the proteasome via Rpn13-Rpn2 and Rpn1, respectively, and serve to trim ubiquitin chains, thus rescuing proteins from proteasomal degradation (Yao et al. 2006, Hamazaki et al. 2006, Qiu et al. 2006).

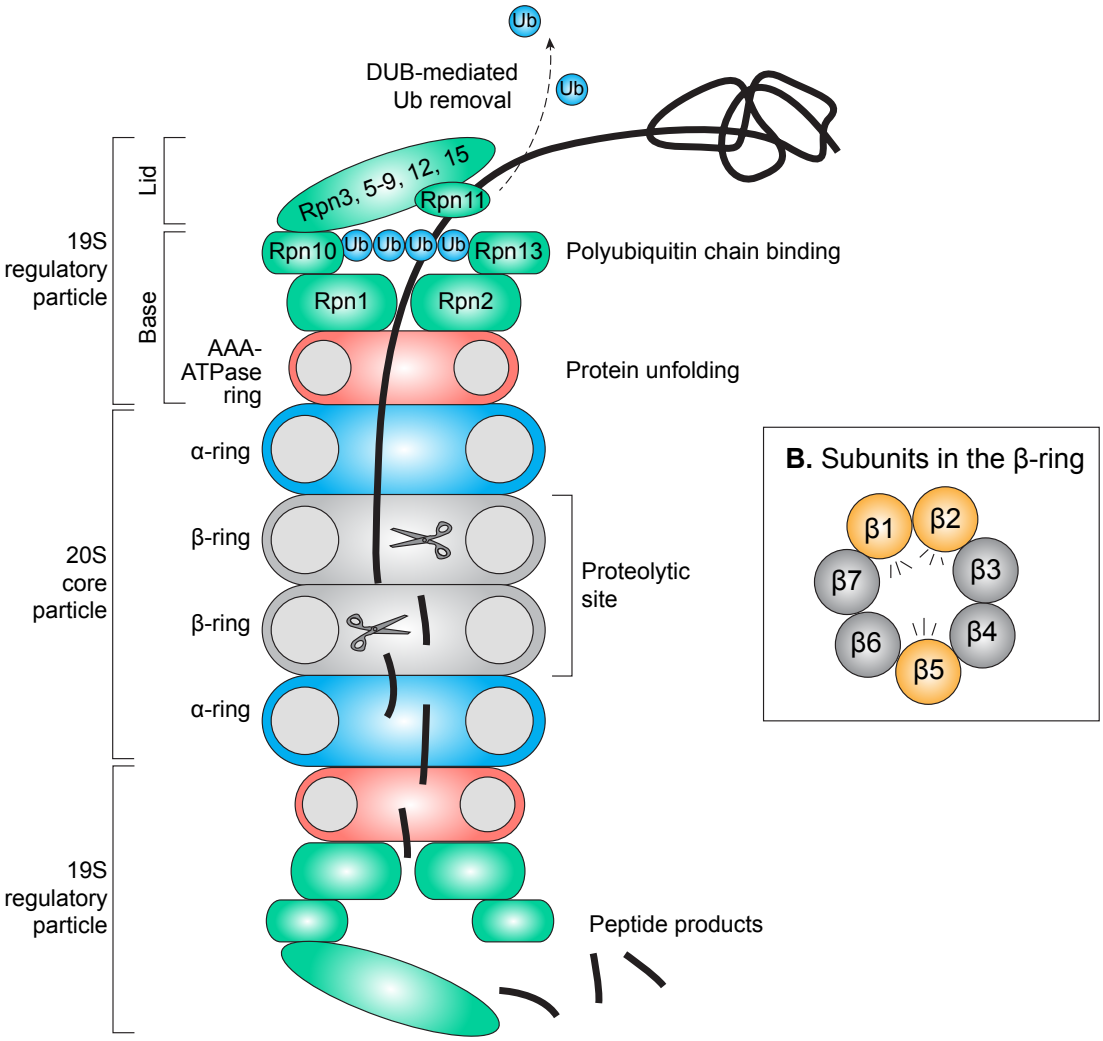

Figure 1.1 Simplified cartoon of the cross section of eukaryotic 26S proteasome and the mechanism of protein degradation.

(A) The eukaryotic 26S proteasome consists of a 20S core particle capped by two 19S regulatory particles. The core particle is further composed of two identical α and two identical β rings, each made up of seven distinct subunits. Ubiquitylated proteins are recognised by the 19S regulatory particle subunit Rpn10 and Rpn 13 and are unfolded by the AAA-ATPase prior to their catalytic degradation by the 20S core particle. Several DUBs mediate recycling of ubiquitin from proteasomal substrates (described in section 1.4).

(B) The β-rings consist of seven subunits. β1, β2 and β5 have catalytic activities for the proteolytic degradation of polypeptide chains.

1.3 Discovery of ubiquitylation as a signal for lysosomal and autophagic degradation

After the discovery of ubiquitin as a tag for selective protein degradation and the identification of the proteasome as an executor of proteolysis, the general consensus was that non-specific bulk turnover of proteins was mediated by the lysosome whereas specific protein turnover was mediated by the proteasome. It was nearly a decade after the discovery of the ubiquitin proteasome system (UPS) that it became apparent that the regulated lysosomal degradation of endocytosed membrane proteins, as well as the selective removal of organelles from the cytosol by autophagy also involves ubiquitin (Hurley and Stenmark 2011, Korolchuk et al. 2010, Clague and Urbé 2010). The ability of one small molecule to dictate the different fate of cellular proteins is derived from the ability of ubiquitin to modify its substrate's surface topology via different ubiquitin 'chains', which will be further discussed in the following section.

1.3.1 Ubiquitin structure

Ubiquitin is a 76-amino acid protein encoded by four different genes, namely *UBB*, *UBC*, *UBA52* and *RB27A*. UBB and UBC express tandem repeats of three and nine ubiquitin moieties, respectively, whereas the UBA52 and RPPS27A genes encode for a single ubiquitin fused to the N-terminus of the ribosomal proteins, L40 and S27a, respectively (Wiborg et al. 1985, Baker and Board 1991). These pro-ubiquitin molecules are constitutively cleaved to generate an intracellular pool of free ubiquitin.

Structurally, ubiquitin consists of four antiparallel β-sheets on one side and an α-helix on the other side, forming a barrel-like structure with a flexible C-terminal tail (Figure 1.2) (Vijay-Kumar et al. 1987). Among the 76 amino acids that comprise ubiquitin, there are seven highly conserved lysine (K) residues, K6, K11, K27, K29, K33, K48 and K63. All seven lysine residues, together with the α-amino group of the N-terminus of ubiquitin, can be conjugated via an isopeptide or peptide bond, respectively, to the C-terminal

glycine of another ubiquitin molecule, forming 8 different types of ubiquitin chains.

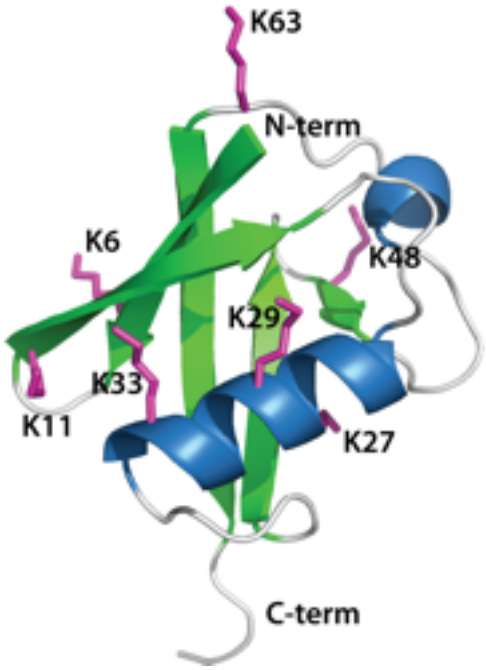

Figure 1.2 Crystal structure of ubiquitin.

Ubiquitin is composed of 76 amino acids. It consists of four antiparallel β-sheets on one side and a α-helix on the other side, forming a barrel-like structure with a flexible C-terminal tail. Ubiquitin has seven lysine residues (orange), which allows for additional ubiquitylation (This figure was kindly generated by Igor Barsukov).

1.3.2 The ubiquitylation cascade

Following the discovery of ubiquitin, Hershko, Ciechanover and colleagues used immobilized ubiquitin as a 'covalent' affinity bait and further identified the three key enzymes that act in concert to catalyse ubiquitin conjugation, namely the E1 (ubiquitin-activating enzyme), E2 (ubiquitin-conjugating enzyme) and E3 (ubiquitin ligase) (Hershko et al. 1983, Ciechanover et al. 1982).

E1, the ubiquitin-activating enzyme, first binds to ATP•Mg^{2+} and ubiquitin to catalyse acyl-adenylation of the C-terminal glycine of ubiquitin (Figure 1.3A). This allows the formation of a thioester linkage between the E1 and the ubiquitin intermediate. Next, the ubiquitin is transferred to the catalytic cysteine of an E2 via transthioesterification, forming an E2~Ub intermediate (Wenzel et al. 2011b). Finally, an E3 ligase binds to both the E2~Ub thioester and the substrate to mediate the transfer of ubiquitin from the catalytic cysteine of the E2 to the substrate (Berndsen and Wolberger 2014).

The ubiquitin-modifying components have a hierarchical structure, with only 2 E1s, 40 E2s and more than 600 E3 ligases (Figure 1.3B) (Li et al. 2008, Berndsen and Wolberger 2014, Deshaies and Joazeiro 2009). Different E2 enzymes have been shown to dictate the length and linkage-type of ubiquitin chains. For example, Baboshina and Haas demonstrated that the E2 enzyme UBE2S only catalyses the formation of K11-linked ubiquitin chains (Baboshina and Haas 1996). Other E2s, such as UBE2G2 and UBC13 have been shown to specifically form K48 and K63-linkages (Liu et al. 2014, Lim et al. 2013).

On the other hand, the high number of E3 ligases provides specificity towards a broad array of substrates. There are three types of E3 ligases, namely the HECT, RING and RING-between-RING (RBR) E3 ligases (Figure 1.3A).

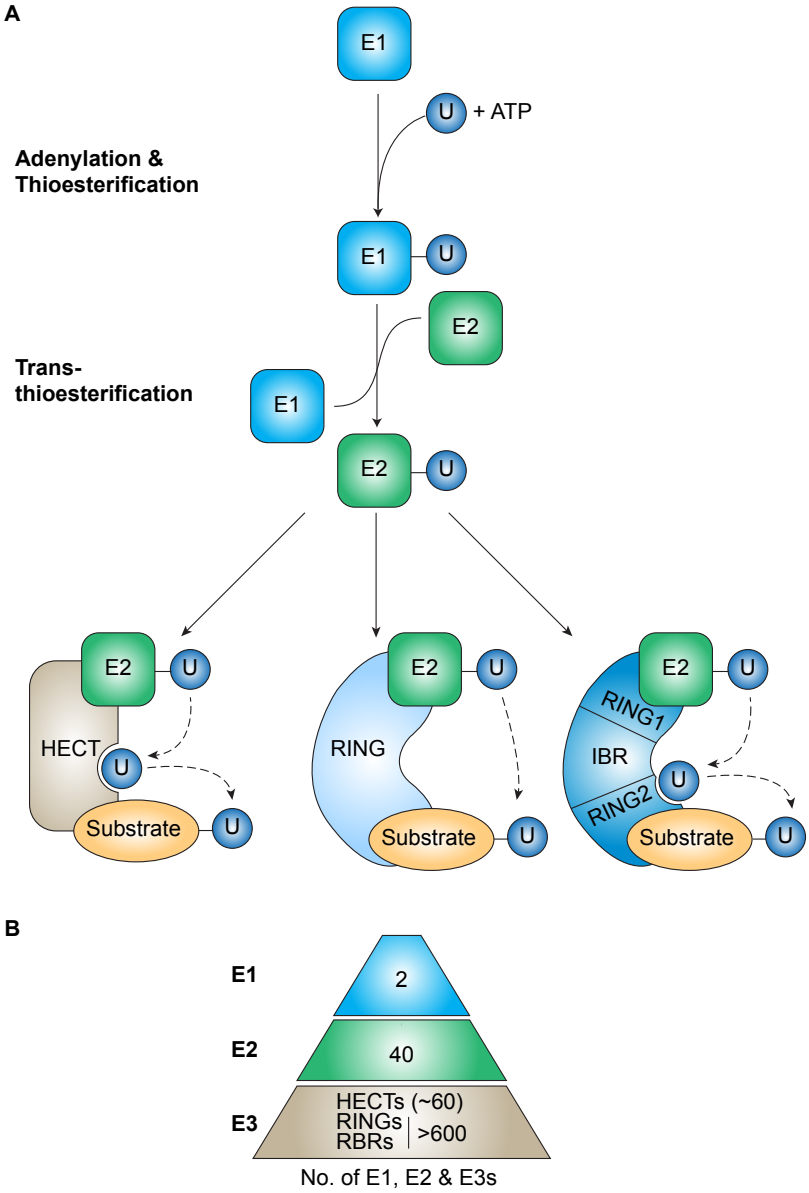

Figure 1.3 Mechanism of the ubiquitylation.

(A) Ubiquitylation is accomplished by the coordinated action of three enzymes, an E1 ubiquitin-activating enzyme; an E2 ubiquitin-conjugating enzyme; and an E3 ubiquitin ligase. The E1 hydrolyses an ATP to activate the C-terminus of ubiquitin by adenylation. The adenylated ubiquitin forms a thioester bond with the E1 active-site cysteine. Ubiquitin is then transferred to the active-site cysteine of an E2 via transthioesterification. The ubiquitin-charged E2 binds to an E3, which transfer the ubiquitin to a substrate protein. HECT-type E3 ligases form an intermediate ubiquitin-thioester bond via an E3 active-site cysteine prior to the formation of an isopeptide bond between the C-terminal of ubiquitin with either the N-terminus of a substrate protein or the ε-amino group of a lysine residue. RING type E3 ligases directly transfer ubiquitin from the E2 to the substrate. The RING-between-RING E3 ligases contain RING domains but also form an intermediate ubiquitin-thioester bond with ubiquitin prior to ubiquitin transfer to the substrate.

(B) There are only two E1s, and approximately 40 E2s in the human genome. The large number of E3s in combination with different E2s provide substrate and linkage specificities during ubiquitylation. cascade (Modified from (Winklhofer 2014, Heride et al. 2014)).

The HECT (homologous to E6AP carboxy terminus) family of E3 ligases catalyses ubiquitylation in a two-step reaction. Ubiquitin is first transferred from the E2 to a catalytic cysteine in the E3 and then subsequently transferred to the substrate. The HECT domain consists of two lobes situated at each of the N- and C-terminus. The N-lobe associates with the E2 while the C-lobe containing the catalytic cysteine forms a thioester bond with ubiquitin (Metzger et al. 2012). Some HECT E3s demonstrate specificity in ubiquitin linkage synthesis. KIAA10 preferentially catalyses K29 and K48-linked chains while E6AP only synthesises K48-linked chains (Mastrandrea et al. 1999, You and Pickart 2001). Nedd4 (Neural precursor cell expressed, developmentally down-regulated 4) and Itch have both been shown to specifically synthesise K63-linked chains, but Itch can also form K29-linked chains to target Deltex (DTX) for lysosomal degradation (Kim and Huibregtse 2009, Maspero et al. 2011, Scialpi et al. 2008, H. T. Kim et al. 2007, Chastagner et al. 2006).

In the case of the RING (really interesting new gene) family of E3 ligases, these enzymes lack a catalytic cysteine and largely serve as scaffolds to recruit the E2 in close proximity to the substrate to facilitate direct transfer of ubiquitin. The RING domain, which is a sequence containing conserved Cys and His residues (typically Cys3HisCys4) allows binding of two zinc cations, forming a cross-brace zinc-finger structure (Freemont et al. 1991). Unlike HECT E3s, a RING E3 does not form a thioester intermediate with ubiquitin and the ubiquitin-linkage specificity is largely conferred by the interacting E2. Therefore, a RING E3 that can bind to different sets of E2s will be able to produce several distinct types of ubiquitin chains.

The RING E3s can be further categorized into single unit RING E3s and multi-subunit Cullin RING ligases (CRLs) (Li et al. 2008). One of the most well-known RING E3s is MDM2. MDM2 ubiquitylates p53, a key protein that regulates the cell cycle, cell proliferation, cell invasion, cell survival and apoptosis (Kubbutat et al. 1997). Loss of p53 and/or overexpression of MDM2 are commonly associated with cancer, including sarcomas, gliomas, melanomas and breast cancers. (Landers et al. 1997, Pykett et al. 1997). An

example of the multimeric RING E3s are the Cullin-RING ligases (CRLs) of which the Skp, Cullin, F-box (SCF) complexes are a subgroup. In the SCF complex, the Cullin-RBX1 RING module binds an E2 while Skp1 binds the opposite end of the Cullin and recruits the F-box protein that confers specificity for substrate recognition (Petroski and Deshaies 2005, Zheng et al. 2002). Interestingly, the activation of the E3 activity of CRLs requires the conjugation of another ubiquitin-like protein, Nedd8, which alters the orientations of the different subunits of the SCF complex, thereby preventing the binding of the CRL inhibitor, CAND1 and improving E2 binding (Saha and Deshaies 2008, Duda et al. 2008).

The RBR family of E3 ligases has only recently been classified as a mechanistically distinct family of E3s that share overlapping features with both HECT and RING E3s. RBR E3s have at least two RING domains, separated by a conserved sequence known as the in-between-ring (IBR) domain (Aguilera et al. 2000). However, unlike the RING E3s, RBR E3s contain catalytically active Cys and can mediate ubiquitylation in a HECT-like mechanism (Wenzel et al. 2011a). The best-studied RBR E3 ligase is Parkin, named after its association with Parkinson's Disease (Wang et al. 2000). Parkin plays a cytoprotective role in the cell via its ability to clear misfolded or aggregated proteins such as α-synuclein, Pael-R, and CDCrel-1, all of which accumulate in patients with Parkinson's Disease (Shimura et al. 2001, Imai et al. 2001, Zhang et al. 2000). In addition, Parkin also regulates the selective removal of mitochondria via autophagy (Jin and Youle 2013). Recently, Müller-Rischart and colleagues reported that Parkin also increases the linear ubiquitination of NEMO formed by linear ubiquitin chain assembly complex (LUBAC), thereby activating the canonical NF-κB pathway (Henn et al. 2007, Muller-Rischart et al. 2013).

1.3.3 Different ubiquitin linkages and their physiological roles

Ubiquitin conjugation occurs between the lysine residues of a protein and the C-terminus of ubiquitin. The conjugation of a single ubiquitin moiety is called monoubiquitylation (Figure 1.4A). The conjugation of multiple ubiquitin moieties to different lysine residues within the same substrate is referred to

as multi-monoubiquitylation. Both monoubiquitylation and multi-monoubiquitylation have been implicated in the internalization of cell surface receptors, including G-protein coupled receptors, epidermal growth factor receptors and platelet-derived growth factor receptors (Terrell et al. 1998, Haglund et al. 2003, Mosesson et al. 2003). In addition, histones (most notably H2A and H2B), are also regulated by monoubiquitylation, extending the roles of monoubiquitylation to chromosome condensation and gene expression (Goldknopf et al. 1975, Robzyk et al. 2000)(reviewed in (Cao and Yan 2012, Fuchs and Oren 2014). Monoubiquitylation of Fanconi anemia group D2 protein (FANCD2) and Proliferating cell nuclear antigen (PCNA) are implicated in interstrand cross-linking (ICL) DNA repair pathway (Smogorzewska et al. 2007, Knipscheer et al. 2009). Monoubiquitylation of p53 by MDM2 has been shown to induce nuclear to cytoplasmic export of p53 for subsequent polyubiquitylation and degradation (Li et al. 2003).

As mentioned before, there are seven lysine residues in ubiquitin, all of which can serve as substrates for the attachment of another ubiquitin, forming different ubiquitin chains. This modification is termed polyubiquitylation (Figure 1.4B). Chain linkages are homogenous if the same lysine residue is modified during elongation and are named according to the lysine residue within ubiquitin that is used for chain formation, namely K6, K11, K27, K29, K33, K48 and K63 linkages. Conversely, “mixed ubiquitin chain” or “heterogenous chain” describes different linkages that are found at succeeding positions of the same ubiquitin chain. Alternatively, multiple modifications on a single ubiquitin can also take place, forming branched ubiquitin chains of unknown function. A linear ubiquitin chain is formed if the C-terminal glycine of an ubiquitin is linked with the N-terminal methionine of another ubiquitin. These different ubiquitin chains adopt different conformations and topologies, allowing for recognition by different ubiquitin-binding proteins (Ikeda and Dikic 2008, French et al. 2005, Hicke et al. 2005, Raasi et al. 2005, Clague et al. 2013). Therefore, different ubiquitin chains can influence the downstream effect of the ubiquitylated protein and constitute another layer of control in the regulation of cellular function (Wong and Cuervo 2010, Komander and Rape 2012, Komander 2009).

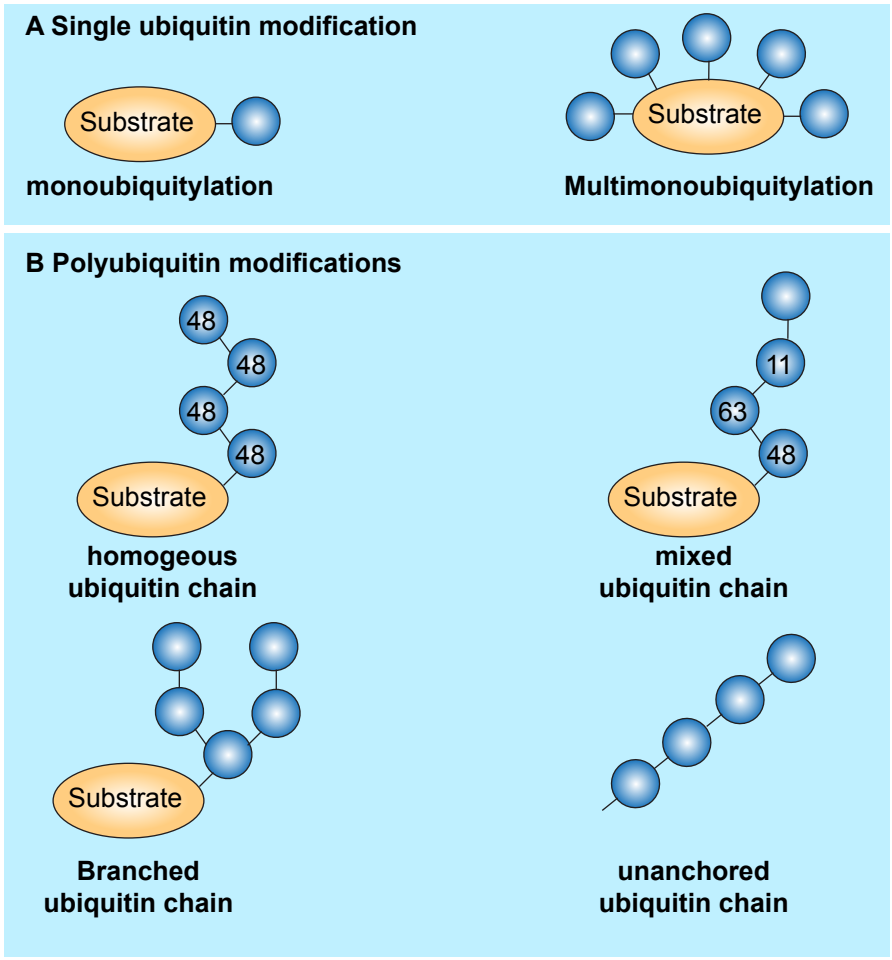

Figure 1.4 The different topologies of ubiquitylation.

(A) Conjugation of a single ubiquitin onto a substrate is called monoubiquitylation. Multiple conjugation of individual ubiquitylation onto different lysine residues of the same substrate is termed multi-monoubiquitylation.

(B) The internal lysine residues of ubiquitin allow the formation of polyubiquitin chains. The different types of ubiquitin chains are described in the figure.

All linkages have been detected in yeast, with K48 and K11-linked chains being the most abundant forms, followed by K63, K6, K27, K29 and K33-linked chains (Xu et al. 2009, Peng et al. 2003). In HEK293 cells, Kaiser and colleagues reported that the majority of the total ubiquitin pool are monoubiquitylated-conjugates (~63%), whereas free ubiquitin and polyubiquitin chains constitute approximately 26% and 11% of the total ubiquitin pool, respectively (Kaiser et al. 2011). Dammmer et al. further demonstrated in the same cell line that Lys48 (52%) and Lys-63 (38%)-linked

chains made up the majority of the polyubiquitin chains, followed by K29-linked chains (8%) (Dammer et al. 2011).

The best-characterised forms of ubiquitylation are K48 and K63 linkages and K48-linked chains are referred to as the ‘canonical’ ubiquitin chains. A chain of four or more ubiquitin moieties extended through K48 can target proteins for proteasomal degradation (Chau et al. 1989). On the other hand, K63-linked ubiquitin chains are implicated in various cellular processes, for example, in the internalization and degradation of cell surface receptors via endocytosis and lysosomal degradation (Conze et al. 2008, Galan and Haguenauer-Tsapis 1997, Geetha and Wooten 2008). Other roles of K63 ubiquitylation include DNA repair, autophagy, NF-κB and Wnt signaling pathway (Tauriello et al. 2010, Tran et al. 2008, Conze et al. 2008, Lim et al. 2013, B. Wang et al. 2007, Sobhian et al. 2007, H. Kim et al. 2007).

The remaining ubiquitin linkages are relatively less well characterised compared to K48 and K63-linked chains and are often referred to as the ‘atypical’ ubiquitin linkages. It is worth noting that all linkages, with the exception of K63-linked chain, may be able to target substrates for proteasomal degradation. Indeed, quantitative mass spectrometry analysis of unique signature peptides of each ubiquitin linkage revealed that all linkages, apart from K63-linked chain, accumulated both in yeast and in mouse neurons upon the inhibition of the 26S proteasome (Bedford et al. 2011, Xu et al. 2009). The reported cellular functions of the different ubiquitin modifications are summarised in Table 1.1.

Type		Cellular function	Reference
Single ubiquitin modification	Mono	Histone regulation	(Robzyk et al. 2000)
		Nuclear-cytoplasmic shuttling of p53	(Li et al. 2003)
		Endocytosis	(Terrell et al. 1998)
		DNA repair	(Huang and D'Andrea 2010)
	Multi	Endocytosis	(Mosesson et al. 2003, Haglund et al. 2003)
Polyubiquitin modification	Linear	NF-κB signaling	(Tokunaga and Iwai 2009, Tokunaga et al. 2009)
	K6	Parkin-mediated mitophagy	(Durcan et al. 2014)
		α-tubulin polymerization during embryogenesis	(Srivastava and Chakrabarti 2014)
		DNA repair	(Morris and Solomon 2004)
		Ascorbic acid conversion	(L. Wang et al. 2009)
	K11	Proteasomal degradation for cell cycle regulation	(Matsumoto et al. 2010, Budhavarapu et al. 2012, Jin et al. 2008)
	K27	Proteasomal degradation during Parkin-mediated mitophagy	(Geisler et al. 2010)
	K29	Proteasomal targeting	(Johnson et al. 1995)
		Lysosomal targeting	(Chastagner et al. 2006)
	K33	Negative regulation of T-cell Receptor signaling	(Huang et al. 2010)
	K29/K33	AMP-kinase inhibition	(Al-Hakim et al. 2008)
	K48	Proteasomal targeting	(Chau et al. 1989)
	K63	Lysosomal targeting	(Geetha and Wooten 2008)
		Autophagy	(Chin et al. 2010, Paul and Kumar 2011)
		Endocytosis	(Galan and Haguenauer-Tsapis 1997, Duncan et al. 2006)
		DNA Damage	(Bailly et al. 1997)
		NF-κB signaling	(Conze et al. 2008)
		Wnt signaling	(Tauriello et al. 2010)
	Heterologous linkage	E3 ligase activation (mixed K6, K27 and K48)	(Ben-Saadon et al. 2006, Tran et al. 2008)
		Internalisation of MHC1 (K63 and K11)	(Boname et al. 2010)

Table 1.1 Types of ubiquitin modification and and proposed cellular functions.

1.3.4 Linkage specific effects and recognition by ubiquitin binding domains

Some proteins have evolved to encode different ubiquitin-binding domains (UBDs) that recognise ubiquitin-conjugated substrates, in a manner similar to SH2 domain that allow for the recognition of phosphorylated proteins. In addition, the different polyubiquitin linkages provide diversity to substrate recognition and interaction with downstream ubiquitin-binding proteins or ubiquitin receptors with different UBDs (Hicke et al. 2005).

The first ubiquitin-binding protein identified was a proteasome subunit S5A/Rpn10, which contains a ubiquitin interacting motif (UIM) (Young et al. 1998, Hofmann and Falquet 2001). This discovery offers an explanation for the ability of the 26S proteasome to recognise and interact with ubiquitylated substrates. Since then, more than 20 UBD families have been reported and they all differ in terms of structure and binding modes (Kirkin and Dikic 2007). The α-helices (e.g. UIM and ubiquitin-associated domain,UBA) and zinc-finger (e.g. Nuclear pore localization 4 zinc finger, NZF and ubiquitin-binding zinc finger, UBZ) UBDs comprise the largest class of UBDs. The α-helices interact with the hydrophobic patch (Ile44) on ubiquitin whereas the zinc-finger domain offers more diversity than the α-helices and can recognise three different regions (Ile44, Asp58 and Gly76) on the surface of ubiquitin (Kirkin and Dikic 2007, Hurley et al. 2006). It is worth noting that UBDs have a low affinity for free ubiquitin to prevent the high levels of free ubiquitin (estimated at 10μM) in the cell from constitutively occupying the UBDs, which would render these unavailable for dynamic binding to ubiquitylated proteins (Hicke et al. 2005). Instead, multiple UBDs are often found in a ubiquitin-binding protein, which work cooperatively to bind to two or more ubiquitin moieties with high avidity. For example, the tandem UIM peptides on Rap80 demonstrate preference for K63 over K48 and monoubiquitin conjugation (Sims and Cohen 2009). Structural analysis of Rap80 revealed that the α-helices of two tandem UIMs and the weakly α-helical linker region between the two allow for the formation of one continuous α-helical structure that binds the two K63-linked ubiquitins simultaneously (Sims and Cohen 2009).

1.4 The deubiquitylases

Similar to most post-translational modification, the conjugation of ubiquitin to its substrate is reversible and the deconjugation of ubiquitin is mediated by the deubiquitylating enzymes (DUBs, also referred to as deubiquitylases). There are more than 90 DUBs that have so far been identified in the human genome. These DUBs can be categorized into five distinct families: ubiquitin-specific proteases (USPs), ubiquitin C-terminal hydrolases (UCHs), ovarian tumour proteases (OTUs), Josephins or Machado-Joseph Disease proteins (MJDs), Jab1/MPN/MOV34 metalloproteases (JAMM/MPN+s) (Komander et al. 2009a, D. Komander 2010, Clague et al. 2013). The number of enzymes identified in each family is summarized in Figure 1.5.

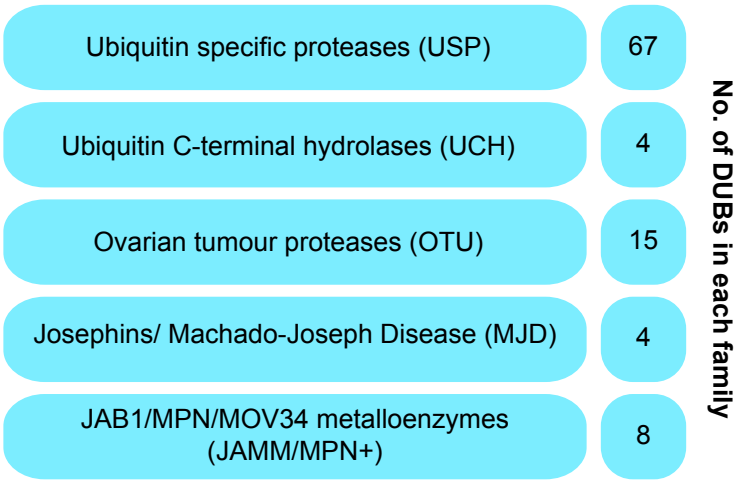

Figure 1.5 The different families of DUBs and the number of DUBs in each family.

The general roles of DUBs can be categorised into three functional groups. Firstly, ubiquitin can be transcribed from several genes, either as a linear fusion of ubiquitin molecules with each other or with ribosomal proteins, which need to be cleaved to generate a cellular pool of free ubiquitin (Figure 1.6A). Secondly, DUBs can remove conjugated ubiquitin chains from proteins, thereby reversing proteasomal or lysosomal degradation or other downstream signalling activities (Figure 1.6B and C). By removing ubiquitin from substrates that are committed to degradation, some DUBs can recycle ubiquitin to maintain cellular ubiquitin homeostasis. Specifically, three DUBs, USP14, UCHL5 and POH1 are found to associate with the human 26S proteasome and their proteolytic activities are required to hydrolyze ubiquitin

chains prior to substrate degradation (Figure 1.6D) (Finley 2009). DUBs can also be used to edit ubiquitin linkages, thereby leading to alterations in the ubiquitin signal and its downstream effects (Figure 1.6E) (Komander et al. 2009a, Clague et al. 2012). In addition, cytosolic ubiquitin chains generated from *en bloc* cleavage of ubiquitin chains from proteins (i.e. directly between the substrate and the proximal ubiquitin) need to be disassembled by DUBs to regenerate the pool of free ubiquitin in the cell (Figure 1.6F). An example of a DUB, which could act in this fashion is Ubp14 (the yeast homolog of USP5/IsoT), which has been shown to bind via its UBD to the free C-terminus of unconjugated ubiquitin to process cytosolic, unanchored ubiquitin chains into single ubiquitin molecules (Amerik et al. 1997, D. Komander 2010).

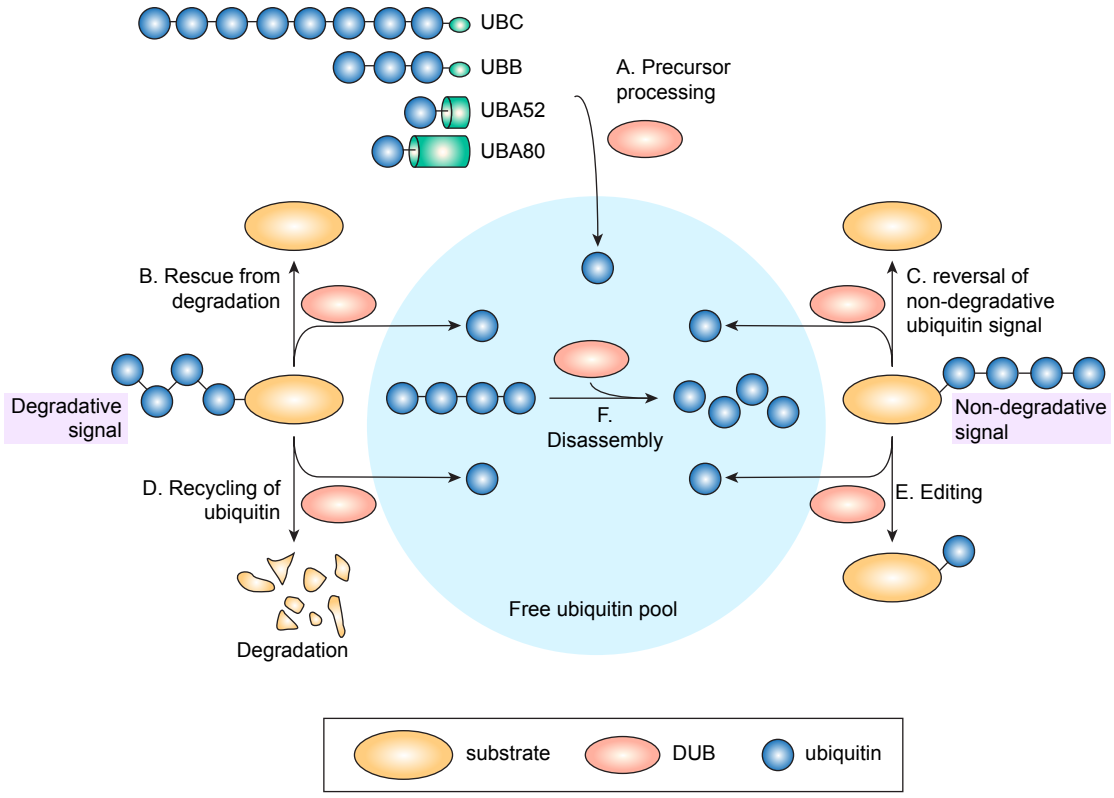

Figure 1.6 General functions of deubiquitylases.

The large number of DUBs in the human genome serves different functions: (A) processing of newly translated tandem ubiquitin repeats or ubiquitin fused to ribosomal proteins; (B) rescuing proteins targeted for proteasomal or lysosomal degradation; (C) reversal of non-degradative signals; (D) recycling of ubiquitin prior to substrate degradation to maintain ubiquitin homeostasis; (E) editing ubiquitin chains and altering ubiquitin signal; (F) disassembling ubiquitin chains generated by en bloc removal from substrates to form individual ubiquitin molecules. (Adapted from Komander et al. 2009).

1.4.1 Structure and catalytic activity of the cysteine-dependent DUBs

The USPs, OTUs, UCHs and Josephins are all cysteine proteases that catalyse the proteolytic reaction between a Lys ε-amino group and a carboxyl group that corresponds to the C-terminus of ubiquitin. Current understanding of the mechanism of cysteine proteases comes from studies of the plant protease, papain (Storer and Menard 1994). Cysteine proteases usually rely on a catalytic triad or diad for their functions. The two crucial amino acid residues for the proteolytic action are a histidine (His) and cysteine (Cys). The side chain of the His residue lowers the pKa of the Cys residue, enabling its nucleophilic attack on the isopeptide bond between the C-terminal of ubiquitin with the lysine residue of the conjugated substrate. Usually, a third residue of either asparagine or aspartic acid aligns and polarizes the catalytic His. However, this is not always essential as some enzymes (e.g. A20) lack the third residue and can still polarize the His by other means. The nucleophilic attack forms a catalytic acyl intermediate between the C-terminus of ubiquitin and the thiol group of the catalytic Cys. Next, a water molecule hydrolyses the acyl-Cys intermediate, thereby releasing the ubiquitin and completing the catalytic cycle (reviewed in (Clague et al. 2013)).

1.4.2 Structure and catalytic activity of the Zinc-metalloprotease DUBs

The JAMM family of DUBs are zinc-dependent metalloproteases. They contain highly conserved His, Asp and Ser residues that coordinate the catalytic zinc (Maytal-Kivity et al. 2002). During catalysis, the zinc ion is coordinated by two His residues, an Asp residue and water molecule. A nearby invariant Glu residue accepts a proton from the water molecule, leaving a hydroxyl ion, which then attacks the carboxyl carbon of the isopeptide bond. The ε-amino group from the proximal ubiquitin that is linked to the carboxyl carbon of the distal ubiquitin is then replaced with the hydroxyl group from the activated water molecule (Komander et al. 2009a, D. Komander 2010, Clague et al. 2013).

1.4.3 Substrate specificity of DUBs

The 98 human DUBs exhibit specificity for their substrates at multiple levels, including the ability to distinguish between ubiquitin and ubiquitin-like modifiers, different ubiquitin linkages and substrates at different subcellular localisations.

Ubiquitin belongs to one of the 17 small ubiquitin-like modifiers (UBLs) encoded by the human genome. While the sequence of the UBLs varies, they all take on a characteristic ubiquitin fold. In addition, several UBLs, including small ubiquitin-like modifier (SUMO), neural precursor cell expressed, developmentally down-regulated 8 (Nedd8), Interferon-stimulated gene 15 (ISG15), ubiquitin D (FAT10) and autophagy related protein 12 (ATG12) use a similar conjugation mechanism to ubiquitin for protein modification, resulting in a similar topological change in the targeted substrate (Hochstrasser 2009). However, DUBs are able to distinguish between ubiquitin and some of these UBLs, partly due to the fact that the C-terminal four residues of ubiquitin preceding the Gly-Gly-motif of are dissimilar to those of SUMO, Atg12 and FAT10. Even though Nedd8 has a similar sequence to Ubiquitin, the fact that arginine at position 72 is replaced by alanine means that this UBL cannot be processed by USPs (Ye et al. 2011). The identical sequence of ISG15 at the four residues with ubiquitin, allows some DUBs, including USP2, USP5, USP13, USP14, USP18 and USP21 to recognise and hydrolyse ISG15 (Gong et al. 2000, Catic et al. 2007, Ye et al. 2011, Clague et al. 2013).

The specificity of DUBs also extends to their ability to recognise different ubiquitin linkages and also different positions within the ubiquitin chain. For example, the JAMM/MPN+ family of DUBs including AMSH, AMSH-LP and BRCC36 display intrinsic specificity for Lys63-linked chains only (Cooper et al. 2009, McCullough et al. 2004, Sato et al. 2008, Komander et al. 2009b). Other examples of DUBs that demonstrates linkage specificity include CYLD (K63-linked) and Cezanne (K11-linked) (Komander et al. 2008, Bremm et al. 2010). Recently, a newly identified DUB, OTULIN that is involved in NF-κB

signaling has been shown to specifically recognise linear ubiquitin chains and several other enzymes of the OTU-family have also been shown to exhibit ubiquitin chain specificity (Keusekotten et al. 2013, Mevissen et al. 2013).

The subcellular localisation of DUBs also provides another level of regulation towards their substrate specificity. For example, USP19 and USP30 both have a transmembrane domain that localises these DUBs to the endoplasmic reticulum and mitochondria, respectively (Hassink et al. 2009, Nakamura and Hirose 2008). USP19 is involved in the ER-associated degradation (ERAD) pathway during unfolded protein response and has been shown to rescue cystic fibrosis transmembrane conductance regulator (CFTR) from proteasomal degradation (Hassink et al. 2009). USP30 has been implicated in the regulation of mitochondrial morphology (Nakamura and Hirose 2008).

1.4.4 USP domain DUBs

The USPs are the largest and most diverse family of DUBs, consisting of 67 distinct members (Clague et al. 2013, David Komander 2010). The USP domain comprises three sub-domains resembling the Palm, Thumb and Fingers of a right hand (Hu et al. 2002). The Fingers bind to a distal ubiquitin, bringing it in close proximity to the catalytic site located at the interface between the Palm and the Thumb.

Most of the USP family enzymes also contain different accessory domains that provide substrate specificity and localization. As mentioned before, USP19 and USP30 both contain transmembrane domains that localize these DUBs to the ER and mitochondria respectively (Lee et al. 2014, Nakamura and Hirose 2008, Hassink et al. 2009). In addition, most DUBs contain one or more UBDs. The most common UBD found in the USPs is the Zinc-finger domain (ZnF-UBP), which has been demonstrated or predicted in at least a subset of USPs (USP3, USP5, USP14, USP16, USP44, USP45 and USP49) to specifically bind to the free C-terminus Gly-Gly motif of ubiquitin (Bonnet et al. 2008, Nicassio et al. 2007, Pai et al. 2007, Reyes-Turcu et al. 2006). The

other UBDs, UBA and UIM are also observed not only in USPs but also in other DUB families (reviewed in (Clague et al. 2013)).

Another domain that is commonly observed in ubiquitin-interacting/modifying proteins, the UBL is also observed in many USPs (Faesen et al. 2012, Xiao Zhu et al. 2007). UBL domains serve variable functions in different proteins. In the context of USP14, the UBL domain is required for its recruitment to the proteasome. The binding of USP14 with the proteasome promotes the catalytic activity of USP14, presumably via conformational change that unblocks the catalytic site (Hu et al. 2005). The five C-terminal UBL domains of USP7 function to promote the catalytic activity of USP7 (Faesen et al. 2011a). In addition USP15 contains a DUSP-UBL double domain, which serves as a binding module for the E3 ligase BRAP, further demonstrating the functional diversity of UBL domains in the USPs (Hayes et al. 2012, Elliott et al. 2011).

Generally, USPs are less selective between polyubiquitin chains. Faesen and colleagues demonstrated that USP1, USP4, USP7, USP8, USP11, USP15 USP21 and USP25 hydrolyse all forms of di-ubiquitin linkages at similar rates, with the exception of linear di-ubiquitin chains, which were only cleaved by in USP4, USP16 and USP21 (Faesen et al. 2011b).

1.4.5 Ubiquitin C-terminus Hydrolases (UCHs)

The UCH family of DUBs consists of only 4 members, namely UCHL1, UCHL3, UCHL5 and BAP1. The UCH domain consists of approximately 210 a.a., which either span the entire protein (UCHL1 and UCHL3) or the N-terminus (UCHL5 and BAP1) (Clague et al. 2013, Komander et al. 2009a). The two smaller UCHs, UCHL1 and UCHL3 demonstrate negligible *in vitro* activity towards K48, K63 and linear ubiquitin chains (Komander et al. 2009b).

One feature that is unique to the UCH family is a large surface loop that forms right over the active site upon ubiquitin binding and ubiquitin needs to

pass through this loop to reach the active site. This restricts the size of ubiquitylated substrates that are allowed assess to the catalytic site and only ubiquitin conjugated to small peptides or molecules is allowed to access the catalytic site. This also explains the inability of UCHL1 and UCHL3 to deubiquitylate ubiquitin chains (Das et al. 2006, Johnston et al. 1997, Johnston et al. 1999, Misaghi et al. 2005). As mentioned before, ubiquitin is synthesised as pro-ubiquitin chains consisting of head-to-tail ubiquitin repeats capped with a short peptide at the C-terminus. UCHL1 and UCHL3 might be involved in the processing of pro-ubiquitin chains to generate free ubiquitin by removing these short peptides. An alternative hypothesis suggests that the unstable ubiquitin thioester intermediates generated during ubiquitin activation may escape the ubiquitylation cascade and undergo thiol or amine modification in the cytosol. UCHL1 and UCHL3 may serve to reverse this process and restore the free ubiquitin levels in the cell. Indeed, the high copy numbers of these DUBs as observed from proteomic studies and the lack of other domains for protein-protein interaction support this hypothesis (Geiger et al. 2012, Schwanhausser et al. 2011). However, a recent paper reported that UCHL1 deubuiquitylates and rescues NOXA (a BH3-only protein that promotes apoptosis), from proteasomal degradation in both human cells and *Caenorhabditis elegans* (Brinkmann et al. 2013). It is also worth mentioning that a point mutation (I93M) in UCHL1 has been associated with Parkinson's Disease, causing a partial decrease in its catalytic activity (Leroy et al. 1998)

The other two larger UCH enzymes, UCHL5 and BAP1, have a more extended crossover loop, which provides more flexibility for larger ubiquitin conjugates (Zhou et al. 2012). Intriguingly, the catalytic activity of both UCHL5 and BAP1 is only activated upon binding to their appropriate physiological partners (Zhou et al. 2012). In the case of UCHL5, the C-terminal extension after the UCH domain is required for its association with the proteaosome subunit Rpn13 (Hamazaki et al. 2006, Qiu et al. 2006, Yao et al. 2006). In *Drosophila*, *dBAP1* (*Calypso*) forms a complex with the Polycomb group (PcG) protein ASX to oppose the monoubiquitylation of H2A

by the E3 ligase complex, PRC1-dRAF (Polycomb repressive complex I – dRing-associated factor) (Scheuermann et al. 2010).

1.4.6 Ovarian tumour proteases (OTUs)

The OTU domain structure does not resemble that of the USP domain. However, the catalytic residues superimpose well with those of the USP and UCH domains (Komander and Barford 2008). Members of the OTU family display variable specificity towards different linkages (Mevissen et al. 2013). OTUD1 and OTUB5/DUBA preferentially act on K63-linked chains whereas OTUB1 are reported to be K48 specific (Kayagaki et al. 2007, Edelmann et al. 2009, T. Wang et al. 2009, Virdee et al. 2010). TRABID was first identified to be a K63-specific DUB, but was later shown to display greater preference for K29 and to a lesser extend K33 and K63-linked chains (Virdee et al. 2010, Tran et al. 2008). OTULIN, a recently discovered OTU family member, has been reported to hydrolyse linear ubiquitin chains only (Keusekotten et al. 2013, Mevissen et al. 2013).

Several OTU enzymes have been implicated in different signaling processes. For example, A20, OTULIN and Cezanne (together with CYLD from the USP family) are involved in NF-κB signaling, TRABID regulates WNT signaling, and OTUD5 modulates IRF3 signaling (Wertz et al. 2004, Enesa et al. 2008, Tran et al. 2008, Kayagaki et al. 2007, Trompouki et al. 2003, Keusekotten et al. 2013). Several other members of the OTU-family have also been shown to exhibit specificity for particular ubiquitin chains (Mevissen et al. 2013). In particular, A20/TNFAIP3 is a unique protein, which comprises both intrinsic DUB and E3 activities at the N- and C-terminus, respectively (Wertz et al. 2004, Heyninck and Beyaert 2005). A20 is transcriptionally upregulated by NF-κB but it operates in a negative feedback loop to suppress the signaling pathway. A20 demonstrates high deubiquitylating activity towards K63-linked chains on receptor-interacting protein 1 (RIP1; an essential mediator of the proximal TNF receptor 1 signaling complex) yet conjugates K48-linked chains onto the same substrate. Formation of K63-linked chains on RIP1 provides platform for the recruitment of an adaptor protein, Mitogen-activated

protein kinase kinase kinase 7 interacting protein 1 (TAB), which in turn recruits Mitogen-activated protein kinase kinase kinase 7 (TAK1) for autophosphorylation and subsequently activates NF-κB. The replacement of K63-linked chain to K48-linked chain by A20 targets RIP1 for proteasomal degradation, thereby suppresing NF-κB signaling. In addition, A20 also disrupts the interaction between various E3s (e.g. TRAF6, an E3 that is involved in NF-κB activation) with the E2s, Ubc13 and UbcH5c, by targeting the E2s for proteasomal degradation, further suppressing NF-κB signaling (Shembade et al. 2010).

1.4.7 Machado-Joseph disease proteins (MJDs)

Ataxin-3 (ATXN3) is the most prominent member of the MJD family. In fact, the name of this DUB family arises from the disease caused by ATXN3 mutation. Machado-Joseph Disease is the major form of spinocerebellar ataxia (Riess et al. 2008). This disease is caused by the C-terminal amplification of an unstable CAG triplet repeat that results in the extension of poly-glutamine (polyQ) in Ataxin 3. The resulting polyQ stretch fails to fold properly, leading to protein aggregation in cells (Williams and Paulson 2008).

The MJD domain is found at the N-terminus of all the MJD family members. All four members of this family, ATXN3, ATXN3L, JOSD1 and JOSD2, have been shown to be catalytically active (Burnett et al. 2003). Nuclear magnetic resonance studies on the MJD domain of ATXN3 revealed that the structure is in a non-productive conformation at steady state, due to the presence of a large helical lever that occludes the active site (Mao et al. 2005, Nicastro et al. 2005, Nicastro et al. 2006). Intriguingly, the Josephin domains of both ATXN3 and JOSD1 have been shown to be mono-ubiquitylated and such ubiquitylation increases the catalytic activity of both DUBs (Winborn et al. 2008, Seki et al. 2013). ATXN3 demonstrates preference for K63-linkages and together with JOSD1, and the closely related family member, ATXN3L, have been implicated in the transcriptional repression of phosphatase and tensin homolog (PTEN) in lung cancer cells (Winborn et al. 2008, Sacco et

al. 2014). In addition, JOSD1 has been implicated in the regulation of membrane dynamics, cell motility and endocytosis (Seki et al. 2013).

1.4.8 JAB1/MPN/Mov4 metalloenymes (JAMM)

The JAMM metalloenzyme family consists of 8 members. These DUBs often operate as part of a multimeric protein complex (David Komander 2010, Clague et al. 2013). For example, POH1/PSMD14 is constitutively incorporated in the 19S regulatory particle of the proteasome and recycles ubiquitin chains from substrates destined for proteasomal degradation (Finley 2009). AMSH and AMSH-LP are both associated with the ESCRT machinery for membrane trafficking (Williams and Urbe 2007, Clague and Urbe 2006). CSN5 is a subunit of the COP9 signalosome that deneddylates the Cullin E3 ligases for inactivation (Cope et al. 2002). BRCC36 is implicated in DNA repair pathway via association with two complexes, the BRISC and BRCA1-RAP180 complexes (Cooper et al. 2009, Shao et al. 2009). MYSM1 associates with the histone acetyltransferase, p300/CBP-associated factor (p/CAF) to coordinate histone acetylation and deubiquitylation (P. Zhu et al. 2007).

Several members of the JAMM family display high specificity for K63-linked ubiquitin chains, including AMSH, AMSH-LP, BRCC36 and POH1/PSMD14 (Cooper et al. 2009, McCullough et al. 2006, McCullough et al. 2004, Sato et al. 2008). POH1 can also cleave ubiquitin chains *en bloc*, a feature important for the rapid removal of ubiquitin chains from proteasome-targeting substrates (Yao and Cohen 2002). MYSM1 on the other hand, has been shown to remove monoubiquitin from H2A (P. Zhu et al. 2007).

1.5 Autophagy

The term ‘autophagy’ arises from the Greek word ‘*auto’* for self and ‘*phagein’* for eating. The first observation of autophagy by Christian de Duve stems from his early discovery of the lysosome (Duve et al. 1953, De Duve and Wattiaux 1966). He coined the term autophagy, to describe the lysosomal degradation of cellular organelles, distinct from that of the degradation of

mediated autophagy (CMA) is different from both macroautophagy and microautophagy as the autophagic cargo is usually a cytosolic protein rather than on organelle or bulk cytoplasmic contents (Kaushik and Cuervo 2012, Massey et al. 2004). The targeted protein usually contains a pentapeptide motif (KFERQ) for the recognition by a cytosolic chaperone, heat shock cognate protein of 70kDa (HSC70) (Dice 1990, Chiang et al. 1989). This substrate-HSC70 complex then interacts with lysosome-associated membrane protein type 2A (LAMP-2A) for lysosomal translocation of the substrate (Cuervo and Dice 1996). In this thesis, I will focus on macroautophagy, hereafter referred to as autophagy.

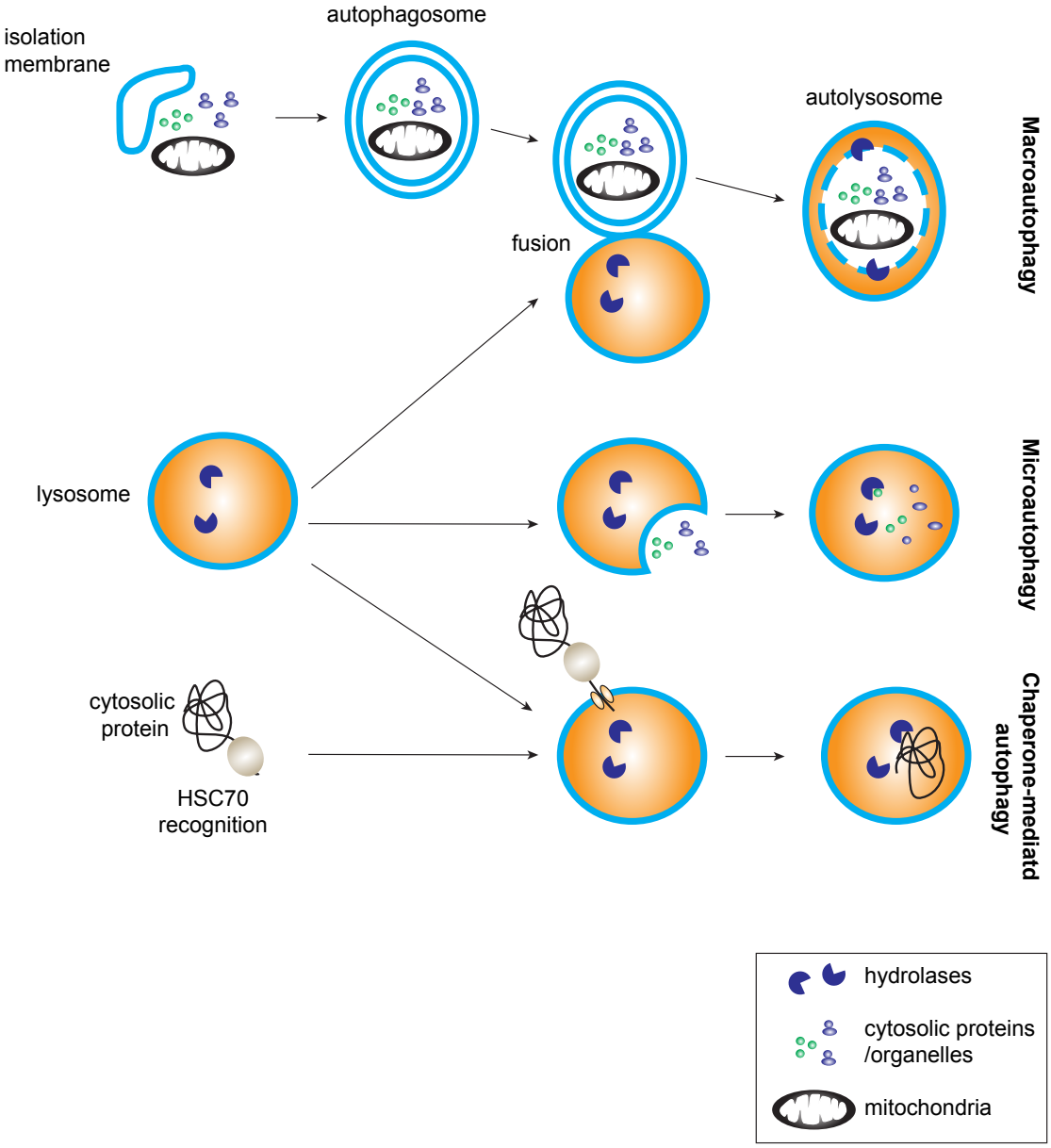

Figure 1.7 Different forms of autophagy.

Autophagic degradation can occur by at least three mechanisms. During macroautophagy, an isolation membrane expands and engulfs autophagic cargo, forming an autophagosome. The autophagosome then fuses with lysosomes to degrade the autophagic content. Microautophagy occurs via the invagination of the lysosomal membrane to engulf cytosolic material, which is then internalized and degraded in the lysosome. During chaperone-mediated autophagy, soluble cytosolic proteins are recognised by heat shock cognate 70 (HSC70) chaperone and its co-chaperones for translocation and import into the lysosome.

other intracellular proteins or endocytosed proteins (Klionsky 2008, Essner and Novikoff 1961).

1.5.1 Different forms of autophagy

For many years, it was thought that autophagy is a non-specific catabolic process to provide new energy sources during cell starvation. However, autophagy is now known to have crucial roles in development, immune defense, programmed cell death, tumor suppression and prevention of neuronal degeneration (Levine and Klionsky 2004, Munz 2006, Shintani and Klionsky 2004). In addition, recent advancement in the field revealed sub-classes of selective autophagic pathways that could specifically remove unwanted or dysfunctional organelles and protein aggregates in response to different stimuli or insults.

Depending on the mechanisms by which cargos are being sequestered into the autophagic pathway, autophagy can be classified into macroautophagy, microautophagy and chaperon-mediated autophagy (CMA) (Klionsky 2005, Wang and Klionsky 2003). Macroautophagy is the most studied form of autophagy. During the initiation of macroautophagy, a double-membraned structure, known as the isolation membrane engulfs the autophagic cargo, forming the autophagosome (Figure 1.7). The autophagosome then fuses with the lysosome, leading to the formation of autolysosomes for the degradation of the autophagic material. The sequestration and engulfment of cargo can either be non-specific (bulk-engulfment) or selectively targeted. Selective macroautophagy can further be specified based on the autophagic cargo, including mitophagy (mitochondria), reticulophagy (endoplasmic reticulum), ribophagy (ribosomes), pexophagy (peroxisomes), lipophagy (lipid droplets), xenophagy (invading pathogens) and aggrephagy (protein aggregates).

In contrast to macroautophagy, microautophagy is the engulfment of cytoplasmic material directly into the lysosome via lysosomal membrane invagination and without the prior formation of autophagosome. Chaperone-

1.5.2 Formation of autophagosome

Although autophagy was discovered at the same time as the lysosome, our current understanding of the molecular mechanism of autophagy truly expanded dramatically upon the discovery of over 30 autophagy-related (ATG) genes through yeast genetic studies in the last few decades (Harding et al. 1995, Klionsky et al. 2003, Thumm et al. 1994, Tsukada and Ohsumi 1993). Most of the ATG genes are conserved in higher eukaryotes, including ATG1 to ATG10 and ATG12 to ATG18 (Table 1.2). These autophagy components can be functionally categorized into three groups following the progression of autophagy: (1) Atg1/unc-51-like kinase (ULK) and its regulators, (2) the VPS34class III PI3K complex I, (3) the Atg9 cycling complex and (4) the ubiquitin-like Atg8/LC3 and Atg12 conjugation pathways (Table 1.2).

	Yeast	Mammal	Functions/ Characteristics
Atg1/ULK kinase complex	Atg1	ULK1/2	Serine/threonine protein kinase
	Atg13	ATG13	Regulator of Atg1 complex through phosphorylation
	Atg17	FIP200/RB1CC1	Component of the Atg1 complex
	Atg29	-	
	Atg31	-	
	-	ATG101/C12orf44	Component of the ULK complex in mammals
Atg9 and its cycling system	Atg9	ATG9	Transmembrane protein
	Atg18	WIPI1/2	Peripheral membrane protein
Class III PI3K complex	Vps15	PIK3R4/VPS15/p150	Serine/threonine protein kinase
	Vps34	PIK3C3/VPS34	PI3K
	Vps30/Atg6	Beclin-1	Component of class III PI3K complex
	Atg14	ATG14	Class III PI3K complex I
	Vps38	UVRAG	Class III PI3K complex II
Ubiquitin-like conjugation systems	Atg3	ATG3	E2-like enzyme for Atg8 conjugation
	Atg4	ATG4A to ATG4D	LC3/Atg8 C-terminal hydrolase; deconjugating enzyme
	Atg5	ATG5	Conjugates with Atg12
	Atg7	ATG7	E1-like enzyme for Atg12 and Atg8
	Atg8	LC3A, B, B2, C, GAPARAP, L1, L2	Ubiquitin-like molecule (Ubl), conjugates to phosphatidylethanolamide (PE)
	Atg10	ATG10	E2-like enzyme for Atg12 conjugation
	Atg12	ATG12	Ubl
	Atg16	ATG16L1, L2	Forms Atg12-Atg5-Atg-16 complex

Table 1.2 Atg and Atg-related proteins that form the core molecular machinery of autophagosome formation.

(Mizushima et al. 2011, Jin and Klionsky 2013).

1.5.2.1 The mTOR complexes

Autophagy is a stress-induced catabolic process. Various stimuli have been shown to trigger autophagy in cells, including nutrient starvation, energy depletion and lack of growth factors (Reviewed in (Yang and Klionsky 2010)). A key player in autophagy is the mammalian target of rapamycin (mTOR).

mTOR is a nutrient and energy sensing kinase that can be activated by various upstream signaling events, for example insulin receptor activation (Klionsky and Emr 2000, Zoncu et al. 2011b). mTOR forms two functionally distinct protein complexes, mTORC1 and mTORC2, both of which share two subunits: the positive regulator, mammalian lethal with SEC13 protein 8 (mLST8/GβL) and the negative regulator, REP domain-containing mTOR-interacting protein (DEPTOR) (Figure 1.8) (Loewith et al. 2002). Accessory subunits that are unique to mTORC1 include the scaffolding protein, RAPTOR (regulatory-associated protein of mTOR) and a negative regulator, PRAS40/AKT1S1 (40kDa Pro-rich Akt substrate). On the other hand, subunits that are unique to mTORC2 include RICTOR (rapamycin-insensitive companion of mTOR; a scaffolding protein), PROTOR1/2 (protein observed with RICTOR1/2; for complex assembly) and mSIN1/MAPKAP1 (mammalian stress-activated map kinase-interacting protein 1; for membrane targeting) (reviewed in (Zoncu et al. 2011b)). The name mammalian target of rapamycin is perhaps slightly misleading as rapamycin does not directly target mTOR itself. Instead, rapamycin forms a complex with FKBP12 (FK506-binding protein of 12kDa), which in turn binds and inhibits RAPTOR-bound mTOR. Since MTORC2 is RICTOR, rather than RAPTOR bound, only mTORC1 is sensitive to rapamycin (Loewith et al. 2002). However, it has been reported that prolonged treatment with rapamycin can also indirectly inhibit mTORC2 as rapamycin-FKBP12 depletes the cellular pool of mTOR, thereby inhibiting the mTORC2 complex formation (Sarbassov et al. 2006).

Both of the mTOR complexes are involved in the suppression of autophagy. However, MTORC2 acts upstream of mTORC1. Their involvement in autophagy regulation will be described in the next section.

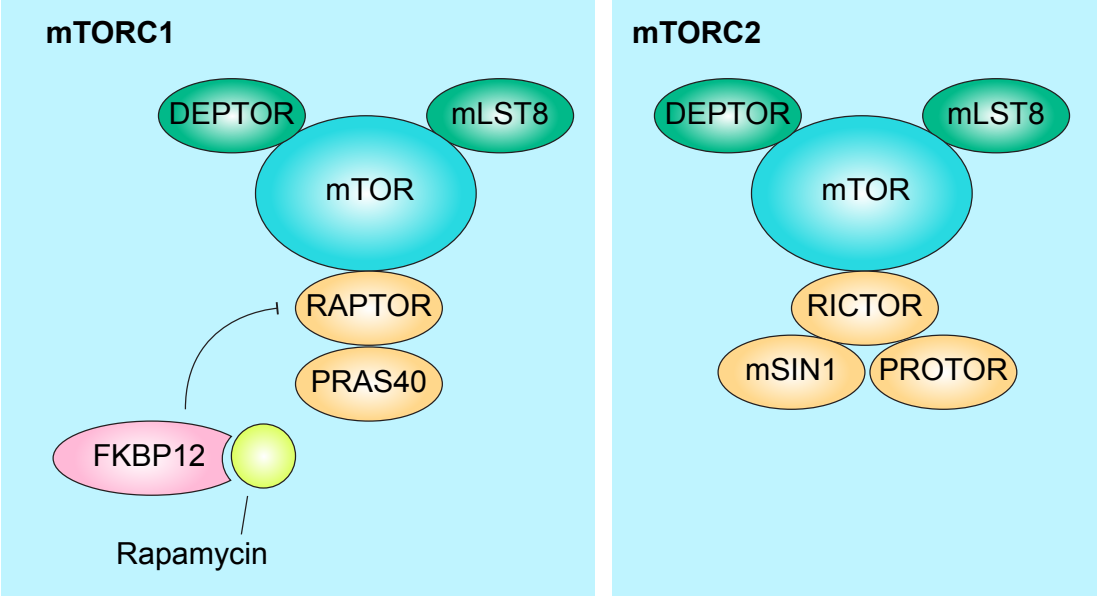

Figure 1.8 Schematic illustration of the organisations of mTOR complex I (mTORC1) and complex II (mTORC2).

Both mTORC1 and mTORC2 contain the core components, mTOR, DEPTOR and mLST8. The accessory subunits unique to mTORC1 are RAPTOR and PRAS40 whereas RICTOR, mSIN1 and PROTOR are only found in mTORC2 (Adapted from (Zoncu et al. 2011b)).

1.5.2.2 ULK1/2 complex activation upon mTORC1 inactivation

In fed cells, activation of growth factor/insulin receptors phosphorylates the insulin receptor substrate (IRS), which then activates class I PI3K to generate PtdIns3,4,5-P_3 (White 1998, Yu et al. 1998). PtdIns3,4,5-P_3 binds and activates PDK1 (Phosphoinositide-dependent kinase-1), which in turn phosphorylates AKT/PKB, among many other kinases (Datta et al. 1999, Liao and Hung 2010). In addition, mTORC2 also phosphorylates AKT/PKB, leading to its activation (Moore et al. 2011). Activated AKT/PKB then phosphorylates and inhibits the function of a GTPase activating protein (GAP) complex, TSC1-TSC2 complex, on RHEB (Ras homolog enriched in brain) (Q. Yang et al. 2006, Frias et al. 2006, Zoncu et al. 2011a).

In parallel, another family of small GTPases, Ras-related GTPases (RAGs) is also involved. RAGs exist in heterodimers, which consist of either RAGA or RAGB paired with RAGC or RAGD. In the presence of high amino acid concentration, the heterodimer is in an active conformation state, characterised by a GTP-bound RAGA/B and a GDP-bound RABC/D (Sancak and Sabatini 2009). This conformation allows the heterodimer to interact with RAPTOR and recruit mTORC1 to the lysosomes or the late endosomes, where both RAG and RHEB reside (Sancak et al. 2008, Sancak et al. 2010). RHEB in turn is an activator of mTOR (Huang and Manning 2008, Zoncu et al. 2011b). Active mTORC1 binds and hyperphosphorylates ULK1/2 and ATG13 disrupting the interaction between the two (Kim et al. 2011, Kamada et al. 2010).

During nutrient starvation, the inactivation of PKB and simultaneous phosphorylation of AMPK (AMP-activated protein kinase) by LKB1 (liver kinase B1) leads to an activating phosphorylation of the TSC complex and subsequently inactivates RHEB (Shackelford and Shaw 2009, Sancak et al. 2008). In addition, low amino acid levels also cause the RAG heterodimer to assume an inactive conformation, such that RAGA/B is now GDP-bound whereas RABC/D is GTP-bound (Kim et al. 2008, Sancak and Sabatini 2009). Subsequently, mTORC1 is inactivated, allowing ATG13, FIP100 and

ATG101 to form a complex with ULK1/2 and promote nucleation of autophagic membranes (Figure 1.9) (Ganley et al. 2009, Chan and Tooze 2009).

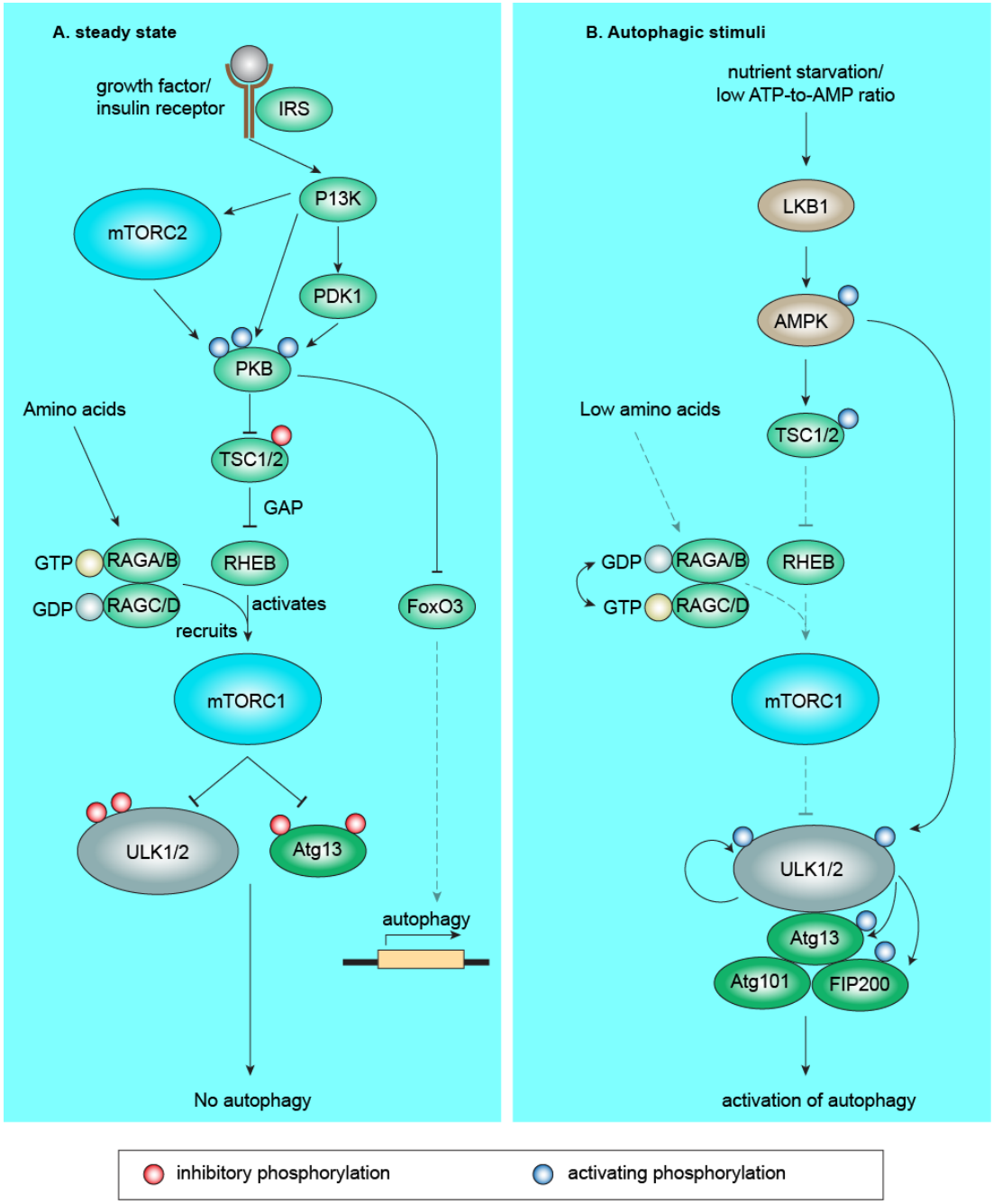

Figure 1.9 ULK1/2 complex activation during autophagy.

(A) Under steady state conditions, constitutive growth factor and/or insulin stimulation activates PKB/Akt, which phosphorylates and inhibits the GAP activity of TSC1/2 complex on RHEB, resulting in the activation the mTORC1 by RHEB. In parallel, high amino acid level in the cell promote GTP-bound and GDP-bound states of RAGA/B and RABC/D, respectively, resulting in an active conformation that recruits mTORC1 to the lysosome or late endosome for activation by RHEB. Activated mTORC1 hyperphosphorylates both ULK1/2 and Atg13, causing

dissociation of the UL1/2 complex and inhibiting downstream activation of autophagy.

(B) During nutrient starvation, the loss of insulin stimulation and decrease in ATP energy results in the phosphorylation of AMPK by LKB1. AMPK1 in turn phosphorylates and activates the GAP activity of TSC1-TSC2 complex on RHEB, leading to the inactivation of mTORC1. In parallel, the absence of amino acid switches the GTP and GDP bound states of RAGA/B and RABC/D, resulting in the release of mTORC1 from the lysosome. The inactivation of mTORC1 removes its suppression on ULK1/2, which can then phosphorylate ATG13, FIP200 and itself for activation of autophagy. A red circle indicates inhibitory phosphorylation, whereas blue circle indicates activating phosphorylation.

1.5.2.3 The VPS34 complex I /II

The activated ULK1/2 complex has been reported to phosphorylate Beclin-1, a core component of the mammalian class III phosphoinositide 3 kinase (PtdIns3K; also referred to as VPS34 complex), thereby promoting autophagy progression (Russell et al. 2013). The VPS34 complex is implicated in the nucleation of the autophagosomal membrane.

The core complex of the Class III PI3K consists of VPS34, VPS15, and Beclin-1. These core components can bind either ATG14L or ultraviolet irradiation resistance-associated gene (UVRAG), forming two distinct complexes, complex I and II, respectively (Figure 1.10A and B) (Kihara et al. 2001, Itakura et al. 2008). ATG14L is found at the ER at steady state and localises to autophagosomal membranes upon starvation. Importantly, depletion of ATG14L impedes the phosphorylation of phosphatidylinositol (PtdIns) to phosphatidylinositol 3-phosphate (PtdIns-3*P*) and its downstream autophagosomal membrane formation and autophagy induction (Figure 1.10A) (Sun et al. 2008, Itakura et al. 2008, Matsunaga et al. 2009, Zhong et al. 2009). Therefore, the VPS34 complex I has been proposed to be involved in the early stages of autophagosome formation. On the other hand, the UVRAG-containing VPS34 complex II acts at the later stages of autophagy maturation (Figure 1.10B). The BAR-domain protein Bif-1 interacts with Beclin-1 via UVRAG and promotes ATG9 trafficking from the Golgi to the autophagosomal membrane (Takahashi et al. 2007, Takahashi et al. 2011). UVRAG also interacts with the homotypic fusion and protein sorting (HOPS)-tethering complex, which promotes the fusion of autophagosomes with late

endosomes and lysosomes (Chong et al. 2008). At steady state, Beclin-1, the subunit of the core complex that is present in both the VPS34 complex I and II binds AMBRA1, which in turn interacts with dynein, tethering the VPS34 complex to the cytoskeleton (Di Bartolomeo et al. 2010). During autophagy induction, ULK1 phosphorylates AMBRA1, resulting in the release of VPS34 complex I and II from dynein and relocalisation to the ER to promote autophagosome formation. The other subunit of the VPS34 core complex, p150, is reported to be required for VPS34 membrane association and activity (Stack et al. 1995).

Recruitment of VPS34 to the isolation membrane promotes the phosphorylation of PtdIns to PtdIns-3*P* (Foster et al. 2003, Vanhaesebroeck and Waterfield 1999). PtdIns-3*P* has been proposed to recruit double FYVE domain-containing protein 1 (DFCP1) via its FYVE (conserved in Fab1, YOTB, Vac1 and EEA1) domain (Axe et al. 2008). Other PtdIns-3*P* effectors, WD repeat domain phosphoinositide-Interacting protein 1 and 2 (WIPI1 and 2) are also recruited to the autophagosomal membrane during autophagy induction (Figure 1.10A) (Proikas-Cezanne and Pfisterer 2009, Su et al. 2011, Polson et al. 2010). WIPI1 and WIPI2 recruitment to the preautophagosomal membrane has been reported to promote LC3 lipidation during autophagy (Mauthe et al. 2011, Dooley et al. 2014, Polson et al. 2010). On the other hand, DFCP1 has been suggested to act as a platform for the recruitment of other ATG proteins to the isolation membrane, such as LC3 and ATG5. However, this remains to be fully investigated.

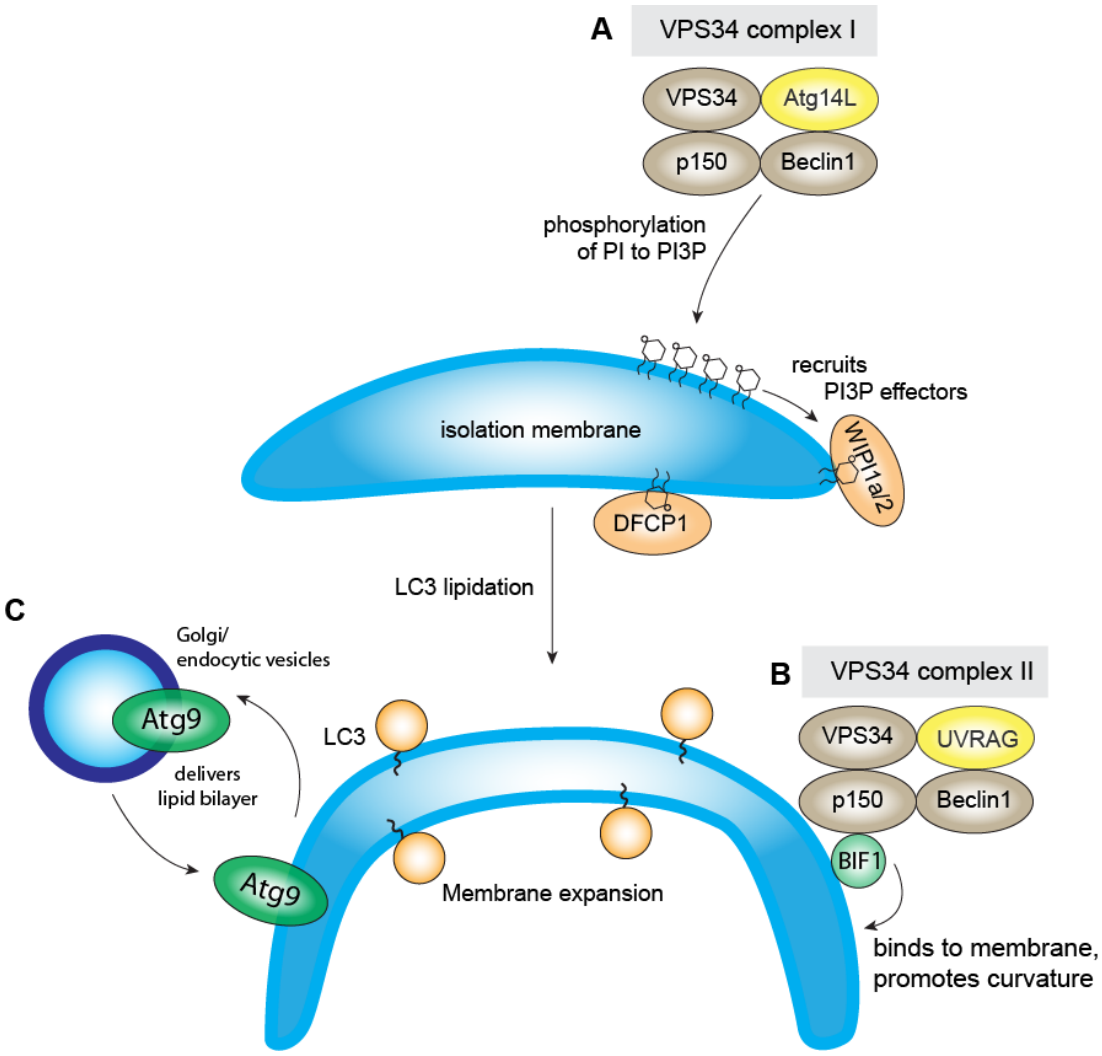

Figure 1.10 The VPS34 complex I /II and the ATG9 cycling system.

(A) Apart from the core components (VPS34, p150 and Beclin1), VPS34 complex I contains an accessory subunit, ATG14L. VPS34 complex I is responsible for the formation of isolation membrane (IM). VPS34 complex I phosphorylates PI to PtdIns-3*P*, which promotes the recruitment of WIPI1/2 and DFCP1 to the IM to promote LC3 lipidation and insertion into the autophagosomal membrane.

(B) VPS34 complex II (with UVRAG instead of ATG14L) is associated with the later stages of autophagy and has been shown to recruit BIF-1, a protein that binds and promote membrane curvature and has been implicated in ATG9 recruitment to the autophagosomal membrane.

(C) ATG9 localises to the Golgi and endocytic vesicles at steady state. Upon autophagy induction, it shuttles between the autophagosome and Golgi or endocytic vesicles. It is proposed to deliver lipid membranes for the formation and expansion of the isolation membrane.

1.5.2.4 The ATG9 cycling system

Another key player in autophagosome formation is ATG9. ATG9 is the only reported multipass transmembrane ATG protein to date. ATG9 is also thought to act at the early stages of autophagosome formation and is proposed to deliver lipid bilayers to the preautophagosome structures as the depletion of ATG9 results in the formation of significantly fewer autophagosome (Figure 1.10C) (Orsi et al. 2012). Interestingly, yeast Atg9 is observed to shuttle between the mitochondria and the preautophagosomal structure (the isolation membrane structure equivalent in yeast) whereas mammalian ATG9 shuttles between either the trans-Golgi network or endocytic vesicles and the isolation membrane (Reggiori et al. 2005, Young et al. 2006, Reggiori and Tooze 2012, Longatti and Tooze 2012). This observation suggests that the autophagosomal membrane could originate from several organellar membranes.

Indeed, the origin of the isolation membrane (IM) has been a constant debate. Longatti and Tooze proposed four models for the origin of autophagosome formation: (1) *de novo* synthesis of lipid bilayers via delivery of lipids, (2) gradual expansion of the IM via heterotypic fusion of vesicles from other organelles, (3) homotypic fusion of a constitutive pool of autophagic vesicles, and (4) membrane remodeling/extension of a pre-existing membrane sheet derived from other organelles, for example, the ER (Longatti and Tooze 2009).

In both the second and fourth models, various organelles have been shown to contribute towards membrane expansion. Several studies demonstrated that ER is a main source of lipid bilayer, as evidenced by the PtdIns-3*P* positive membrane structures that stem from the ER membrane upon autophagy induction. These membranes were termed omegasomes as they are frequently observed to form a Ω-shape. Omegasomes have been shown to mature into autophagosomes, which bud off from the ER and stain positive for ATG8 and ATG5 (Axe et al. 2008). Apart from the ER, the mitochondria have also been reported to participate in autophagosome biogenesis (Hailey

et al. 2010). In addition, ER-mitochondria contact sites are known to regulate various processes, including lipid exchange, mitochondria fusion/fission and Ca^{2+} exchange has also been shown to give rise to autophagosomes (Hamasaki et al. 2013). Ravikumar and colleagues also provided evidence that the plasma membrane contributes to the formation of pre-autophagosomal membranes and also the expansion of existing autophagosomal membranes (Ravikumar et al. 2010b, Ravikumar et al. 2010a). Recently, Longatti and Tooze reported that the overexpression of a RAB11 GTPase effector, TBC1D14 inhibited autophagy. Since RAB11 is involved in the regulation of endocytic recycling, this observation suggests that the recycling endosomes are also necessary for autophagosome formation (Longatti and Tooze 2012). It is likely that multiple sources could contribute to the nucleation and expansion of the autophagosomal membrane in either a cell type and/or stimulus-dependent manner.

1.5.2.5 Autophagosome expansion

Two ubiquitin-like (UBL) conjugation systems are involved in the expansion of the isolation membrane (Figure 1.11). In the first ubiquitin-related system, Atg12 is conjugated to Atg5, via the sequential action of Atg7 and Atg10, which act as E1 and E2-like enzymes, respectively (Figure 1.11C). The Atg12-Atg5 complex then interacts with Atg16L, forming a trimeric structure that further homodimerises to form a multimeric complex called the Atg16L complex (Mizushima et al. 2003).

LC3 (ATG8) is synthesized as pro-LC3. Prior to its conjugation to phosphatidylethanolamide (PE), the C-terminal residues of pro-LC3 are cleaved off by a cysteine protease, Atg4B, to expose its glycine residue for covalent conjugation to PE (Ichimura et al. 2000, Kirisako et al. 2000). A second ubiquitin-related system involving Atg7 (E1-like enzyme), Atg 3 (E2-like enzyme) and the Atg5-Atg12-Atg16L complex (E3-like enzyme) conjugates LC3 to PE in the isolation membrane, thereby determining the site of LC3 lipidation (Figure 1.11) (Hanada et al. 2007, Fujita et al. 2008). The cleaved, soluble form of LC3 is termed LC3-I and the PE-conjugated, membrane-bound form of LC3 is referred to as LC3-II (Klionsky et al. 2008).

LC3-II is inserted into both sides of the lipid bilayer. However, LC3-II on the cytoplasmic surface can be extracted by Atg4 whereas LC3-II in the autophagosomal lumen remains bound to the autophagic membranes and is degraded together with the autophagic cargo (Kirisako et al. 2000). Therefore, LC3-II also serves as an important biomarker to monitor autophagy progression.

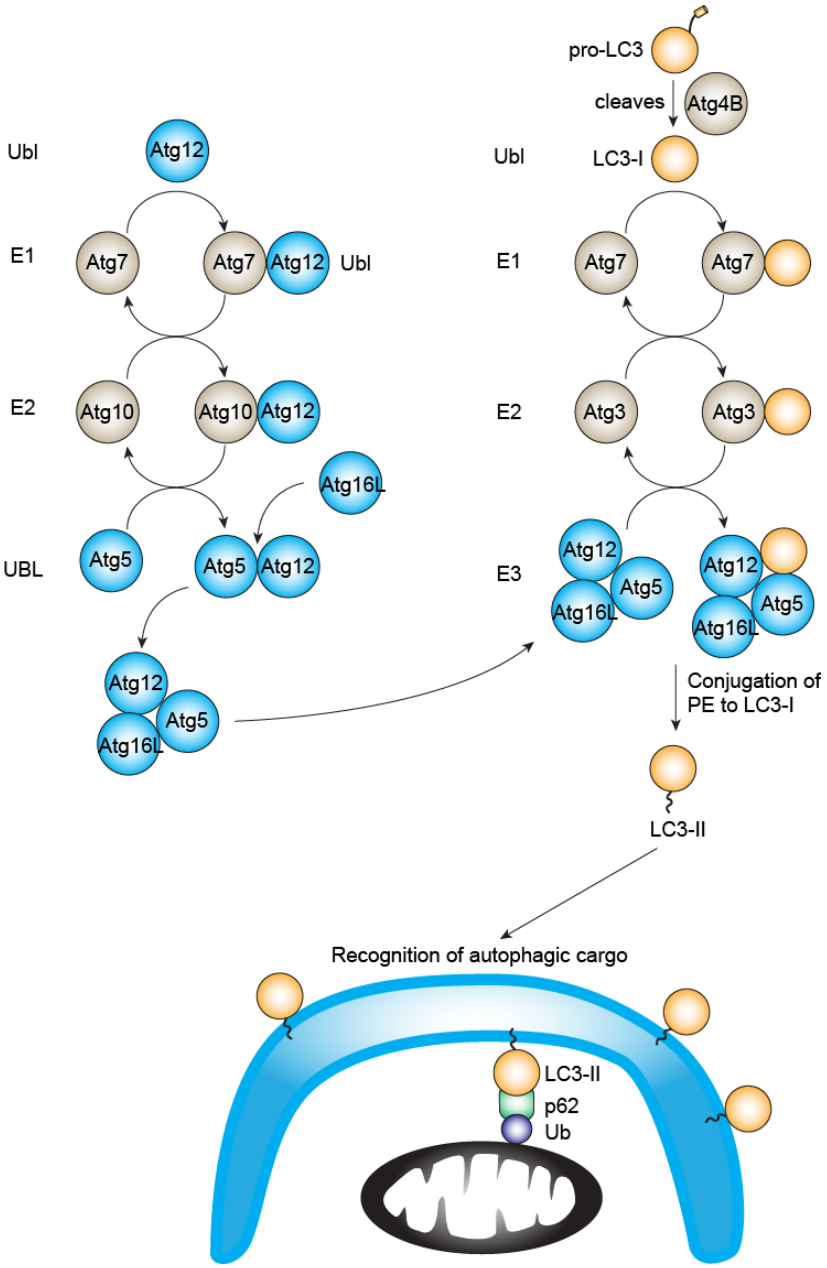

Figure 1.11 The two UBL conjugation systems.

In the first ubiquitin-lke conjugation system, Atg12 acts as a UBL that is conjugated to Atg5 and Atg16L, via sequential conjugations with Atg 7 (E1-like enzyme) and Atg10 (E2-like enzyme). In this case, there is no E3-like enzyme involved. The Atg5-Atg12-Atg16L complex is involved in another UBL conjugation system for the lipidation of LC3. LC3 is synthesized as a precursor (pro-LC3). It is constitutively cleaved by Atg4B into LC3-I. LC3-I acts as a UBL that is sequentially conjugated to Atg7 (E1-like enzyme), Atg3 (E2-like enzyme), and the previously described Atg5-Atg12-Atg16L complex (E3-like enzyme). LC3-I is finally lipidated with phosphatidylethanolamide (PE), forming LC3-II for its insertion into autophagosomal membranes. LC3-II can bind to LIR-containing adaptor proteins such as p62, which recognise ubiquitylated proteins on the surface of damaged organelles during selective autophagy.

1.5.3 Selectivity of autophagy

Similar to proteasomal and lysosomal degradation, the selectivity of autophagic cargo is tightly regulated by post-translational modifications, most notably phosphorylation and ubiquitylation. Proteins on the surface of damaged or malfunctioning organelles, for example, the ER and mitochondria, are ubiquitylated by specific E3 ligases, such as GP78 and Parkin (Fang et al. 2001, Narendra et al. 2009). The ubiquitylated proteins can then be recognized by molecular adaptors such as p62, NBR1 and optineurin (Lamark et al. 2009, Birgisdottir et al. 2013). These adaptors contain two domains: a LIR (LC3-interacting region) for interaction with ATG8 family proteins, and a C-terminal UBA domain for interaction with ubiquitin, thereby recruiting the autophagosomal membrane to the ubiquitin-tagged organelles (Figure 1.11) (Lamark et al. 2009, Birgisdottir et al. 2013). In the next section, I will discuss in detail the selective autophagy of mitochondria via PINK1 and Parkin-mediated mitophagy as this pathway is explored in this project.

1.6 Selective removal of mitochondria by autophagy

1.6.1 Mitochondria

Mitochondria, often referred to as the 'powerhouse of the cell', are primarily responsible for the generation of ATP via aerobic respiration. Mitochondria are also involved in various housekeeping functions, including the biosynthesis of amino acids and steroids, fatty acid oxidation, cytosolic calcium homeostasis and mitochondrial antiviral signaling (MAVS) (reviewed in (Johri and Beal 2012)). Last but not least, mitochondria also play a pivotal role in the orchestration of apoptosis.

Considering the multiple roles of mitochondria in the cell, it is not surprising that defects in mitochondrial function have significant impacts on the physiology of the cell and the health of an individual. In particular, mitochondrial dysfunction has been linked to neurodegenerative disease, most notably to Parkinson's Disease (PD). The etiology of PD is diverse, with both environmental and genetic factors contributing to the loss of dopaminergic neurons and the accumulation of α-synuclein positive inclusions, termed Lewy bodies (LB), in the substantia nigra. PD patients are clinically diagnosed based on several characteristic features, including tremor, rigidity, slowness of movement and postural instability (reviewed in (Sherer et al. 2002, Saito et al. 2000, Nuytemans et al. 2010, Morrison 2003)).

The environmental and genetic risks of PD converge at least partially on mitochondrial dysfunction. Exposure to rotenone, paraquat and MPTP (1-methyl-4-phenyl-1,2,3,6-tetrahydropyridine), three chemical compounds that disrupt the mitochondrial electron transport chain (ETC) and result in the accumulation of reactive oxygen species (ROS), have all been linked to increase risk of Parkinson Disease (Tanner et al. 2011, Bove et al. 2005).

At least three genes for which mutation has been associated with PD are functionally related to the mitochondria: Parkin (PARK2), PINK1 (PARK6) and DJ1 (PARK7) (Nuytemans et al. 2010). All three genes are associated

with early onset familial PD. In particular, extensive studies in *Drosophila* revealed that the PINK1 and Parkin loss-of-function mutants result in strikingly similar phenotypes, including locomotor defects (apoptosis of indirect flight muscle), male sterility (defect in spermatogenesis) and reduced lifespan (Greene et al. 2003, Park et al. 2006). Strikingly, the phenotype observed with the PINK1 mutant can be rescued by Parkin overexpression but not vice versa, suggesting that Parkin acts downstream of PINK1 in a common pathway (Clark et al. 2006, Y. Yang et al. 2006). Indeed, it was later discovered that PINK1 and Parkin act sequentially to mediate the selective elimination of impaired mitochondria by mitophagy (Narendra et al. 2008, D. P. Narendra et al. 2010, Vives-Bauza et al. 2010).

1.6.2 Parkin structure

Parkin belongs to the RBR family of E3 ubiquitin ligases, which combines the features of both the RING and HECT E3 ligases (Nuytemans et al. 2010, Riley et al. 2013, Wenzel et al. 2011a). Structurally, Parkin contains a N-terminal UBL domain, followed by an atypical RING domain (RING0) and a RBR domain at the C-terminus. The RBR domain at the C-terminus comprises two different RING domains, RING1 and RING2, separated by an in-between RING (IBR) domain (Figure 1.12A). Under steady state conditions, Parkin is auto-inhibited because the multi-domain protein folds into a compact structure, resembling a coiled snake (Figure 1.12B). The RING0 domain blocks the catalytic cysteine found in the RING2 domain (C431). On the other hand, a short sequence named the repressor element of Parkin (REP) sequence located between the IBR and RING2 domains binds to RING1, thereby preventing the interaction between RING1 and the ubiquitin-charged E2 (Hristova et al. 2009, Trempe et al. 2013, Riley et al. 2013, Wauer and Komander 2013).

Understanding the structure of Parkin provides clues that help interpret the effects of the different Parkin mutations associated with PD (Figure 1.12A). In general, the mutations can be classified into three groups. The first group of mutations lead to a change in protein domain folding such as R42P, K211N,

C212R, C289G, T351P, C441R (Figure 1.12A; colour-coded in blue). In particular, the cysteine mutations in the RING domains abolish their zinc binding ability, thereby altering the domain folding. The C431F mutation affects the catalytic sites at the RING2 domain (C431F; colour-coded in green). The last group of mutations affects interactions between domains (colour-coded in orange). For example, the G328E mutation between RING1 and IBR alters its 'hinge' property and thereby affecting the conformational flexibility. On the other hand, the R33Q mutation may promote interaction between the UBL domain and the IBR domain that is structurally in close proximity (Trempe et al. 2013).

While the auto-inhibited structure of Parkin at steady state has been revealed, the conformational changes occurring upon ubiquitin and substrate binding remain unsolved. Three different groups have recently reported that PINK1 activates Parkin in a 'feed-forward' mechanism: mitochondrial depolarisation stabilizes PINK1 on the mitochondrial surface. PINK1 then phosphorylates the UBL domain of Parkin and, surprisingly, ubiquitin at a positionally equivalent serine (S65) (Kane et al. 2014, Kazlauskaite et al. 2014, Koyano et al. 2014). The phosphorylated ubiquitin in turn can activate and recruit Parkin to the mitochondria. To date, it remains to be seen whether the phosphorylated ubiquitin is in fact incorporated into Parkin substrates.

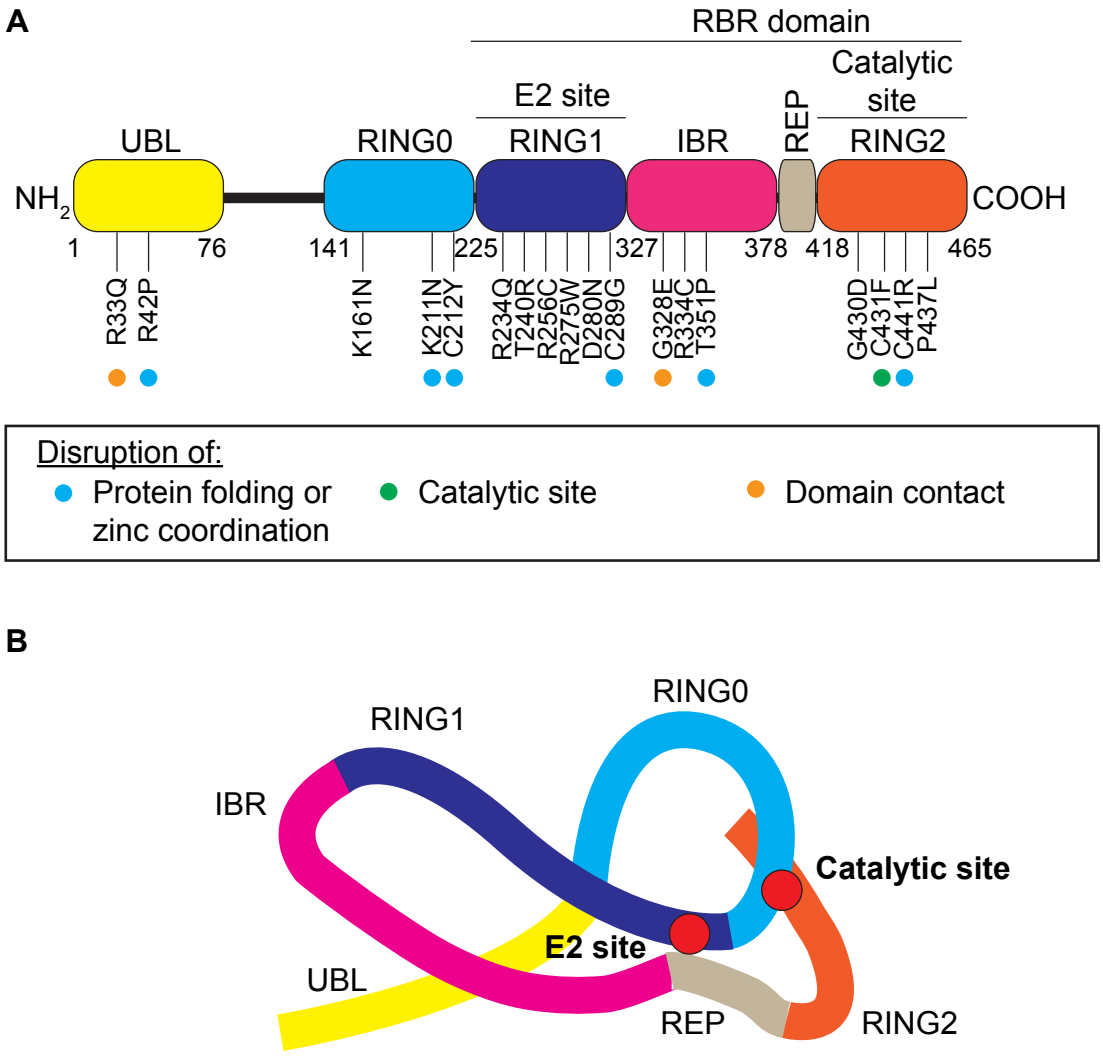

Figure 1.12 Parkin domain architecture and structure.

(A) Domain architecture illustrating the linear arrangement of the five Parkin domains and the REP sequence. The RBR domain is subdivided into RING1, IBR and RING2. RING1 is responsible for Parkin interaction with ubiquitin-charged E2 whereas the RING2 contains the catalytic cysteine (C431). The reported PD mutations are annotated as shown and colour coded according to proposed effects of mutations based on the crystal structure of Parkin (Spratt et al. 2013, Trempe et al. 2013, Wauer and Komander 2013).

(B) Parkin folds into a compact structure, loosely resembling a coiled snake. Each coloured segment corresponds to the domains indicated in (A). The red dots represent the occlusion of the interaction between RING1 with E2 by the REP sequence and the blockage of the catalytic cysteine of RING2 by the hydrophobic region of RING0. (Adapted and modified from (Dove and Klevit 2013, Trempe et al. 2013).

1.6.3 The protective roles of Parkin

Studies in *Drosophila* and human cell lines indicate that Parkin serves cytoprotective roles in response to different stress paradigms, including mitochondrial and ER stress, misfolded protein aggregation, excitotoxicity and proapoptotic stimulation (reviewed in (Winklhofer 2014)). To date, more than 30 bona fide Parkin substrates have been discovered (Dawson and Dawson 2010). Parkin-dependent ubiquitylation of these substrates can lead to different cellular fates: proteasomal degradation is most common but there are a few instances where ubiquitylation by Parkin results in activation of different cell signaling pathways. Based on the identified substrates, the cytoprotective activity of Parkin can be attributed to three distinct areas: (1) selective removal of damaged mitochondria via mitophagy; (2) promoting proteasomal degradation of toxic/aggregated proteins; and (3) modulating non-degradative signaling for cell death or survival pathways. These functions of Parkin will be discussed in the next sections.

1.6.3.1 PINK1 and Parkin-mediated Mitophagy

PTEN-induced putative kinase-1 (PINK1) is a serine/threonine kinase (Woodroof et al. 2011). It has a N-terminal mitochondrial targeting signal (MTS; a.a.1-94) and a transmembrane region consisting of a series of positively charged amino acids (TM; a.a. 94-110) (S. M. Jin et al. 2010).

Under normal condition, mitochondrial membrane potential drives PINK1 into the mitochondria via the translocase of outer mitochondrial membrane (TOM) and translocase of inner mitochondrial membrane (TIMM) complex. The mitochondria-targeting signal (MTS) is first cleaved by mitochondrial processing peptidase (MPP) and the transmembrane domain (TM) is then cleaved by both mitochondrial processing peptidase (MPP) and presenillin-associated rhomboid-like protease (PARL) to produce the shorter 53kDa ΔN-PINK1 fragment (Figure 1.13) (Deas et al. 2011, Seok M. Jin et al. 2010, Lin and Kang 2008, Meissner et al. 2011, Whitworth et al. 2008, Greene et al. 2012). The cleaved ΔN-PINK1 fragment exposes the bulky and hydrophobic phenyalanine (F104), which can then be recognised and ubiquitylated by several E3 ligases including UBR1, UBR2 and UBR4 for degradation by the proteasome via the N-end rule pathway (Yamano and Youle 2013).

When mitochondria are impaired, there is a loss of membrane potential, causing an inhibition of PINK1 translocation into the mitochondria (Lin and Kang 2008). Instead, PINK1 interacts with the TOM complex, forming a 700kDa complex on the outer mitochondrial membrane (OMM), with the kinase domain facing the cytosol (Lazarou et al. 2012). OMM-localised PINK1 autophosphorylates at Ser228 and Ser402, an event that is required for the subsequent phosphorylation of Parkin (Okatsu et al. 2012). The activated Parkin can ubiquitylate many OMM proteins including MFN1/2, MIRO1/2, voltage-dependent anion channels VDAC1/2/3, subunits of the TOM complex (TOMM20, TOMM70A and TOMM22) and the BCL-2 family members including MCL1, BAK and BAX (Sarraf et al. 2013, Lazarou et al. 2012, Gegg et al. 2010, Wang et al. 2011, Kane and Youle 2011, Sun et al. 2012). In fact, quantitative proteomic study of CCCP-treated HeLa, SH-SY5Y and HCT116 cells overexpressing Parkin revealed widespread Parkin-dependent ubiquitylation, suggesting that Parkin activation induces major OMM remodeling, at least when ectopically expressed (Sarraf et al. 2013).

The influence of PINK1 extends beyond the activation of Parkin. At least two OMM Parkin substrates, the two GTPases, MIRO and MFN2, are phosphorylated by PINK1 for their recognition by Parkin (Wang et al. 2011, Kane and Youle 2011, Chen and Dorn 2013, Ziviani et al. 2010). The ubiquitylation of OMM proteins may either lead to their extraction by p97 and subsequent proteasomal degradation (for example, MCL1 and MFN) or act as docking signal for the recruitment of p62 (Tanaka et al. 2010, Xu et al. 2011, Yoshii et al. 2011). The selective degradation of MFN inhibits mitochondrial fusion, thereby segregating depolarised mitochondria from the healthy population of mitochondria. In addition, the degradation of MIRO dissociates mitochondria from the microtubules and arrests mitochondrial movement to allow efficient mitophagy (Wang et al. 2011). The role of p62 in the context of PINK1/Parkin-mediated mitophagy remains controversial. Geisler and colleagues reported that p62 is required for mitophagy while two other groups (Narendra et al. and Okatsu et al.) reported that depletion of

p62 resulted in a loss of perinuclear clustering of mitochondria but did not inhibit mitophagy (Derek Narendra et al. 2010, Okatsu et al. 2010).

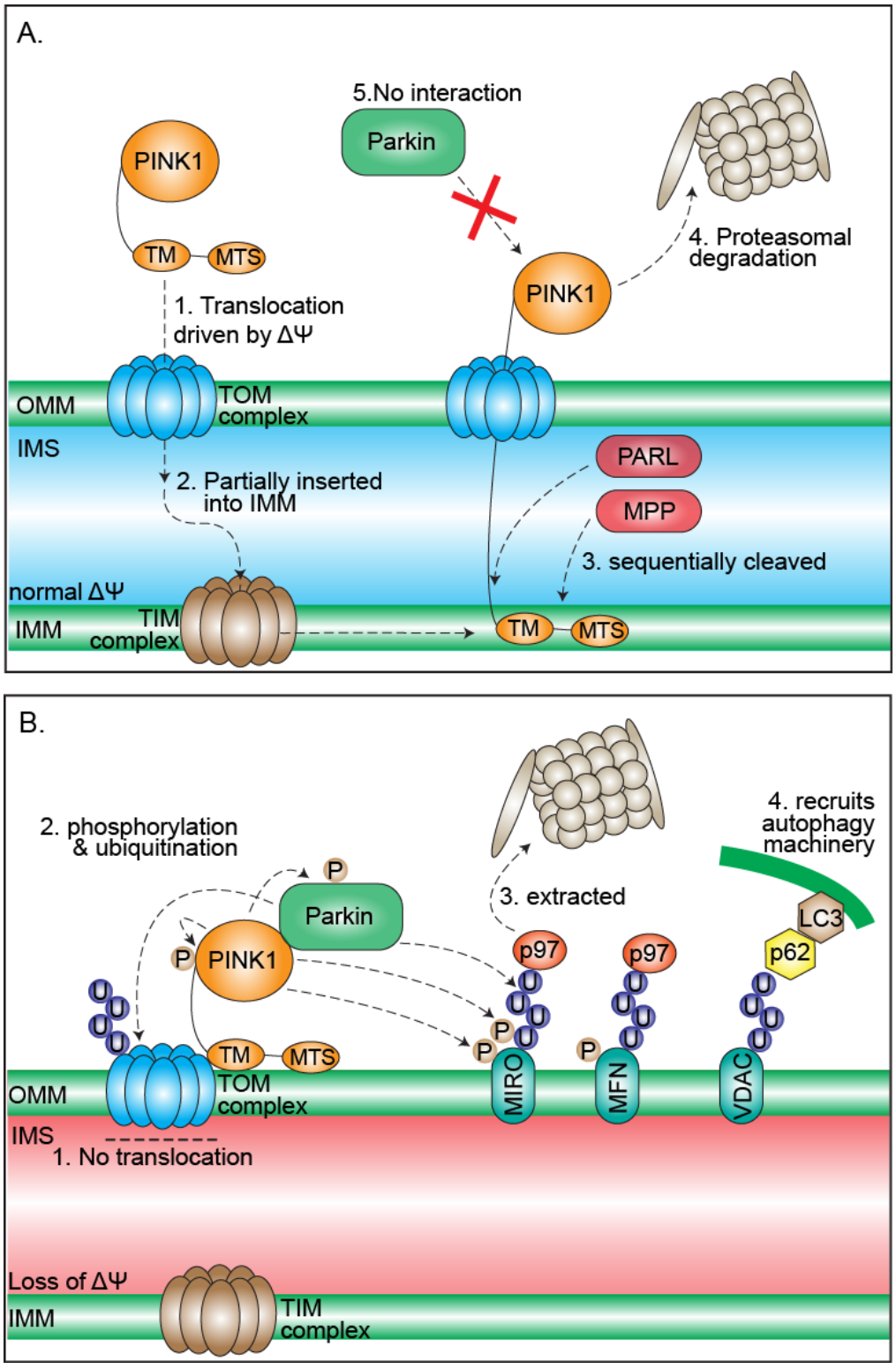

Figure 1.13 Mechanism of PINK1 stabilisation, Parkin recruitment and mitophagy progression during mitochondrial depolarisation.

(A) At steady state, (1) PINK1 is driven by the membrane potential to (2) partially translocate into the intermitochondrial membrane space (IMS) and is inserted into the inner mitochondrial membrane (IMM). (3) The mitochondrial-targeting signal (MTS) and the transmembrane domain (TM) are sequentially cleaved by mitochondrial processing peptidase (MPP) and presenillin-associated rhomboid-like

protease (PARL), respectively. (4) Cleaved PINK1 is proposed to be released into the cytosol and degraded constitutively via the proteasomal degradation pathway.
(B) When the mitochondrial membrane potential is disrupted, (1) PINK1 is not translocated into the mitochondria. Instead it interacts with the TOM complex and physically recruits Parkin. (2) PINK1 phosporylates itself and Parkin for its activation. In addition, PINK1 also phosphorylates MIRO and MFN for their recognition by Parkin. (3) Ubiquitinated outer mitochondrial membrane (OMM) proteins can either be extracted by p97 AAA-ATPase for proteasomal degradation, or, (4) recruit autophagy machinery including p62 and LC3 to promote the formation of autophagosomal membrane around the mitochondria.

1.6.3.2 Parkin-mediated degradation of toxic substrates

The ubiquitylating activity of Parkin extends beyond mitophagy. Several proteins that are mutated and/or accumulated in neuronal cells during familial autosomal recessive PD, particularly in the intracytoplasmic inclusions, known as Lewy bodies (LB), have also been reported to be substrates of Parkin. These proteins include *O*-linked glycosylated α-synuclein (α-sp22), CDCrel-1, synphilin-1 and PAEL-R (Shimura et al. 2001, Imai et al. 2001, Zhang et al. 2000, Chung et al. 2001).

The discoveries of CDCrel-1 and α-synuclein as substrates of Parkin were made around the same time. Zhang et al. reported that Parkin ubiquitylates and degrades CDCrel-1 in an UbcH2 (E2)-dependent process (Zhang et al. 2000). CDCrel-1 is a member of the Septin family, with intrinsic GTPase activity and is predominantly expressed in the nervous system (Beites et al. 1999). In addition, CDCrel-1 co-precipitates with synaptic vesicles via its interaction with syntaxin and has been speculated to modulate dopamine release, thereby contributing towards neurodegeneration (Zhang et al. 2000, Beites et al. 1999).

Shimura and colleagues demonstrated by immunohistochemistry and affinity purification that Parkin colocalises with α-synuclein in Lewy bodies. Further co-immunoprecipitation experiments showed that Parkin binds to two E2 conjugating enzymes, UbH7 and, to a weaker extend, UbcH8. E2 binding allows Parkin to ubiquitylate α-synuclein (Shimura et al. 2001). In addition, Chung and colleagues also reported that an α-synuclein-interacting protein,

synphilin-1 is also ubiquitylated by Parkin. Synphilin-1 co-localises with α-synuclein in the Lewy bodies observed in PD (Chung et al. 2001).

Another Lewy body-component, Pael-R is also a substrate of Parkin (Murakami et al. 2004). Imai and colleagues showed that CHIP (carboxyl terminus of the Hsc70-interacting protein), Hsp70, Parkin and Pael-R form a dynamic complex both *in vitro* and *in vivo*. Upon ER stress, CHIP plays dual roles in the ubiquitylation and subsequent degradation of Pael-R. Firstly, CHIP association with the complex is enhanced during ER stress, removing the association and inhibitory action of Hsp70 on Parkin and Pael-R. Secondly, CHIP acts as an E4-like, ubiquitin-elongation enzyme to promote Parkin-mediated ubiquitylation of Pael-R. Importantly, overexpression of Pael-R correlates with increased cell death and this can be rescued by the expression of Parkin, suggesting a cytotoxicity effect of Pael-R accumulation in cells (Imai et al. 2001).

It is worth noting that, unlike sporadic cases of PD, the majority cases of autosomal-recessive juvenile Parkinsonism (AR-JP) with loss-of-function Parkin mutations do not accumulate Lewy bodies (Saito et al. 2000, Morrison 2003). This supports the idea that the formation of Lewy bodies requires the E3 activity of Parkin. Indeed, the co-expression of Parkin, α-synuclein and synphilin-1 (an interacting protein of α-synuclein) resulted in the formation of Lewy-body-like ubiquitin-positive cytosolic inclusions (Chung et al. 2001). It is most likely that the pathophysiological effect of Parkin loss-of-function is mediated through other mechanisms, such as the accumulation of damaged mitochondria due to mitophagy defects. Hardy et al. proposed that the loss of function of Parkin might result in direct cell death without Lewy body formation in contrast to incomplete loss of function of Parkin or mutation of other PD associated genes (Hardy et al. 2003). Further pathological studies of patients with different forms of Parkin mutations need to be carried out to support this hypothesis.

Another protein that is degraded via Parkin-mediated ubiquitylation is FBXW7/FBXO7/FBX7. FBXW7 is a cytosolic substrate-binding adaptor

protein of the SCF multi-subunit E3 ligase complex. FBXW7 was first reported to form a complex with Parkin to mediate the degradation of cyclin E1. High levels of cyclin E1 have been associated with neuronal apoptosis (Padmanabhan et al. 1999). Consistent with this, Burchell et al. reported that depletion of FBWX7 affects Parkin recruitment during mitophagy (Burchell et al. 2013). Parkin was also shown to directly ubiquitylate FBXW7 for proteasomal degradation during mitophagy (Ekholm-Reed et al. 2013). Since SCF^{FBWX7} ubiquitylates and promotes the degradation of MCL1, a pro-survival BCL2 family member, this Parkin-dependent loss of FBXW7 was proposed to promote MCL1 accumulation and cell survival.

1.6.3.3 Parkin-mediated cell viability and apoptotic pathways

Apart from the proteasomal and lysosomal degradation of mitochondrial proteins and mitochondria, Parkin can also transcriptionally promote mitochondrial biogenesis. This is achieved via the ubiquitylation of PARIS (Parkin Interacting Substrate, ZNF746), a Kruppel-associated box (KRAB) domain-containing transcriptional repressor that regulates the transcription of many genes involved in cellular metabolism. Of relevance here, PCG-1α (peroxisome proliferator-activated receptor gamma coactivator 1-alpha), a gene involved in mitochondrial biogenesis, respiration and ROS metabolism, is one of the genes that is also suppressed by PARIS. Consistent with this, accumulation of PARIS following the expression of a loss-of-function mutant of Parkin affects mitochondrial biogenesis and leads to neurodegeneration in a mouse model (Shin et al. 2011, St-Pierre et al. 2006).

Parkin has also been shown to upregulate NF-κB pathway in response to different cellular stresses including ROS accumulation (CCCP), ER stress (thapsigargin) and wide spectrum kinase inhibition (staurosporine) (Henn et al. 2007, Muller-Rischart et al. 2013, Sha et al. 2010). Using mouse embryonic fibroblasts deficient in NEMO, it was demonstrated that the cytoprotective role of Parkin, at least in the face of these stimuli, depend on the linear ubiquitylation of NEMO and was independent of Parkin-mediated mitophagy as selective knockdown of PINK1, ATG5, or p62 did not affect the

stress protective phenotype. NEMO has been previously shown to be ubiquitylated by LUBAC (linear ubiquitin chain assembly complex), which consists of two RBR E3 ligases, HOIL-1L and HOIP (Muller-Rischart et al. 2013, Kirisako et al. 2006, Tokunaga et al. 2009). Under cellular stress, Parkin is recruited to HOIP and significantly enhances the linear ubiquitylating activity of LUBAC on NEMO (Figure 1.14). It remains to be determined whether Parkin enhances linear ubiquitylation of NEMO directly or indirectly by promoting the activity of LUBAC. One of the downstream transcriptional genes of NF-κB is the mitochondrial GTPase, OPA1 (optic atrophy 1). OPA1 is an inner mitochondrial membrane protein that is involved in the regulation of mitochondrial cristae arrangement. Inhibition of the electron transport chain complex I has been reported to cause cristae disintegration and increase cell death (Ramonet et al. 2013). While it might not be the only protein upregulated via this pathway, it certainly is an essential protein involved in Parkin-mediated NF-κB activation during cell stress as OPA1 knockdown in SH-SY5Y cells or knockout in mouse embryonic fibroblasts abrogated the pro-survival effects of Parkin expression (Muller-Rischart et al. 2013).

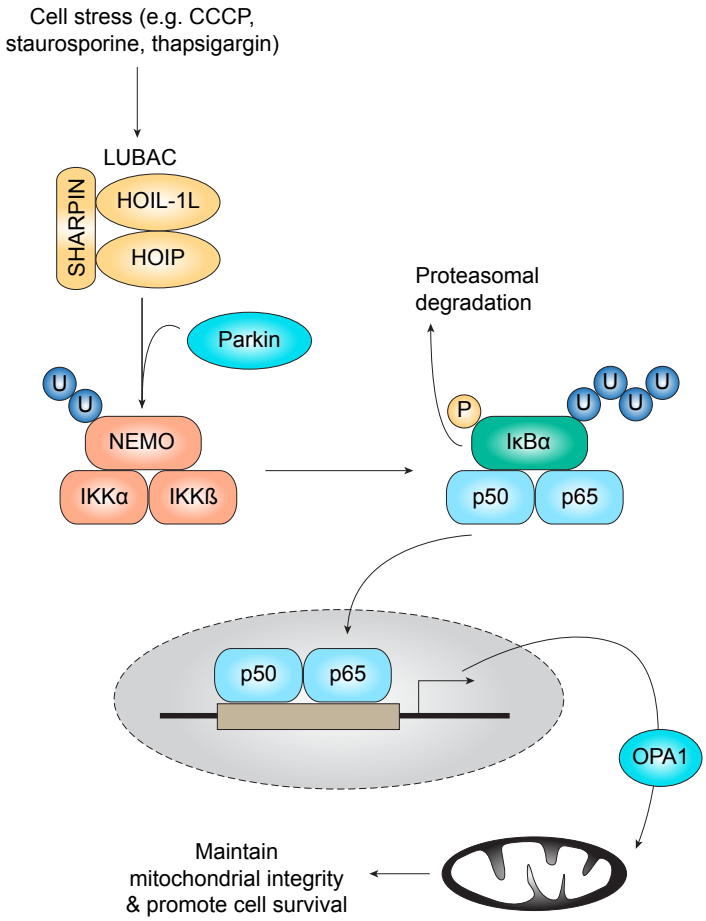

Figure 1.14 Parkin-mediated NF-κB pathway activation to promote mitochondrial integrity and cell survival.

During cell stress, Parkin is recruited to the LUBAC complex (consisting of HOIL-1L, HOIP and SHARPIN) and increases linear ubiquitylation of NEMO, an essential regulatory component of the IκB kinase complex. Once activated, this phosphorylates IκBα for subsequent proteasomal degradation, releasing the NF-κB dimers (p50/p65) for translocation into the nucleus to regulate transcription of target genes, which include OPA1. OPA1 is localised in the inner mitochondrial membrane and helps to maintain mitochondrial integrity, hence is indirectly involved in the promotion of cell survival (adapted from (Winklhofer 2014)).

In addition to its crosstalk with the NF-κB pathway, ectopic expression of Parkin in Drosophila suppressed the constitutively active form of Hempipterous (Hep(CA)), a JNK kinase that normally induces apoptosis in the eye imaginal disc and causes an with eye degeneration phenotype. Parkin overexpression also suppresses the Drosophila JNK, Basket (Bsk), preventing the formation of extra vein (Hwang et al. 2010). In line with this, Parkin expression in monkey kidney fibroblasts (COS1 cells) significantly suppresses JNK activity (Cha et al. 2005, Hwang et al. 2010).

In conclusion, Parkin is involved in a wide spectrum of pathways that converge to oppose cell death and promote cell survival. As a consequence, the loss of Parkin or its loss-of-function mutation during cell stress, either mediated by the degradative substrates of Parkin (both mitochondrial proteins and aggregate-prone cytosolic proteins) or its non-degradative substrates (activation of different cellular pathways) may cause cells to undergo apoptosis.

1.7 Apoptosis

The word ‘apoptosis’ originates from the Greek word meaning ‘falling off’, such as leaves from a tree. This term was coined in 1972 by Kerr and colleagues, who described a specific morphological pattern of scattered single cell death, with pyknotic nuclei (condensed chromatin), and formation of small spherical cytoplasmic fragments (membrane blebbing) (Kerr et al. 1972). Cytoplasmic fragments known as apoptotic bodies are often formed, with altered chemical composition (externalization of phosphatidylserine, PS) that signal neighbouring cells or macrophages to engulf them, causing minimal disruption to the overall tissue integrity with no inflammation.

In fact, apoptosis was first referred to as ‘shrinkage necrosis’, due to the observation of cell shrinkage, which baffled Kerr and colleagues (Kerr 1971). In necrotic cells, ionic pumps stop functioning, leading to the accumulation of intracellular lactate, which promotes the osmotic entry of water. As a result, necrotic cells swell and eventually rupture. The idea that apoptosis is a form

of programmed cell death that plays a complementary but opposing role to mitosis and cytokinesis arises from the observation that the growth and development of *Caenorhabditis elegans* involves the invariant apoptosis of 131 somatic cells (out of the 1090 cells that are present) (Sulston et al. 1983, Sulston and Horvitz 1977). Trump and Berezesky later demonstrated that in contrast to the passive progression of necrosis, cells execute apoptosis via a calcium and ATP energy-dependent mechanism (Trump and Berezesky 1995, Lockshin and Zakeri 2001).

1.7.1 Activation of the caspase cascade

Apoptosis is mediated by a family of cysteine proteases known as caspases, (c for cysteine and asp for aspartic acid). As the name suggests, these proteases cleave their target proteins at specific aspartic acids. The caspase family can be divided into two groups based on their position in the apoptotic signaling cascade: (1) the initiator caspases (Casp-2, 8, 9 and 10) and (2) the effector/executioner caspases (Casp-3, 6 and 7). There is another subset of caspases that are not involved in apoptosis. Instead, these groups of caspases (Casp1, 4 and 5) are involved in the inflammatory response.

To avoid aberrant, non-specific proteolytic cleavage in the cell, caspases are synthesized as inactive precursors, known as pro-caspases (Parrish et al. 2013, Boatright and Salvesen 2003). Upon stimulation, two initiator caspases are brought together by an adaptor protein, which promotes their dimerization and 'close-proximity' activation (Figure 1.15A) (Baliga et al. 2004, Wachmann et al. 2010). Following dimerization, the initiator caspases are weakly activated, allowing them to undergo autocatalytic cleavage to remove their prodomains, further improving their catalytic activity and complex stability for downstream cleavage of effector caspases (Baliga et al. 2004, Wachmann et al. 2010).

For their activation, effector procaspases need to be cleaved at two specific aspartic acid sites (by the activated initiator caspases) to remove the prodomain and to generate one large and one small fragment. These two

fragments dimerise and assemble with another heterodimer to form the final active tetramer (Figure 1.15B) (Boatright and Salvesen 2003). The activated effector caspases can then further cleave other caspases, thereby amplifying the apoptotic signal (Figure 1.15C). In addition, effector caspases also cleave a wide array of cellular proteins, ranging from Bid (BH3-only protein) to actin, γ-catenin, vimentin, lamin A, PARP (poly-ADP-ribose polymerase), topoisomerase I, XIAP (X-linked inhibitor of apoptosis protein) and ICAD (inhibitor of caspase-activated DNAse, CAD). This results in cytoskeletal and plasma membrane remodeling, breakdown of nuclear lamina, DNA fragmentation, cell cycle arrest and further amplification of apoptotic signal (reviewed in (Slee et al. 2001, Jin and El-Deiry 2005)).

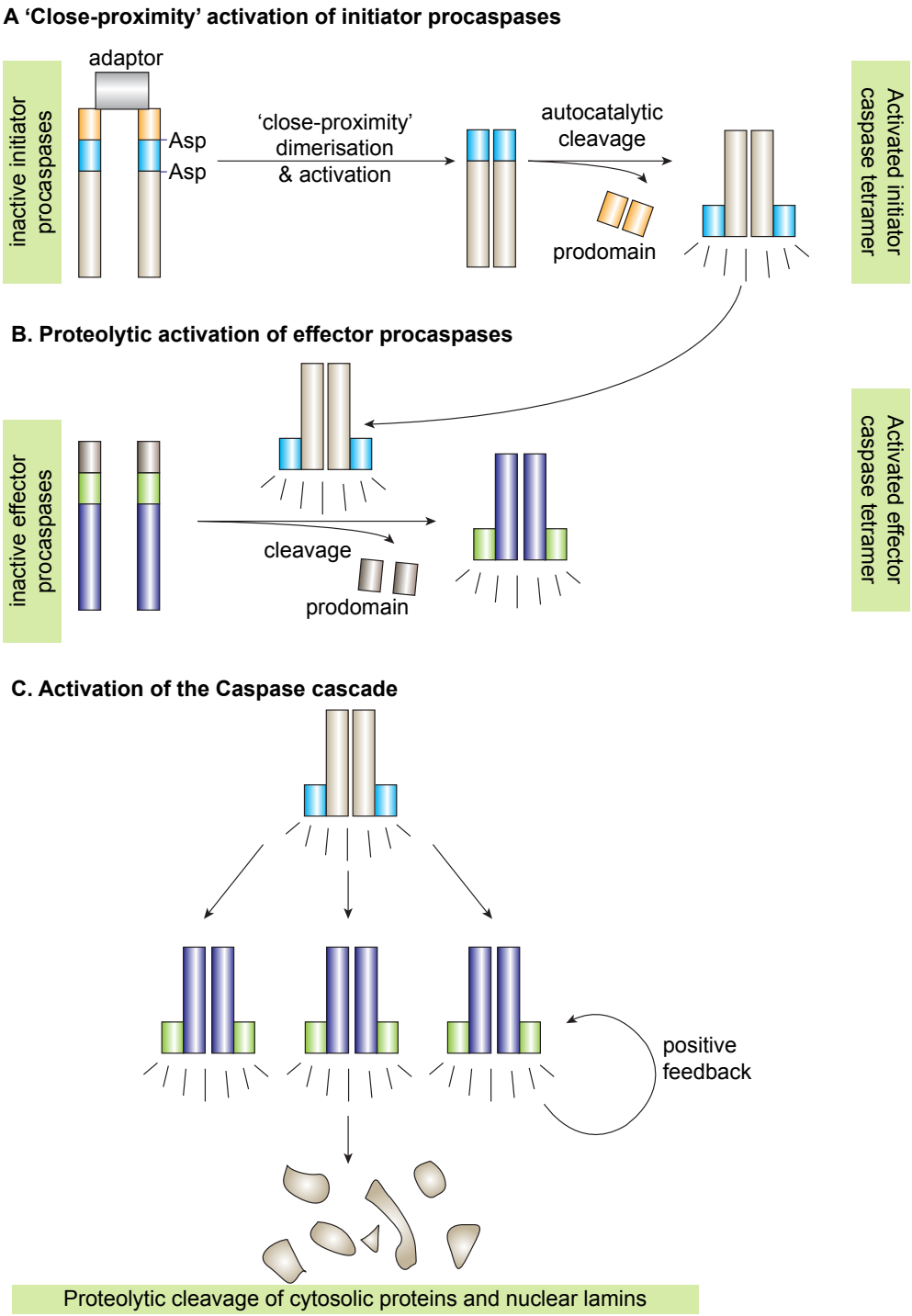

Figure 1.15 Activation of procaspases during apoptosis .

(A) Caspases are synthesized as inactive procaspases. During activation of apoptosis, initiator caspases are recruited to adaptor proteins, leading to 'close-proximity' activation of their catalytic activity. The initiator caspases then undergo autocatalytic cleavage at two specific aspartic acid residues, removing the prodomains and generating the long and short caspase fragments. Two caspases (with two fragments each) associate to form a tetramer. (B) Effector procaspases are activated via the proteolytic cleavage by (already activated) initiator caspases. The activated caspases cleave the effector procaspases at two similar aspartic acid residues, and generate similar fragments, which also form tetramer similar to that of the initiator caspases. (C) The upstream initiator caspase can cleave and activate many executioner procaspases, who in turn, can cleave other caspases, producing

an amplifying proteolytic cascade. In addition, the executioner caspases can also cleave a range of key proteins in the cell, causing the phenotypic changes observed during apoptosis.

1.7.2 The BCL2 family proteins

The B-cell lymphoma 2 (BCL2) family proteins are involved in the regulation of mitochondria-mediated apoptosis (Cory and Adams 2002, Ola et al. 2011, Burlacu 2003). The BCL2 family members are characterised by the presence of at least one BH domain (block homology) (Figure 1.16). The pro-apoptotic and anti-apoptotic family members have four BH domains (BH1-4) whereas the BH3-only proteins, as the name suggests, only has the BH3 domain. In addition, most of the pro-apoptotic and anti-apoptotic family members (with only a few exceptions) and some of the BH3-only proteins have a transmembrane domain, which allows the protein to be inserted into the outer mitochondrial membrane. Some of the members are constitutively localized to the outer mitochondrial membrane (e.g. BAK, MCL1 and BCL-xL), while some (for e.g. BAX) adopt a conformation that tucks away the transmembrane domain until activation by cytotoxic signals (Griffiths et al. 1999, Suzuki et al. 2000).

A main characteristic of the BCL2 family members is their ability to form homo and heterodimers among each other. At steady state, the relative amounts of the pro- and anti-apoptotic proteins are in equilibrium and the anti-apoptotic BCL2 members bind and inhibit the oligomerisation of the pro-apoptotic members, which can induce mitochondrial outer membrane permeabilization (MOMP), causing the release of cytochrome C (Kluck et al. 1997). The BH3-only proteins are responsible for the initiation of apoptotic signals. Upon a trigger, the BH3-only proteins can either sequester the anti-apoptotic proteins away from the pro-apoptotic members, or they can directly activate the pro-apoptotic members (Figure 1.16B) (reviewed in (Czabotar et al. 2014)). The functions of the BCL2 family members are further discussed in the next section.

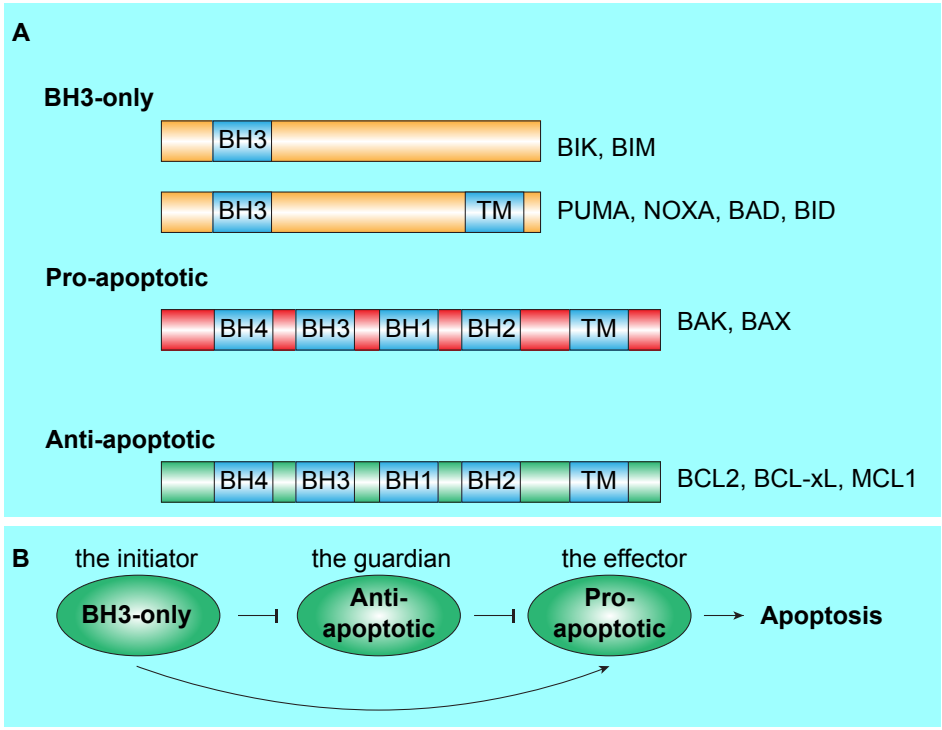

Figure 1.16 The domain architecture of BCL2 family proteins and the mode of action.

(A) The BH3-only proteins contain one BH (block homology) domain. Some of the BH3-only proteins also contain a transmembrane (TM) domain. Both the pro- and anti-apoptotic family members have four BH domains and most of the proteins within these two categories also have a TM domain.

(B) The anti- and pro-apoptotic proteins exist in equilibrium at basal state. Upon cytotoxic trigger, the BH3-only proteins bind with the anti-apoptotic proteins, thereby releasing the pro-apoptotic proteins to oligomerise on the outer mitochondrial membrane, releasing cytochrome C and inducing apoptosis.

1.7.3 Extrinsic and intrinsic apoptotic pathways

A wide array of stimuli may trigger apoptosis in mammalian cells via two major apoptotic pathways, the extrinsic and intrinsic pathways, both of which converge on the activation of the effector caspases.

Upon activation of the intrinsic apoptotic pathway, for example, due to DNA damage or ER stress, p53 accumulates in the cell (Figure 1.17). p53 transcriptionally upregulates BCL2 homology 3 (BH3)-only proteins, PUMA and NOXA (P. Wang et al. 2007, Akhtar et al. 2006, Chipuk et al. 2005). PUMA and NOXA bind and inhibit the BCL2 anti-apoptotic family members, BCL2, BCL-xL and MCL1, alleviating their inhibition of the pro-apoptotic

BCL2 family members, BAX and BAK (Yee and Vousden 2008). BAK and BAX can then oligomerise on the mitochondrial outer membrane, inducing mitochondrial outer membrane permeabilisation (MOMP). Alternatively, p53 has also been shown to directly translocate to the mitochondria and bind competitively with BCL2 and BCL-xL, resulting in the release of BAK and BAX for MOMP induction (Mihara et al. 2003, Mikhailov et al. 2003, Basanez et al. 2002, Kuwana et al. 2002).

MOMP results in the release of several pro-apoptotic proteins from the mitochondrial intermembrane space (IMS), including cytochrome C, Omi/htrA2 (high-temperature requirement) and Smac/DIABLO (second mitochondrial activator of caspases) to initiate or regulate caspase activation (Riedl and Salvesen 2007, Li et al. 1997, Yang et al. 1997, Kluck et al. 1997). Upon release from the mitochondria, these proteins promote apoptosis in various ways. Cytochrome C release induces the formation of an intracellular multicomplex structure, termed 'apoptosome' that contains APAF1 (apoptotic protease-activating factor 1) and procaspase 9 (Riedl and Salvesen 2007, Li et al. 1997). Procaspase 9 is activated in the apoptosome, which in turn cleaves and activates the downstream effector caspases, most notably, caspase 3 (Li et al. 1997, Jiang and Wang 2000). Both Smac/DIABLO and Omi/htrA2 bind and neutralize the inhibitory activity of the IAP family members (inhibitors of apoptosis) against caspases (Martins 2002, Martins et al. 2002, Verhagen et al. 2000, Du et al. 2000). In addition, Omi/htrA2 has also been reported to cleave ped/pea-15, an anti-apoptotic protein (Trencia et al. 2004).

On the other hand, the extrinsic apoptotic pathway is activated by cell surface death receptors, including Fas, TNF (tumour necrosis factor), and TRAIL (TNF-related apoptosis-inducing ligand) receptors (Figure 1.17) (reviewed in (Jin and El-Deiry 2005). Binding of the respective ligands triggers homotrimerisation of the receptors and recruits an adaptor protein, FADD (Fas-associated death domain). FADD in turn recruits caspase-8 (the initiator caspase) to form a death-inducing signaling complex (DISC) (Figure 1.17). Caspase-8 is autoactivated at the DISC, allowing it to proteolytically

cleave and activate downstream effector caspases, including caspase-3, caspase-6 and caspase-7 (Jin and El-Deiry 2005, Ashkenazi and Dixit 1998). Alternatively, caspase-8 can also amplify the apoptosis cascade by cleaving Bid. The truncated form of Bid (tBid) then oligomerises with BAK and BAX, leading to the release of cytochrome C and subsequent activation of caspase-9 follows the same downstream events as in the intrinsic apoptotic pathway (Wei et al. 2000).

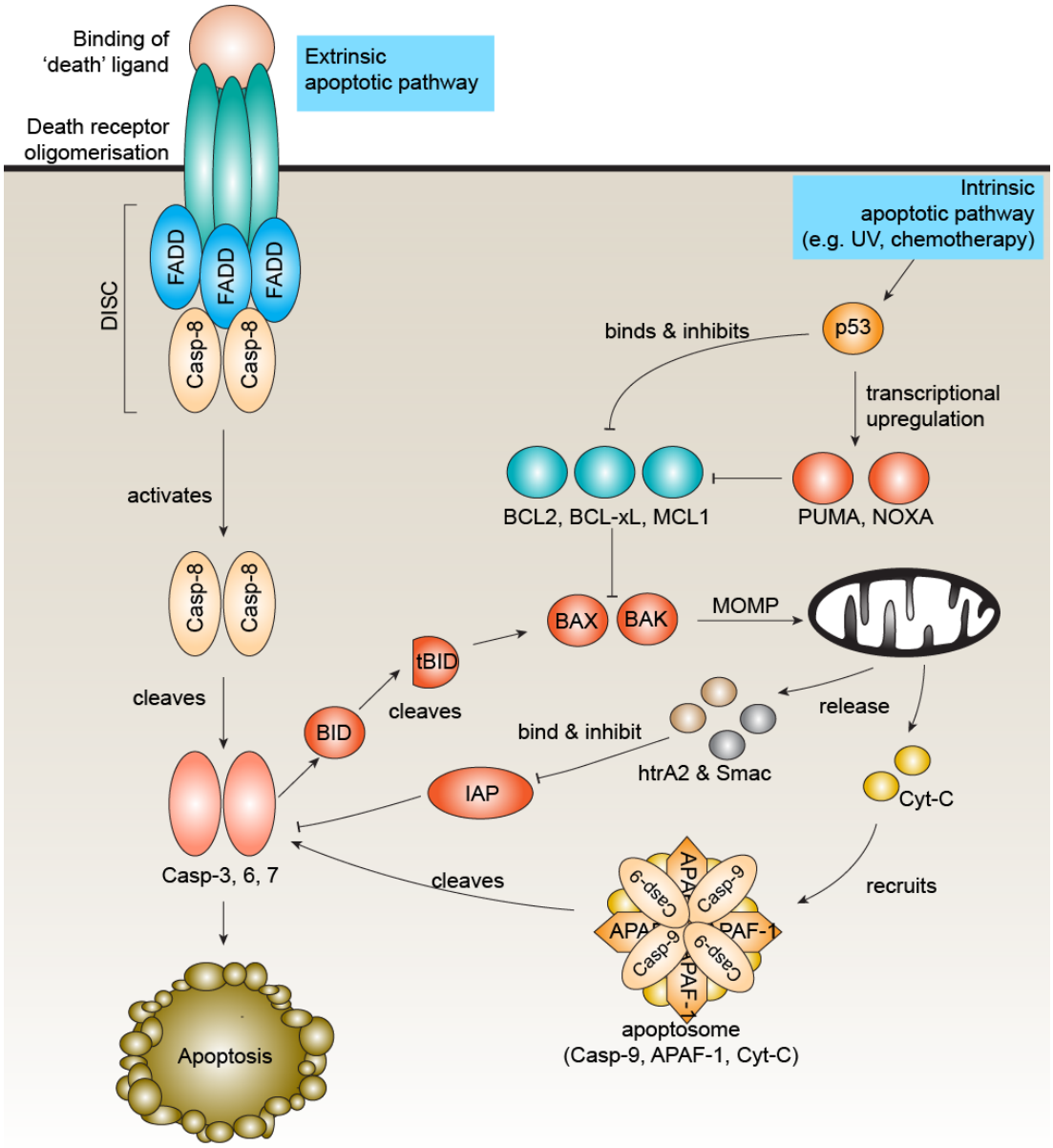

Figure 1.17 Key events in extrinsic and intrinsic apoptotic signaling pathways.

Intrinsic apoptotic signal triggers the accumulation of p53. p53 transcriptionally upregulates the BH3-only proteins, PUMA and NOXA. PUMA, NOXA and p53 can bind and neutralize the inhibition of the BCL2 anti-apoptotic family members (BCL2, BCL-xL and MCL1) towards the BCL2 pro-apoptotic family members (BAK and BAX), causing them to oligomerise on the OMM and form pores that lead to mitochondrial outer membrane permeabilisation (MOMP). Several apoptosis regulators, including cytochrome C, Omi/htrA2 and Smac/DIABLO are release into the cytosol. Cytochrome C binds with APAF-1 and procaspase 9, forming the multicomplex 'apoptosome'. The activation of caspase 9 by the apoptosome results in the downstream activation of effector caspases (caspase 3, 6, 7) and apoptosis. Both htrA2 and Smac bind and inhibit the IAPs, further amplifying the apoptotic signal.

The extrinsic pathway is activated by the binding of 'death' ligands to the death receptors (including FAS, TNF and TRAIL receptors). The activated receptors then oligomerise and recruit both FADD and caspase-8, forming the DISC complex, which activates caspase 8. Caspase 8 can either directly activate caspase 3, 6 and

7, or, it can cleave Bid, forming tBid. tBID can then bind to BAX and BAK to promote their oligomerisation on the OMM, converging with the intrinsic apoptotic pathway.

1.8 Autophagic cell death

Autophagy plays dual roles in cells. While moderate autophagy confers cytoprotective roles in response to nutrient starvation or growth factor deprivation, autophagy has also been observed in apoptotic cell death during excessive stress (He and Klionsky 2009, Eisenberg-Lerner et al. 2009). Indeed, the interplay between autophagy and apoptosis is highly complex and can be generalised into two different types as described below.

1.8.1.1 The antagonist

Autophagy acts as an alternative pathway to apoptosis (Figure 1.18A). For example, ER stress activates autophagy to selectively remove protein aggregates and misfolded proteins, thereby dampening the unfolded protein response (UPR) that could lead to apoptosis (Ogata et al. 2006, Castino et al. 2005). In addition, the selective removal of depolarised mitochondria via autophagy prevents the accumulation of ROS, which otherwise can cause DNA damage and activation of apoptosis (I. Kim et al. 2007). This antagonistic relationship between autophagy and apoptosis is often employed by cancer cells to evade cell death under unfavorable conditions, such as hypoxia and DNA damage. Ito and colleagues demonstrated that inhibition of autophagy using 3-methyladenine and bafilomycin A1 sensitises human malignant glioma cells to radiation-induced cell death, although these inhibitors would also interfere with the lysosomal pathway itself (Ito et al. 2005).

1.8.1.2 The partner / the enabler

Apoptosis and autophagy may occur simultaneously, either in parallel, or cooperatively (often with one predominating the other) to cause cell death (Figure 1.18B). The idea is that if one pathway is inhibited or defective, the other serves as a back-up to ensure efficient cell death. (Eisenberg-Lerner et al. 2009). Alternatively, autophagy can assist apoptosis without directly

causing cell death (Figure 1.18C). This is best represented by the generation of cellular ATP via autophagy for the energy-dependent processes during the activation of apoptosis (Eguchi et al. 1999, Zamaraeva et al. 2005). For example, membrane blebbing during apoptosis requires ATP to drive acto-myosin contraction (Inbal et al. 2002). Indeed, several known activators of apoptosis can also activate autophagy, including etoposide (in mouse embryonic fibrolasts), ceramide (breast and colon cancer cells) and the activation of the TRAIL receptors (various human cancer cell lines, including MCG-7, HCT116 and U87MG) (Park et al. 2007, Pattingre et al. 2009, Feng et al. 2005). In these cases, it is unclear whether autophagy occurs together with apoptosis to trigger cell death, or to generate ATP energy for subsequent apoptosis.

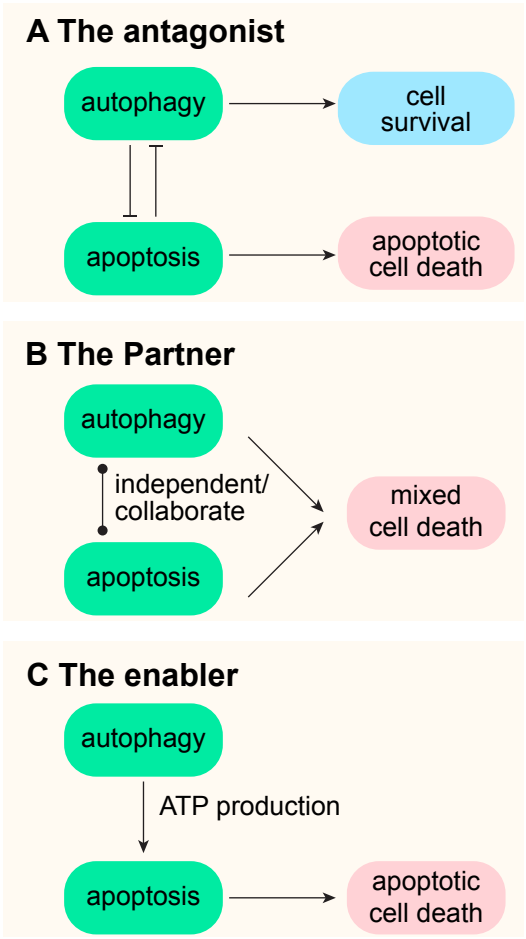

Figure 1.18 Schematic representation of the interplay between autophagy and apoptosis during cell stress.

(A) Autophagy and apoptosis act as alternative mechanisms to induce cell death.

(B) Autophagy and apoptosis can occur together during cell stress but in mutually exclusive pathways. In this case, autophagy may or may not contribute to cell death.

(C) Autophagy assists the progression of apoptosis via ATP production, leading to apoptotic cell death.

1.9 Aims of this study

In this chapter, I have introduced the ubiquitin system, from the ubiquitin structure to the ubiquitin-modifying family of E1, E2, E3 and DUBs that are involved in reversible ubiquitylation. I also discussed our currently knowledge on the autophagy pathway, focusing especially on the involvement of ubiquitylation in selective autophagy of specific organelles. Mitophagy, the selective autophagy of mitochondria by PINK1 and Parkin was introduced in detail as the loss-of-function mutations of this kinase and E3 ligase, respectively, have been reported to cause neuronal cell death in AR-JP (autosomal recessive-juvenile Parkinsonism). The mechanism and key players involved in apoptosis as well as the interplay between autophagy and cell death were also introduced in this chapter.

Our laboratory has a long-standing interest in the involvement of DUBs in various ubiquitin-mediated cellular processes. At the start of this project, the identity of DUBs that are involved in Parkin-mediated mitophagy, either opposing or assisting the E3 activity of Parkin was unknown. Therefore, the aims of my research project are:

- To characterise Parkin-mediated mitophagy in cell lines expressing either endogenous or exogenous Parkin levels
- To characterise the effects of different mitochondrial depolarizing drugs on mitophagy
- To biochemically dissect the different stages of mitophagy by western blotting
- To develop robust assays for both visual inspection and western blot analysis of Parkin-mediated mitophagy
- To utilize these assays as readouts for DUB siRNA screens
- To identify and deconvolute DUBs involved in Parkin-mediate mitophagy
- To understand the mechanisms by which the identified DUBs regulate Parkin-mediated mitophagy.

Chapter 2: Materials and Methods

2.1 Molecular biology

2.1.1 Reagents

Taq DNA Polymerase (BIO-21040) was purchased from Bioline (London, UK). Deoxynucleotide mix (100mM, #200415) and PfuUltra HF DNA Polymerase (#600390) were from Agilent (La Jolla, CA, USA). DH5α subcloning efficiency cells (#18265-017), S.O.C medium (#1554-034) and electrophoresis grade agarose powder were from Invitrogen (Paisley, UK). TAE buffer was obtained from National Diagnostics (Hull, UK). XL1-Blue supercompetent cells (#200236) were purchased from Agilent Technologies (Santa Clara, CA, USA). Miniprep (#27106), HiSpeed Maxiprep (@12633), RNeasy Mini (#74106), gel extraction (#28604) and PCR purification (#28704) kits were all from QIAGEN (Crawley, UK). Quick Ligation Kit (#M2200S), 1kDa DNA ladder (#N3232) and 100bp DNA ladder (#N3231) were purchased from New England Biolab (Herts, UK). PCR nucleotide Mix (#C1441), RNasin® plus RNAse inhibitor (#N2611) and nuclease free water (#P1193) were obtained from Promega (Madison, WI, USA). All primers were ordered from Eurofins MWG Operon (Ebersberg, Germany). All other chemicals were obtained from Sigma Aldrich (Poole, UK) unless otherwise stated.

2.1.2 Polymerase Chain Reaction (PCR)

DNA amplification by PCR was performed to clone RFP from pRFP-c1 vector to be used later to replace a GFP-tag from USP30-siRNARes1-GFP plasmid (Mullis et al. 1992). PfuUltra HF DNA polymerase was used to amplify RFP from pRFP-c1 vector and to insert *BamHI* and *NotI* restriction sites at each end of the RFP, forming *BamHI*-RFP-*NotI*. The primer sequences are shown in Table 2.1. PCR mixture was set up as shown in Table 2.2 and run using

according to the thermal cycle programmes as shown in Table 2.3 using a Techne TC-3000 Thermal Cycler (Scientific Laboratory Supplies Ltd., Hessle, UK).

Target	Primer No.	5'-3'		T_m
RFP	1837	F	gaGGATCCatggcctcctccgaggacgtc	69
	1838	R	gaGCGGCCGCttaggcgccggtggagtgg	72

Table 2.1 PCR primer sequences for amplification of RFP from pRFP-c1.

Capital letters in the primer sequence represents the insertion of sequence for recognition by *BamHI* (forward) and *Not1* (reverse) restriction enzymes.

Plasmid (100ng/µl)	1µl
10x PCR buffer	5µl
dNTP (25mM each)	0.4µl
5' primer (100ng/µl)	1.0µl
3' primer (100ng/µl)	1.0µl
PfuUltra HF	1µl
Sterile water	y µl
Total volume	50 µl

Table 2.2 PCR reaction mixture.

Segment	Step	No. of cycles	Temperature	Duration
1	Initial Denaturation	1	95˚C	5 min
2	Denaturation	34	95˚C	1 min
	Annealing		T_m-5˚C*	1 min
	Extension		68˚C	1 min /kb
3	Final Extension	1	68˚C	5 min

Table 2.3 Thermal cycler programme for PfuUltra Hotstart DNA polymerase. Asterisk: annealing temperature is set 5˚C below the melting temperature.

2.1.3 TOPO blunt-end cloning

TOPO blunt-end cloning was catalyzed by topoisomerase I that was covalently bound to the phosphate group of thymidine residue at each end of the linearized pCR4®Blunt-TOPO vector. The open reading frame (ORF) of interest was first amplified by PCR and resolved on a DNA agarose gel (Section 2.1.7). The amplified construct was then cut out from the gel and eluted using the gel extraction kit from Qiagen according to manufacturer's instructions. The eluted PCR product was then ligated with pCR4®Blunt-TOPO vector with the cloning reaction described in Table 2.4 at room

temperature for 5min. The ligated plasmids were transformed into TOP10 *Escherichia coli* as described in the next section.

Reagent	**Volume**
pCR4®Blunt-TOPO vector	1µl
Salt solution	1µl
PCR product	1µl
Sterile water	3µl
Total volume	**6 µl**

Table 2.4 TOPO cloning reaction mixture.

2.1.4 Bacteria transformation

Bacteria transformation was carried out using either TOP10 or DH5α *Escherichia coli* cells. Prior to transformation, 50µl of bacteria (per transformation reaction) was thawed on ice. 2µl of PCR product (from 50µl of PCR mixture) or approximately 100ng of DNA was added to the competent cells and left to incubate on ice for 20min. The cells were then heat-shocked at 42°C in water bath for 30sec and placed back on ice for 2min. 250µl of S.O.C. (super optimal broth with catabolite repression) medium was added to the bacteria suspension. The bacteria were shaken at 250rpm for 1hr and then inoculated on selective lysogeny broth (LB) agar plates with the appropriate antibiotic selection (Kanamycin: 10mg/ml, Ampicillin: 100mg/ml) and incubated at 37°C overnight.

3-5 bacteria colonies per condition were selected for overnight culture in 5ml of LB medium with the appropriate antibiotic selection. DNA was purified from the bacteria culture using Qiagen MiniPrep Kit. Purified DNA samples were test-digested and positive constructs were sent for sequencing. All DNA constructs generated were sequenced at the DNA Sequencing Service (University of Dundee, UK). Bacteria with sequence-verified constructs were further expanded in 250ml of LB medium for DNA extraction using the Qiagen MaxiPrep Kit and glycerol stock was made as described in the next section.

2.1.5 Glycerol stock

5ml of overnight-growth bacteria cultured in LB medium was centrifuged at 2,700xg to collect the bacteria pellet. The pellet was then resuspended in 40% glycerol in LB medium and kept at -80°C.

2.1.6 Restriction digest

Restriction digest mixture was set up as shown in Table 2.5. In general, 500ng of DNA sample was used for test digest and 5µg of DNA sample was used for restriction cloning. The reaction mixture was incubated for 1hr and optimal incubation temperature varies according the restriction endonuclease(s) used (mostly 37°C).

DNA sample	x µl
Restriction endonuclease	0.4 µl
10x Reaction buffer	1.0 µl
BSA (optional depending on restriction endonuclease)	1.0 µl
Sterile water	y µl
Total volume	**10 µl**

Table 2.5 Reaction mixture for restriction digest.

2.1.7 Agarose gel electrophoresis

Agarose gels were prepared by mixing electrophoresis grade agarose (Invitrogen) with TAE buffer (40mM Tris-acetate, 1mM Na_2-EDTA) and heated in a microwave for approximately 4min (until the agarose had completely dissolved in the buffer). A final concentration of 0.5µg/ml of ethidium bromide was added to allow visualization of DNA using an ultraviolet (UV) light source. The gel was then poured and left to set at room temperature. Prior to loading, 10x sample buffer (5% w/v glycerol, 0.1mM EDTA, 0.04% bromophenol w/v blue) was added to DNA samples at 1:10 dilution. DNA samples were resolved using TAE buffer in a horizontal midi electrophoresis tank (Fisher Scientific, Loughborough, UK) at 120V for 30 to 60min. 10µl of Quickload 1kb DNA ladder standard was loaded alongside the samples. DNA bands were checked using the UVIDoc (UVITECH, Cambridge, UK) .

2.1.8 RNA extraction and quality control

RNA from monolayer of cells was harvested using Qiagen RNeasy Kit as per manufacturer guidelines. The RNA concentration was determined using a NanoDrop Spectrophotometer ND1000 at 260nm. The quality of the nucleic acids was assessed by the ratios between 260nm to 230nm and 260nm to 280nm. A high 260/280 ratio (>2.0) indicates low level of protein contamination whereas a high 260/230 ratio (>2.0) indicates low level of other contaminants such as salts, ethanol, guanidinium, or phenol. 5µl of RNA was also resolved on a 1.2% agarose gel with ethidium bromide (0.5µg/ml) by electrophoresis to visualize the 28S and 18S RNA bands which indicate the absence of RNAse and RNA degradation.

2.1.9 Reverse Transcription

A 10µl solution of 1µg of RNA in sterile water was prepared. The solution was then incubated with 1µl of oligo dT primers at 70°C for 5min to prime the poly(A) tails of mRNA. Afterwards, 8µl of reaction buffer was added to the diluted mRNA and oligo dT primers (see Table 2.6 for buffer composition). The tube was incubated at 37°C for another 5min before 1µl of MuLV reverse transcriptase was added to the tube. The reaction was carried out at 42°C for 1hr, followed by 70°C for 10min. The final reaction mixture was made up to 100µl with sterile water.

5X reverse transcription buffer	4 µl
PCR nucleotide mix	2 µl
RNasin	0.5 µl
Nuclease free deionised water	1.5 µl
Total volume	**8 µl**

Table 2.6 Reaction buffer mixture for reverse transcription.

2.1.10 Quantitative real-time polymerase chain reaction (qRT-PCR)

The primer pairs used for qRT-PCR were summarized in Figure 2.8. All qRT-PCR primers were designed to contain 50-55% GC content, a melting temperature of approximately 58-60˚C and with a final amplicon of approximately 100-200bps. In addition, the primers also span an intron to

avoid amplification of genomic DNA. Designed primers were ordered from Eurofins MWG Operon (Ebersberg, Germany). Prior to use by qRT-PCR, the primers were tested by PCR with reverse-transcribed cDNA samples and resolved by gel electrophoresis to visualize the amplified DNA band (as described in section 2.1.9). As a negative control, RNA samples that were reverse-transcribed without dT-primers were used to ensure that no genomic DNA was amplified.

cDNA generated from reverse transcription was used for qRT-PCR (Higuchi et al. 1992). A negative control was also included by replacing cDNA sample with nuclease free deionised water to ensure no amplification of contaminants. The reaction buffer was prepared using iTaq^{TM} Universal SYBR® Green Supermix (Bio-Rad) according to manufacturer's instruction (see Table 2.7). The cDNA sample was diluted 3-fold and 3µl of the diluted cDNA sample was added to the reaction mixture to reduce pipetting error. qRT-PCR was performed in triplicates using the CFX Connect^{TM} Real-Time PCR Detection System (Bio-Rad). cDNA samples were first denatured at 95°C for 3min, followed by a two-step amplification protocol of 95°C (10sec) and 60°C (30sec) for 40 cycles. Melt curve was analysed after 40 cycles. The Ct values for test genes were normalized to actin and relative expression was represented as $2^{-[\Delta\Delta Ct]}$.

At the early stage of my project, qRT-PCR was routinely used to monitor the knockdown efficiency of USP30 due to the lack of specific antibody for USP30. qRT-PCR was also used to assess the knockdown efficiency of USP31, USP42 and USP43 knockdown efficiency.

	X1 Rxn
2x SYBR Mastermix	5µl
H2O	1.66µl
Forward Primer (20µM)	0.17µl
Reverse Primer	0.17µl

Total	7µl
Vol Per well	7µl
Vol. cDNA per well	3µl

Table 2.7 iTaq Universal SYBR Green reaction buffer.

Gene	5'-3'		Tm (˚C)	Location in Transcript (bp)
Actin	F	CACCTTCTACAATGAGCTGCGTGTG	58	1068-1155
	R	ATAGCACAGCCTGGATAGCAACGTAC	59	
MIRO1	F	ATCCAGAGAGGGAGACACGA	58	1167-1351
	R	GCTCATCAGGTGACAAAGCA	58	
MIRO2	F	AGTGGGCAACAAGTCAGACC	59	462-655
	R	GCTTGGCCTCAGGGTCATAG	60	
USP30	F	GCACCTTCTGAAAGCCTTGT	59	467-575
	R	CGTGAGCATCCTGTTCTTCA	58	
USP31	F	CCTCCTCTGAAGCCACCATC	58	760-964
	R	CATAGAGAGGCCTTGTGTGGG	58	
USP42	F	TCACCAGCTTGGAGACTGTCG	60	4018-4134
	R	CAATCACCCTGGCCATACTCA	60	
USP43	F	AGAAGCTTCCGCCTGAAGC	60	728-905
	R	TGGCGCAAGGGGATAGGTA	60	

Table 2.8 List of primers used for qRT-PCR.

2.2 Cell biology

2.2.1 Materials and Reagents

GeneJuice® transfection reagent was obtained from EMD Millipore (Darmstadt, Germany). Carbonyl cyanide m-chlorophenylhydrazone (CCCP; #C2759), DBeQ (SML0031), oligomycin A (#75351) and antimycin A (#A8674) were purchased from Sigma-Aldrich (poole, UK). Epoxomicin (#324800) and folimycin (#344085) were from Merck Milipore (Darmstadt, Germany). ABT-263 (#S1001) and ABT-737 (#S1002) were purchased from Stratech (Suffolk, UK). Oligofectamine™ (#12252-011), Lipofectamine™ RNAiMAX (#13778150) trypsin-EDTA (#15400), and Opti-MEM (#409864) transfection reagents and most cell culture reagents were purchased from Invitrogen (Paisley, UK) unless otherwise indicated. All plastic wares for cell culture were obtained from Corning Inc. (NY, USA).

2.2.2 Cell culture

Parental human telomerase reverse transcriptase-immortalized retional pigment epithelial (hTERT-RPE1) and HeLa S3 cells were provided by Francis Barr (University of Oxford, Oxford, UK). hTERT-RPE1 cells stably expressing YFP-Parkin were a gift from Dr. Jon Lane (University of Bristol, Bristol, UK). SH-SY5Y neuroblastoma, U2-OS osteosarcoma and A549 non-small cell lung cancer cells were purchased from ECACC (Salisbury, UK). Parental hTERT-RPE1, hTERT-RPE1-YFP-Parkin and SH-SY5Y cells were maintained in Dulbecco's Modified Eagle's Medium/Nutrient Mixture F-12 Ham (DMEM/F12). U2-OS, A549 and HeLa S3 cells were cultured in Dulbecco's Modified Eagle's Medium (DMEM). Both types of media were supplemented with 10% heat-inactivated fetal bovine serum (FBS), 0.1mM MEM non-essential amino acids (NEAA) and 100units/ml each of Penicillin and Streptomycin. All cells were cultured in a humidified 5% CO_2 atmosphere at 37°C. For maintenance, confluent cells were split every 2-3 days at 1:4 – 1:6 dilutions as appropriate using trypsin-EDTA. Briefly, cells were rinsed once in pre-warmed PBS and 1ml of trypsin was added to the cells and

incubated for 3-5mins in the incubator. Cells were then resuspended in complete medium and split accordingly.

2.2.3 siRNA transfection in 6-well plates and 15cm^2 dishes

siRNA transfection of HeLa S3 cells was performed using Oligofectamine. For a 6-well plate setting, HeLa S3 cells were seeded overnight. On the next day, the cells were washed with PBS and replaced with 800µl of no addition DMEM (DMEM without FBS, NEAA and penicillin/streptomycin). 2µl of 20µM siRNA oligos was first incubated with 180µl of OptiMEM (Invitrogen). In parallel, 2µl of Oligofectamine was added to 18µl of OptiMEM. Both solutions were left to incubate at room temperature for 5min. The two solutions were then mixed and left at room temperature for 20min. The transfection mixture was then added dropwise to each well. The final siRNA oligo concentration in each well is 40nM. The cells were then incubated for 4hr and FBS was added to the medium to a final of 10% concentration. The next day, the medium and siRNA transfection mixture were replaced with 2ml of fresh complete DMEM (supplemented with FBS, NEAA, and penicillin/streptomycin). For the SILAC experiments (described in chapter 7), cells were cultured and transfected in 15cm dishes. The volume of transfection reagents, siRNA oligos, OptiMEM and growth media were scaled up by 15 times of that for a transfection in a 6-well plate.

siRNA transfection of SH-SY5Y, HEK293T, U2-OS, parental hTERT-RPE1, hTERT-RPE1-YFP-Parkin cells was carried out using Lipofectamine RNAiMAX transfection reagent following the 'Reverse Transfection' protocol. In the 'Reverse Transfection' protocol, cells were seeded and transfected at the same day. For a 6-well plate setting, 2µl of 20µM siRNA oligos was first incubated with 83µl of OptiMEM. In parallel, 2µl of Lipofectamine RNAiMAX was incubated with 83µl of OptiMEM. Both solutions were left to incubate at room temperature for 5min before being mixed together, vortexed and left at room temperature for 20min. Meanwhile, cells were trypsinised, and resuspended in complete medium (supplemented with FBS and NEAA but without penicillin/streptomycin). The desired number of cells was seeded per well to a final volume of 830µl. After 20min, 170µl of siRNA and transfection

reagent mixture was added dropwise to each well, giving a final concentration of 40nM of siRNA oligos per well. The next day, the medium and siRNA transfection mixture were replaced with 2ml of fresh complete medium (supplemented with FBS, NEAA, and penicillin/streptomycin). Unless stated otherwise, siRNA transfections for qRT-PCR were carried out for 24hr whereas siRNA transfections for protein lysate or fixation were normally carried out for 72hr. The siRNA oligo sequences used are summarized in Table 2.9.

Target	Type	Oligo No.	Target sequence
NT1	siOTP	NT1	TGGTTTACATGTCGACTAA
USP30	Custom order	D1*	CAAATTACCTGCCGCACAA
	siGenome	D3**	ACAGGATGCTCACGAATTA
	siGenome	D4	GCCAAGAAGTTACTGATGA
	siOTP	D6	CCAGAGTCCTGTTCGATTT
	siOTP	D7	GGACATAAACCTAGTCAAC
	siOTP	D8	CGTCAGATATAAAGTCATG
	siOTP	D9	GTCATTACCTCGTCATTGG
	Qiagen	Q2	CACACCAGTATTTATCCTTAA
	Qiagen	Q5*	AACAAATTACCTGCCGCACAA
	Qiagen	Q6	CTCCGATGACACTGTCCGCAA
	Qiagen	Q7**	CTCACGAATTATTCCATGTCA
MIRO1	siGenome	D9	TGTGGAGTGTTCAGCGAAATT
	siGenome	D10	GCAATTAGCAGAGGCGTTATT
	siGenome	D11	CCAGAGAGGGAGACACGAATT
	siGenome	D12	GCTTAATCGTAGCTGCAAATT
MIRO2	siGenome	D9	GCGTGGAGTGTTCGGCCAATT
	siGenome	D10	CCTCAAGTTTGGAGCCGTTTT
	siGenome	D11	GAGGTTGGGTTCCCTGATTATT
	siGenome	D12	AGGAGATCCACAAGGCAAATT
PINK1	siOTP	D6	GCAAATGTGCTTCATCTAA
	siOTP	D7	GCTTTCGGCTGGAGGAGTA
	siOTP	D8	GGACGCTGTTCCTCGTTAT
	siOTP	D9	GAGACCATCTGCCCGAGTA
PARKIN	siOTP	D5	GUAAAGAAGCGTACCATGA
	siOTP	D6	GAACATCACRRGCATTACG
	siOTP	D7	GATAGTGTTTGTCAGGTTC
	siOTP	D8	TTAAAGAGCTCCATCACTT

USP7	siOTP	D5	AAGCGTCCCTTTAGCATTA
	siOTP	D6	GCATAGTGATAACCTGTA
	siOTP	D7	TAAGGACCCTGCAAATTAT
	siOTP	D8	GTAAAGAAGTAGACTATCG
USP28	custom order	A1	CUGCAUUCACCUUAUCAUUTT
	custom order	A2	UUGGUUUAGUGCUGUUAUUTT
	Ambion	A9	GUGAUUGCUUUAUACCGA
	Ambion	A10	GATTATAGTTTGTTCCGAA
Caspase 8	Qiagen	Q11	GAGTCTGTGCCCAAATCAATT
Caspase 9	Qiagen	Q7	GTGACATCTTTGTGTCCTATT
USP33	siOTP	D6	GGGCATGTCTGGAGAATAGTT
VPS35	siOTP	D5	GAACATATTGCTACCAGTA
	siOTP	D6	GAAAGAGCATGAGTTGTTA
	siOTP	D7	GTTGTAAACTGTAGGGATG
	siOTP	D8	GAACAAATTTGGTGCGCCT
BAX	siOTP	D7	AAGTGGAGCTGACATGTTT
	siOTP	D8	TGCCGGAACTGATCAGAAC
	siOTP	D9	GCAAACTGGTGCTCAAGGC
	siOTP	D10	CATCATGGGCTGGACATTG
BAK	siOTP	D6	CGACATGAACCGACGCTAT
	siOTP	D7	TATGAGTACTTCACCCCGA
	siOTP	D8	GACGGCAGCTCGCCATCAT
	siOTP	D9	AATCATGACTCCCAAGGGT

Table 2.9 siRNA oligo sequences used for transfection.

siRNA oligos are purchased from Dharmacon (siGenome and siONTARGETplus; siOTP), Qiagen or Ambion. Note that the Qiagen DUB siRNA oligos that are used for initial deconvolution only are described in the Qiagen siRNA oligo library (shown in appendix).

* USP30 siRNA oligo D1 (from Dharmacon) and Q5 (from Qiagen) are the same sequence, with two additional nucleotides present in oligo Q5.

** USP30 siRNA oligo D3 and Q6 have 11 overlapping nucleotides.

2.2.4 Transfection protocol for DUB siRNA screen in 96-well plates and 6-well plates

For the purpose of DUB siRNA screens (one live-cell imaging screen and two western blot screens described in Chapter 5), two custom-made DUB siRNA libraries were purchased from Qiagen. The first DUB siRNA library consists of siRNA against 92 DUBs, of which, each contains 4 individual siRNA oligos targeting the same DUB. At the later stage of my project, a second DUB siRNA library was obtained from Qiagen, which was an upgrade of the first library, containing two additional DUBs that were discovered later, namely, FAM105B/OTULIN and C14orf28. The usage of each of the DUB siRNA library and the cell types used are summarized in Table 2.10. The siRNA sequences used to target each of the 94 DUBs are listed in Supplementary Table 1.

For the first siRNA screen (live-cell imaging), transfection was carried out in a 96-well plate using RNAiMAX according to the 'Reverse Transfection' protocol described in the previous section. However, the volumes of transfection reagent, OptiMEM and growth media were scaled down by 8.5 times of that for a standard 6-well plate transfection. The 10μM siRNA oligo stocks were also further diluted to 1.2μM prior to transfection so that 2μl of 1.2μM of siRNA oligos were used per transfection to reduce pipetting error (final siRNA concentration 20nM).

The second and third screens for western blot analysis were carried out in 6-well plates and the siRNA transfection protocol follows exactly of that described in the previous section for hTERT-RPE1-YFP-Parkin cells and SH-SY5Y cells.

	siRNA stock concentration	Cell types
First DUB siRNA library Live-cell imaging screen (96-well plate format)	10μM → 1.2μM (further dilution prior to use)	hTERT-RPE1-YFP-Parkin cells (5000 cells/well)
Second DUB siRNA library Western blot screen (6-well plate format)	10μM	hTERT-RPE1-YFP-Parkin cells (3x10E5 cells/well)
		SH-SY5Y cells (3x10E5 cells/well)

Table 2.10 Usage of different DUB siRNA libraries for different siRNA screens and cell lines.

2.2.5 DNA transfection

GeneJuice was used for transient DNA transfection in all the cell lines. For a 6-well plate setting, cells were seeded into each well and incubated overnight at 37°C. The next day, the medium in each well was replaced with 1ml of fresh full DMEM. For DNA transfection, 1μg of plasmid was added to 100μl of OptiMEM and mixed by gently vortexing. Then, 3μl of GeneJuice was added in, vortexed and the mixture was left at room temperature for 20min before adding the mixture dropwise into each well. In the case of hTERT-RPE1 (both parental and YFP-Parkin expressing cells), 5μl instead of 3μl of Genejuice were used to improve transfection efficiency. Unless stated otherwise, cells were harvested or fixed either 24 or 48hr post-transfection. For high expression DNA plasmids, the amount of plasmid was reduced and made up to 1μg by replacing the plasmid of interest with pBlueScript. In the case of expression for immunoprecipitation experiments, 3μg of DNA plasmids were used per 6cm dish of cells.

2.2.6 Drug treatments

Except during titration and in specified experiment, cells were treated with 10μM of CCCP in complete medium (supplemented with NEAA and FBS). Oligomycin A and antimycin A were both used at 1μM. Epoxomicin and Folimycin were both used at 100nM. DBeQ was used at 5, 10 and 20μM. z-VAD-FMK was used at 20μM. ABT-263 and ABT-737 were both used at 10μM.

2.3 Protein Biochemistry

2.3.1 Materials

Mitochondria isolation kit (#130-094-872) was purchased from Miltenyi Biotech (Surrey, UK). BCA protein assay kit (#23225) was obtained from Pierce Biotechnology (Rockford, IL, USA). Protran nitrocellulose membrane (#B3-0042), ProtoGel Resolving Buffer (#B9-0010), ProtoGel Stacking Buffer (#B9-0014), SDS PAGE Tank Buffer, 10x (#B9-0032), ProtoGel (#A2-0072) were purchased from GeneGlow (Elmhurst, UK). Prestained broad range molecular weight marker (#P7708S) and unstained broad range molecular weight marker (#P7702S) were from New England Biolabs (NEB; Hitchin, UK). Bovine IgG (Immunoglobulin G), 2-mercaptoethanol (#M6250), Ponceau S (#P7170), ammonium persulphate (APS) (#A3678), digitonin (D141) mammalian protease inhibitors (#P8340), *N*-ethylmaleimide (NEM; #E1271) were from Sigma-Aldrich (Poole, UK). Mammalian phosphatase inhibitor cocktail was from Roche (Sussex, UK). Marvel skimmed milk powder was from Premier Brands, UK. DRAQ7 (#7406) and annexin V-AF350 (#A23202), DAPI (4',6-Diamidino-2-Phenylindole, Dihydrochloride; #D1306), NuPaGE Bis- Tris 4-12% gels (10 well 1mm: #NP0321BOX, 10 well 1.5mm: #NP0303BOX, 12 well 1.0mm: #NP0322BOX, 15 well 1.5mm: #NP0336, 20 well 1mm: #W61402A, 26-well 1mm: #WG1003), NuPAGE antioxidant (#NP0005), NuPAGE MES (#NP0002-02) and MOPS (#NP0001-02) buffers, Colloidal stain kit (#LC6025) were all from Invitrogen (Paisley, UK). Mowiol (#475904) was purchased from Merck Millipore (Darmstadt, Germany).

2.3.2 Cell lysis for protein harvest

A monolayer of adherent cells were washed three times with ice-cold PBS on ice and harvested with either Nonidet P-40 (NP-40) lysis buffer (0.5% w/v NP-40, 25mM Tris-HCl pH7.5, 100mM NaCl, 50mM NaF), Radioimmunoprecipitation assay (RIPA) lysis buffer (1% Nonidet P-40, 10mM Tris-HCl, pH7.5, 150mM NaCl, 1% sodium deoxycholate, 0.5% SDS), or ‘hot lysis buffer’ (1% SDS, 50mM NaF and 1mM EDTA at 110°C). Both

NP-40 and RIPA lysis buffers were supplemented with mammalian proteinase inhibitor cocktail. In specified experiments, *N*-ethylmaleimide (NEM) and mammalian phosphatase inhibitor cocktail were also added to NP-40 and RIPA lysis buffers to a final concentration of 10 mM to inactivate cysteine proteinases. Lysates were pre-cleared by centrifugation at 14,000 x g for 5min. 'Hot lysate' samples were harvested by washing cells three times with room temperature PBS. The cells were then scraped with rubber policemen in pre-heated 'hot lysis buffer' at 110°C on a heat block. The harvested 'hot lysate' samples were boiled at 110°C for 10min, with vigorous vortexing every 2min interval to shear the DNA content in the samples.

2.3.3 Protein Assay

BCA protein assay kit was used to measure the protein concentration of cell lysates according to manufacturer's instructions. Bovine IgG was used to establish a standard curve. Table 2.11 shows a typical BCA protein assay. Samples were measured in triplicates and were read at OD_{562}.

	Water (µl)	**1mg/ml IgG (µl)**	**Lysis buffer (µl)**	**Cell lysate (µl)**	**BCA Mixture* (µl)**
Standard curve	10	-	3	-	200
	8	2			
	6	4			
	4	6			
	2	8			
	0	10			
Sample	10	-	-	3	

Table 2.11 Typical BCA protein assay. * BCA mixture was made by mixing 50 part of BCA Reagent A with 1 part of BCA Reagent B (50:1, Reagent A:B).

2.3.4 Mitochondria fractionation by TOMM22 antibody-affinity purification

This mitochondria enrichment protocol was modified from Hornig-Do et al. (2009). Cells were rinsed twice with ice-cold phosphate-buffered saline (PBS). Cells were scraped using a rubber policeman in 5ml of cold PBS and spun down at 1000 x g for 2min at 4°C. The cell pellet was gently resuspended in 500µl of HIM buffer (200mM mannitol, 70mM sucrose, 1mM EGTA, 10mM HEPES, pH7.5, 1x mammalian protease inhibitor) and spun down at the same condition as before. Cell suspension was passed through a 23G needle 4-6 times to break the cell membrane. A small amount of the cell lysate was checked under the light microscope to assess the efficiency of homogenisation. The sample was centrifuged at 600g for 10min at 4°C to pellet the nucleus. The post-nuclear supernatant (PNS) was further centrifuged at 7000 x g for 15min at 4°C to pellet the mitochondria. The mitochondrial pellet was resuspended in 10ml of ice-cold separation buffer with 100µl of anti-TOM22 conjugated with iron microbeads from the mitochondria isolation kit (MACS Miltenyi Biotec). The suspension was incubated for 1hr at 4°C using a tube rotator. The antibody-bound mitochondria were then isolated by passing the suspension through a LS column attached to a MACS magnetic separator. The column was then washed three times with 3ml of separation buffer. The column was detached from the MACS separator and 1.5ml of separation buffer was pipetted into the column to elute the mitochondria. The mitochondria were spun down at 13,000 x g for 2min at 4°C and resuspended in 50ul of NP-40 lysis buffer. Iron microbeads were pelleted by centrifugation using Beckman TLA100.2 rotor at 184,000xg for 20min at 4°C.

2.3.5 Crude mitochondria fractionation by centrifugation

Before harvesting, cells from a 10cm dish were washed with ice-cold phosphate-buffered saline (PBS) and scraped off in PBS using a rubber policeman. Cells were centrifuged at 500 x g for 2min and resuspended in 500µl of HIM buffer (200mM D- mannitol, 70mM sucrose, 1mM EGTA, 10mM

HEPES, pH7.5) supplemented with mammalian protease inhibitor. The cells were homogenized by passing through a 23G needle 4-6 times and then centrifuged at 700 x g for 5min. The PNS was further centrifuged at 7000 x g for 15min to pellet the mitochondria. The mitochondrial fraction was resuspended in 50µl of RIPA lysis buffer supplemented with mammalian protease inhibitor.

2.3.6 Cytochrome-C release assay with Digitonin permeabilization

Digitonin was dissolved in water at 1% (w/v) and stored at 4°C. Prior to use, digitonin solution was briefly heated at 95°C for 10sec to dissolve precipitated digitonin. To measure Cyt-C release from mitochondria, cells were scraped from a 10cm dish using a rubber policeman in ice-cold PBS. Cells were then spun down at 700 x g for 5min. The cell pellet was then resuspended gently (by flicking the tube) in 200µl of HIM buffer supplemented with mammalian protease inhibitor and phosphatase inhibitor and 0.025% of digitonin. The cell suspension was incubated on ice for 10min followed by 5min centrifugation at 20,000 x g. The supernatant was collected in a separate tube and the pellet was resuspended in 200µl of RIPA lysis buffer supplemented with mammalian protease and phosphatase inhibitors. The pellet and supernatant fractions were resolved on a NU-PAGE at 1:3 (v/v).

2.3.7 Immunoprecipitation

Protein concentration of pre-cleared lysates (as described in section 2.3.2 and 2.3.3) were determined and adjusted to equal concentration using lysis buffer. Typically, 500-800µg of lysates were used per immunoprecipitation. The lysates were incubated with 1µg of anti-GFP antibody (provided by Ian Prior, University of Liverpool, UK), and 30µl of 50% slurry protein-G agarose. The mixture was incubated on a rotating wheel at 4°C for 1-2hr. Beads were precipitated at top speed in a bench top centrifuge and washed three times with YP-IP buffer (0.1% Nonidet P- 40, 25mM Tris/HCl, pH7.5, 150mM NaCl), followed by a final wash with 10mM Tris/HCl, pH7.5. The pellet was

then resuspended in 20-30µl of 1.5 x SDS-PAGE sample buffer and boiled at 98°C for 5min to retrieve proteins that were bound to the beads.

An alternative immunoprecipitation method was also used in specified experiments using nanotrap, a 13-kDa GFP-binding fragment derived from a llama single-chain antibody (Rothbauer et al. 2008). Similar to the former immunoprecipitation protocol, pre-cleared lysates were incubated with 30µl of 50% slurry of nanotrap cross-linked with beads for 2hr at 4°C. Beads were washed three times with YP-IP buffer (0.1% Nonidet P- 40, 25mM Tris/HCl, pH7.5, 150mM NaCl) and once with 10mM Tris/HCl, pH7.5. The pellet was then resuspended in 20-30µl of 1.5 x SDS-PAGE sample buffer and boiled at 98°C for 5min to retrieve proteins that were bound to the beads.

2.3.8 Sodium dodecyl sulfate polyacrylamide electrophoresis (SDS-PAGE)

Protein samples were resolved by SDS-PAGE using the precast NUPAGE® 4-12% Bis-Tris gels (Invitrogen, Paisley, UK). Protein samples were standardized to the same concentration. Samples harvested in NP-40 or RIPA lysis buffer were then resuspended in 5x sample buffer (50% w/v glycerol, 310mM Tris-HCl, pH6.8, 15% w/v SDS, 16% w/w 2-Mercaptoethanol, 0.05% w/v Bromophenol Blue) and boiled at 98°C for 5min prior to loading onto gel. ‘Hot lysates’ were resuspended in 10x ‘hot lysis’ sample buffer (1M DTT and 1% Bromophenol Blue) and boiled at 110°C for 5min before loading onto gel. Depending on the abundance of the protein of interest, 10-20µg of protein lysates were usually loaded.

The Invitrogen NUPAGE system was used for most of the experiments using precast NUPAGE Bis-Tris 4-12% gradient gels in either an XCell SureLock Mini-Cell System (10,12 or 15 wells) or XCell SureLock Midi-Cell System (20 or 26 wells). Generally, 3-(N-morpholino)propanesulfonic acid (MOPS) buffer was typically used in most experiment. 2-(N-morpholino)ethanesulfonic acid (MES) buffer was used to separate low molecular weight proteins. In general, gels were run at 180V for 60min (mini gel) or 75min (midi gel).

2.3.9 Western blotting

Western blotting (Burnette 1981) was performed by transferring protein from SDS-PAGE onto 0.45µm Protran ® nitrocellulose membrane in transfer buffer (20ml methanol, 80ml water, 3.03g Tris and 14.4g glycine) at a constant current of 0.9A, 24V for an hour in in a Genie blotter (Research Products International Corp., Ill, USA). Following transfer, the nitrocellulose membrane was stained with Ponceau-S stain (Sigma Aldrich) to monitor the efficacy of transfer and to check for equal protein loading. The Ponseau-S stain was washed off with PBS. The membrane was then blocked for at least 30min in 5% Marvel milk powder in PBS containing 0.1% Tween-20 (w/v) (PBS-T) at room temperature. Primary antibody incubation was carried out at the indicated time of either 1hr at room temperature or overnight at 4°C (Table 2.12). Unbound antibody was washed off with PBS-T (three times for 5min each), followed by incubation with IRDye conjugated-secondary antibody (LICOR Biosciences; Table 2.13) at room temperature for 30min. Unbound secondary antibody was washed off with PBS-T (three times for 5min each) followed by a final wash with PBS for 5min. Image acquisition was carried out using LI-COR Odyssey imaging system. Protein band intensities were quantified using ImageJ. Note that the blots were routinely cut into 2 or 3 parts to maximize the number of probings.

Antibody name	Target protein	Spec-ies	Source/ Cat. No.	Dilution/ Duration
Actin	Actin	R	Sigma, A2206	1:2000, 1hr
Actin	Actin	M	Abcam, Ab6276	1:10000, 1hr
ACTN4	ACTN4	R	from Kazufumi Honda, NA	1:1000, 1hr
AGR2	AGR2	M	From Laurent Dumartin, NA	1:500, 1hr
AHCYL2	AHCYL2	R	GeneTex, GTX112212	1:1000, 1hr
alpha-Tubulin	alpha-Tubulin	M	Sigma, T5168	1:100, o/n
BAK (G-23)	BAK	R	Santa Cruz, SC-832	1:1000, 1hr
BAX	BAX	M	BD Transduction, 610982	1:1000, 1hr
BCL-XL	BCL-XL	R	Cell Signaling, 2764S	1:1000, 1hr
BCL2	BCL2	M	Abcam, AB692	1:1000, 1hr
Caspase 3	Caspase 3	M	Cell Signalling, 9668	1:1000, o/n
Caspase 8	Caspase 8	R	R&D, AF1650	1:1000, 1hr
Caspase 9	Caspase 9	M	Enzo, ADI-AAM-139-E	1:1000, 1hr
Cytochrome C	Cytochrome C	Sh	Sigma, C5723	1:1000, o/n
DJ-1	DJ-1	R	Bethyl, A300-744A	1:1000, o/n
FKBP38 (c391505)	FKBP38/ FKBP8	M	R&D systems, MAD3580	1:1000, o/n
GFP	GFP	Sh	Ian Prior, NA	1:1000, 1hr
IkB-a	IkB	R	Cell Signaling, 9242	1:1000, o/n
LC3 (5F10)	LC3	M	Nanotools, 5F10	1:200, o/n
MCL1 (S-19)	MCL1	R	Santa cruz, sc-819	1:1000, 1hr
MFN2	MFN2	R	Sigma, M6444	1:1000, o/n
MGST1	MGST1	M	From Ralf Morgenstern, NA	1:500, 1hr
MIRO1	MIRO1	R	Sigma , HPA010687	1:1000, 1hr
MUL1	MUL1/ MULAN	R	ABCAM, ab84067	1:500, o/n
Myc (4A6)	Myc	M	Millipore, 05-724	1:1000, 1hr
OPA1	OPA1	R	Abcam, ab54046	1:1000, o/n
p53-DO1	p53	M	Santa Cruz, sc-126	1:1000, o/n
Parkin	Parkin	M	Santa Cruz, sc32282	1:250, o/n
PARP p85 (ASP214)	PARP-p85	M	Cell Signalling, 9546	1:2000, o/n
PINK1	PINK1	R	Novus Biologicals, BC100-494	1:500, o/n
RAB35	RAB35	R	GeneTex, GTX112212	1:500, 1hr
RFP	RFP	R	Ian Prior, NA	1:5000, 1hr
TIMM44	TIMM44	R	Sigma, HPA043052	1:2000, o/n
TOM20	TOM20	M	Sigma , HPA011562	1:1000, 1hr
TOM20	TOM20	M	BD transduction	1:1000, o/n

			laboratories, 612278	
USP15 (1C-10)	USP15	M	Abnova, H00009958-MO1	1:1000, o/n
UCHL5	UCHL5	R	Epitomics, 3904-1	1:1000, o/n
TOM22 (1C9-2)	TOM22	M	Sigma, sc-58308	1:1000, 1hr
USP30	USP30	R	Gift from Genentech, NA	1:250, o/n
USP28	USP28	R	Bethyl, IHC-00176	1:1000, o/n
USP21	USP21	R	Sigma, HPA028397	1:1000, o/n
USP33	USP33	R	Bethyl, A300-925A	1:1000, 1hr
USP8	USP8	R	Sigma, HPA004869	1:1000, o/n
USP7	USP7	R	Abcam, ab4080	1:1000, 1hr
VPS35	VPS35	G	ABCAM, AB10099	1:1000, o/n

Table 2.12 Primary antibodies for western blotting. (R: rabbit; M: mouse; Sh: sheep; G: goat; NA: Not applicable; o/n: overnight incubation)

Secondary Antibody	**Catalogue No.**	**Dilution**
Donkey anti-mouse IRDye 800CW	926-32212	1:15000
Donkey anti-mouse IRDye 680CW	926-32222	1:15000
Donkey anti-rabbit IRDye 800CW	926-32213	1:15000
Donkey anti-rabbit IRDye 680CW	926-32223	1:15000
Donkey anti-sheep IRDye 800CW	926-32214	1:15000
Donkey anti-sheep IRDye 680CW	926-32224	1:15000

Table 2.13 Secondary antibodies for western blotting.

2.3.10 Immunofluorescence staining

Cells cultured on coverslips were washed three times with room temperature PBS. For most of the immunofluorescence staining, cells were fixed with 4% paraformaldehyde (PFA) in PBS for 15min. PFA was then quenched with 50mM of ammonium chloride in PBS for 10min. Cells were then permeabilised with 0.2% Triton-X100 in PBS for 5min before blocking with 10% goat serum in PBS for 20min.

For LC3 staining, cells were first fixed with 4% PFA in PBS for 15min, followed by permeabilization with methanol for 5min at room temperature before blocking with 10% goat serum in in PBS for 20min.

Next, cells were incubated with primary antibody in 5% goat serum in PBS for 1hr (Table 2.14), followed by three washes with PBS. Cells were then incubated with secondary antibody in 5% goat serum in PBS for 30min (Table 2.15). After that, cells were washed three times with PBS, rinsed with water and mounted onto glass slides with Mowiol plus 4',6-diamidino-2-phenylindole (DAPI). Immunofluorescence images were taken using either a Nikon Ti-Eclipse with a CFI Plan Apo VC 60x oil objective or a Leica confocal SP2 AOBS with a HCX PL APO CS, 63×, 1.40 oil objective.

2.3.11 Live-cell microscopy

Cells were placed in a humidified chamber with 5% CO_2 at 37°C. Images were taken using a Nikon Ti-Eclipse microscope. The Perfect Focus System (PFS) was used to ensure accurate focusing. In specified experiments, DRAQ7 (0.3μM) and annexin V-AF350 (5μl per 1ml) were added to visualize dead cells and apoptotic cells, respectively. Images were captured using a CFI S Plan Fluor ELWD 20x objective. For comparison of different treatment conditions, video collages were made using Nikon NIS-Element software and exported as AVI files. Videos were labeled and time-stamped using ImageJ before being downsized into JPEG format and saved at 3 frames per second.

Antibody name	Target protein	Species	Source/ Cat. No.	Fixation	Dilution
Caspase-3 (Active)	Cleaved Casp-3	R	R&D systems, AF835	PFA	1:200
cPARP (Asp214) clone D64E10	Cleaved PARP	R	Cell Signaling, 5625	PFA	1:400
Cyt-C	Cyt-C	R	BD Pharmigen, 556432	PFA	1:200
FK2	ubiquitin	M	Enzo, PW8810	PFA	1:2000
LC3 clone 5F10	LC3	M	Nanotools, 5F10	PFA & methanol	1:200
Myc Clone 4A6	Myc	M	Millipore, 05-724	PFA	1:500
TOM20	TOM20	M	Sigma , HPA011562	PFA	1:1000

Table 2.14 Primary antibodies used for immunofluorescence staining. (R: rabbit; M: mouse; PFA: paraformaldehyde)

Secondary Antibody	Catalogue No.	Dilution
Donkey anti-mouse AF350	A10035	1:200
Donkey anti-rabbit AF350	A10039	1:200
Donkey anti-sheep AF488	A11015	1:500
Donkey anti-sheep AF594	A11016	1:500
Donkey anti-rabbit AF488	A21206	1:500
Donkey anti-rabbit AF594	A21207	1:500
Donkey anti-mouse AF488	A21202	1:500
Donkey anti-mouse AF594	A21203	1:500

Table 2.15 Secondary antibodies used for immunofluorescence staining. All secondary antibodies were from Invitrogen.

2.4 Mass spectrometry

2.4.1. Materials

HPLC grade Acetonitrile (#20060320) and Water (#23595328) were from VWR (Lutterworth, UK). Trypsin Gold (#V5280) was obtained from Promega (Southampton,UK). LoBind Eppendorf tubes (#022431081) were purchased from Eppendorf (Hamburg, Germany). Stainess steel blades were sourced from Swann-Morton (Sheffield,UK). All other chemicals were obtained from Sigma Aldrich (Poole, UK) unless otherwise stated.

2.4.2 Stable isotope labeling by amino acids in cell culture (SILAC)

HeLa S3 cells were cultured in DMEM with 10% dialyzed FBS (Dundee Cell Products). Different amino acids were supplemented to generate light (L-lysine, Lys0; L-arginine, Arg0), medium (L-lysine-$^{2}H_{4}$, Lys4; L-arginine-$^{13}C_{6}$, Arg6) and heavy (L-lysine-$^{2}H_{6}$-$^{15}N_{2}$, Lys8; L-arginine-$^{13}C_{6}$-$^{15}N_{4}$, Arg10) SILAC labeled cells. All L-lysines were supplemented at 146mg/L and all L-arginines were supplemented at 28mg/L. 200mg/L of L-proline was also supplemented to prevent arginine to proline conversion (Bendall et al. 2008). Cells were grown in the SILAC media for at least five passages prior to use for experiment to ensure maximal isotopic labeling.

2.4.3 In-gel Digestion

Protein samples (40-60µg) were run on a 4-12% NU-PAGE precast gel and stained using Colloidal Blue Staining Kit (Invitrogen) according to manufacturer's instruction. Briefly, the gel was incubated in a fixing solution while gently shaking for 10min (seeTable 2.16), followed by a further 10min incubation in a staining solution (see Table 2.17). 5ml of Stainer B solution was then added into the staining solution and the gel was incubated for 3hr. After that, the staining solution was decanted and the gel was left in 200ml of deionized water and gently shaken overnight at room temperature to remove background staining. The visible protein bands were excised and diced into small pieces using a stainless steel blade. The gel pieces were transferred

into a LoBind eppendorf tube and destained using 20µl of 1:1 volume of 50mM ammonium bicarbonate and 50% acetonitrile (ACN). De-staining was carried out at 37°C for 10min each time. This step was repeated two to three times until gel pieces became transparent. The de-stain solution was discarded and replaced with 20µl of 1.5mg/ml DTT in 100mM ACN and further incubated at 37°C for 30min. The DTT solution was replaced with an equal volume of 55mM chloroacetamide (CAA) and further incubated at 37°C for 30min in the dark. The gel pieces were then dehydrated using 10µl of 100% acetonitrile and incubated at 37°C for 10min. This step was repeated two to three times until gel pieces shrank and turned white. The solvent was removed and the residual solvent was left to evaporate with the lid of the LoBind tube open in a fume hood. 20µl of 1ng/µl of trypsin in 50mM of acetic acid was added to the gel pieces and incubated at 37°C for 1hr. A further 10µl (or more, to completely cover the gel pieces) of ammonium bicarbonate was added and the samples were incubated at 37°C overnight.

The next day, the solution was collected and an equal volume of 1% formic acid was added to the gel pieces and incubated for 20min before combining with the previous solution. The gel pieces were dehydrated by incubation with 100% ACN for 10min and the supernatant was collected in the same tube as the previous step. The collected mixture was dried using SpeedVac Concentrator Plus (Eppendorf) at 60°C. The dried samples were resuspended in 30µl of 0.05% trifluoroacetic acid (TFA).

Reagents	Volume (ml)
Methanol	100ml
Acetic acid	20ml
Ultrapure water	80ml

Table 2.16 Fixing solution for NU-PAGE precast gel.

Reagents	Volume (ml)
Deionized water	55ml
Methanol	20ml
Stainer A	20ml

Table 2.17 Staining solution for NU-PAGE gel.

2.4.4 Detection and identification of peptides

5µl of each sample was loaded on high performance liquid chromatography column coupled to an LTQ-Orbitrap XL (Thermo Fisher) fitted with a Proxeon nanoelectrospray source. Samples were resolved on a 1-62% linear ACN gradient over 21mins. MS spectra were acquired by the Orbitrap at a resolution of 30,000 and MS/MS was performed on the TOP 5 ions. All spectra were acquired using Xcalibur software (version 2.0.7; Thermo Fisher Scientific). Raw MS spectra were searched against human.ipi.library and analyzed using MaxQuant (Cox et al. 2009, Cox and Mann 2008).

2.4.5 Bioinformatic and statistical analysis

The gene ontology (GO) terms of each protein identified were annotated by Database for Annotation, Visualization and Integrated Discovery (DAVID) (Dennis et al. 2003). To maximize the identification of mitochondrial proteins, the list of proteins identified was also cross-referenced to the Mitocarta Database (Pagliarini et al. 2008). The significance A value for the change in SILAC protein ratio of each protein was analysed using Perseus (Cox and Mann 2012).

Chapter 3: Characterisation of Parkin-mediated Mitophagy

3.1 Introduction

Mitophagy is the selective removal of mitochondria by autophagy. Autophagy, similar to proteasomal and lysosomal degradation, involves the ubiquitylation of proteins as a signal for the recruitment of the autophagic machinery (Clague and Urbé 2010). In the context of mitophagy, the best-characterised ubiquitin E3 ligase is Parkin. In this chapter, I describe the work that I carried out to characterise the cell lines to investigate Parkin-mediated mitophagy with the following aims: (1) to assess the level of Parkin in different cell lines, (2) to compare different mitophagic stimuli, and (3) to characterise the ubiquitylation and turnover of mitochondrial proteins during mitophagy.

3.2 Characterisation of cell lines expressing endogenous Parkin

3.2.1 HEK293T cells express endogenous Parkin

I first set out to analyse the levels of endogenous Parkin in a few cell lines available in the laboratory. The cell lines include: HeLa, HeLa S3, MCF7, HEK293T and A549 cells (Figure 3.1A). In addition, I also included a human telomerase reverse transcriptase-immortalised retinal pigment epithelial cell line stably expressing yellow fluorescence-tagged Parkin (hTERT-RPE1-YFP-Parkin) as a positive control (gift from Jon Lane, University of Bristol). As shown in Figure 3.1A, hTERT-RPE1-YFP-Parkin cells express YFP-Parkin at very high levels (indicated by arrow; 77kDa). Of the cells that I have analysed, only HEK293T cells showed a band corresponding to the molecular weight of endogenous Parkin (indicated by §; 51.6kDa). The ratio of protein band intensities (as measured with the Licor ImageStudio software associated with the Odyssey) suggests an approximately 87-fold

overexpression of Parkin in hTERT-RPE1-YFP-Parkin cells compared to HEK293T cells.

Next, I characterised Parkin-mediated mitophagy progression in HEK293T cells (Figure 3.1B). For this, I used carbonyl cyanide *m*-chlorophenyl hydrazone (CCCP), a potent small molecule membrane-permeable protonophore to disrupt the inner mitochondrial membrane potential. Upon CCCP treatment, I observed rapid cleavage of long OPA1 (L-OPA1) to short OPA1 (<4hr). This event occurs only in respiration-compromised mitochondria and serves as a good readout in my experiments to reflect the potency of drugs to induce inner mitochondrial membrane (IMM) depolarization (Ishihara et al. 2006). In addition, PINK1 accumulated in the cells upon CCCP treatment at 4hr and peaked at 8hr. I also observed a gradual increase in a higher molecular weight form of MIRO, indicative of ubiquitinated MIRO, whilst the unmodified form of MIRO and other outer mitochondrial membrane (OMM) and IMM proteins, including TOM20 and TIMM44, remained unchanged over the course of 24hr. Note that the apparent decrease of TIMM44 levels at times 8 and 24hr shown in the representative experiment in Figure 3.1B is most likely due to underloading of the lanes (compare Actin levels of these timepoints).

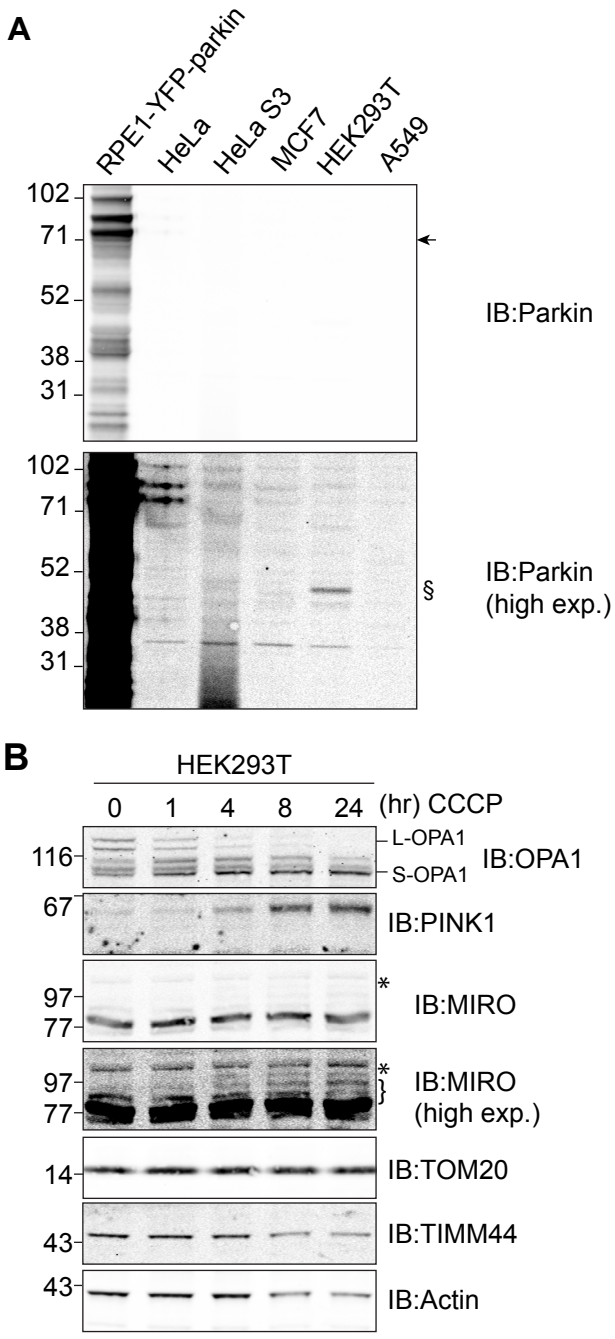

Figure 3.1 Characterisation of endogenous Parkin level in different cell lines.

(A) 20µg of NP40 lysates from hTERT-RPE1-YFP-Parkin, HeLa, HeLa S3, MCF7, HEK293T and A549 cells (non-stimulated) were immunoblotted with Anti-Parkin antibody. Arrow: YFP-Parkin. §: endogenous Parkin. High exp.: Intensity of blots was leveled in Adobe Photoshop to show the higher molecular weight species of MIRO. A representative blot is shown.
(B) HEK293T cells were treated with 10µM of CCCP. Cells were harvested with NP40 lysis buffer at the indicated time. 20µg of lysates were immunoblotted as indicated. Asterisk: non-specific band. Bracket: high molecular weight, ubiquitylated MIRO (n=1).

3.2.2 SH-SY5Y cells express endogenous Parkin

Since Parkin and PINK1 mutations have been associated with neurodegeneration in Parkinson's disease, I also analysed the level of endogenous Parkin and investigated mitophagy in SH-SY5Y cells, a dopaminergic neuroblastoma cell line that is commonly used as an *in vitro* cell model for Parkinson's disease (Xie et al. 2010). Similar to HEK293T cells, CCCP treatment induced accumulation of PINK1 starting at 4hr and peaked at 8hr in SH-SY5Y upon CCCP treatment (Figure 3.2A). I also observed the appearance of high molecular weight forms of MIRO in these cells, indicative of ubiquitylated MIRO. Note that the seemingly gradual loss of TIMM44 over time parallels the decrease in Actin and therefore is most likely due unequal SDS-PAGE to nitrocellulose membrane transfer.

Since the Parkin antibody that I used detected multiple weak bands at high exposures in SH-SY5Y cells, I depleted Parkin by siRNA to visualize the band specific to Parkin (51.6kDa; Figure 3.2B). I found that a fuzzy band above the 43kDa marker was lost upon treatment with Parkin-specific siRNA, indicating that this is the endogenous Parkin. Further characterization work carried out by a colleague in the laboratory (Aitor Martinez) revealed that SH-SY5Y cells weakly express endogenous Parkin compared with hTERT-RPE1-YFP-Parkin cells and at a level similar to endogenous Parkin in HEK293T cells.

I also used oligomycin A and antimycin A (O+A), which are inhibitors of the electron transport chain complex V and complex III, respectively as an alternative, more specific option to depolarise the mitochondria. Upon 24hr of O+A treatment, L-OPA1 is fully converted to S-OPA1. Interestingly the endogenous Parkin is depleted in the non-targeting control siRNA-transfected cells (NT1, Ctrl IX). The low level of endogenous Parkin and its subsequent rapid depletion during mitophagy could potentially explain the general lack of mitophagy in these cells as indicated by the stable levels of TIMM44 over the course of O+A treatment. Surprisingly, PINK1 depletion by siRNA interference did not fully rescue the protein level of endogenous Parkin during O+A treatment.

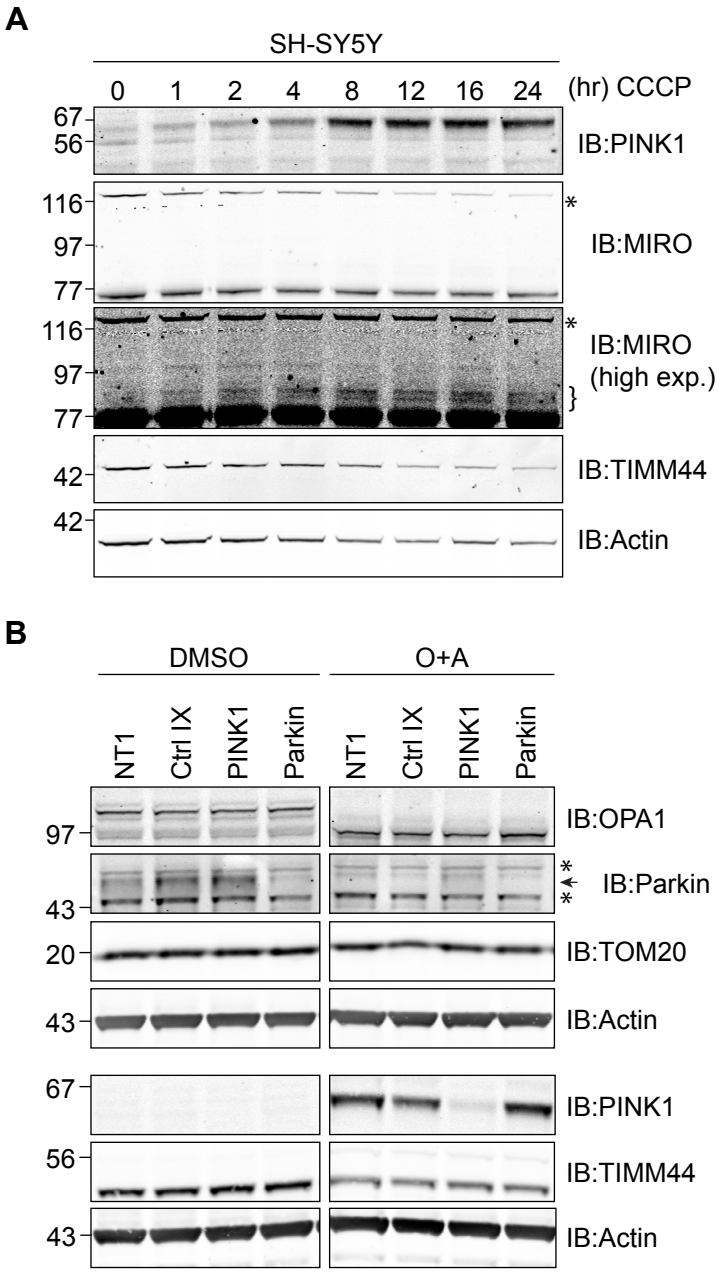

Figure 3.2 Characterisation of Parkin-mediated mitophagy in SH-SY5Y cells.

(A) SH-SY5Y cells were treated with 10μM of CCCP for the depicted time. The cells were then harvested in NP40 lysis buffer and immunoblotted for the respective proteins. Asterisk: non-specific band. Bracket: high molecular weight, ubiquitylated MIRO. A representative blot is shown.
(B) SH-SY5Y cells were transfected with 40nM of either non-targeting controls (NT1 and control IX) or siRNA oligos against PINK1 and Parkin for 72hr. Cells were then treated with 1μM of oligomycin A and 1μM of antimycin A (O+A) for 24hr. Cells were lysed with RIPA lysis buffer and immunoblotted as indicated. Asterisk: non-specific band; arrow: endogenous Parkin (n=1).

3.3 Mitophagy in Parkin-overexpressing cells

Since cell lines with endogenous Parkin expression do not undergo robust mitophagy, I proceeded to induce mitophagy in hTERT-RPE1 cells stably expressing YFP-Parkin (hTERT-RPE1-YFP-Parkin).

3.3.1 Characterisation by immunofluorescence microscopy

I first characterised mitophagy in these cells by immunofluorescence microscopy (Figure 3.3A). I counterstained fixed cells with anti-TOM20 antibody to visualize the mitochondria. Under basal conditions, YFP-Parkin is expressed and localised to the cytosol. YFP-Parkin is recruited to the mitochondria as shown by TOM20 colocalisation as early as 1hr after CCCP treatment. At 4hr, the Parkin punctae gradually form larger perinuclear aggregates. These Parkin-decorated mitochondrial aggregates will henceforth be referred to as Parkin aggregates. At 8hr, approximately 40% of the Parkin aggregates are lost. By 12hr, up to 80% of the cells have undergone complete mitophagy and newly synthesised Parkin is cytosolic again. Cells that do not express Parkin still retain their mitochondria, although these are fragmented.

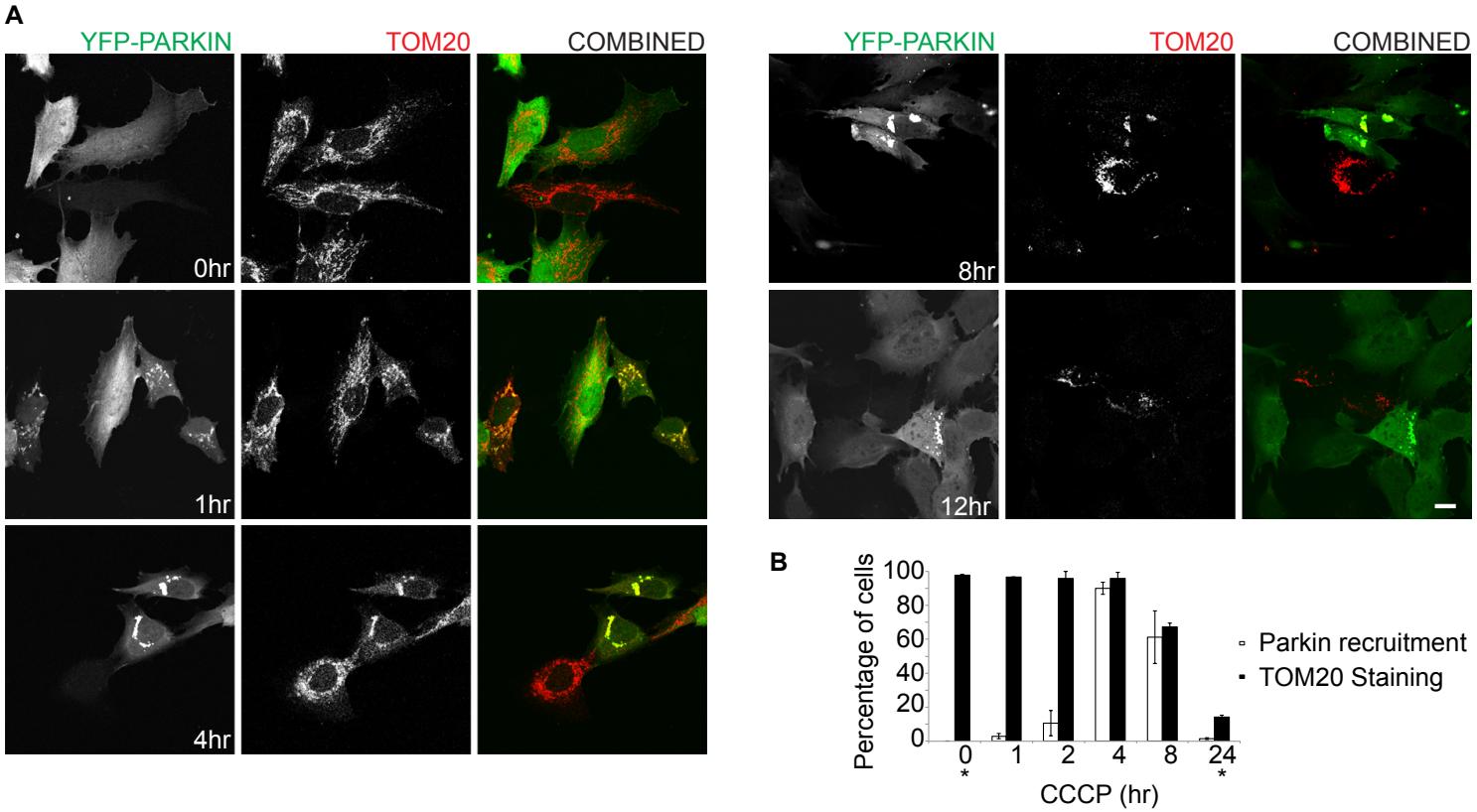

Figure 3.3 Timecourse of CCCP treatment in hTERT-RPE1-YFP-Parkin cells.

(A) hTERT-RPE1-YFP-Parkin cells were treated with CCCP for the indicated times. The cells were fixed and stained with anti-TOM20 (mouse). Single confocal sections were taken using a Leica confocal microscope at 63x magnification. Scale bar: 10μm.
(B) The number of cells that showed Parkin recruitment (colocalisation with TOM20) and the number of cells that are positive for TOM20 staining were counted and expressed as a percentage of total cells. ~200 cells per condition were quantified. Error bar represents standard deviation of 3 or 5 (*) independent experiments.

3.3.2 Western blot analysis of mitophagy

I also assessed the progression of mitophagy biochemically using western blotting. To this end, I compared lysates from hTERT-RPE1-YFP-Parkin cells in parallel with those from SH-SY5Y and also hTERT-RPE1 cells (Figure 3.4). In all three cell lines, PINK1 gradually accumulates over time. The accumulation of PINK1 is slower and weaker in SH-SY5Y cells. The OMM protein, MIRO, is ubiquitinated upon CCCP treatment in SH-SY5Y and hTERT-RPE1-YFP-Parkin cells but not in the parental hTERT-RPE1 cells. Nonetheless, the ubiquitylation pattern of MIRO is different in SH-SY5Y cells and hTERT-RPE1-YFP-Parkin cells. The data also show that both OMM and IMM proteins, as represented by MIRO and TIMM44 respectively, are only visibly degraded when there is an excessive amount of Parkin. I also observed an intriguing increase in the accumulation of PARP-p85, a cleaved fragment of PARP (Poly ADP-ribose polymerase) that is cleaved by caspase 3 during apoptosis (Tewari et al. 1995). This observation will be further discussed in detail in chapter 4.

3.3.3 Spatial and temporal analysis of PINK1 accumulation and Parkin activation

To further characterise the accumulation of PINK1 at the OMM and Parkin recruitment to the mitochondria in hTERT-RPE1-YFP-Parkin cells, I carried out a crude mitochondria enrichment (Figure 3.5). As controls for the mitochondria enrichment, I probed for different mitochondrial proteins, including MIRO (OMM protein), TIMM44 (IMM protein) and Cyt-C (mitochondria intermembrane space protein). These proteins were only present in the mitochondria-enriched fraction (MF). CCCP treatment also led to ubiquitylation of MIRO, as shown by the characteristic ubiquitin laddering that appeared at 2-4hr after CCCP treatment. MIRO, TIMM44 and Cyt-C levels decreased at 6hr of CCCP treatment. Interestingly, PINK1 and Parkin were present both in the post-mitochondrial supernatant (PMS) and the MF.

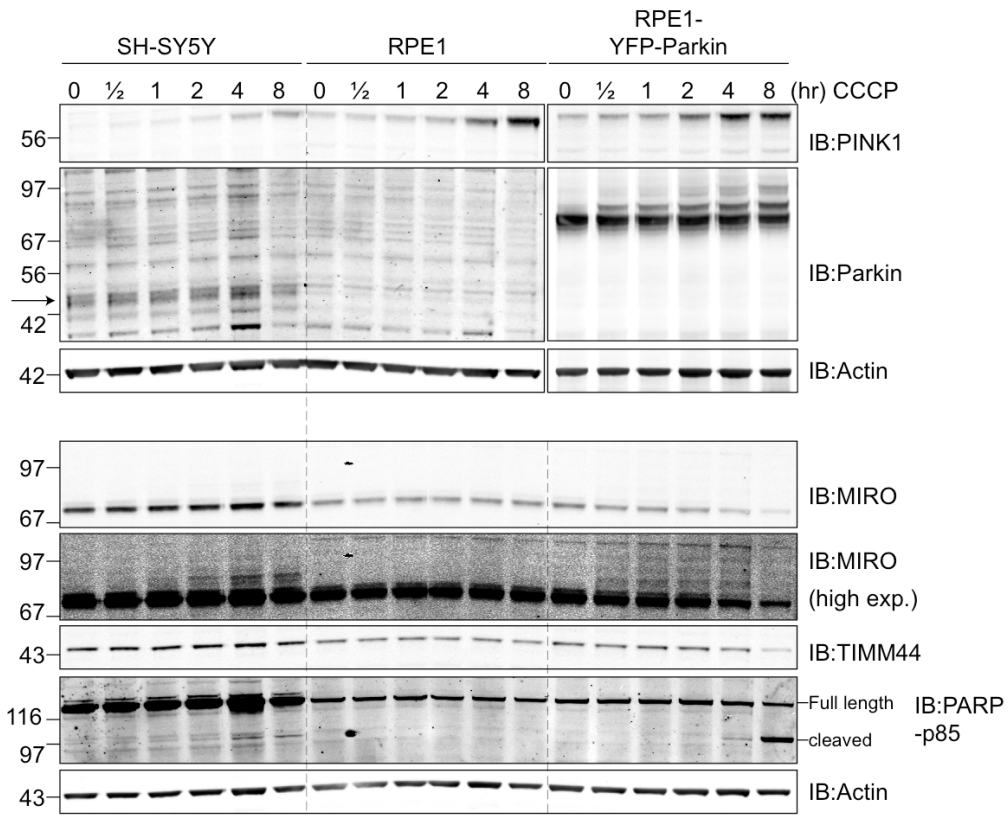

Figure 3.4 Comparative biochemical dissection of the progression of mitophagy in SH-SY5Y, hTERT-RPE1 and hTERT-RPE1-YFP-Parkin cells.

The three different cell lines were treated with 10μM of CCCP for the indicated times. The cells were lysed in NP40 lysis buffer and probed for the depicted proteins. For the PINK1 and Parkin western blot, the RPE1-YFP-Parkin lysate samples were resolved and exposed separately to that for SH-SY5Y and RPE1. A representative blot is shown. Arrow: Endogenous Parkin.

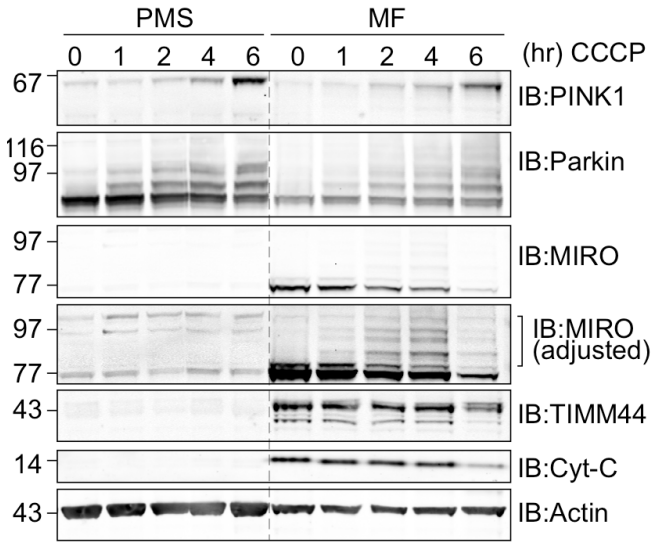

Figure 3.5 Spatial and temporal analysis of PINK1 and Parkin localisation during CCCP treatment.

hTERT-RPE1-YFP-Parkin cells were treated with CCCP (10μM) and harvested in PBS by gently scraping the cells using a rubber policeman at the indicated times. Mitochondria fractions (MF) were enriched using the crude mitochondria fractionation method (described in chapter 2, section 2.3.5) and resuspended in RIPA lysis buffer. 10μg of lysates from each fraction were resolved to probe for the indicated proteins. Shown is a representative blot. PMS: post-mitochondrial supernatant; MF: mitochondrial fraction. Bracket: Ubiquitin laddering of MIRO.

3.4 Optimisation of mitophagy-stimuli

3.4.1 Selection of drugs to induce mitophagy in hTERT-RPE1 cells

Mitophagy is generally triggered by the loss of mitochondrial membrane potential, whereupon, PINK1 fails to be imported into the mitochondria, interacts with the TOM complex and recruits Parkin to the mitochondrial outer membrane (Jin et al. 2010). The experiments I described prior to this section were mostly carried out using CCCP treatment. Although CCCP has been widely used in the study of mitophagy, its non-selective ability to increase proton conductance in any organellar membrane also extends to the lyososomal membrane, raising concern on its effect on the lysosome during autophagy (Padman et al. 2013). Therefore, I compared CCCP-induced mitophagy with a selection of other chemical compounds (see Table 3.1).

Chemicals	Description and mechanism of action
CCCP	Small membrane permeable ionophore; depolarizes mitochondrial membrane potential (and dissipates proton gradients in other membranes)
Rotenone	Inhibitor for electron transport chain (ETC) complex I (NADH-coenzyme Q reductase)
Oligomycin A	Inhibitor of the ETC complex V (F0/F1-ATP synthase)
Antimycin A	Inhibitor of the ETC complex III (Cytochrome C oxidoreductase)

Table 3.1 Selection of chemical compounds tested to induce mitophagy

3.4.2 Carbonyl cyanide C-chlorophenyl hydrazine (CCCP)

CCCP was the first choice to induce mitophagy as it has been extensively used in the field to induce mitochondrial membrane depolarization. In earlier experiments, I took reference from published literature and used 10μM of CCCP to induce mitophagy (general working concentration of CCCP ranges from 5-20μM) (W. X. Ding et al. 2010, MacVicar and Lane 2014, Tanaka et al. 2010, Narendra et al. 2010, Narendra et al. 2008, Sarraf et al. 2013). Since I can observe robust translocation of Parkin to the mitochondria and also the loss of mitochondrial proteins, I decided not to increase the concentration of CCCP to avoid non-specific effects. Instead, I tested lower concentrations of CCCP. 0.1 or 1μM of CCCP were not sufficient to induce Parkin recruitment to the mitochondria in these cells (Figure 3.6).

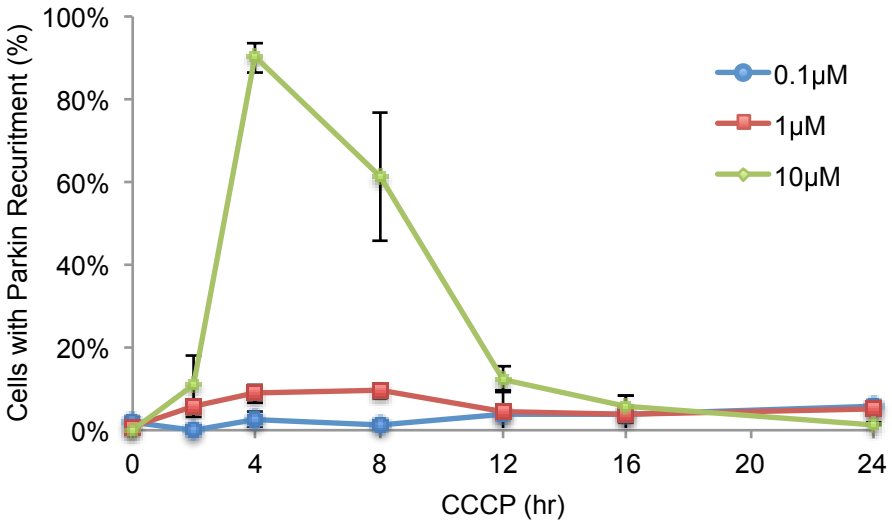

Figure 3.6 Titration of CCCP concentration in hTERT-RPE1-YFP-Parkin cells.

hTERT-RPE1-YFP-Parkin cells were treated with 0.1, 1 and 10μM of CCCP up to 24hr. The cells were fixed in 4% PFA and mounted onto glass slides using Mowiol with DAPI. 200 cells per condition were counted. Error bar represents standard deviation of 3 independent experiments.

3.4.3 Rotenone does not induce mitophagy

We asked if a more specific inhibitor of the mitochondrial ETC could induce mitophagy. I first tested rotenone, a compound that selectively inhibits NADH oxidation via the NADH-ubiquinone oxide reductase complex (complex I) (Hartley et al. 1994). As shown in Figure 3.7, 10μM of CCCP efficiently induced mitophagy in hTERT-RPE1-YFP-Parkin cells. In contrast, 100nM of rotenone did not induce mitophagy, as evidenced by the lack of TOM20 and TIMM44 degradation. Moreover, rotenone treatment did not induce L-OPA1 cleavage, a process that depends on mitochondria depolarisation in either parental or Parkin-overexpressing hTERT-RPE1 cells. This suggests that rotenone treatment alone is insufficient to trigger mitochondrial damage.

I further titrated the concentration of rotenone ranging from 0.1μM to 100μM for 8hr (Figure 3.7B). No OPA1 cleavage or PINK1 recruitment was observed. In addition, both MIRO and TIMM44 levels remained unchanged at all concentrations of rotenone. At higher concentrations (10μM and 100μM), I observed slightly higher levels of both LC3-1 and LC3-II. I concluded that rotenone does not induce mitophagy, although it may induce some general autophagy in these cells.

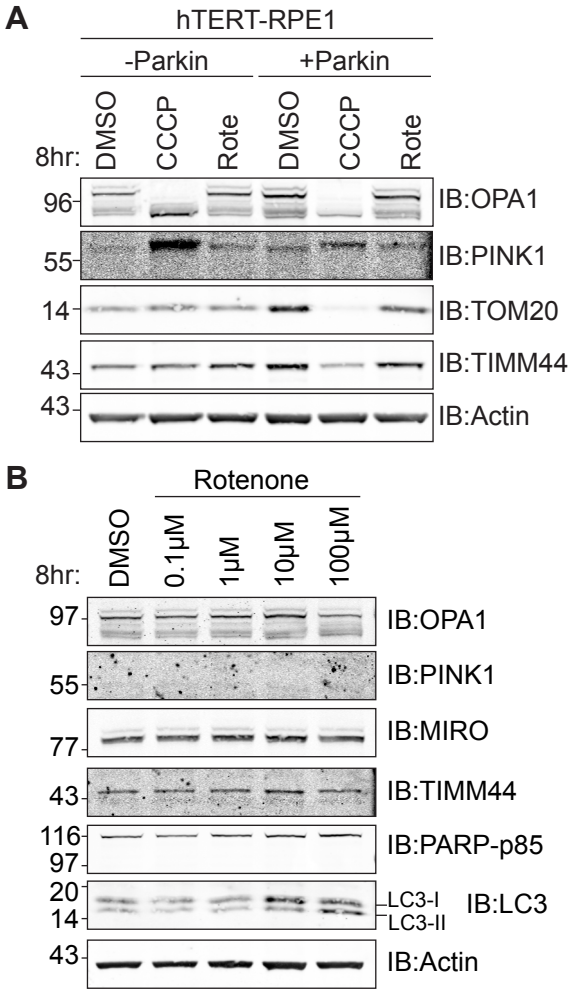

Figure 3.7 Comparison of CCCP and rotenone treatment for mitophagy induction.

(A) hTERT-RPE1 (parental and YFP-Parkin expressing) cells were treated with 10μM of CCCP or 100nM of rotenone for 8hr. Cells were lysed in RIPA lysis buffer. 10μg of lysates were immunoblotted as indicated.
(B) hTERT-RPE1-YFP-Parkin cells were treated with varying concentration of rotenone (0.1μM to 100μM) for 8hr. Cells were lysed in RIPA lysis buffer. 10μg of lysates were immunoblotted as indicated.

3.4.4 Oligomycin A and antimycin A synergistically induce mitophagy

Oligomycin A and antimycin A are inhibitors of the ETC complex V and III, respectively. To test if these two drugs induce mitophagy in hTERT-RPE1-YFP-Parkin cells, I followed their effects using live-cell imaging of YFP-Parkin. Treatment with either of these two drugs individually at 0.1 and 10μM did not induce any Parkin recruitment, up to 12hr of exposure. At a higher concentration (100μM), 90% of the antimycin A treated cells show Parkin recruitment (Figure 3.8). Oligomycin A treatment at 100μM did not induce any Parkin recruitment. However, approximately 90% of the cells simultaneously treated with just 100nM of oligomycin A and antimycin A underwent Parkin recruitment. Moreover, the kinetics of Parkin recruitment, increased with the concentration of the drugs.

The induction of mitophagy by oligomycin A and antimycin A can also be seen with western blotting, as Parkin was autoubiquitylated 1hr after application (Figure 3.2). It is also apparent that 10μM of CCCP and 1.0μM of oligomycin A and Antimycin A (O+A) treated cells had faster OPA1 cleavage (1hr instead of 4hr) compared to 0.1μM of O+A. In addition, MIRO degradation is also enhanced (seen first at 1hr instead of 4hr). Similar to CCCP treatment, I observed PARP cleavage with O+A treatment, reflecting the presence of cell death during the treatment. The level of PARP-p85 directly correlates with the concentration of O+A used.

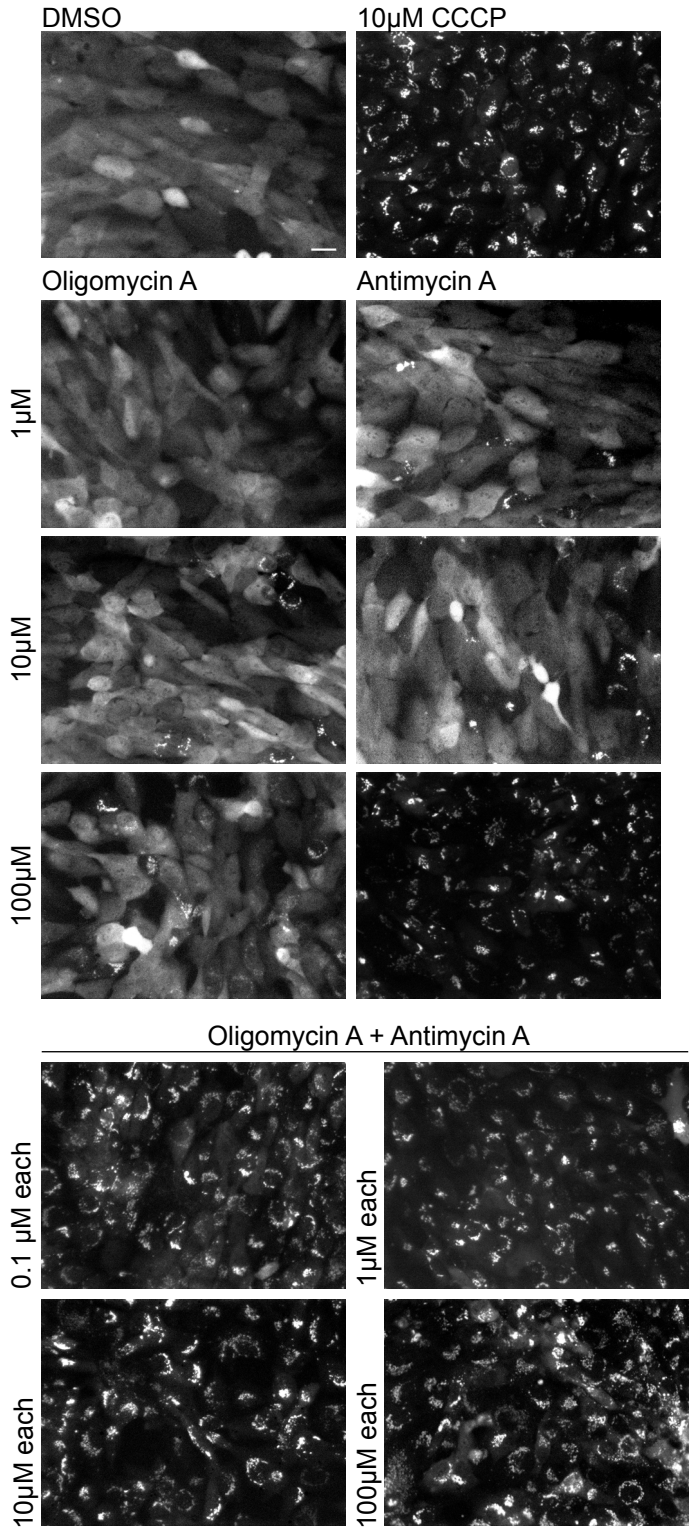

Figure 3.8 Simultaneous treatment of oligomycin A and antimycin A induced Parkin recruitment.

hTERT-RPE1-YFP-Parkin cells were treated with DMSO, CCCP (10μM) and different concentrations of oligomycin A and antimycin A as indicated. YFP-Parkin recruitment was monitored by live-cell imaging. Images show representative still frames at 4hr of treatment. Scale bar: 20μm.

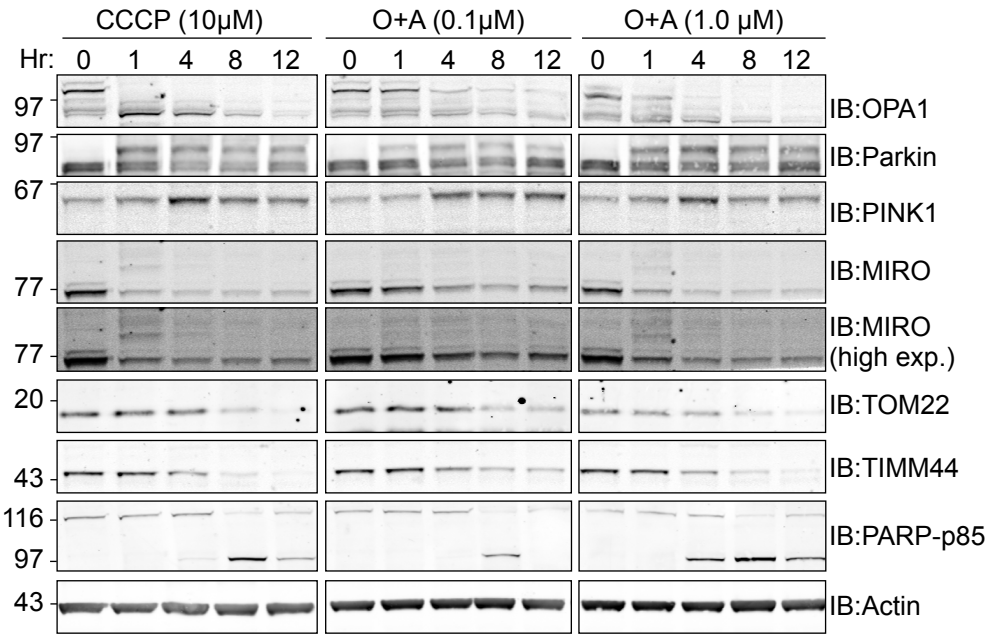

Figure 3.9 Comparison of CCCP, Oligomycin A and Antimycin A treatment.

hTERT-RPE1-YFP-Parkin cells were treated with either 10μM of CCCP or oligomycin A and antimycin A (O+A; 0.1μM each or 1μM each) for the indicated times. The cells were harvested with NP40 lysis buffer supplemented with mammalian protease inhibitor. 10μg of lysates were immunoblotted as indicated. Shown is a representative blot.

3.5 Discussion

In this chapter, I summarized the work I carried out to characterise the expression of Parkin in several cell lines and the link between Parkin expression level and the ability of cells to undergo mitophagy. Of the cell lines that I have tested, I observed no endogenous Parkin expression in HeLa or A549 cells. Consistent with the literature, SH-SY5Y and HEK293 cells, from which HEK293T cells are derived from, express endogenous Parkin and are commonly used in the field to study Parkin biology (Van Humbeeck et al. 2011a, Narendra et al. 2008, Van Humbeeck et al. 2011b, Zhao et al. 2003, Ren et al. 2003, Finney et al. 2003). Endogenous Parkin levels in HEK293T and SH-SY5Y cells were expressed at very low levels and high intensity imaging was required during western blotting to visualize the band. Upon mitochondrial depolarization in HEK293T and SH-SY5Y cells using CCCP and O+A, respectively, I found that MIRO is ubiquitylated. However, the unmodified form of MIRO and other mitochondrial markers,

including TOM20 (OMM protein) and TIMM44 (IMM protein) were not degraded.

Importantly, I found that 24hr of O+A treatment in SH-SY5Y cells depleted endogenous Parkin. This observation is consistent with the notion that mitochondrial depolarization induced PINK1-dependent activation of the E3 ligase activity of Parkin, leading to its self-ubiquitylation and proteasomal degradation (A. Rakovic et al. 2013, Shiba-Fukushima et al. 2012). It has previously been demonstrated that in the presence of two E2 conjugating enzymes, UbcH7 and UbcH8, Parkin has the ability to self-ubiquitylate and target itself for proteasomal degradation both *in vivo* and *in vitro* (Zhang et al. 2000). Finney and colleagues further demonstrated using truncated Parkin constructs that the self-ubiquitylation and degradation of Parkin is dependent on the N-terminal UBL, without which, the level of the truncated Parkin is markedly stabilised (Finney et al. 2003).

While translocation of endogenous Parkin to depolarized mitochondria has been demonstrated in HEK293 and SH-SY5Y, endogenous Parkin in general does not induce robust mitophagy. In most studies in the literature, stable cell lines overexpressing Parkin are employed to amplify the effect of Parkin-mediated mitophagy (Aleksandar Rakovic et al. 2013, Narendra et al. 2008). Most notably, Grenier and colleagues reviewed and compared comprehensively the differences in the response of immortalized cell lines and primary neurons to CCCP (Grenier et al. 2013). They hypothesized that primary neurons, unlike immortalized cells, are heavily dependent on mitochondria for ATP generation via oxidative phosphorylation (OXPHOS) and are incapable of utilizing glycolysis to generate energy (Almeida et al. 2001). Subsequently, complete degradation of mitochondria is unlikely a default mechanism of these cells upon mitochondrial depolarisation. This hypothesis is further supported by Kanki and Klionsky (2008) who demonstrated that amino acid starvation of yeast cultured in non-fermentable carbon source (lactate) induced low level of mitophagy while amino acid starvation of yeast cultured in fermentable carbon source (glucose) induced high levels of mitophagy (Kanki and Klionsky 2008). In mammalian cells,

MacVicar and colleagues have also made similar observations. Conditioned in galactose-based medium, hTERT-RPE1 cells become resistant to CCCP-induced OPA1 cleavage by OMA1 and therefore are more resistant to mitophagy (MacVicar and Lane 2014). These reports suggest that global mitophagy is unlikely to be the 'default' mechanism for neuronal and OXPHOS-dependent cells in the face of complete mitochondrial depolarization by CCCP as this could severely affect the bioenergetics in neuronal cells. Instead, it is likely that the low and 'self-limiting' endogenous level of Parkin exists in neuronal cells to selectively remove small pools of dysfunctional mitochondria from the healthy population of mitochondria.

I next characterised mitophagy induction in Parkin-overexpressing hTERT-RPE1 cells. This cell line was kindly provided to us by Jon Lane and has previously been shown to undergo bulk mitophagy upon CCCP treatment (MacVicar and Lane 2014). CCCP induced rapid recruitment of Parkin to the surface of mitochondria within the first 4hr of treatment. At 12hr, most of the cells have cleared their Parkin aggregates. Titration on the concentration of CCCP showed that that 10μM of CCCP is the minimal concentration that is required to induce mitophagy in these cells. Intriguingly, CCCP treatment at 8hr also induced cell death in these cells. The cell death was observable under the light microscope and was further confirmed by western blotting with anti-PARP-p85 antibody. Since Parkin-mediated mitophagy has been reported to confer cytoprotection, this observation is unexpected and is further characterised in Chapter 4 (Ekholm-Reed et al. 2013, Johnson et al. 2012).

Another important question in Parkin-mediated mitophagy concerns the type of stimuli that should be used to induce mitochondrial damage. Carbonyl cyanide m-chlorophenylhydrazone (CCCP) is the most commonly used chemical compound to depolarize the mitochondria. CCCP is a lipid-soluble weak acid that acts as a protonophore, capable of increasing the conductance of lipid bilayers by several order of magnitude (Kasianowicz et al. 1984). This property of CCCP has been applied to dissipate the proton gradient that is actively generated by the electron transport chain, thereby

collapsing the inner mitochondrial membrane potential and inhibiting ATP generation by OXPHOS. However, CCCP does not specifically target the inner mitochondrial membrane only. Instead, CCCP depolarizes any organellar membranes with proton gradient, including the lysosomes and peroxisomes (Jankowski et al. 2001, Padman et al. 2013). Since autophagosomes fuse with lysosomes at the later stage of autophagy, the use of CCCP raises concern whether lysosome acidification could be inhibited with CCCP treatment. Currently, the jury is still out as opposing observations were made on the effect of CCCP on the lysosome. Padman and colleagues demonstrated using electron microscopy that remnants of mitochondria remains in cells after 24hr of CCCP treatment (20μM) in HeLa cells expressing Parkin (Padman et al. 2013). On the other hand, Ding et al. reported the release of GFP from GFP-LC3 during CCCP treatment (30μM) as evidence for functional lysosomes in the same cell line as the former (Wen-Xing X. Ding et al. 2010). In my case, CCCP treatment (10μM) on hTERT-RPE1-YFP-Parkin cells induced Parkin activation and also loss of the IMM protein, TIMM44. Since IMM proteins are inaccessible to the proteasome, the loss of IMM proteins during mitophagy is generally considered to take place via the autolysosomal pathway. Therefore, it is most likely that CCCP does not affect the lysosomal activity in these cells. However, to unequivocally address this issue, one should measure the pH of the lysosome (for example, using lysotracker or acridine orange) or the degradation of a known lysosomal substrate such as the epidermal growth factor receptor (EGFR) (Pierzynska-Mach et al. 2014, Opresko et al. 1995).

Epidemiological studies showed correlation between the exposure of pesticides and increased risk of Parkinson's Disease (PD) (Gorell et al. 1998, Menegon et al. 1998). Interestingly, exposure to rotenone, a high affinity inhibitor of the ETC complex I that is commonly used as a broad-spectrum insecticide and pesticide, has also been associated with an increased risk of Parkinson's Disease. Rotenone-treated rats exhibited many characteristics of PD, including nigrostriatal dopaminergic degeneration caused by caspase 3 activation and Lewy body-like cytoplasmic inclusions with alpha-sycnuclein accumulation ((Betarbet et al. 2000, Betarbet et al. 2002, Sherer et al. 2002,

Alam and Schmidt 2002, Sherer et al. 2003a, Sherer et al. 2003b). In addition, exposure of rats to another ETC complex I inhibitor, 1-methyl-4-phenyl-2,3-dihydropyridinium (MPP+), the active metabolite of *N*-methyl-4-phenyl-1,2,3,6-tetrahydropyridine (MPTP), also induced similar Parkinson-like symptoms.

Therefore, I sought to determine if inhibition of ETC complex I by rotenone treatment could induce mitophagy in hTERT-RPE1-YFP-Parkin cells. Using rotenone concentrations ranging from 100nM to 100μM, I did not observe any loss of MIRO or TIMM44 up to 8hr of treatment. This observation is consistent with most studies, which showed that inhibition of the ETC complex I with rotenone does not induce mitophagy (Tanaka et al. 2010, Chan et al. 2011). Chan et al. (2011) suggested that localized mitochondrial dysfunction *per se* might not be sufficient to induce activation of Parkin. Instead, a severe mitochondrial depolarisation is required for the recruitment and activation of Parkin at the mitochondria (Chan et al. 2011). Indeed, it has been shown that rotenone treatment has a modest effect on overall ATP production in cells (30% decrease at 1μM of rotenone treatment) and even less effect on mitochondria depolarization (10%) (Chu et al. 2013, Li et al. 2003). Nonetheless, long duration of rotenone treatment induces a chronic accumulation of ROS and has been shown to trigger cell death after 36hr of treatment in HL-60 (human promyelocytic leukemia cells) and HT-1080 (human fibroscarcoma cells) (Li et al. 2003). Since I only treated my cells with rotenone for 8hr, this might explain the lack of visible changes in the cells. It is worth noting that rotenone (1μM) has recently been shown to induce mitophagy independent of Parkin and p62 recruitment in rat cortical neurons (Chu et al. 2014, Chu et al. 2013). This rotenone-induced mitophagy is mediated by the externalisation of cardiolipid, a diphosphatiylglycerol lipid that normally exists in the IMM, which subsequently recruits LC3 directly to the mitochondria (Chu et al. 2014, Chu et al. 2013).

I also investigated the effect of chemical inhibition of complex III and complex V of the ETC by antimycin A and oligomycin A, respectively on Parkin recruitment to the mitochondria. At 10μM or lower concentrations, oligomycin

A and antimycin A did not induce Parkin recruitment to the mitochondria. At 100μM, antimycin A induced Parkin recruitment. Simultaneous treatment of antimycin A and oligomycin A (O+A) effectively induced mitophagy at a concentration as low as 100nM each. 1μM each of O+A treatment induced similar Parkin activation and mitophagy kinetics as CCCP treatment. This finding corroborates with most of the studies on Parkin-mediated mitophagy, which reported that O+A treatment effectively induces mitophagy, in a similar fashion to CCCP treatment (Vives-Bauza et al. 2010, Allen et al. 2013, Hollville et al. 2014). Intriguingly, I observed PARP cleavage during O+A and CCCP treatment. This observation is further characterised in the next chapter.

3.6 Conclusion

In conclusion, through the work presented in this chapter, I showed that endogenous levels of Parkin are insufficient to induce bulk mitophagy. Overexpression of Parkin at high levels is required for global clearance of mitochondria. I also investigated the ability of different chemical compounds to induce mitophagy. CCCP, as a non-selective membrane depolarizer, effectively induced mitophagy. Simultaneous inhibition of the ETC complex III and complex V by antimycin A and oligomycin A, respectively, also induced mitophagy whereas the ETC complex I inhibitor, rotenone, did not. These characterization studies lay the foundation for my subsequent work to develop an assay to screen for deubiquitylase(s) that are involved in Parkin-mediated mitophagy.

Chapter 4: PINK1/Parkin-mediated Mitophagic Cell Death

4.1 Introduction

PINK1 and Parkin mutations associated with Parkinson's Disease are recessive, and the loss of their kinase and E3 ligase functions, respectively, are detrimental for cell survival. Consistent with their cytoprotective roles, PINK1 and Parkin expression have been reported to reduce protein aggregations and increase longevity in flies (Anil Rana et al. 2013). In this chapter, I describe a contradicting observation: induction of mitophagy in Parkin-overexpressing hTERT-RPE1 cells induces cell death in a small population of cells. Intriguingly, proteasome inhibitor halts this type of mitophagic cell death.

4.2 PINK1 depletion protects hTERT-RPE1 cells against cell death

Since PINK1 acts upstream of Parkin in the induction and progression of mitophagy, depletion of PINK1 by siRNA transfection provides a good control to assess the siRNA transfection efficiency. It also serves as a positive control for mitophagy induction (See Video 1). Upon CCCP treatment, the control cells (NT1) accumulate PINK1 and lose MIRO and TIMM44 (Figure 4.1A). On the contrary, depletion of PINK1 prevents the loss of MIRO and TIMM44. LC3 conversion from LC3-I (top band) to LC3-II (bottom band) occurs in both conditions, indicating that the activation of general autophagy is not dependent on PINK1, but rather, is triggered by the accumulation of intracellular ROS levels in response to CCCP treatment. Intriguingly, I consistently observed cell death at the late stages of CCCP treatments (6-8hr), as reflected by the appearance of PARP-p85, a cleaved PARP fragment that is generated by activated caspase 3 during apoptosis (Tewari et al. 1995). This observation is also confirmed by live-cell imaging of the progression of mitophagy upon CCCP treatment (Video 1 and Figure 4.1B). A membrane impermeable dye (DRAQ7) that is only taken up by membrane-

compromised (dead) cells was added to the medium during CCCP treatment to visualize dead cells. A striking accumulation of DRAQ7-positive cells (pink spot) was observed over time only in control but not PINK1-depleted cells.

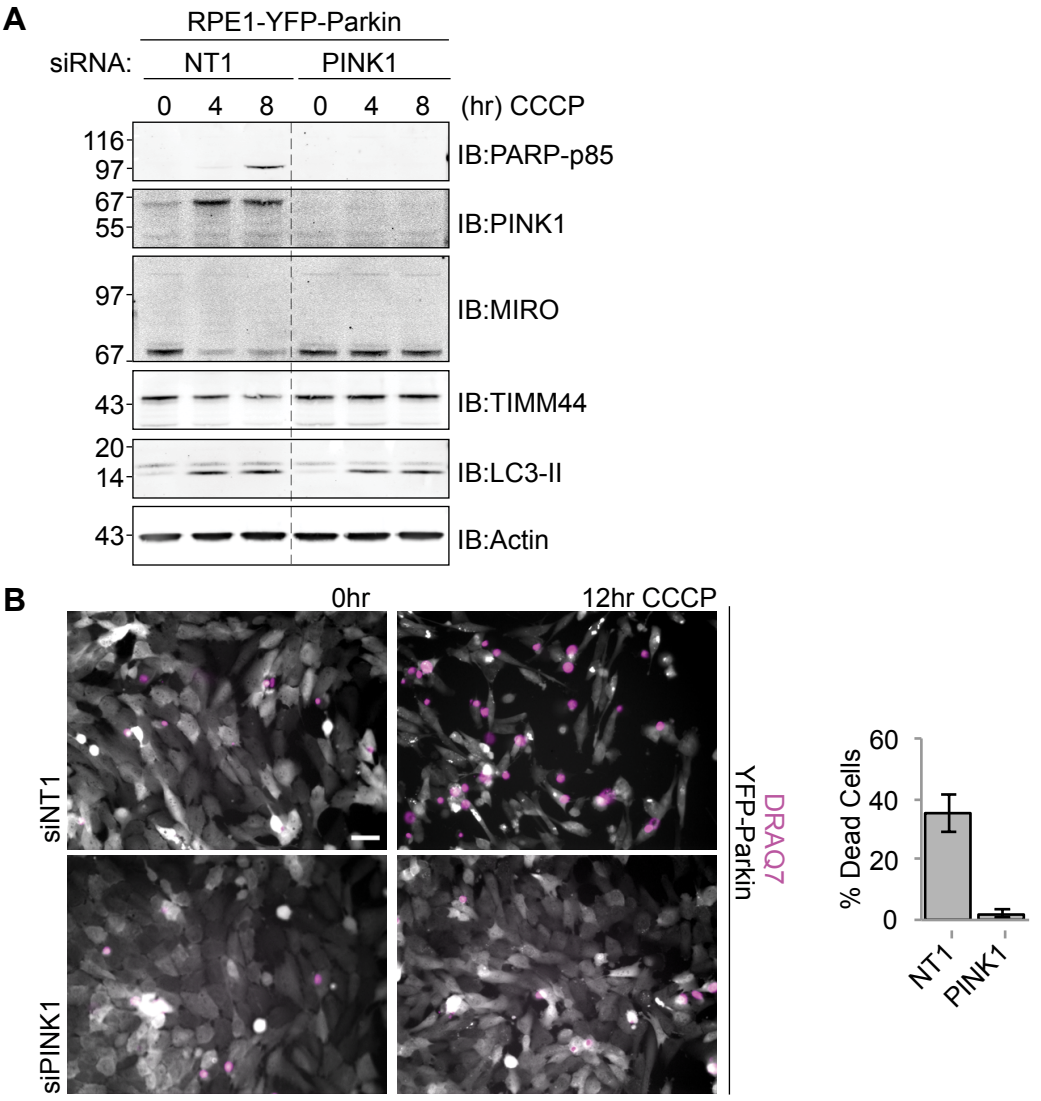

Figure 4.1 siRNA depletion of PINK1 in hTERT-RPE1-YFP-Parkin cells protects against cell death.

(A) hTERT-RPE1-YFP-Parkin cells were transfected for 72hr with either a non-targeting control siRNA oligo (NT1) or siRNA oligo targeting. Cells were then treated with CCCP (10μM) and lysed with NP40 lysis buffer at the indicated times. 15μg of lysates were probed with the indicated antibodies.
(B) hTERT-RPE1-YFP-Parkin cells were transfected as described in (A). Cells were then treated with CCCP (10μM) in the presence of a membrane impermeable dye, DRAQ7 (0.3μM). Images were taken at 15min interval with Nikon Ti-Eclipse and CFI S Plan Fluor ELWD 20x objective. Shown are frames before and after CCCP treatment (T=12hr). Scale bar: 40μm.

4.3 Mitophagic cell death is dependent on Parkin

Since PINK1 and Parkin act in concert to promote mitophagy, the role of Parkin in the observed cell death was also investigated. To this end, I compared parental hTERT-RPE1 cells and hTERT-RPE1-YFP-Parkin cells (Figure 4.2A). While PINK1 accumulates in both cell lines during CCCP treatment, PARP cleavage (PARP-p85) is only observed in hTERT-RPE1-YFP-Parkin cells. It is worth noting that the full length PARP (FL) was not observed consistently across different experiments. This may not be surprising as the antibody used was raised to detect cleaved PARP fragment (PARP-p85; Cell Signaling, 9546). YFP-Parkin is auto-ubiquitylated during CCCP treatment, indicating that Parkin is activated and mitophagy is taking place.

In addition, siRNA-mediated depletion of Parkin in hTERT-RPE1-YFP-Parkin cells also partially reduced the levels of PARP-p85 (Figure 4.2B). The very high Parkin expression level in these cells makes it difficult to fully deplete Parkin. Nevertheless, reduction of Parkin levels clearly protected the cells from apoptosis whilst mitochondrial protein degradation (MIRO and TIMM44 loss) was not affected. This suggests that the residual Parkin levels are sufficient for mitophagy and it is the excessive levels of Parkin that cause cell death.

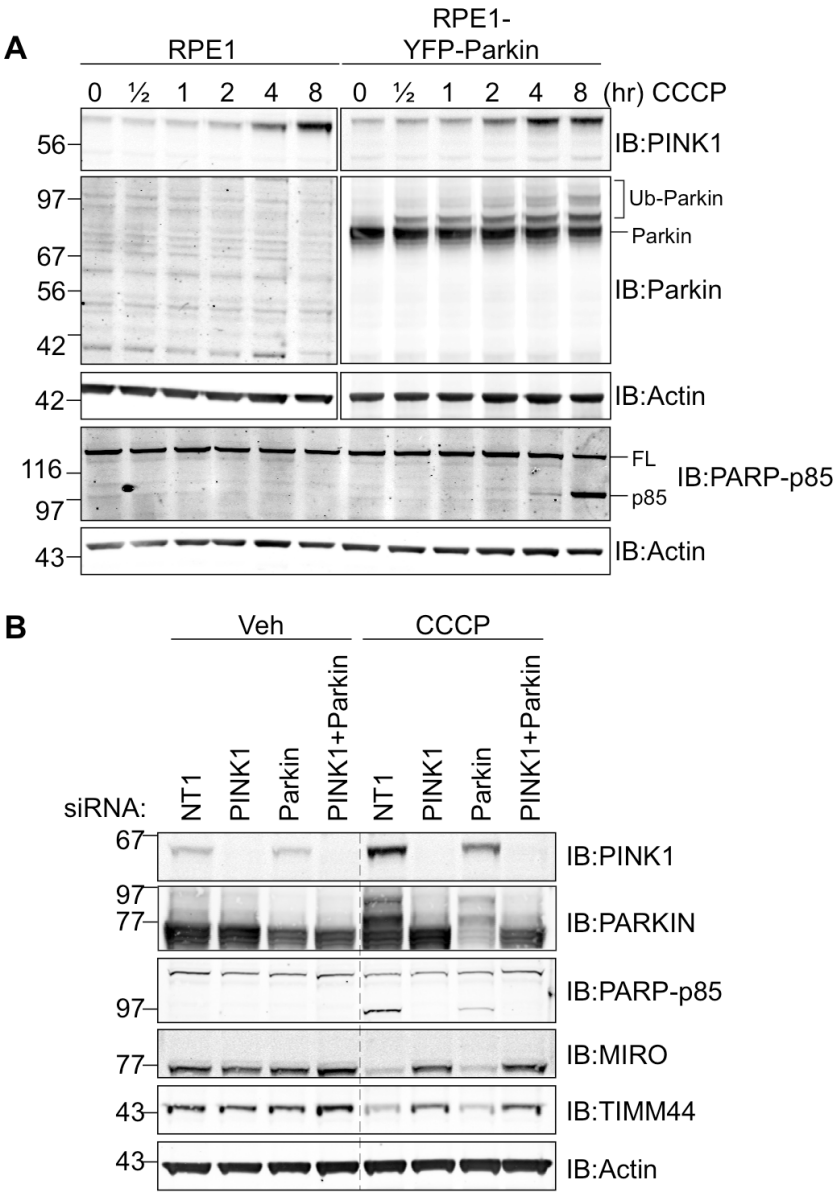

Figure 4.2 Parkin expression is required for mitophagic cell death.

(A) Parental hTERT-RPE1 cells and hTERT-RPE1-YFP-Parkin cells were treated with CCCP (10μM). Cells were lysed in NP40 lysis buffer at the indicated times. and 15μg of lysates were probed with the indicated antibodies. FL: full length PARP; p85: p85 fragment of PARP. Note that this is the same blot as shown in Fig 3.4.

(B) hTERT-RPE1-YFP-Parkin cells were transfected for 72hr with either non-targeting siRNA control (NT1), siRNA targeting PINK1 or siRNA targeting Parkin. Cells were then treated with CCCP (10μM) for 8hr and lysed with RIPA lysis buffer. 15μg of lysates were probed with the indicated antibodies.

4.4 Dissection of the Parkin-dependent mitophagy pathway and cell death using inhibitors of protein degradation

Next, I wanted to know if the cell death observed is a consequence of proteasomal degradation of OMM proteins or the end result of autolysosomal degradation. To understand this, I inhibited the proteasome and the lysosome using epoxomicin and folimycin, respectively. In addition, I also inhibit p97, an AAA-ATPase that has been described to extract OMM proteins for proteasomal degradation, using DBeQ (Chou et al. 2011, Xu et al. 2011).

4.4.1 Different cell fates with selective inhibition of the proteasomal and lysosomal degradation pathways

Co-treatment of cells with CCCP and epoxomicin, the proteasome inhibitor, accumulated MIRO in both unmodified and higher molecular weight, ubiquitylated forms. On the other hand, co-treatment of cells with CCCP and folimycin, a vacuolar ATPase inhibitor, inhibited the degradation of TIMM44 and promoted the accumulation of LC3-II. Unexpectedly, folimycin treatment partially affects the turnover of MIRO. This suggests that MIRO turnover (and possibly other OMM proteins) during mitophagy is not strictly dependent on the proteasome. On the other hand, epoxomicin treatment also partially prevented CCCP-induced loss of TIMM44, suggesting that proteasomal degradation of OMM proteins is required for the progression of mitophagy. Strikingly, co-treatment of hTERT-RPE1-YFP-Parkin cells with CCCP and proteasomal inhibitor (Epoxomicin) but not lysosomal inhibitor (Folimycin) protects the cells from cell death (Figure 4.3).

One possible interpretation for the inhibition of cell death by epoxomicin is that the physical extraction of OMM proteins could damage the outer mitochondrial membrane. Therefore, proteasomal inhibition protects the integrity of the OMM, thereby preventing the release of Cyt-C into the cytosol.

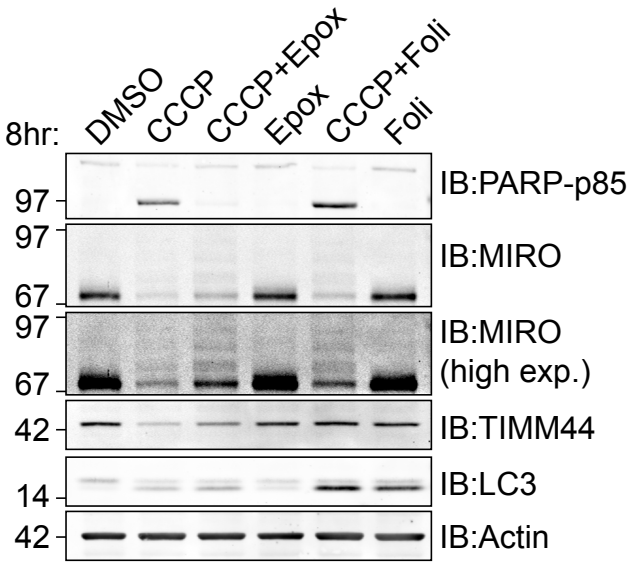

Figure 4.3 Proteasomal but not lysosomal inhibition protects cells from CCCP-induced, Parkin-dependent apoptosis.

hTERT-RPE1-YFP-Parkin cells were treated with CCCP (10μM), epoxomicin (Epox; 100nM) or/and folimycin (Foli; 100nM) for 8hr. The cells were then harvested in NP40 lysis buffer and 15μg of samples were probed with the indicated antibodies.

4.4.2 DBeQ, a p97 inhibitor does not prevent mitophagic cell death

The extraction of two OMM proteins, MCL1 and MFN1 for degradation has been shown to be mediated by p97, a AAA+ family member, prior to proteasomal degradation (Xu et al. 2011). Therefore, I wondered if DBeQ, a p97 inhibitor, could phenocopy the effect of proteasome inhibitor. I first titrated the concentration of DBeQ (Figure 4.4A). Since DBeQ has been reported to block the maturation of autophagosomes, I probed for LC3 as a readout for the efficacy of the inhibitor (Chou et al. 2011). Indeed, at 10 and 20μM, DBeQ treatment alone promotes accumulation of LC3-II, suggesting inhibition of the autophagy pathway. At 20μM, DBeQ also induces OPA1 cleavage, and a partial loss of MIRO, suggesting that high concentration of DBeQ alone can trigger mitophagy or general autophagy. Epoxomicin treatment alone induced the accumulation of a 52kDa fragment of PINK1. Intriguingly, I also observed mild accumulation of the 52kDa fragment of PINK1 with 20μM of DBeQ treatment. At steady state, this 52kDa fragment is normally constitutively degraded by the proteasome (Jin et al. 2010). The observation of this cleaved fragment at high DBeQ concentration suggests that the proteasomal degradation process might be affected by DBeQ. Upon co-treatment with CCCP, DBeQ induced higher levels of cell death as shown by the increase in cleaved PARP, contrary to the protective effect seen with epoxomicin. I also assessed the efficacy of DBeQ by blotting for MCL1 (Figure 4.4B). Consistent with the prior observations in the literature, DBeQ alone elevated the level of MCL1 (Xu et al. 2011).

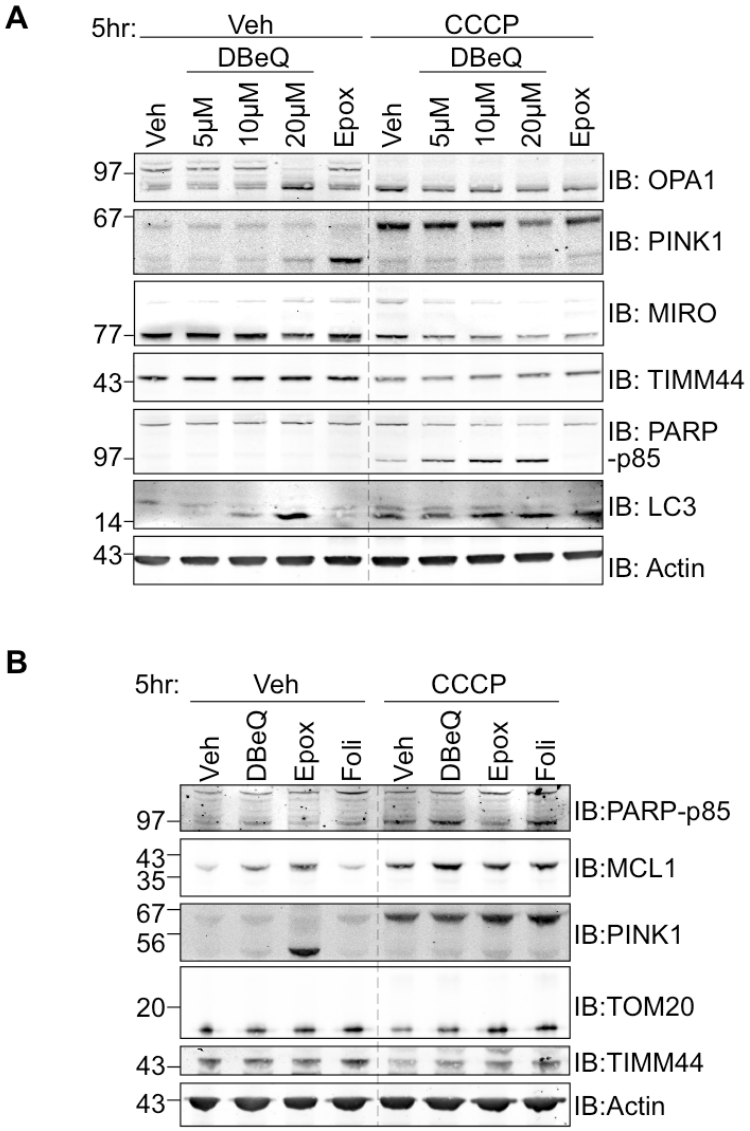

Figure 4.4 p97 inhibition exacerbates mitophagic cell death.

(A) hTERT-RPE1-YFP-Parkin cells were treated with varying concentrations of DBeQ or epoxomicin (Epox: 100nM) in the absence or presence of CCCP (10μM) for 5hr. Epoxomicin (Epox) treatment (100nM) was used as a negative control for PARP cleavage. Cells were lysed in RIPA lysis buffer and samples were probed with the indicated antibodies.
(B) hTERT-RPE1-YFP-Parkin cells were treated with DBeQ (10μM), epoxomicin (Epox; 100nM) and folimycin (Foli; 100nM) for 5hr in the presence or absence of CCCP (10μM). Cells were lysed in 'hot lysis' SDS buffer and samples were probed with the indicated antibodies.

4.5 Immunofluorescence characterization of the effect of epoxomicin, folimycin and DBeQ on mitophagy

Following a series of interesting observations from the proteasome, lysosome and p97 inhibition experiments, we decided to visualize the effects of these inhibitors on mitophagy by immunofluorescence microscopy. For the visualization of mitochondria, I stained the cells with anti-TIMM44 antibody. After 8hr of treatment with DBeQ alone, I observed perinuclear-aggregation of Parkin-positive mitochondria in ~20% of the cells. This is consistent with the biochemical data in Figure 4.4A whereby high concentration of DBeQ promotes OPA1 cleavage, an early event that precedes Parkin-mediated mitophagy. In addition, I observed that ~40% of the cells had short and swollen mitochondria. When cells were co-treated with DBeQ and CCCP, there was a dramatic delay or inhibition of Parkin clearance at 8hr compared with the control cells. Both epoxomicin and folimycin co-treatment with CCCP also delayed or inhibited clearance of Parkin aggregates. However, epoxomicin treated cells had 2-3 enlarged Parkin aggregates per cells whereas folimycin treated cells had numerous small Parkin aggregates.

4.5.1 Proteasomal inhibition affects clearance of mitophagic vesicles

Since proteasomal inhibition delays or possibly inhibits the clearance of mitophagic vesicles, one hypothesis would be that the clearance of some OMM proteins by the proteasome is required for the subsequent recruitment of autophagy components including p62 and LC3 to the mitochondria. To investigate this, I stained cells treated with CCCP with or without epoxomicin with p62 and LC3 antibodies (Figure 4.6A and B). After 8hr of CCCP treatment, Parkin aggregates co-localized with p62 staining and by 12hr, most of the Parkin aggregates were cleared (Figure 4.6A). However, when cells were treated with both CCCP and epoxomicin, the Parkin aggregates were present even after 12hr, consistent with previous observations in Figure 4.5. These Parkin aggregates also stained positive for p62, suggesting that the recruitment of p62 is not impeded during proteasomal inhibition.

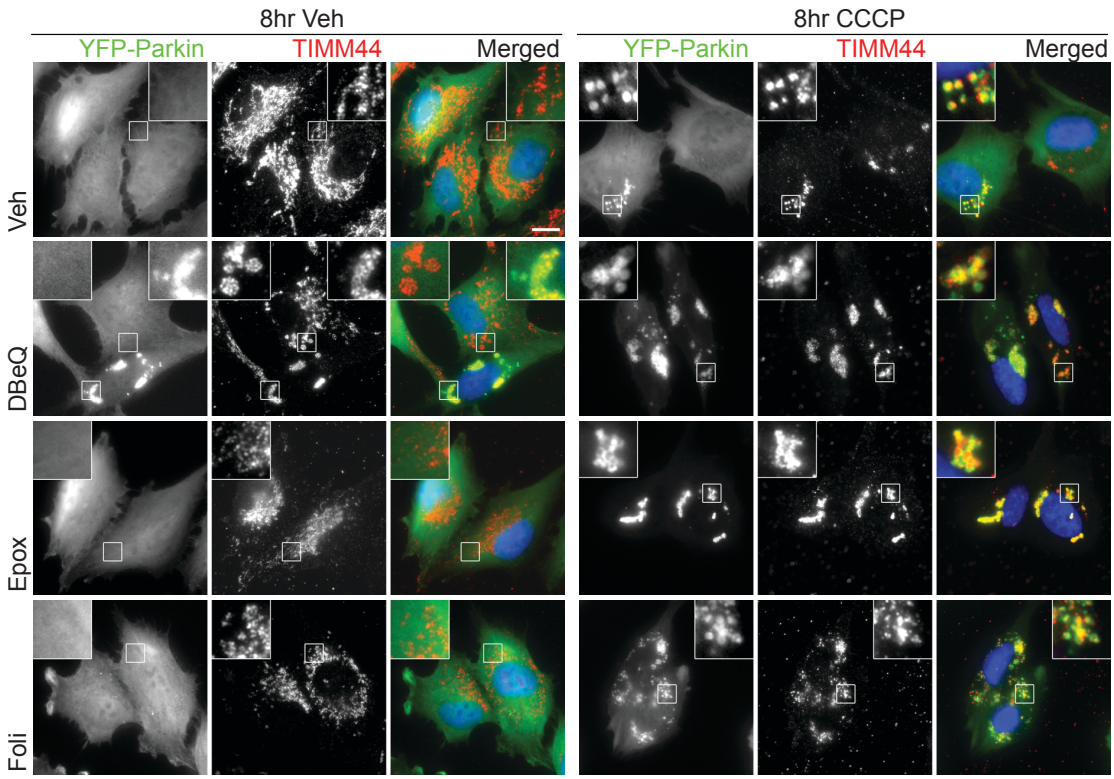

Figure 4.5 Differential effects of p97-targeted, proteasomal and lysosomal inhibitors on Parkin recruitment and mitophagy.

hTERT-RPE1-YFP-Parkin cells were treated with CCCP (10μM), DBeQ (10μM), epoxomicin (Epox; 100nM), and folimycin (Foli; 100nM) for 8hr. The cells were then fixed with PFA and stained with anti-TIMM44 antibody. The coverslips were mounted using mowiol with DAPI to stain the nuclei (blue in merged image). Scale bar: 10μm.

Similar observations are also made with the LC3 staining. After 8hr of CCCP treatment, smaller Parkin aggregates were enveloped by LC3, which forms a circle around the aggregates (see 8hr CCCP + DMSO treatment; left inset) while bigger Parkin aggregates were decorated with spots of LC3 (see the same condition as previous; right inset). CCCP and epoxomicin treated cells contained only large Parkin aggregates (both 8 and 12hr) that were decorated by spots of LC3, which do not complete surround the aggregates.

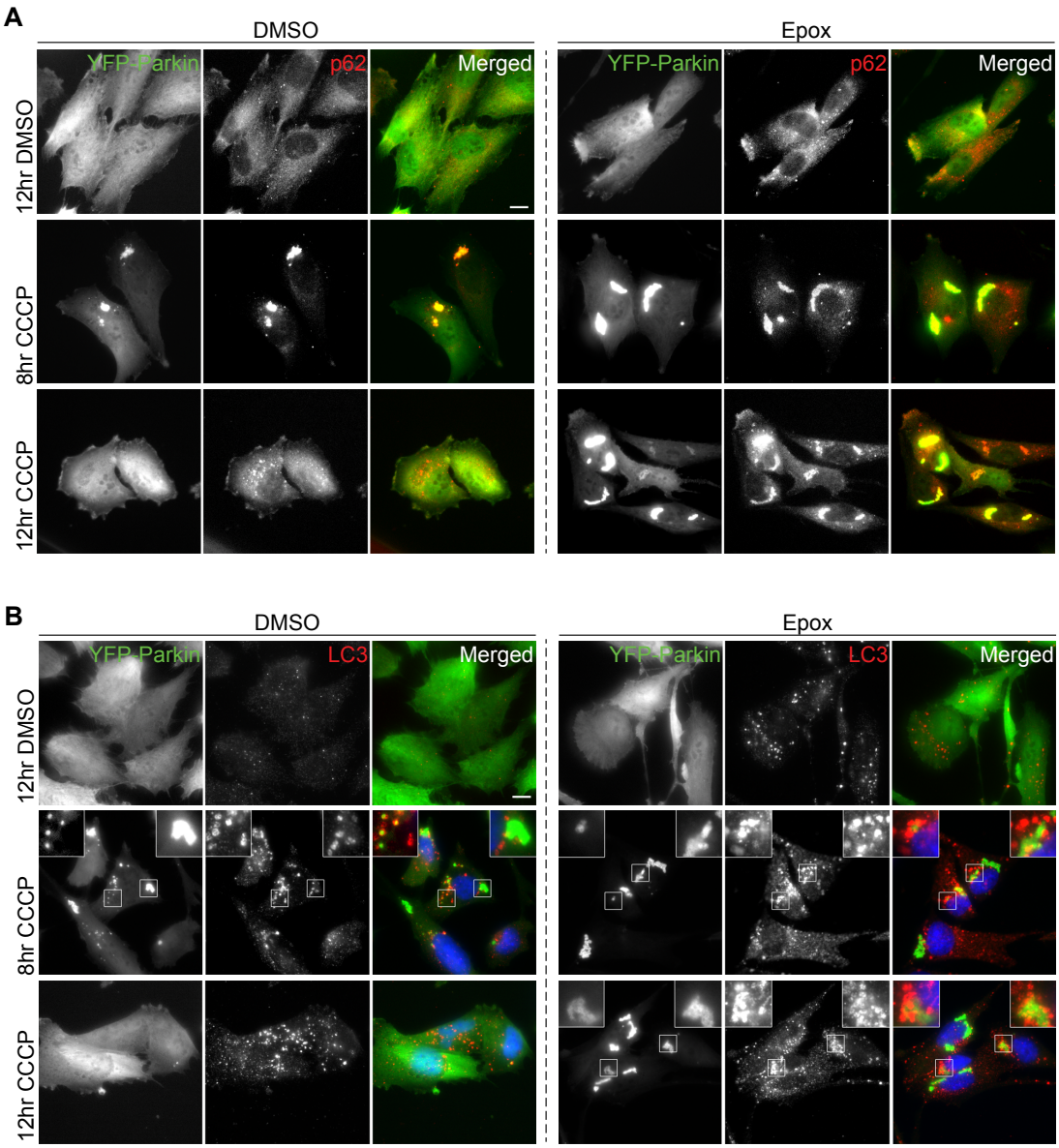

Figure 4.6 Epoxomicin treatment delays mitophagic vesicle clearance.

(A) hTERT-RPE1-YFP-Parkin cells were treated with CCCP (10μM) and epoxomicin (Epox; 100nM) for the indicated times. The cells were then fixed with PFA and stained with anti-p62 antibody. The coverslips were mounted using mowiol. Scale bar: 10μm.
(B) hTERT-RPE1-YFP-Parkin cells were treated as described in (A). The cells were then fixed with PFA followed by methanol. Cells were stained with anti-LC3 antibody The coverslips were mounted using mowiol with DAPI (blue in merged image). Scale bar: 10μm.

4.6 Cytochrome-C is released from the mitochondria during mitophagic cell death

If the ubiquitylation and degradation of OMM proteins induce rupture of OMM, Cytochrome-C (Cyt-C) should be released, leading to the activation of apoptosis. To test this hypothesis, I fixed and stained CCCP treated hTERT-RPE1-YFP-Parkin cells with anti-Cyt-C antibody to check for Cyt-C release from the mitochondria using immunofluorescence microscopy (Figure 4.7A). After 6hr of CCCP treatment, I observed a mixture of cytosolic and mitochondrial Cyt-C in approximately 20% of the cells, whereas in DMSO treated cells, the Cyt-C staining was restricted to the mitochondria.

Cyt-C release from the mitochondria was also confirmed using digitonin-permeabilised cells. For this, I incubated CCCP-treated cells in HIM buffer with varying digitonin concentrations for 10min on ice. I then harvested and centrifuged the cells at 14,000xg for 3min to separate the permeabilised cells from the released cytosolic fraction (Figure 4.7A, detailed protocol described in Chapter 2, section 2.3.6). At lower digitonin concentrations (0.01 and 0.25%), Cyt-C is only released in the CCCP treated cells. At higher (0.075%), Cyt-C is released in both DMSO and CCCP-treated cells. As a control to show that inner mitochondrial membrane proteins were not released into the cytosol during digitonin treatment, I also probed the blot for TIMM44 (inner mitochondrial transmembrane protein).

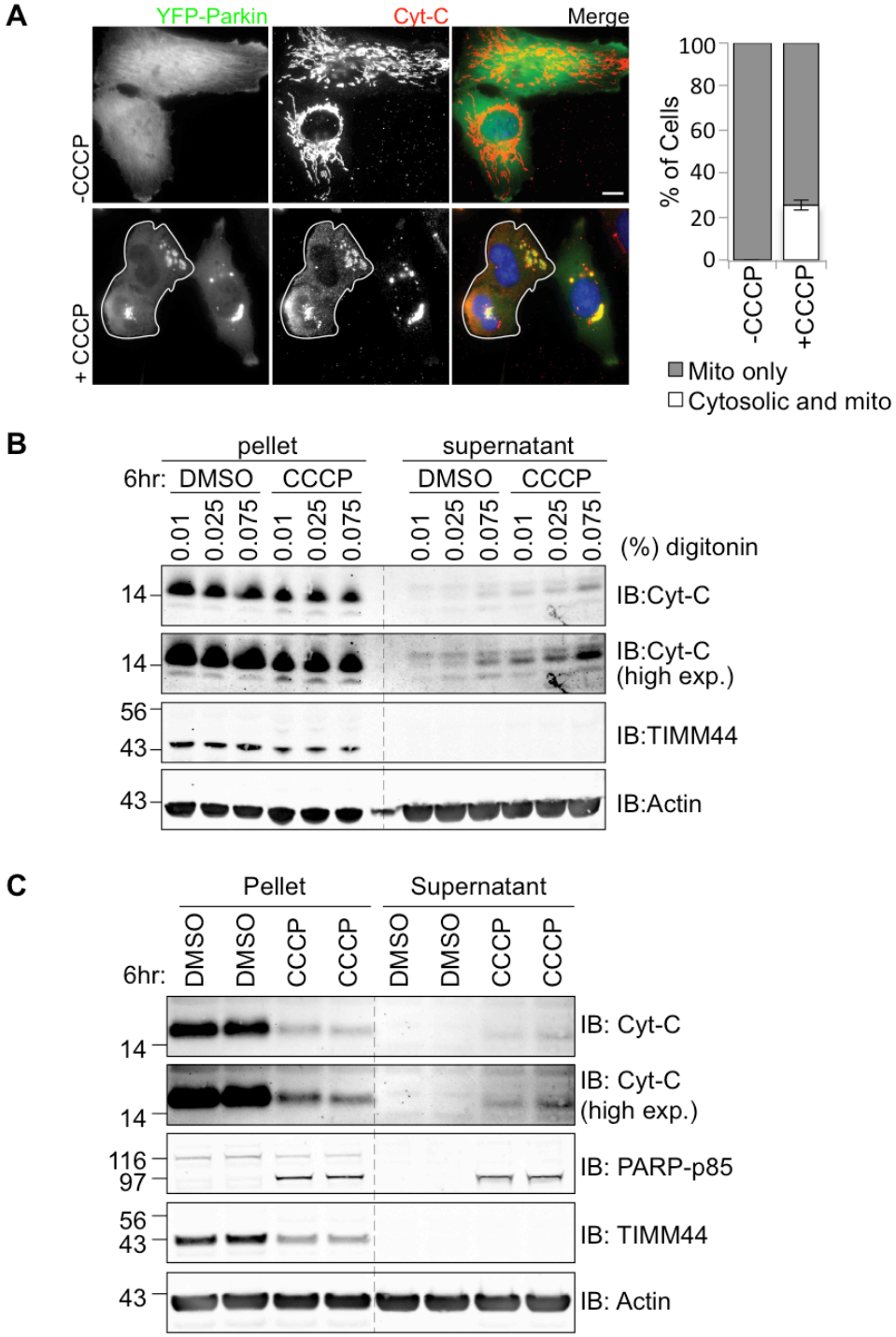

Figure 4.7 Cyt-C is released during Parkin-mediated mitophagy.

(A) hTERT-RPE1-YFP-Parkin cells were treated with CCCP (10μM) for 6hr. The cells were then fixed with PFA and stained with anti-Cyt-C antibody. Coverslips were mounted onto glass slides with mowiol and DAPI (blue in merged image). Scale bar: 10μm. Graph represents quantitation of cells with exclusively mitochondrial Cyt-C or a mixture of cytosolic and mitochondrial Cyt-C staining. Error bar represents standard deviation from 3 independent experiments.
(B) hTERT-RPE1-YFP-Parkin cells were treated with CCCP (10μM) for 6hr. Cells were then treated with different concentration of digitonin for 10min in HIM buffer. The treated samples were then centrifuged at 14,000rpm for 3min. The pellet and

supernatant fractions were loaded at 1:3 (volume:volume) on a NU-PAGE to probe for the depicted proteins.
(C) hTERT-RPE1-YFP-Parkin cells were treated with CCCP (10μM) for 6hr. Cells were then treated with 0.025% of digitonin for 10min in HIM buffer. The treated samples were then centrifuged at 14,000rpm for 3min. The pellet and supernatant fractions were loaded in duplicates at 1:3 (volume:volume) on a NU-PAGE to probe for the depicted proteins.

4.7 Mitophagic cell death occurs via apoptosis

4.7.1 Phosphatidylserine and phosphatidylethanolamide externalization precedes mitophagic cell death

The observation of PARP cleavage and Cyt-C release during CCCP treatment suggests that the cell death is apoptosis. Another hallmark of apoptotic cell death is the externalisation of phosphatidylserine (PS) and phosphatidylethanolamide (PE) from the cytosolic side of the cell membrane (Fadok et al. 1992, Martin et al. 1995, Emoto et al. 1997). I treated hTERT-RPE1-YFP-Parkin cells with CCCP in the presence of annexin V (a Ca^{2+}-dependent phospholipid-binding protein that has high affinity for PS and PE) and the membrane impermeable dye, DRAQ7. I monitored the progression of mitophagy and cell death by live-cell imaging. As shown in Figure 4.8, annexin V stained the plasma membrane after 8hr of CCCP treatment. In contrast, cells were only DRAQ7-positive after 12hr. This strongly supports the notion that the mitophagic cell death is apoptotic.

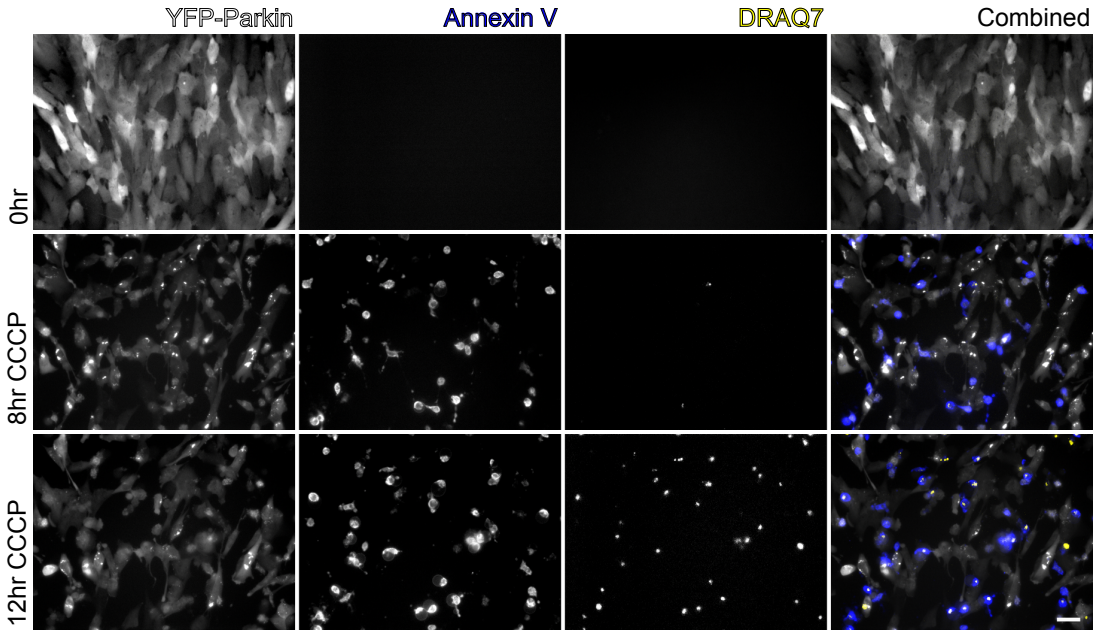

Figure 4.8 Phosphatidylserine and phosphatidylethanolamide externalization precedes cell death.

hTERT-RPE1-YFP-Parkin cells were treated with CCCP (10μM) and imaged in the presence of DRAQ7 (0.3μM) and annexin V-AF350 (Invitrogen; 5μl annexin V/ml of medium, supplemented with 2.5mM of $CaCl_2$). Mitophagy progression was imaged every 30min up to 16hr. YFP-Parkin was pseudo-coloured grey, annexin V was in blue and DRAQ7 was in yellow. Scale bar: 40μm.

4.7.2 Mitophagic cell death is prevented by Z-VAD-FMK

Next, I treated the hTERT-RPE1-YFP-Parkin cells with CCCP and a broad-spectrum caspase inhibitor, benzyloxycarbonyl-Val-Ala-Asp (OMe) fluoromethyl ketone (Z-VAD-FMK) (Slee et al. 1996, Sun et al. 1999). Live-cell imaging of mitophagy progression with DRAQ7 staining to monitor for dead cells demonstrated that Z-VAD-FMK effectively inhibited cell death without affecting the progression of mitophagy (Video 2 and Figure 4.9). This was also confirmed by western blotting (Figure 4.9B). Activation and progression of mitophagy, indicated by the loss of MIRO, TOM20 and TIMM44, occurred normally in both CCCP and CCCP with Z-VAD.FMK treatment. However, PARP cleavage (PARP-p85) is inhibited when cells are treated with Z-VAD.FMK.

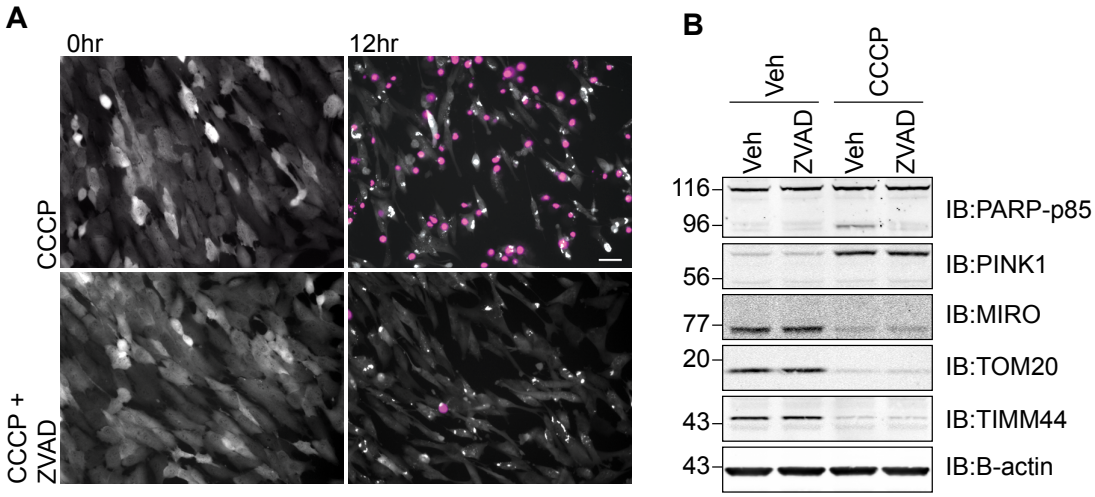

Figure 4.9 The broad-spectrum caspase inhibitor, Z-VAD-FMK prevents mitophagic cell death.

(A) hTERT-RPE1-YFP-Parkin cells were treated with CCCP (10μM) or CCCP with Z-VAD-FMK (ZVAD; 20μM). The progression of mitophagy and cell death were recorded by live-cell imaging at 15min intervals in the presence of the membrane impermeable dye, DRAQ7 (0.5μM). Shown are single frames (T=12hrs) from a representative video, with YFP-Parkin shown in grey and DRAQ7 shown in pink. Scale bar:40μm.
(B) hTERT-RPE1-YFP-Parkin cells were treated the same as in (A). The cells were lysed in RIPA lysis buffer. 10μg of lysates were immunoprobed as indicated.

4.7.3 Mitophagic cell death is dependent on both caspase 8 and caspase 9

Next I wanted to investigate whether the cell death is triggered via the intrinsic or extrinsic apoptotic pathway. I induced mitophagy in cells depleted of caspase 8 (Casp-8) and caspase 9 (Casp-9) by RNA interference. The current understanding is that Casp-8 cleavage and activation is generally required for the activation of the extrinsic apoptotic pathway while Casp-9 activation is required mostly for the intrinsic pathway. However, Casp-9 can also be activated in the extrinsic pathway to amplify the apoptotic cascade. Interestingly, both Casp-8 and Casp-9 were required for mitophagic cell death (Figure 4.10). Consistent with the data from the Z-VAD-FMK treatment, inhibition of apoptosis by knocking down Casp-8 and Casp-9 did not block mitophagy, as indicated by the loss of TOM20 in all three conditions. It is worth pointing out that while I could observe the efficient depletion of both Casp-8 and Casp-9 in their respective knockdown conditions, I only observed the p43/p41 cleaved Casp-8 fragments that are commonly observed in the literature (Sohn et al. 2005, Sawai 2013, Ferreira et al. 2012). I did not detect any Casp-9-derived fragment (either p37 or p35) in these cells (Del Bello et al. 2003, Zou et al. 2003).

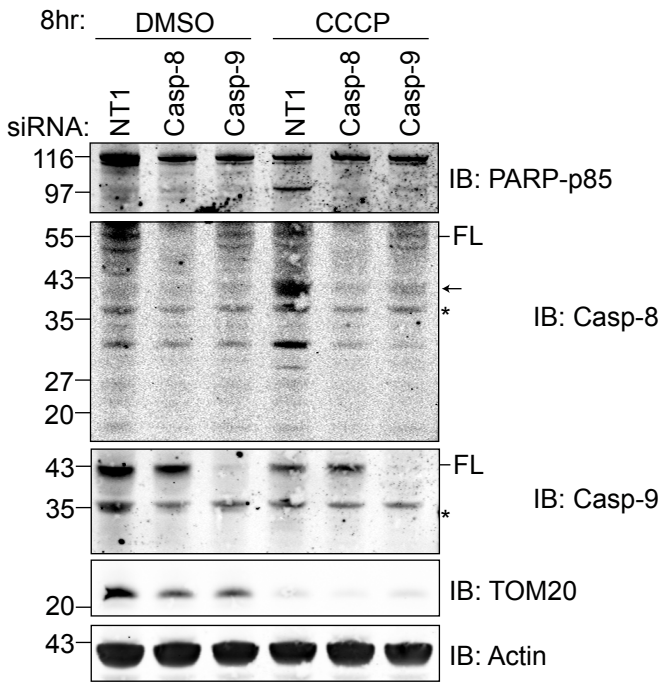

Figure 4.10 Mitophagic cell death occurs via Casp-8 and Casp-9 dependent apoptosis

hTERT-RPE1-YFP-Parkin cells were transfected for 72hr with either non-targeting siRNA control (NT1), siRNA targeting caspase 8 (Casp-8) or siRNA targeting caspase 9 (Casp-9). The cells were then treated with CCCP (10μM) for 8hr and harvested in 'hot lysis' SDS buffer. 25μg of lysates were probed with the indicated antibodies.
Asterisk: non-specific band. Arrow: cleaved caspase 8 fragment.

4.8 Discussion

For many years, PINK1 and Parkin have been assigned cytoprotective roles in various organisms. Rana and colleagues demonstrated that the overexpression of Parkin in neurons promoted the lifespan of *Drosphila*. This was attributed to the efficient turnover of *drosophila* Mitofusin and the maintenance of normal mitochondrial morphology and respiratory activity by Parkin (A. Rana et al. 2013). Johnson and colleagues demonstrated in Parkin-expressing mouse embryonic stem cells that BAX is targeted for ubiquitylation and proteasomal degradation during activation of mitophagy, and subsequently prevents Cytochrome-C release (Johnson et al. 2012). Furthermore, Parkin has been shown to promote cell survival by stabilising MCL1 indirectly, via the degradation of FBXW7, an E3 ligase that ubiquitylates and promotes the degradation of MCL1 (Inuzuka et al. 2011, Ekholm-Reed et al. 2013).

While the concept of PINK1 and Parkin-induced cell death is contradicting our current understanding of the cytoprotective roles of PINK1 and Parkin, our observation is supported by Yoshii et al. (2011) who demonstrated that Parkin overexpression leads to disruption of mitochondrial membrane integrity (Yoshii et al. 2011). Yoshii and colleagues discovered that overexpression of Parkin in mouse embryonic fibroblasts (MEFs) promotes widespread ubiquitylation and proteasomal degradation of OMM proteins during mitophagy (e.g. TOM20, TOM40, TOM70a and OMP25). Using electron microscopy, they observed mitochondrial swelling, rupture of the OMM, and loss of cristae structure and suggested that the proteasomal degradation of these proteins may damage the integrity of the OMM and lead to the rupture to the OMM. They further showed that proteasomal inhibition could protect the integrity of the mitochondrial double membranes. Consistent with their observation, the cell death that I observed can also be inhibited by proteasomal inhibition whereas inhibition of the lysosome by vacuolar ATPase by folimycin did not rescue the cell death. While the authors did not detect cell death based on caspase 3 activation or nuclear fragmentation in their setting, it is possible that the cell death that I observed

in our system is also caused by the rupture of OMM, causing cytochrome C release into the cytosol.

Immunofluorescence microscopy revealed that both proteasomal and lysosomal inhibition blocked the clearance of Parkin aggregates. However, proteasomal inhibition promoted the accumulation of large Parkin aggregates (2-3 aggregates per cell) while lysosomal inhibition accumulated numerous small Parkin aggregates. Further investigation of the effect of proteasomal inhibition on Parkin-mediated mitophagy revealed that p62, the adaptor for the recruitment of LC3, as well as LC3 itself were recruited to the mitochondria during both CCCP and CCCP plus epoxomicin treatments, suggesting that the initiation of autophagic process, including the ubiquitylation of mitochondrial proteins and the lipidation of LC3 were not affected by proteasomal inhibition. However, I observed that the Parkin aggregates were larger in epoxomicin co-treated cells, with LC3 punctae decorating the edges of the aggregates. In contrast, in the absence of epoxomicin, cells had smaller Parkin aggregates that were completely enveloped by LC3 (in a ring morphology). This suggests that smaller Parkin aggregates might be turned over more efficiently compared to larger Parkin aggregates. It is likely that the degradation of certain OMM proteins by the proteasome is required for the dissociation of large Parkin aggregate into smaller aggregates prior to lysosomal degradation. For example, the degradation of mitochondrial proteins that are involved in the fusion and fission machinery (e.g. MFN1/2) and the movement of mitochondria (e.g. MIRO1/2) might be impeded, affecting the dissociation of the Parkin-decorated mitochondrial aggregates (Fransson et al. 2006, Fransson et al. 2003, Chen et al. 2003). Both MFN1/2 and MIRO1/2 are known substrates of Parkin during mitophagy and the degradation of the two have been shown to promote mitophagy (Ziviani and Whitworth 2010, Gegg et al. 2010, Wang et al. 2011).

P97, an AAA-ATPase, has been shown to retrotranslocate MCL1 and MFN1 from the mitochondria OMM to the cytosol prior to proteasomal degradation (Xu et al. 2011, Tanaka et al. 2010). To further test if the physical action of

protein extraction from the mitochondria by p97 is responsible for the damage of the OMM, I used DBeQ, a p97 inhibitor. I observed that high concentrations of DBeQ treatment alone could induce OPA1 cleavage and Parkin recruitment, suggesting that mitophagy was induced upon p97 inhibition. Unlike proteasomal inhibition, p97 inhibition did not rescue the cells from cell death. Instead, simultaneous treatment of cells with CCCP and DBeQ exacerbated cell death. Since p97 is involved in a wide array of functions, ranging from chromatin remodelling, endocytic vesicle maturation, autophagosomal maturation to ER-associated degradation (ERAD), it is possible that the cell death observed is not a direct result of mitophagic cell death but a combined effect from multiple cellular stresses (Meyer et al. 2012, Chou et al. 2011). Indeed, Chou and colleagues reported that DBeQ is highly potent in activating caspase 3 and caspase 7 via a mechanism that is not yet understood (Chou et al. 2011). Therefore, no strong conclusion can be drawn from the effect of p97 on mitophagic cell death.

Cyt-C release is generally associated with apoptotic cell death (Jiang and Wang 2000). Indeed, I observed Cyt-C release during CCCP treatment using digitonin permeabilisation of the cell membrane. This was further supported by the observation of a small population of cells (20%) with partial cytosolic localization of Cyt-C.

In healthy cells, phospholipids are assymetrically-distributed between the outer and inner membranes. The outer membrane is composed mostly of cholinephospholipids, such as phosphatidylcholine and sphingomyelin whereas the inner membrane is composed mostly of aminophospholipids, including phosphatidylserine (PS) and phosphatidylethanolamide (PE). The distribution of PS and PE is actively maintained by the enzyme aminophospholipid translocase (‘flippase’) (Diaz and Schroit 1996). During apoptosis, an enzyme known as the phospholipid scramblase is cleaved and activated by effector caspases, which promotes bidirectional movement of phospholipids, thereby exposing PS and PE to the cell surface (Zhou et al. 1997, Martin et al. 1995). The externalized PS and PE can be recognized and bound by annexin V in a Ca^{2+}-dependent manner. Therefore, annexin V

affinity to the plasma membrane serves as an alternative read out for apoptosis. I treated the cells with CCCP in the presence of annexin V conjugated with a fluorescent dye and a membrane impermeable dye, DRAQ7. During CCCP treatment, annexin V was seen to localize to the plasma membrane (at 8hr) and this event precedes the incorporation of DRAQ7 (at 12hr).

The apoptotic nature of this cell death is also confirmed by its sensitivity of Z-VAD-FMK, a broad spectrum caspase inhibitor (Slee et al. 1996). However, Z-VAD-FMK does not differentiate between the intrinsic and extrinsic pathway. The current view is that caspase 8 is cleaved and activated during extrinsic apoptotic activation, which could either cleave caspase 3 to directly trigger apoptosis, or cleave Bid into tBid to activate Bak and Bax oligomerisation on the OMM, resulting in Cyt-C release into the cytosol. Cyt-C then triggers the assembly of the apoptosome that subsequently activates Caspase 9. Caspase 9 cleaves Caspase 3 to promote apoptosis. On the other hand, intrinsic apoptosis is triggered directly via the mitochondria where internal insults trigger the release of Cyt-C from the mitochondria, sharing the same downstream mitochondria-mediated pathway as described above for extrinsic apoptosis (Mukhopadhyay et al. 2014).

In our setting, it seems that both caspase 8 and caspase 9 are required for the activation of apoptosis. We postulate two explanations to the observation (Figure 4.11). In the first scenario, cell death might take place via the extrinsic pathway but activation of caspase 8 alone is insufficient to activate caspase 3. Instead, the activation of caspase 9 via Bid cleavage and Cyt-C release might be required to amplify the caspase cascade. This is less likely to be the case as the extrinsic triggers are usually Fas, TNF or TRAIL ligands that bind to their respective receptors to activate the extrinsic pathway. In the alternative, and more likely scenario, cell death might take place via the intrinsic pathway. In a situation where a small subset of damaged mitochondria is not efficiently engulfed by the lysosomes, only a small amount of Cyt-C is released into the cytosol. This low level of Cyt-C might not be sufficient to activate apoptosis. Instead, a positive feedback loop via

the activation of caspase 3, which has been reported to cleave caspase 8 might be required to further activate tBid and pemeabilise the OMM to amplify the caspase cascade (Figure 4.11)(Sohn et al. 2005, Viswanath et al. 2001). Viswanath and colleagues demonstrated in rat adrenal medulla cell line (PC12 cells) that 1-methyl-4-phenyl-1,2,3,6- tetrahydropyridine (MPTP) treatment (150μM) induces caspase 9 activation within 2hr of treatment, followed by caspase 3 activation (2-4hr). Caspase 8 activation and Bid cleavage did not occur until late stages (4-6hr). They further demonstrated that inhibition of caspase 9 using LEHD-FMK, a cell-permeable caspase-9 specific inhibitor, prior to MPTP treatment did not block Cyt-C release but inhibited caspase 8 activation and the subsequent cell death (Viswanath et al. 2001). Therefore, it is possible that the cell death observed in our cell line follows a similar intrinsic apoptotic pathway as PC12 cells.

Very recently, Zhang and colleagues reported that HeLa cells expressing Parkin underwent apoptosis after valinomycin and mitophagy after CCCP treatment (Zhang et al. 2014). They demonstrated that the differential response was due to the selective ubiquitylation and degradation of MCL1 by Parkin during valinomycin but not CCCP treatment, which dictate whether cells undergo mitophagy or apoptosis. While I have not tested valinomycin in hTERT-RPE1-YFP-Parkin cells, I propose that the trigger and mechanism for our cell death observation is most likely different from that described by Zhang and colleagues. MCL1 degradation induces apoptosis by allowing BAK and BAX oligomerisation on the OMM for Cytochrome-C release. In chapter 6, I will demonstrate that BAK and BAX knockdown does not affect CCCP-induced cell death, which argues against the upstream effect of MCL1 degradation.

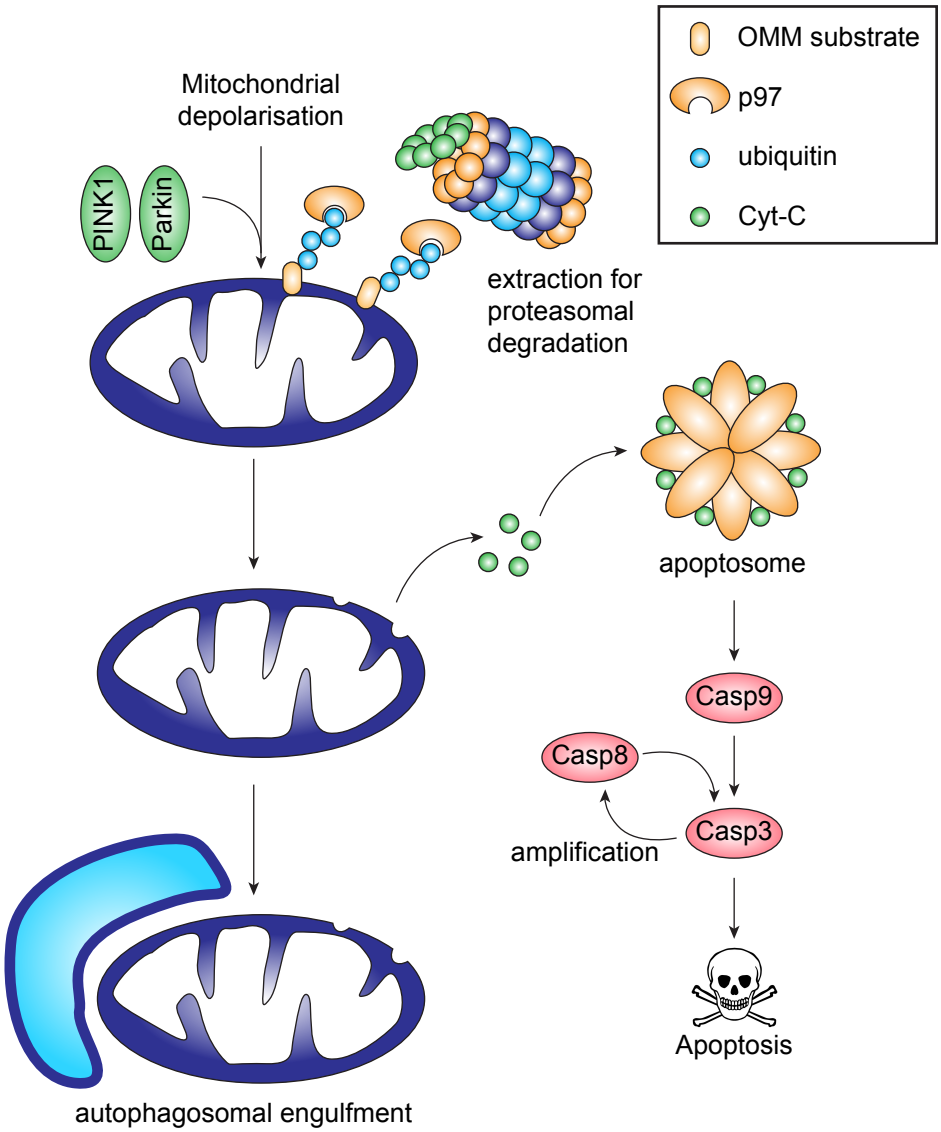

Figure 4.11 Proposed model for the involvement of caspase 8 and caspase 9 in Parkin-mediated mitophagic cell death.

Mitochondrial depolarisation triggers PINK1 and Parkin recruitment to the outer mitochondrial membrane (OMM). High expression of Parkin causes aberrant ubiquitylation of OMM proteins, resulting in their extraction by p97 for proteasomal degradation, which affects the integrity of the outer mitochondrial membrane. Cytochrome-C is release from the mitochondrial intermembrane space, triggering the intrinsic apoptotic pathway. The assembly of the apoptosome activates caspase-9, which then activates caspase 3. Caspase 3 and caspase 8 can inter-activate each other, further amplifying the caspase cascade to trigger apoptosis.

Chapter 5: Identification of Deubiquitylases Involved in Parkin-mediated Mitophagy

5.1 Introduction

Parkin is an ubiquitin-E3 ligase that is involved in mitophagy. During mitochondrial depolarisation, Parkin is recruited to the OMM via its interaction with PINK1 and subsequently phosphorylated by PINK1. This activates Parkin to ubiquitylate several OMM proteins, leading to their degradation or the recruitment of the autophagic machinery, which efficiently removes malfunctioning mitochondria. While the Parkin-mediated ubiquitylation event is well characterized during mitophagy, the DUBs that oppose or regulate these events remain relatively uncharacterized. This chapter reports on work carried out to identify DUBs that are involved in the regulation of PINK1/Parkin-mediated mitophagy.

The aims discussed in this chapter are: (1) to develop a live-cell imaging, medium-throughput assay to visualise Parkin recruitment and mitophagy progression in hTERT-RPE1-YFP-Parkin cells, (2) to perform a focused siRNA screen using a targeted DUB siRNA library to identify potential DUBs that can regulate PINK1/Parkin-mediated mitophagy, and (3) to validate the top-hits from this siRNA screen.

5.2 Live cell imaging screen for DUBs involved in Parkin-mediated mitophagy

hTERT-RPE1 cells stably expressing YFP-tagged Parkin provide a nice visualization tool of (YFP-) Parkin recruitment to the mitochondria during mitochondria depolarization. Having characterised the timeline of YFP-Parkin recruitment, aggregation and clearance during mitophagy in chapter 3, I decided to carry out a DUB siRNA screen by imaging the progression of mitophagy in these cells (Figure 5.1).

A custom-made DUB siRNA library supplied by QIAGEN consisting of siRNA pools targeting 92 DUBs was used for this screen. The oligo pools were each comprised of 4 individual siRNA oligos. hTERT-RPE1-YFP-Parkin cells were transfected with the siRNA pools (20nM) using Lipofectamine RNAiMAX according to the 'reverse transfection' protocol described in Chapter 2. Briefly, the siRNA oligos, OptiMEM, and RNAiMAX transfection reagent were mixed in a 96-well plate. After incubation, 5,000 cells were seeded into each of the wells.

CCCP (10μM) was used to depolarize the mitochondria and trigger Parkin recruitment. The progression of mitophagy was recorded by live-cell imaging using a Nikon Ti-Eclipse microscope with a CFI S Plan Fluor ELWD 20x objective. I first set up the 96-well plate on a motorised microscope stage contained within a humidified chamber with 5% CO_2 at 37°C. I manually selected 1 position per well for imaging using the Perfect Focus System (PFS) to ensure the cells remain in focus across all timepoints. Images were taken every 10min for up to 12hr.

Candidate DUBs, for which depletion altered the response to CCCP, were selected based on Parkin recruitment at 2hr, Parkin aggregation at 4hr and Parkin clearance at 12hr. These DUBs were then selected for further deconvolution using the individual siRNA oligos to eliminate off-target effects.

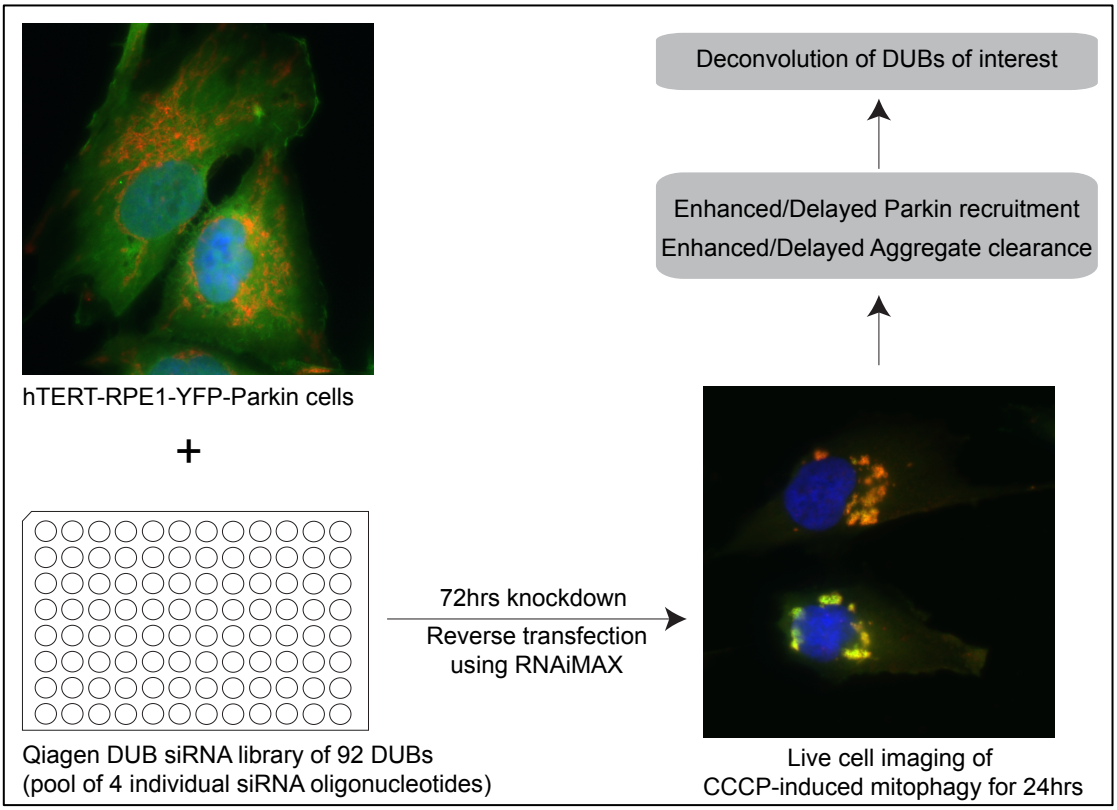

Figure 5.1 Experimental workflow of the live-cell imaging screen for DUBs involved in Parkin-mediated mitophagy.

hTERT-RPE1-YFP-Parkin cells were transfected for 72hrs with siRNA pool oligos (20nM) using RNAiMAX transfection reagent. The siRNA oligos were obtained as a custom-made library targeting 92 DUBs (20nM). The initial screen was carried out with a pool of four individual siRNA oligos targeting each DUB. CCCP (10μM) was used to depolarize the mitochondria and activate Parkin recruitment. The progression of mitophagy was recorded by live-cell imaging using the Nikon Ti-Eclipse microscope. Candidate DUBs for which depletion altered mitochondrial response to CCCP were identified based on visual inspection of Parkin recruitment, aggregation and clearance. DUB candidates that were selected were further deconvoluted with individual siRNA oligos to eliminate off target effects.

5.2.1 Optimisation of the siRNA transfection protocol and transfection efficiency

Routinely, I carried out all of my siRNA transfections using 40nM of siRNA oligos in a 6-well plate. However, all the previous siRNA screens that were carried out in our laboratory using the Qiagen DUB siRNA library were based on 20nM siRNA oligos. Therefore, I wanted to check whether transfection with 20nM siRNA is sufficient to deplete the proteins of interest in hTERT-RPE1-YFP-Parkin cells. I carried out a test transfection with a previously characterised siRNA oligo against USP33 (oligo 6) in a 96-well plate using Lipofectamine® RNAiMAX transfection reagent using the exact reverse transfection protocol that I would want to use later in my screen. USP33 siRNA transfection was used for this purpose as this protein has been well studied in our laboratory and the USP33 antibody that we routinely use is specific and sensitive (Thorne et al. 2011). 72hrs after transfection, I pooled the cell lysates from 12 wells of a 96-well plate and assessed the siRNA transfection efficiency by western blotting. As shown in Figure 5.2, both 20nM and 40nM of siRNA oligos knocked down USP33 to comparable levels in these cells. Therefore, I decided to use 20nM of siRNA oligos for the DUB siRNA screen.

5.2.2 Transfection of NT1 and PINK1 siRNA oligos as controls to assess knockdown efficiency and efficacy of CCCP treatment

Since PINK1 acts directly upstream of Parkin during mitophagy, depletion of PINK1 prevents Parkin recruitment to the mitochondria during CCCP treatment. This provides a good visual assessment for the knockdown efficiency and also serves as a positive control for CCCP-induced mitophagy. As shown in Figure 5.2B, siRNA-mediated depletion of PINK1 blocked Parkin recruitment upon CCCP treatment in up to 80% of the cells. In addition, I chose the non-targeting oligo (NT1), which should not target any mRNA as a negative control that should not affect mitophagy.

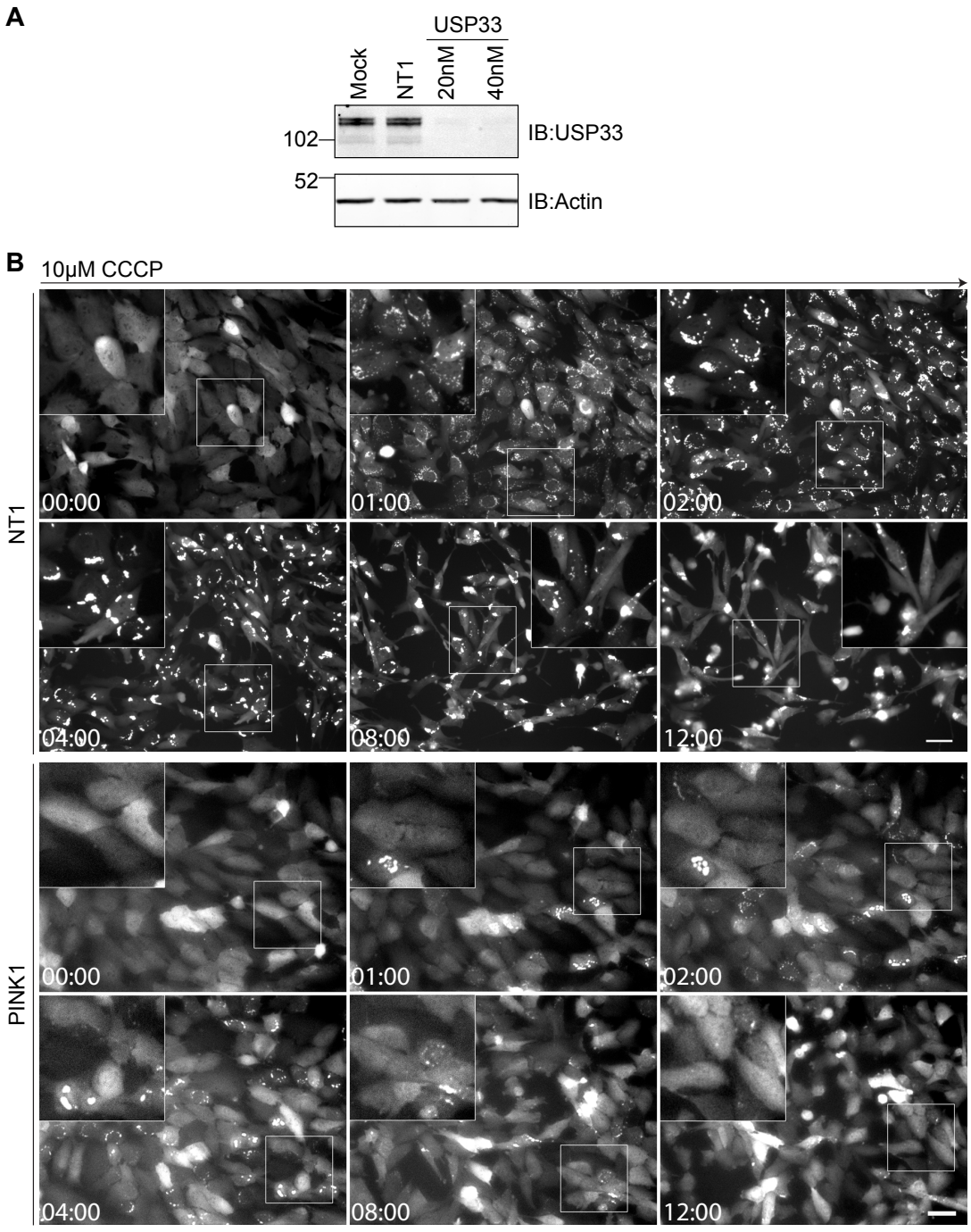

Figure 5.2 Optimisation of the siRNA transfection protocol including positive and negative controls for the mitophagy screen.
(A) hTERT-RPE1-YFP-Parkin cells were transfected for 72hr with 20nM of either non-targeting control (NT1) or siRNA oligo targeting UPS33 (D6). Cells were harvested in NP40 lysis buffer and 20μg of lysates were probed with anti-USP33 and anti-Actin antibodies.
(B) hTERT-RPE1-YFP-Parkin cells were transfected for 72hr with NT1 or PINK1 targeting siRNAs(20nM). Cells were then treated with 10μM of CCCP. Mitophagy progression was imaged live with frames captured in 15min intervals. Representative frames at the indicated times after CCCP (10μM) addition are shown for both NT1 and PINK1 siRNA transfected cells. Scale bar: 40μm.

5.2.3 Identification and deconvolution of DUBs of interest

As demonstrated in Figure 5.3, normal Parkin recruitment to the mitochondria occurs within the first two hours, with the formation of first small and numerous Parkin punctae. These punctae gradually aggregate and form larger spots at 4hr, with most cells clearing the Parkin aggregates between 8-12hr (Figure 5.3). While I attempted to quantitatively measure the area and number of Parkin aggregates based on the YFP-Parkin fluorescence intensity, this method falls short for the following reasons: (1) Parkin expression levels vary greatly across different cells and different wells, (2) some cells undergo mitophagic cell death (as discussed in Chapter 4) and these apoptotic cells usually round up and have high fluorescence intensity, and (3) early Parkin recruitment to the mitochondria forms smaller Parkin punctae that have weaker intensity compared to the larger Parkin aggregates formed at the later stages of mitophagy. The difference in fluorescence intensity and size of Parkin punctae and aggregates made it difficult to set a uniform fluorescence intensity threshold for all the wells for quantitation. In the end, I visually assessed the effect of DUB depletion on Parkin recruitment at 2hr, Parkin aggregation at 4hr and Parkin clearance at 8hr with reference to the non-targeting 1 (NT1) siRNA oligo-transfected cells.

I carried out the DUB siRNA screen twice with pooled siRNA oligos. DUBs, which upon depletion showed the same effect on Parkin-mediated mitophagy in both of the screens were selected for further deconvolution. While there are a few subtle differences in Parkin recruitment and aggregation upon knockdown of some of the DUBs, the most striking effect that I observed was delayed recruitment of Parkin to the mitochondria during the first 2 to 4hr of CCCP treatment. In most cases, the delay in Parkin recruitment did not visibly affect Parkin clearance at the later stage (8-12hr). In fact, in some cases, the cells with delayed Parkin recruitment seemed to proceed to Parkin clearance faster than the control (NT1) cells. At this stage, since I did not have a mitochondrial marker in the screen, it is not possible to tell if this phenotype represents an enhanced mitophagy or simply a transient recruitment of Parkin to the mitochondria that eventually dissociates without

activating ubiquitylation. For simplicity, I refer to this observation as a 'reduced response (RR)' as assessed at the 4hr timepoint of CCCP treatment, followed with either normal Parkin aggregate clearance (NC) or faster Parkin aggregate clearance (FC; see Table 5.1). An example of reduced response with faster Parkin aggregate clearance during CCCP treatment is shown with the knockdown of USP43 (Figure 5.3).

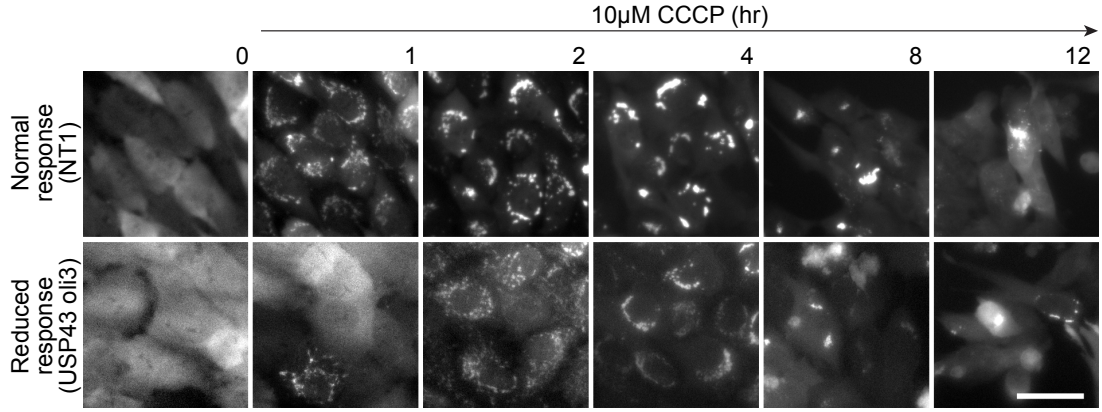

Figure 5.3 Comparison of normal response and reduced response towards CCCP treatment.

hTERT-RPE1-YFP-Parkin cells were transfected for 72hr using either non-targeting control siRNA oligo (NT1) or USP43 siRNA oligo 3 (20nM). Cells were then treated with CCCP (10μM). Mitophagy progression was recorded by live-cell imaging. Scale bar:40μm.

I shortlisted 10 DUBs, for which depletion showed a reduced response towards CCCP treatment. To eliminate off target effects, I further deconvoluted these 10 DUBs using 4 individual siRNA oligos, each used at 20nM (Table 5.1). Based on the deconvolution result, I selected 8 DUBs, which showed a consistent phenotype in at least two out of four individual oligos. DUBs that deconvoluted with two oligos include: BAP1, ZRANB1, USP30 and USP38 whereas USP10, USP42 and USP49 deconvoluted with three. USP43 presented the most promising result, with all four oligos showing the same phenotype (Figure 5.4 to Figure 5.11). Since only one oligo recapitulated the siRNA pool effect for both ATXN3 and OTUD4, these two DUBs were not followed up.

I also observed more cell death with USP30 depletion. This effect was seen with two individual siRNA oligos (Oligo 2 and Oligo 3) as demonstrated by staining with the cell impermeable dye, DRAQ7 during live-cell imaging (Figure 5.12). This effect will be further discussed in the next chapter.

DUB Family	DUB	Screen	Deconvolution					Oligos with the same effects
		Pool	Pool	Oli 1	Oli 2	Oli 3	Oli 4	
UCH	**BAP1**	RR	RR, FC	N	RR, FC	RR, FC	N	2
USP	**USP10**	RR	RR, FC	RR, FC	N	N	RR, FC	3
	USP30	RR	RR, FC, X	N	RR, FC, X	X	RR, FC	2
	USP38	RR	RR, FC	RR, FC	X	DR, FC	N	2
	USP42	RR	RR, FC	RR, NC	RR, FC	RR, NC	N	3
	USP43	RR	RR, FC	RR, FC	RR, FC	RR, FC	RR, FC	4
	USP49	RR	RR, FC	N	RR, FC	RR, FC	RR, FC	3
OTU	**ZRANB1**	RR	RR, FC	RR, FC	*, FC	N	RR, NC	2
	OTUD4	RR	RR, DC	RR, DC	Sick**	N	N	1
MJD	**ATXN3**	RR	N	N	N	RR, NC	N	1

Table 5.1 Overview of shortlisted DUBs from live-cell imaging screen with follow up deconvolution of pool oligos to assess the effect of the DUBs upon siRNA depletion on Parkin-mediated mitophagy.

N: Normal response; NR: Normal recruitment; RR: Reduced response; NC: Normal clearance; FC: Faster clearance; DC: Delayed clearance; X: Cell death

* Cells transfected with ZRANB1 oligo 2 have weak Parkin expression at steady state.

** Cells transfected with OTUD4 oligo 2 looked sick and have very low cell density at steady state.

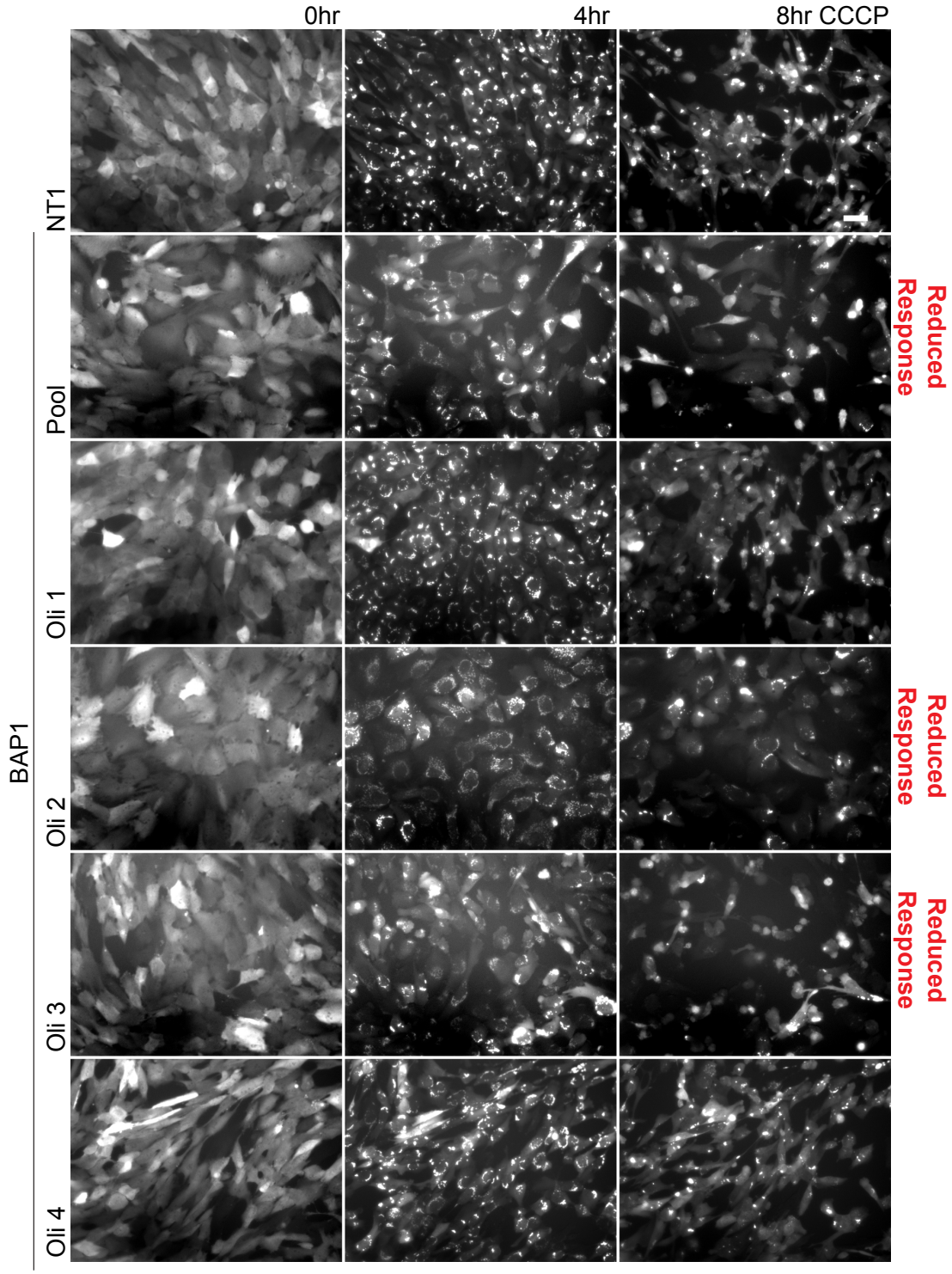

Figure 5.4 BAP1 depletion reduces the mitophagic response during CCCP treatment in hTERT-RPE1-YFP-Parkin cells.

hTERT-RPE1-YFP-Parkin cells were transfected for 72hr with either non-targeting control siRNA (NT1) or siRNA oligos targeting BAP1 (Qiagen pool oligos and 4 individual oligos; Oli 1-4). Cells were then treated with CCCP (10μM). Progression of mitophagy was recorded by live-cell imaging at 30min interval. Representative still frames at 0, 4 and 8 hr after CCCP treatment are shown. Scale bar: 40μm.

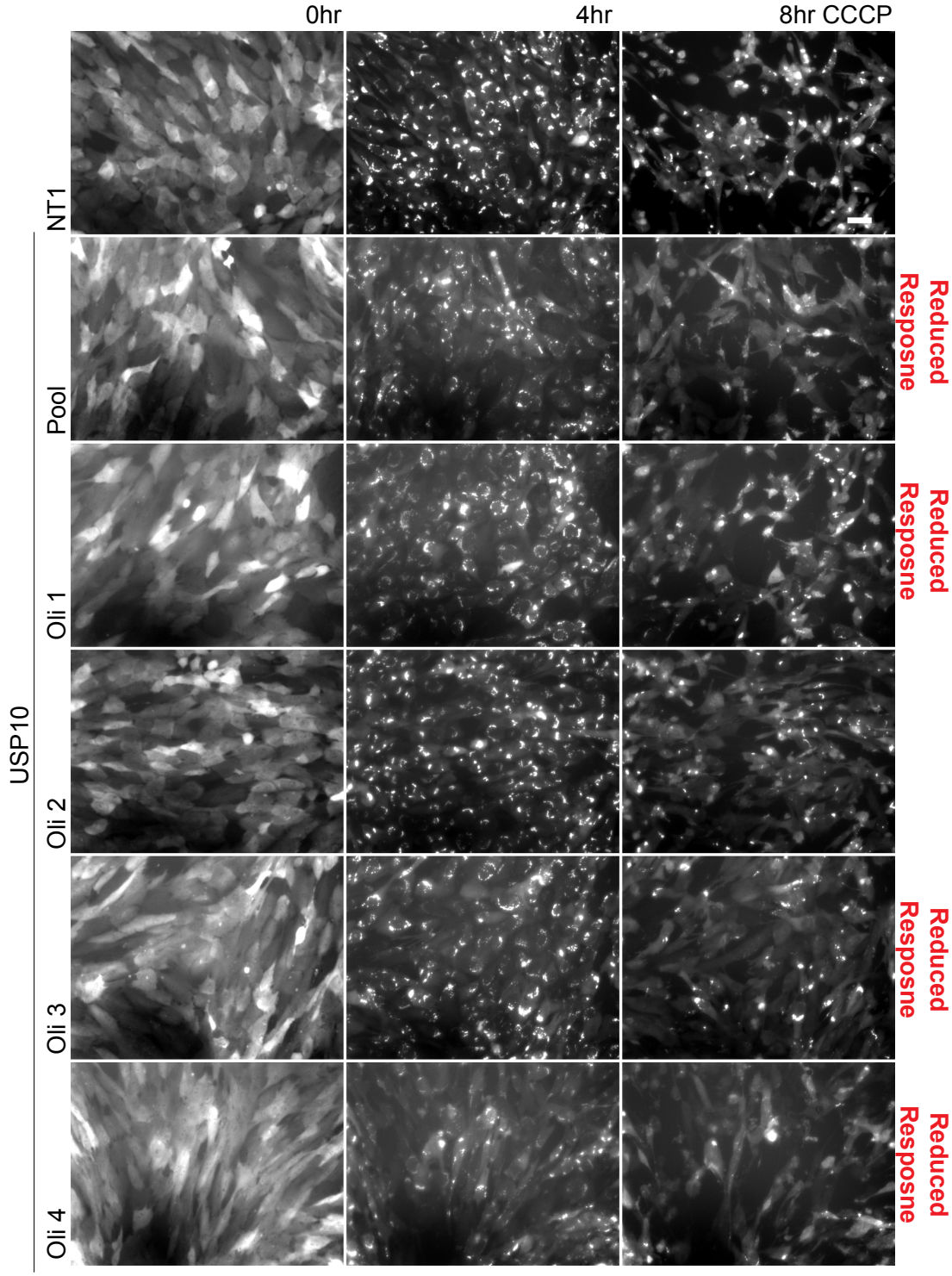

Figure 5.5 USP10 depletion reduces the mitophagic response during CCCP treatment in hTERT-RPE1-YFP-Parkin cells.

hTERT-RPE1-YFP-Parkin cells were transfected for 72hr with either non-targeting control siRNA (NT1) or siRNA oligos targeting USP10 (Qiagen pool oligos and 4 individual oligos; Oli 1-4). Cells were then treated with CCCP (10μM). Progression of mitophagy was recorded by live-cell imaging at 30min interval. Representative still frames at 0, 4 and 8hr after CCCP treatment are shown. Scale bar: 40μm.

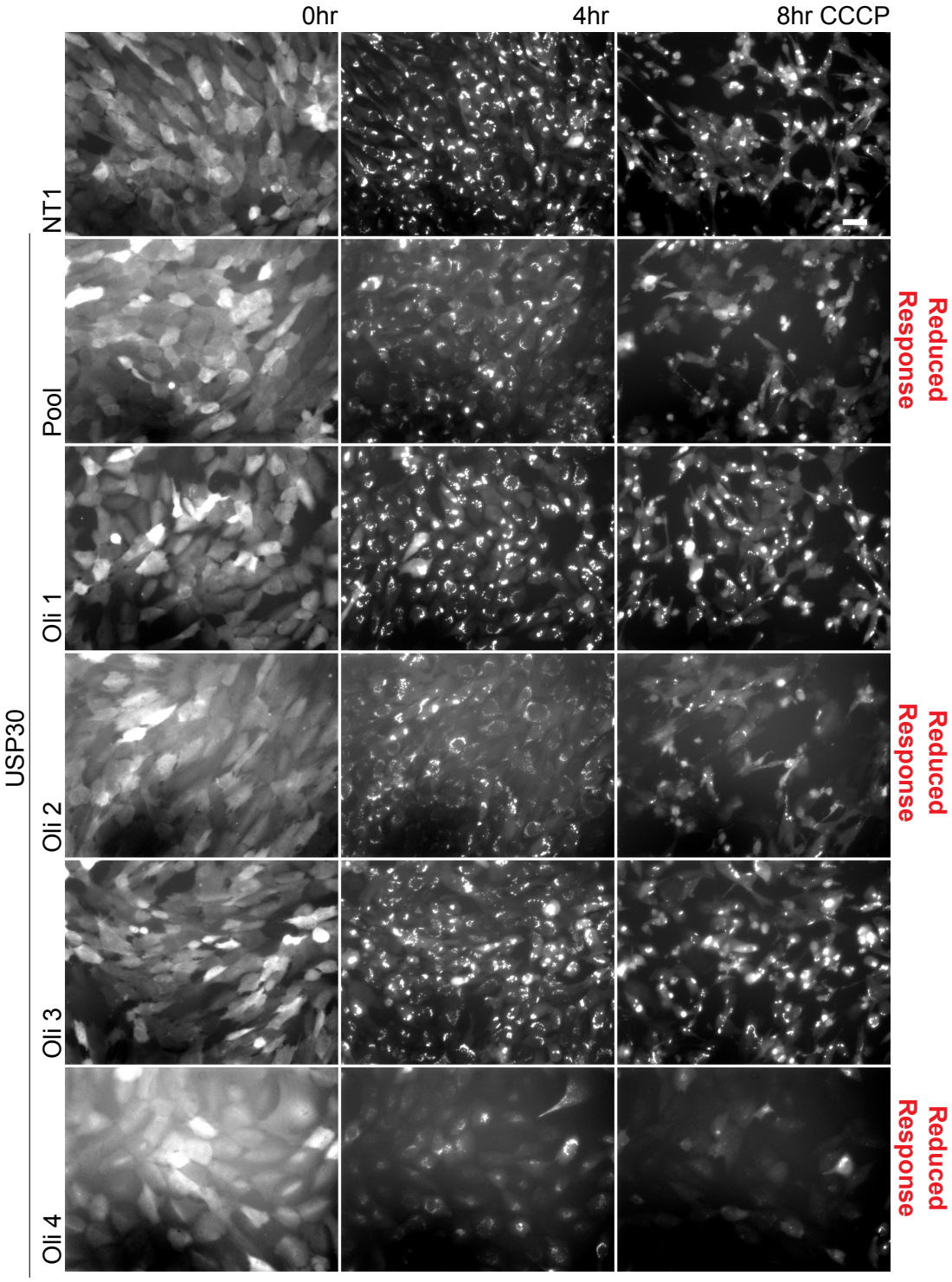

Figure 5.6 USP30 depletion reduces the mitophagic response during CCCP treatment in hTERT-RPE1-YFP-Parkin cells.

hTERT-RPE1-YFP-Parkin cells were transfected for 72hr with either non-targeting control siRNA (NT1) or siRNA oligos targeting USP30 (Qiagen pool oligos and 4 individual oligos; Oli 1-4). Cells were then treated with CCCP (10μM). Progression of mitophagy was recorded by live-cell imaging at 30min interval. Representative still frames at 0, 4 and 8hr after CCCP treatment are shown. Scale bar: 40μm.

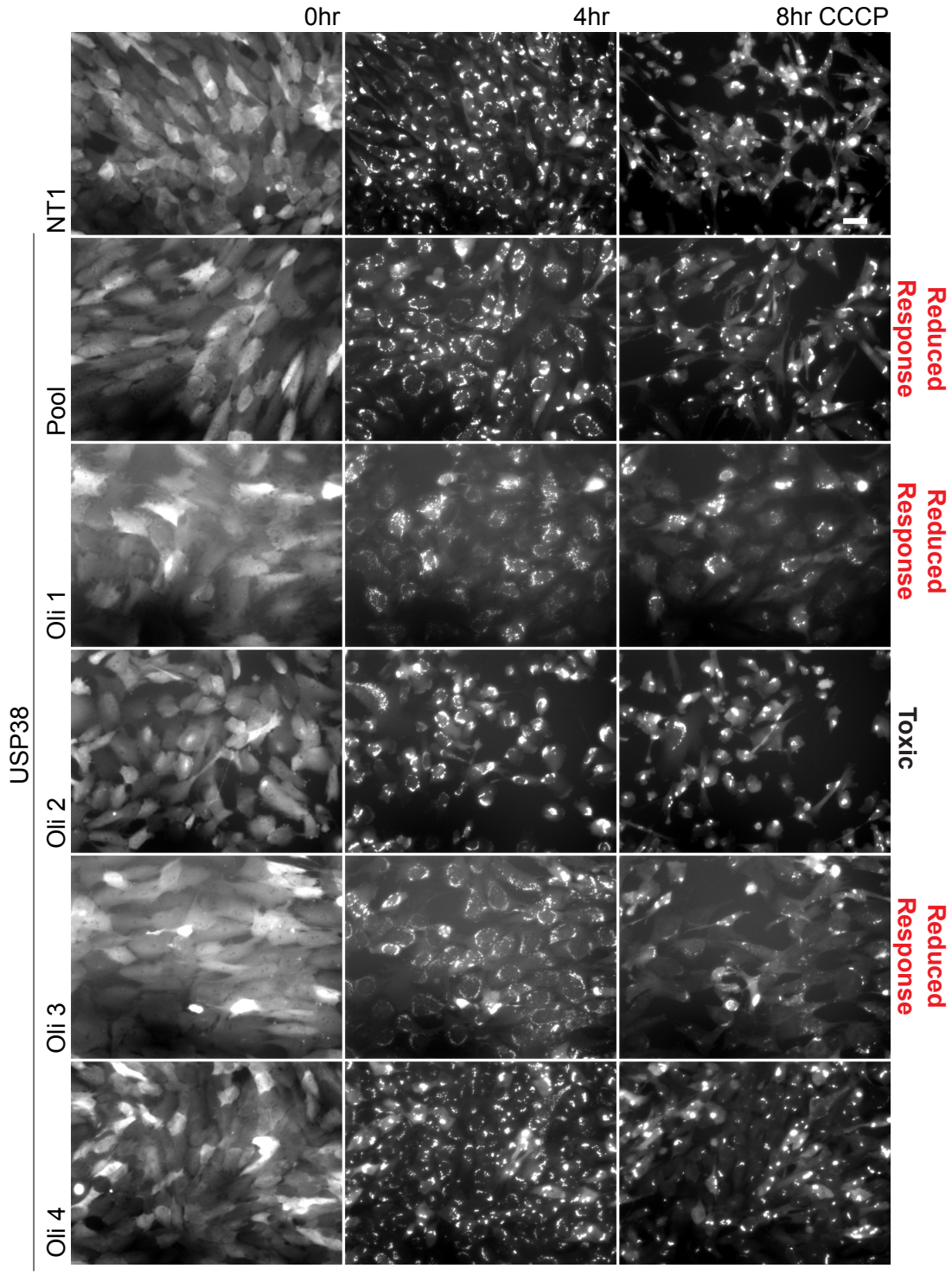

Figure 5.7 USP38 depletion reduces the mitophagic response during CCCP treatment in hTERT-RPE1-YFP-Parkin cells.

hTERT-RPE1-YFP-Parkin cells were transfected for 72hr with either non-targeting control siRNA (NT1) or siRNA oligos targeting USP38 (Qiagen pool oligos and 4 individual oligos; Oli 1-4). Cells were then treated with CCCP (10μM). Progression of mitophagy was recorded by live-cell imaging at 30min interval. Representative still frames at 0, 4 and 8hr after CCCP treatment are shown. Note that transfection with USP38 oligo 2 causes cell death during CCCP treatment. Scale bar: 40μm.

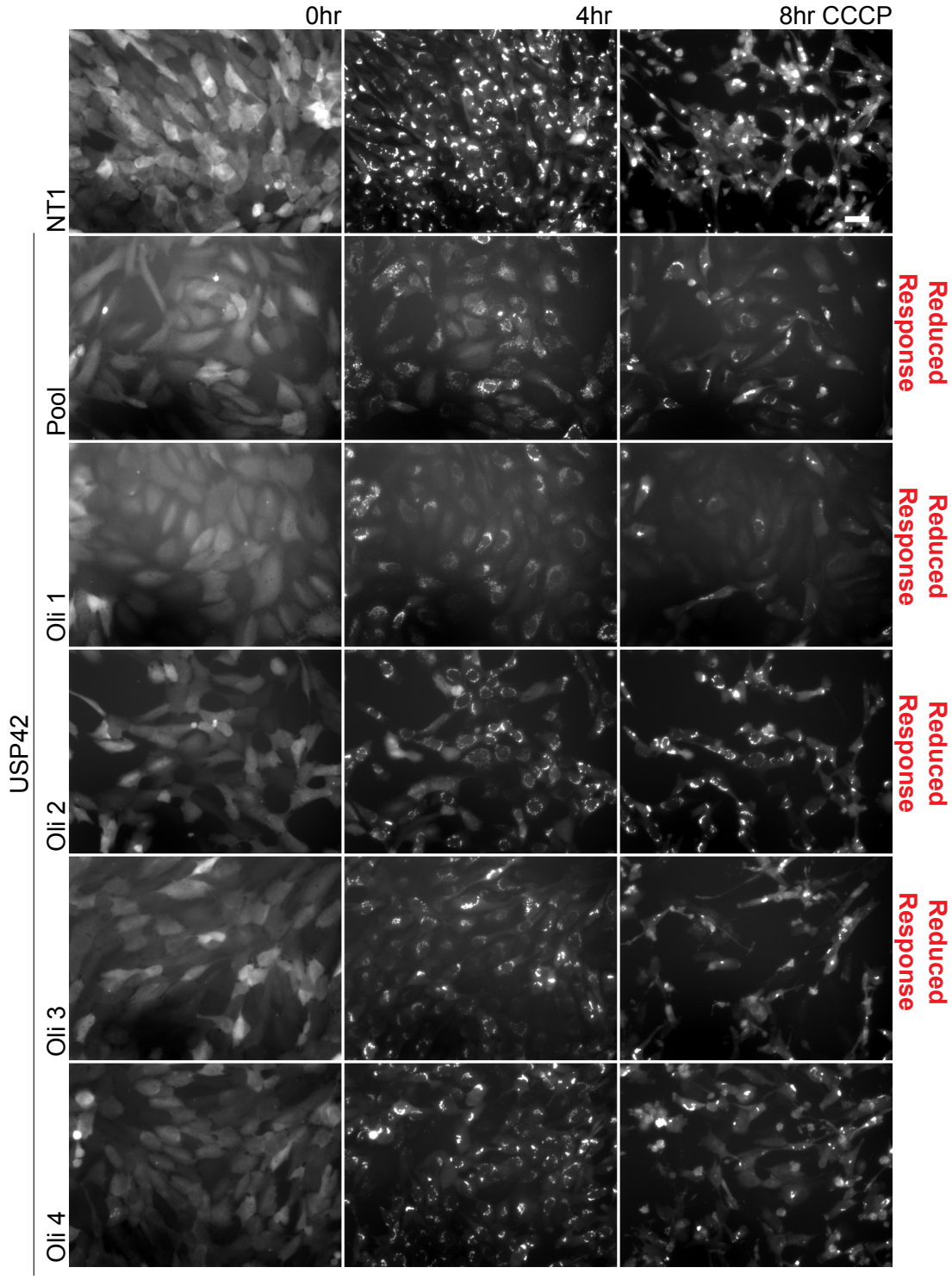

Figure 5.8 USP42 depletion reduces the mitophagic response during CCCP treatment in hTERT-RPE1-YFP-Parkin cells.

hTERT-RPE1-YFP-Parkin cells were transfected for 72hr with either non-targeting control siRNA (NT1) or siRNA oligos targeting USP42 (Qiagen pool oligos and 4 individual oligos; Oli 1-4). Cells were then treated with CCCP (10μM). Progression of mitophagy was recorded by live-cell imaging at 30min interval. Still frames at 0, 4 and 8hr after CCCP treatment are shown. Scale bar: 40μm.

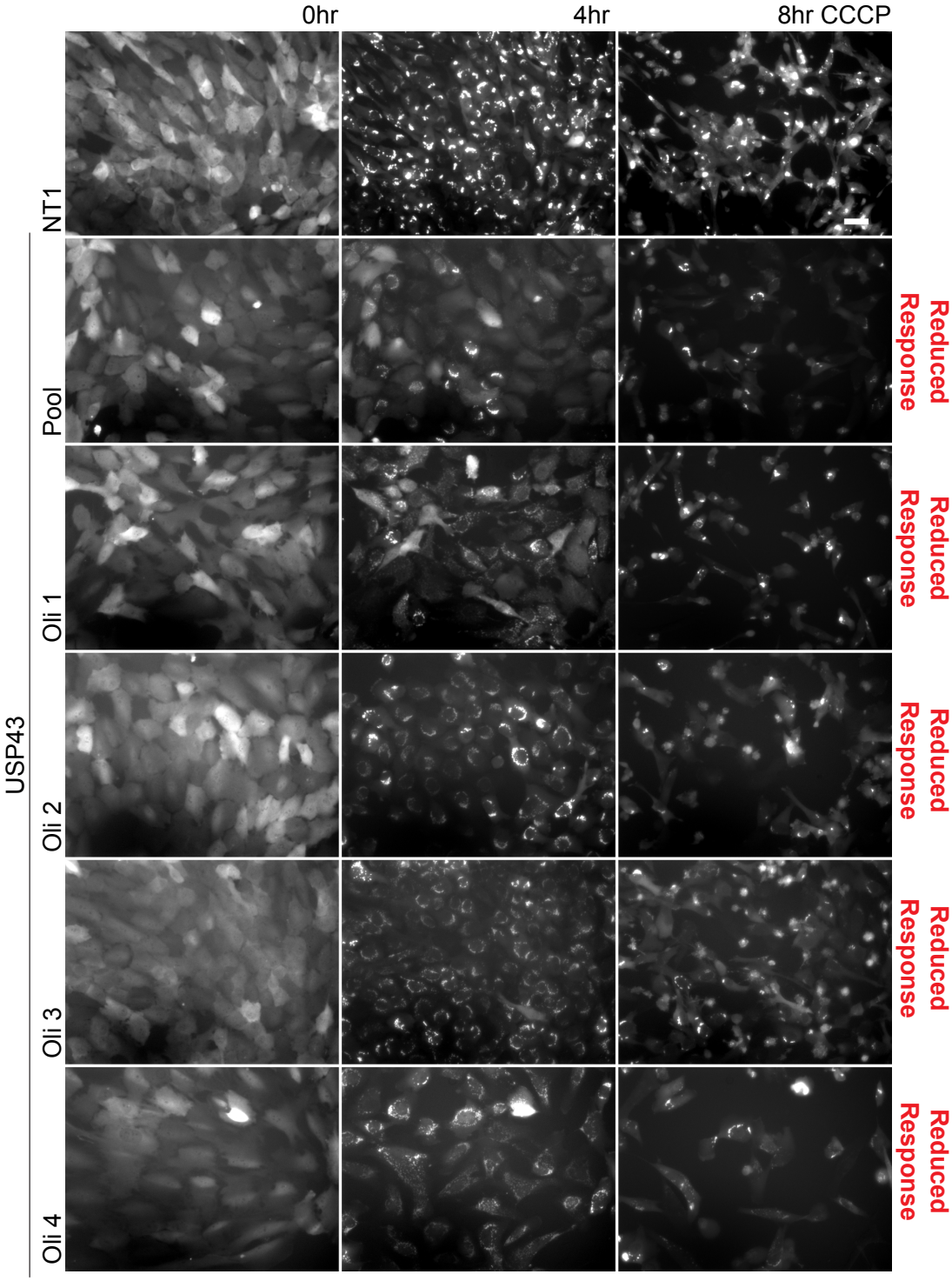

Figure 5.9 USP43 depletion reduces the mitophagic response during CCCP treatment in hTERT-RPE1-YFP-Parkin cells.

hTERT-RPE1-YFP-Parkin cells were transfected for 72hr with either non-targeting control siRNA (NT1) or siRNA oligos targeting USP43 (Qiagen pool oligos and 4 individual oligos; Oli 1-4). Cells were then treated with CCCP (10μM). Progression of mitophagy was recorded by live-cell imaging at 30min interval. Still frames at 0, 4 and 8hr after CCCP treatment are shown. Scale bar: 40μm.

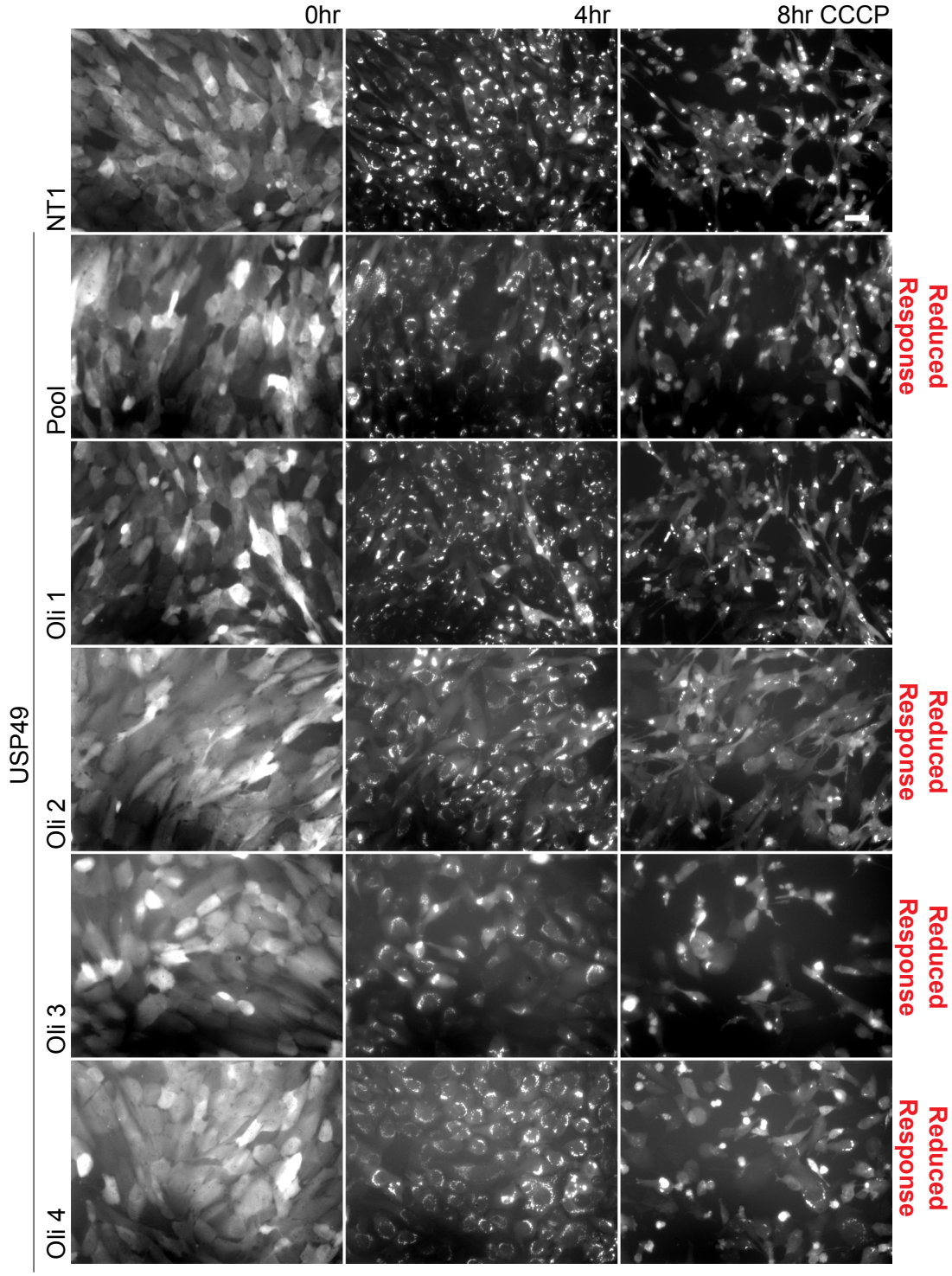

Figure 5.10 USP49 depletion reduces the mitophagic response during CCCP treatment in hTERT-RPE1-YFP-Parkin cells.

hTERT-RPE1-YFP-Parkin cells were transfected for 72hr with either non-targeting control siRNA (NT1) or siRNA oligos targeting USP49 (Qiagen pool oligos and 4 individual oligos; Oli 1-4). Cells were then treated with CCCP (10μM). Progression of mitophagy was recorded by live-cell imaging at 30min interval. Representative still frames at 0, 4 and 8hr after CCCP treatment are shown. Scale bar: 40μm.

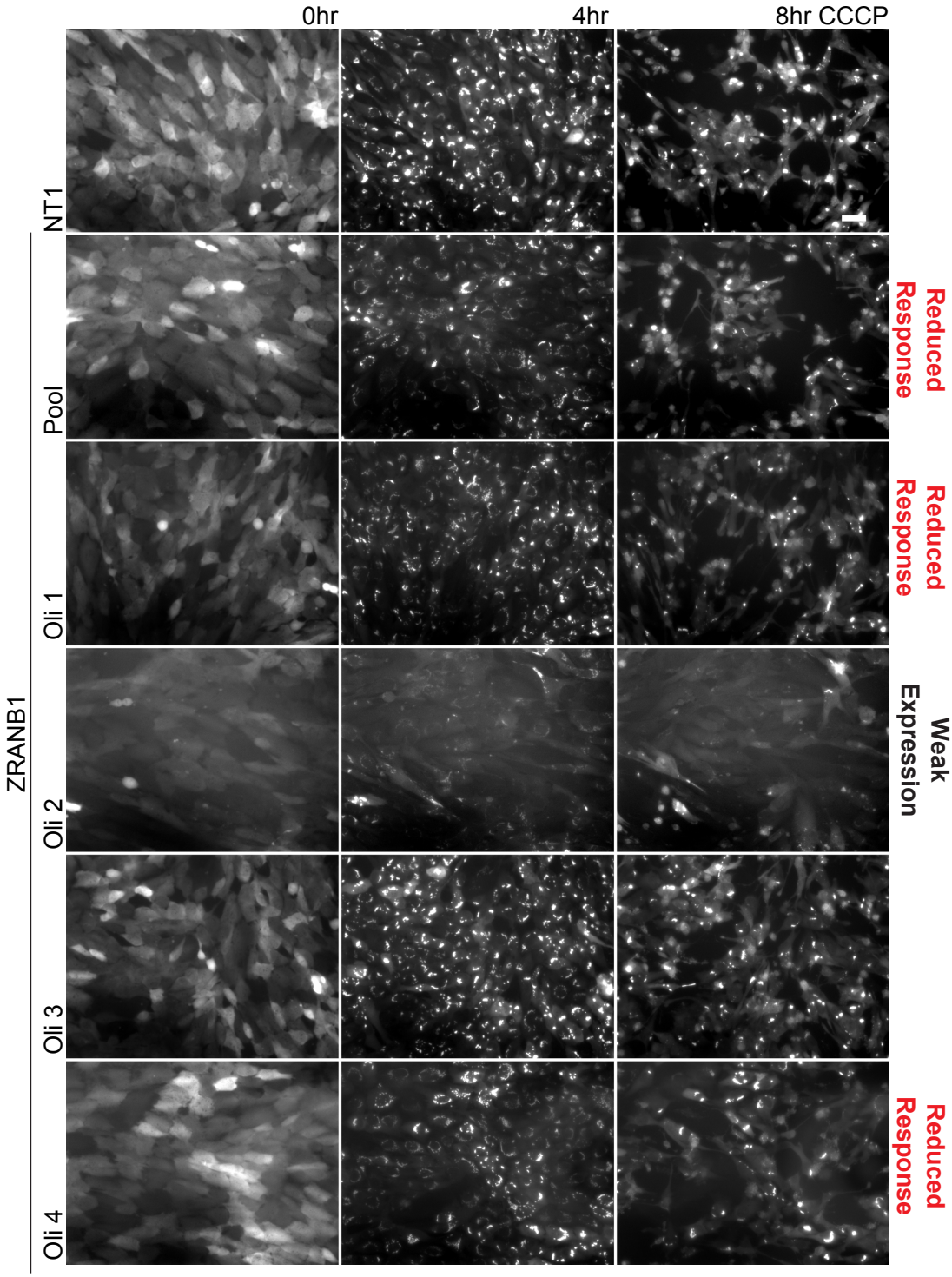

Figure 5.11 ZRANB1 depletion reduces the mitophagic response during CCCP treatment in hTERT-RPE1-YFP-Parkin cells.

hTERT-RPE1-YFP-Parkin cells were transfected for 72hr with either non-targeting control siRNA (NT1) or siRNA oligos targeting ZRANB1 (Qiagen pool oligos and 4 individual oligos; Oli 1-4). Cells were then treated with CCCP (10μM). Progression of mitophagy was recorded by live-cell imaging at 30min interval. Representative still frames at 0, 4 and 8hr after CCCP treatment are shown. Note that transfection with oligo 2 resulted in weak Parkin expression. Scale bar: 40μm.

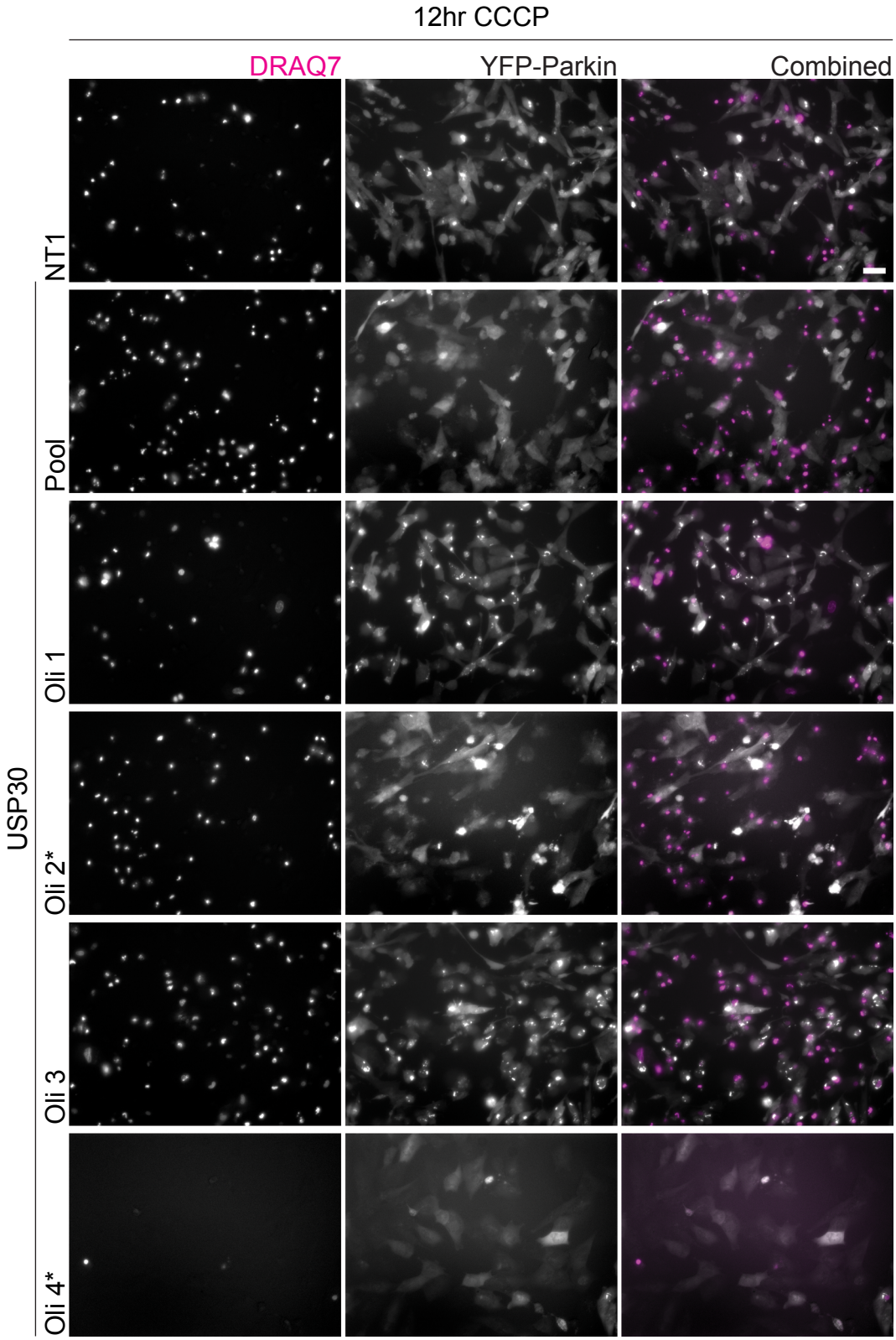

Figure 5.12 USP30 depletion enhanced mitophagic cell death.
Representative still frames at 12hr of CCCP treatment in USP30 depleted cells from the same experiment shown in Figure 5.6. Membrane impermeable DRAQ7 dye was used to visualize dead cells (pseudocoloured in pink). Scale bar: 40µm. Asterisk: Oligos that showed a reduced mitophagic response at 4hr.

5.2.4 Western blot analysis of the effects of selected DUB siRNAs on Parkin-mediated mitophagy

Live-cell imaging of YFP-Parkin translocation to the mitochondria provides limited information regarding the ubiquitylation of mitochondrial proteins and their subsequent degradation. On the contrary, a biochemical analysis of the cell lysates after CCCP treatment by western blotting, allows one to probe for multiple proteins of interest and provides more information regarding mitophagy activation and progression. Therefore, I followed up on the top hits from the live-cell imaging screen with a western blotting approach (Figure 5.13). Note that USP30 was not included in this analysis, as it will be fully characterised in Chapter 6.

I first assessed cleavage of L-OPA1 to S-OPA1 in these cells. OPA1 cleavage is one of the indicators of mitochondrial fragmentation, which in turn, is one of the earliest responses towards mitochondrial depolarization. NT1 and PINK1 both showed partial OPA1 cleavage at 4hr and near complete OPA1 cleavage after 8hr of CCCP treatment. Intriguingly, all of the siRNAs targeting the candidate top hits either partially or completely inhibited OPA1 cleavage. This effect is particularly apparent in USP42 and USP43-depleted cells, which did not exhibit OPA1 cleavage. PINK1 accumulation during CCCP treatment in these cells was also reduced compared to the other DUB siRNA samples. Consistent with this, USP42 and USP43-depleted cells showed increased levels of unmodified and less ubiquitylated Parkin. USP42 and USP43-depleted cells also displayed higher basal levels of MIRO, which remained steady even after 8hr of CCCP treatment. These observations strongly indicate that USP42 and USP43-depleted cells have an impaired response to CCCP-induced mitochondrial depolarisation.

Knockdown of the remaining DUBs, including USP10, USP49, BAP1 and ZRANB1 resulted in partial OPA1 cleavage and also weaker PINK1 accumulation compared to control NT1. This also translates into weaker Parkin autoubiquitylation and less MIRO degradation. These observations corroborate the reduced CCCP response I observed by live-cell imaging.

Interestingly, USP49 depletion reduced the basal protein levels of MIRO, indicating that USP49 might affect its stability. For these reasons, I proceeded by deconvoluting the siRNA oligo pools targeting USP42, USP43 and USP49.

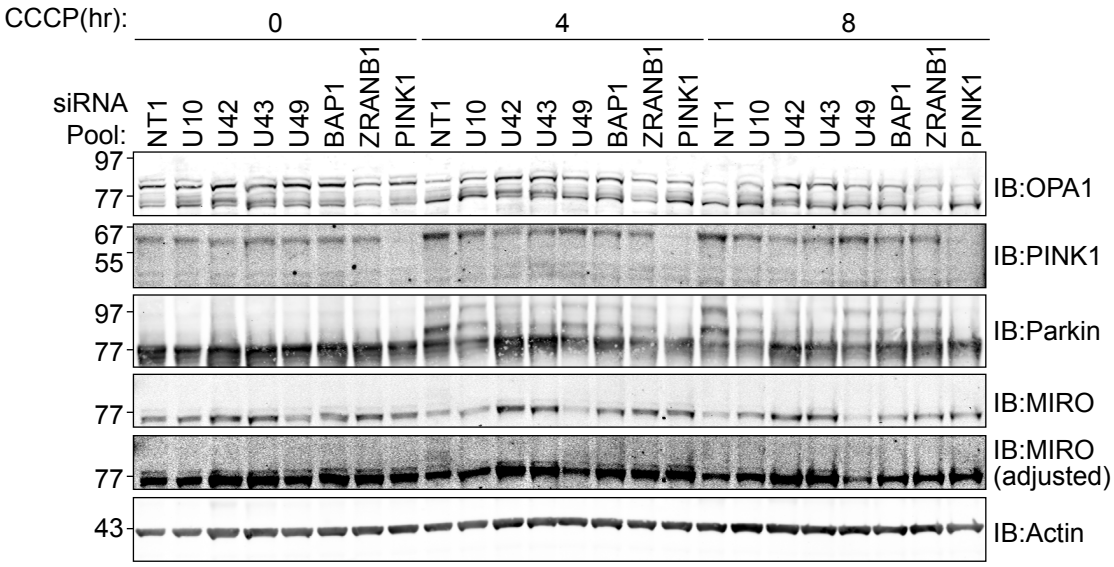

Figure 5.13 Biochemical analysis of DUBs shortlisted from the visual screen.

hTERT-RPE1-YFP-Parkin cells were transfected for 72hr with either the non-targeting siRNA control (NT1) oligo or the indicated Qiagen pooled siRNA oligos. Cells were then treated with CCCP (10μM) and harvested using NP40 lysis buffer at the indicated times. 10μg of lysates were probed for the indicated proteins.

5.2.5 Deconvolution of USP49 siRNA oligos in hTERT-RPE1-YFP-Parkin cells

I first assessed MIRO protein levels upon transfection with four individual siRNA oligos targeting USP49 (Figure 5.14). Only transfection with oligo Q8 recapitulated the reduced MIRO levels observed with the pool of siRNA oligos in Figure 5.13. In addition, TIMM44 and TOM20 levels were also reduced. This suggests that USP49 oligo Q8 might cause global reduction in mitochondria in cells. While I did not assess the knockdown efficiency, the fact that only one oligo recapitulated the effect of the pool suggests that this is most likely an off-target effect.

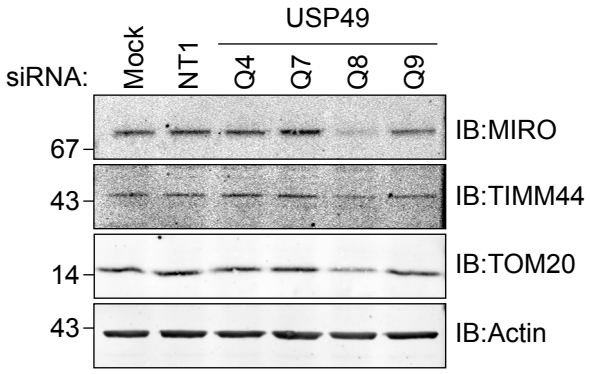

Figure 5.14 USP49 siRNA deconvolution.

hTERT-RPE1-YFP-Parkin cells were transfected for 72hr with either mock (transfection reagent without siRNA oligo), non-targeting siRNA oligo (NT1), or siRNA oligos targeting USP49 (Q4, Q7, Q8 and Q9). Cells were harvested in RIPA lysis buffer. 10µg of lysates were probed as indicated.

5.2.6 Characterisation of the effects of USP42 and USP43 depletion on Parkin depending mitophagy

5.2.6.1 USP42 and USP43 depletion impedes mitophagy

Deconvolution of USP42 oligos showed that three (Q5, Q6 and Q7) out of the four siRNA oligos inhibited or delayed PINK1 accumulation and Parkin activation (Figure 5.15). Subsequently, MIRO, MFN2, TOM20 and TIMM44 were not degraded. This recapitulated the effects seen with the pooled oligos in Figure 5.13.

Since USP42 has previously been described as a DUB for p53(Hock et al. 2011), I also assessed p53 levels in USP42 depleted cells. In the control cells, I observed that CCCP treatment induced accumulation of p53. Two out of four oligos (Q5 and Q7) targeting USP42 prevented the accumulation of p53. In order to assess the knockdown efficiency, I measured the mRNA levels of USP42 after 24hr of siRNA transfection using qRT-PCR (Figure 5.15B). Transfection with all four oligos decreased USP42 mRNA level by 30-60%. While transfection with oligo Q2 reduced the mRNA levels by 60%, it did not inhibit PINK1 accumulation, Parkin activation or degradation of MIRO, MFN2, TOM20 and TIMM44. One possibility is that oligo Q2 transfection has other off-target effects that override the inhibition of mitophagy caused by USP42 depletion.

USP43 depletion with oligos Q2, Q5 and Q6 has similar, but weaker effects on CCCP-induced mitophagy than USP42 depletion. In NT1-transfected cells, PINK1 and Ub-Parkin accumulated by 4hr of CCCP treatment. USP43 Q5 and Q6 transfected cells only showed low levels of both PINK1 and Ub-Parkin even after 8hr of CCCP treatment. MIRO, MFN2, TOM20 and TIMM44 degradation was also inhibited with Q2 and delayed with oligo Q5 and Q6. As the cells transfected with USP43 oligo Q7 at 8hr of CCCP treatment were infected, that sample was not included in the analysis. Two out of four oligos prevented p53 accumulation. As there is no commercially

available USP43 antibody, I also assessed the relative knockdown efficiency by measuring USP43 mRNA levels 24hr post-transfection. Transfection with all four oligos decreased USP43 mRNA levels by 30-50%.

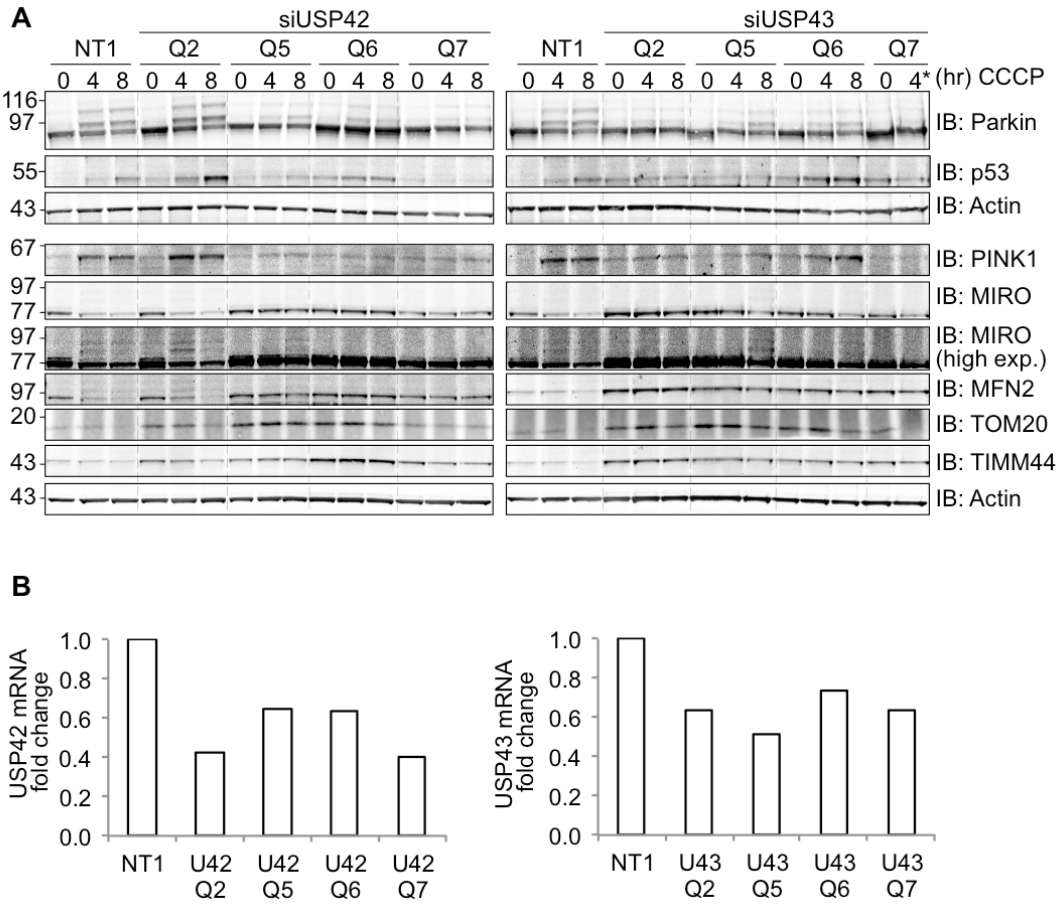

Figure 5.15 siRNA deconvolution for USP42 and USP43.

(A) hTERT-RPE1-YFP-Parkin cells were transfected for 72hr with either non-targeting siRNA control oligo (NT1) or siRNA oligos targeting USP42 (Q2, Q5, Q6 and Q7) and USP43 (Q2, Q5, Q6 and Q7). Cells were then treated with CCCP (10μM) and harvested with RIPA lysis buffer at the indicated times. 15μg of lysates were probed as indicated.
(B) hTERT-RPE1-YFP-Parkin cells were transfected for 24hr in parallel with cells shown in (A). Cells were then harvested for reverse transcription and qRT-PCR. cDNA levels of USP42 and USP43 were normalized to actin and expressed as relative fold change compared to NT1 (n=1).

5.2.6.2 USP42 and USP43 depletion partially inhibits OPA1 cleavage

Since OPA1 cleavage precedes, and is independent of Parkin recruitment, this suggests that the inhibitory effect of USP42 and USP43 depletion lies most likely upstream of PINK1 and Parkin activation. Indeed, also in parental hTERT-RPE cells, USP42 and USP43 depletion followed by 8hr of CCCP treatment partially inhibited the cleavage of L-OPA1 and the accumulation of S-OPA1 (Figure 5.16A). In addition, PINK1 accumulation was also reduced in USP42 and USP43 depleted cells. These results suggest that USP42 and USP43 depletion reduces the mitochondrial response to membrane depolarisation. However, USP42 and USP43 depletion in HEK293T cells did not prevent CCCP-induced OPA1 cleavage, suggesting that this may be a cell type-dependent effect (Figure 5.16B).

One hypothesis for the inhibition of OPA1 cleavage could be decreased sensitivity of the cells towards CCCP treatment upon USP42 and USP43 depletion. Therefore, I asked if the partial inhibition of OPA1 cleavage could be overcome by increasing the concentration of CCCP. Indeed, by doubling the concentration of CCCP used, from 10μM to 20μM, the inhibitory effect on OPA1 cleavage was abolished. Subsequently, PINK1 accumulation, Parkin activation and mitochondrial protein degradation (MIRO, TOM20 and TIMM44) were now also observed in USP42 and USP43 depleted cells (Figure 5.16C).

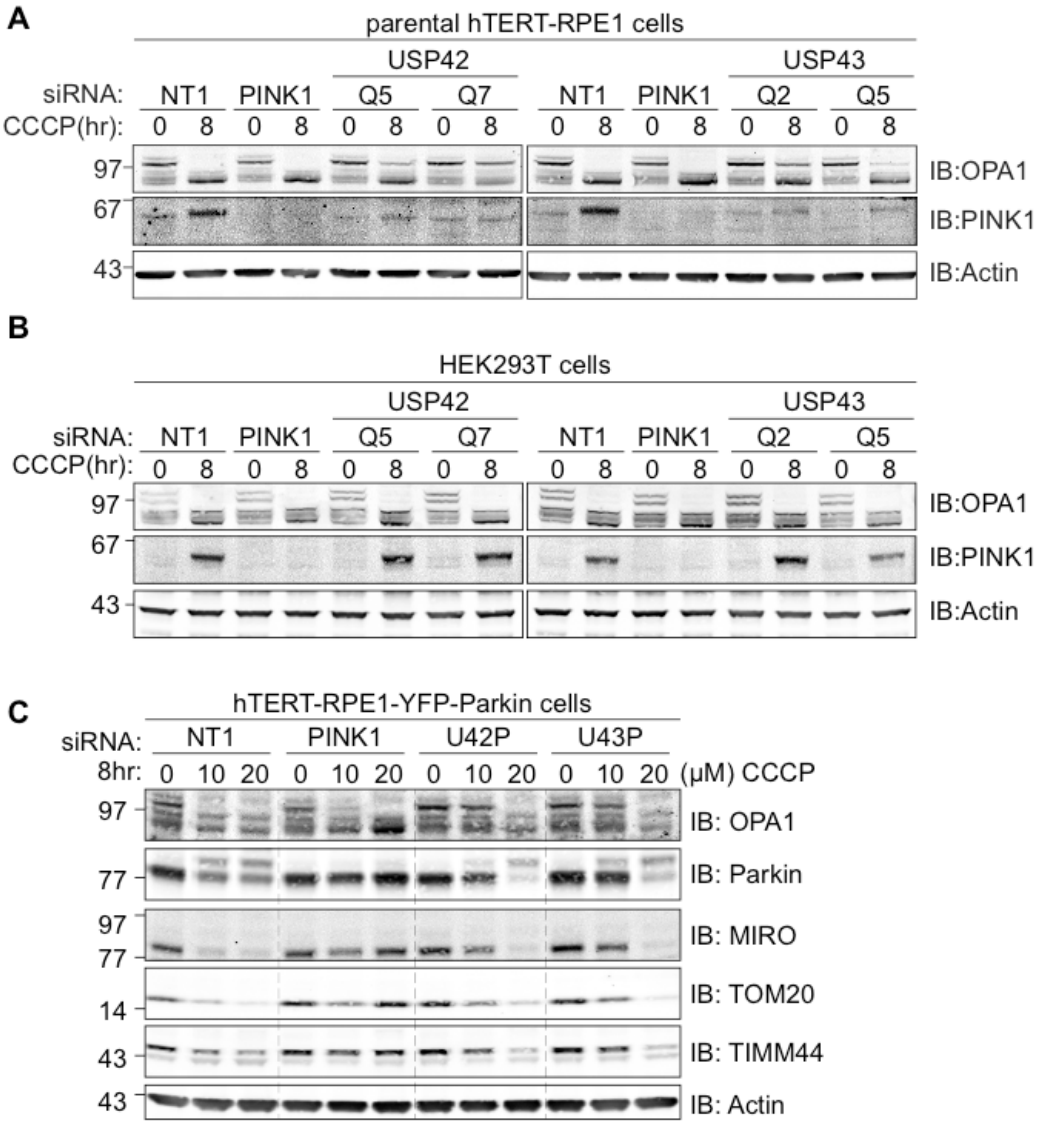

Figure 5.16 Delayed OPA1 cleavage observed in USP42 and USP43 depleted cells is independent of Parkin but can be overcome by high concentrations of CCCP.

(A) Parental hTERT-RPE1 cells were transfected for 72hr with either non-targeting siRNA control (NT1) oligo or siRNA oligos targeting USP42 (Q5 and Q7) and USP43 (Q2 and Q5) for 72hr. Cells were then treated with CCCP (10μM) for 8hr and harvested with RIPA lysis buffer. 10μg of lysates were probed as indicated.
(B) HEK293T cells were transfected and treated the same as in (A).
(C) hTERT-RPE1-YFP-Parkin cells were transfected with 40nM of siRNA against USP42 (Qiagen pool oligos) and USP43 (Qiagen pool oligos) for 72hr. Cells were then treated with either 0, 10 or 20μM of CCCP for 8hr. Cells were harvested in RIPA lysis buffer. 10μg of lysates were immunoprobed as indicated.

Next, I chose two siRNA oligos each for USP42 (Q5 and Q7) and USP43 (Q2 and Q5) to follow up on the effects of USP42 and USP43 depletion on mitochondria by fixed-cell immunofluorescence (Figure 5.17). Based on staining with TOM20 antibodies, I did not observe obvious changes in mitochondrial morphology upon USP42 and USP43 depletion. After 8hr of CCCP treatment, TOM20 staining was either lost or co-localised with YFP-Parkin aggregates in NT1 cells. In contrast, TOM20 staining remained strong in PINK1, USP42 and USP43-depleted cells and did not co-localise with YFP-Parkin. However, unlike PINK1-depleted cells in which mitochondria appeared fragmented, USP42 and USP43-depleted cells still presented with elongated mitochondria. This observation is in agreement with the lack of OPA1 cleavage first seen in delayed/inhibited degradation of MIRO, TOM20 and TIMM44 observed in Figure 5.13.

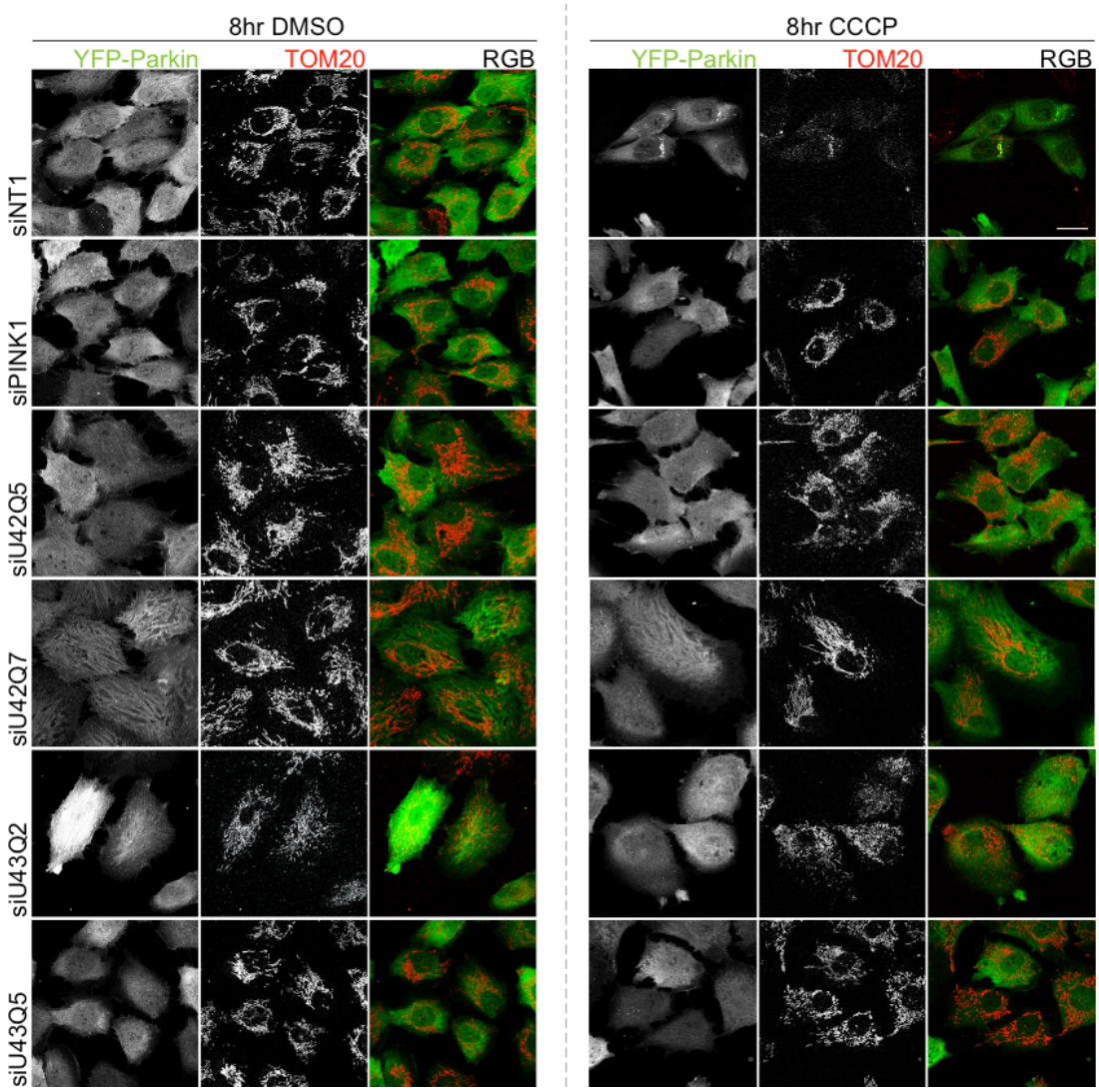

Figure 5.17 siUSP42 and USP43 prevent mitochondrial fragmentation and loss of mitochondria in CCCP-treated hTERT-RPE1-YFP-Parkin cells.

hTERT-RPE1-YFP-Parkin cells were transfected for 72hr with either non-targeting siRNA control (NT1) oligo or siRNA oligo targeting PINK1, USP42 (Q5 and Q7) or USP43 (Q2 and Q5). Cells were then treated with CCCP (10μM). After 8hr, cells were fixed and stained with anti-TOM20. Images were taken using confocal microscope. Scale bar: 20μm.

5.2.6.3 USP43 depletion does not affect VPS35 protein levels

One of the reported interactors of USP43 is VPS35, a subunit of the retromer complex (Sowa et al. 2009). Interestingly, VPS35 mutations have been reported in Parkinson's Disease (Zimprich et al. 2011, Vilarino-Guell et al. 2011). I assessed VPS35 protein levels under basal and CCCP-treated conditions. USP43 depletion over 72hrs did not affect VPS35 protein levels.

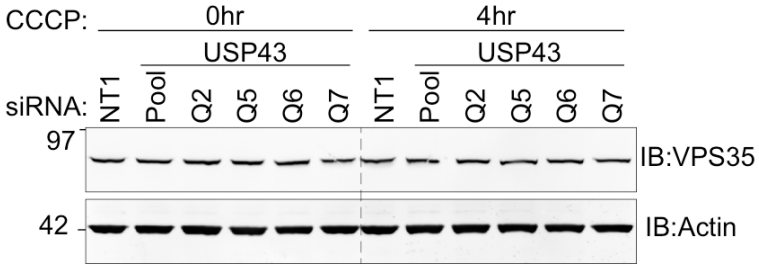

Figure 5.18 USP43 siRNA deconvolution to assess the levels of VPS35.
hTERT-RPE1-YFP-Parkin cells were transfected for 72hrs with either non-targeting siRNA control (NT1) or siRNA targeting USP43 (Q2, Q5, Q6, Q7) for 72hr. Cells were then treated with CCCP (10μM) for 4hr. Cells were harvested in RIPA lysis buffer and 20μg of lysates were probed as indicated.

5.3 Biochemical screen for DUBs involved in Parkin-mediated mitophagy in hTERT-RPE1-YFP-Parkin cells

At a later stage of my project, I decided to carry out a full siRNA DUB screen by western blotting assess the different stages during mitophagy:

(1) Mitochondrial depolarization and fragmentation (L-OPA1 to S-OPA1 cleavage)
(2) Activation of Parkin (PINK1 accumulation and Parkin ubiquitylation)
(3) Proteasomal degradation of OMM proteins (MIRO loss)
(4) Autophagosomal degradation of mitochondria (TIMM44 and S-OPA1 loss)

I first carried out a biochemical screen in hTERT-RPE1-YFP-Parkin cells. For this screen, I used a new customized DUB siRNA library provided by QIAGEN consisting of siRNA pools comprised of four individual siRNA oligos targeting 94 DUBs. This DUB siRNA library is identical to the previous 92-DUB siRNA library described in the previous screen but upgraded with two newly identified DUBs, namely FAM105B (OTULIN) and C14orf28. I performed the screen using a total of 18x 6-well plates. On top of the 94 siRNA pools, I also included two non-targeting siRNA oligos (NT1, NT3) as negative controls whereas an siRNA pool targeting PINK1 was used as a positive control. For internal comparison as well as comparison across different blots, I also included mock controls (transfection reagent without siRNA) of pre- and post-treatment (named Mock T0 and T8) to be loaded onto each gel.

Instead of CCCP, I decided to use a combination of 1μM each of oligomycin A and antimycin A (O+A) for 8hr, which I showed in chapter 3 to effectively induce Parkin-mediated mitophagy by specifically inhibiting the mitochondrial electron transport chain complex V and complex III. I split the 18x 6-well plates into four batches, for which I staggered O+A treatment of each batch in 30min interval to allow sufficient time for harvesting.

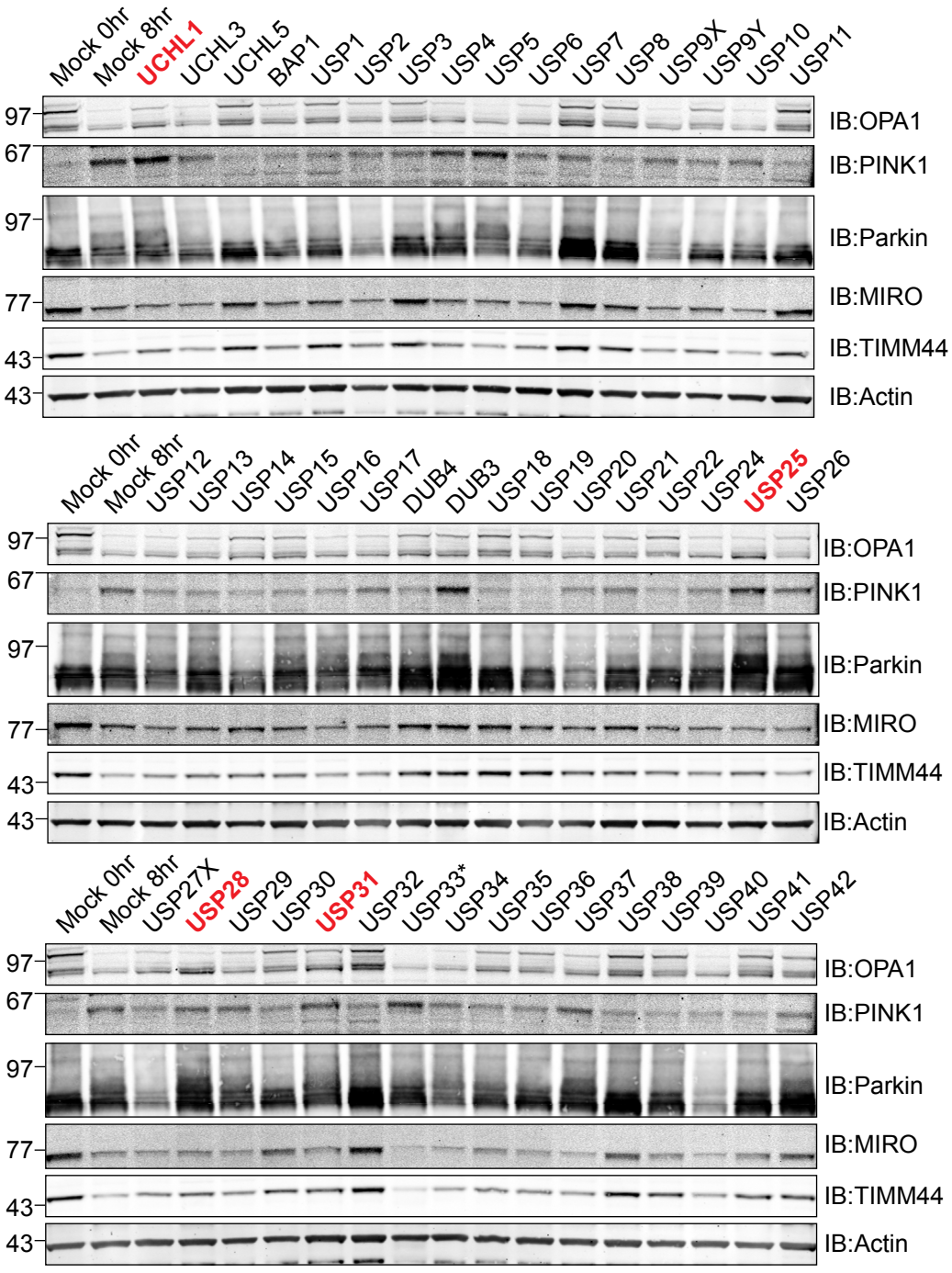

Figure 5.19 Biochemical Screen for DUBs regulating Parkin-dependent mitophagy in hTERT-RPE1-YFP-Parkin cells.

hTERT-RPE1-YFP-Parkin cells were treated for 72hr with either mock (transfection reagent without siRNA oligo), non-targeting siRNA oligos (NT1 and NT3), PINK1, or siRNA oligos targeting 94 DUBs (20nM). Cells were treated with oligomycin A and antimycin A (1μM each) for 8hr and harvested in RIPA lysis buffer. 10μg of lysates were probed as indicated. Asterisk: infected sample. DUBs labeled in red: shortlisted hits.

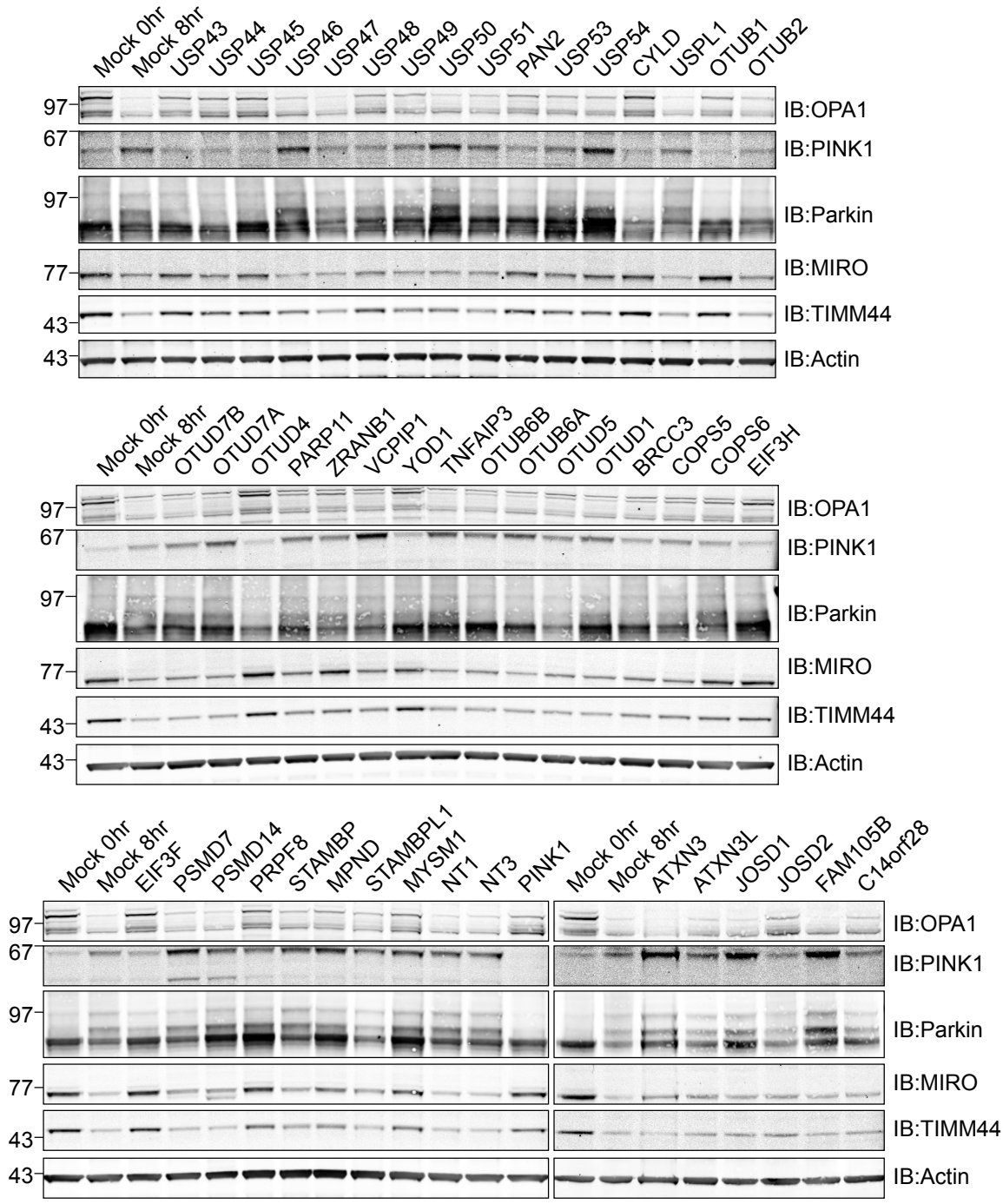

Figure 5.20 Biochemical Screen for DUBs regulating Parkin-dependent mitophagy in hTERT-RPE1-YFP-Parkin cells (continued from Figure 5.19).

hTERT-RPE1-YFP-Parkin cells were treated for 72hr with either mock (transfection reagent without siRNA oligo), non-targeting siRNA oligos (NT1 and NT3), PINK1, or siRNA oligos targeting 94 DUBs (20nM). Cells were treated with oligomycin A and antimycin A (1μM each) for 8hr and harvested in RIPA lysis buffer. 10μg of lysates were probed as indicated.

The first striking observation from the screen was the high number of DUBs-targeting siRNA that either partially or completely inhibited OPA1 cleavage after 8hr of O+A treatment (Figure 5.19 and Figure 5.20). This is demonstrated by the scatter plot in Figure 5.21. DUB siRNAs positioned on the top right-hand quadrant (e.g. USP7 and OTUD4) represents proteins with high protein band intensities for both L-OPA1 and S-OPA1, indicating the lack of L-OPA1 cleavage and the lack of downstream mitophagic degradation of OPA1. DUB-siRNAs that are distributed more towards the bottom left-hand quadrant promote cleavage of L-OPA1 and lower levels of S-OPA1 due to efficient mitophagy (e.g. ATXN3 and USP47). On the other hand, DUB-siRNAs that are distributed more towards the top left-hand quadrant (e.g. USP25 and USP28) represents proteins with L-OPA1 cleavage but accumulated S-OPA1 due to inhibited mitophagy.

Proportionally, DUB depletions that led to partial cleavage of OPA1 showed weaker PINK1 accumulation, Parkin ubiquitylation and loss of MIRO and TIMM44. Since PINK1 accumulation and Parkin ubiquitylation requires the preceding cleavage of OPA1, it is not possible to assess whether these DUBs affect the downstream events of mitophagy.

I next assessed the proteasomal and lysosomal degradation of mitochondrial proteins in DUBs for which depletion did not affect, or only partially affected OPA-1 cleavage. To this end, I assessed MIRO levels (proteasomal degradation) and TIMM44 levels (lysosomal degradation). In addition, OPA1 is also an IMM protein. While L-OPA1 is cleaved and accumulated as S-OPA1, the latter, is degraded in lysosomes. This is illustrated by a good correlation between S-OPA1 and TIMM44 protein levels across the dataset (R^2=0.595; Figure 5.22A). In contrast, whilst proteasomal degradation of MIRO is usually followed by TIMM44 degradation, the correlation between TIMM44 and MIRO protein levels is lower compared to that between S-OPA1 and TIMM44 (R^2=0.357; Figure 5.22B), revealing a differential regulation of the proteasomal and lysosomal degradation pathways.

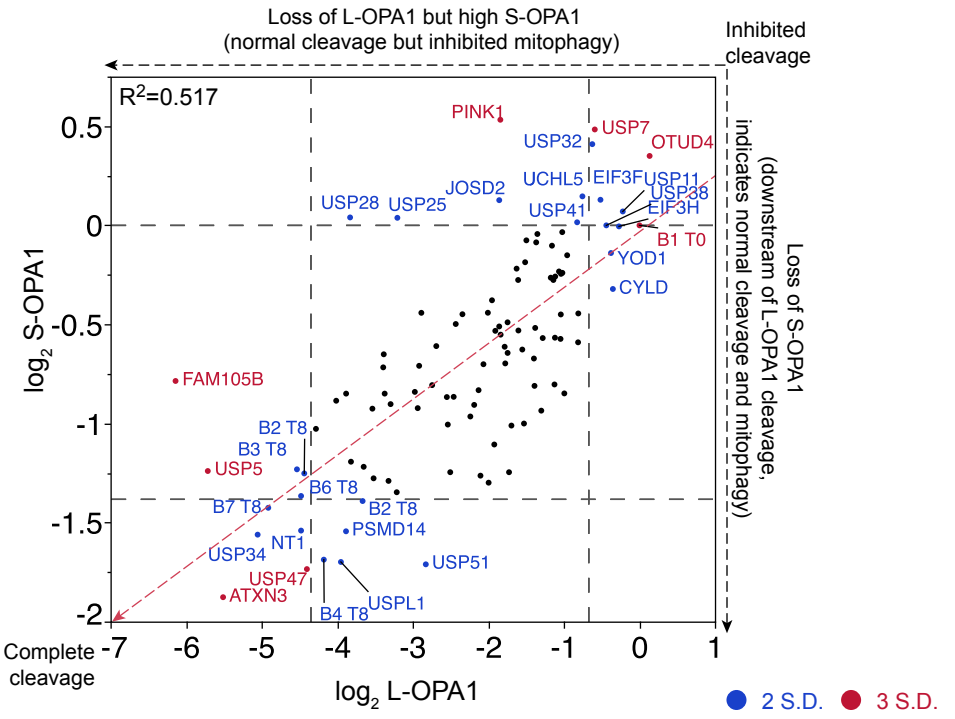

Figure 5.21 Statistical analysis of OPA1 cleavage upon 8hr of oligomycin A and antimycin A-induced mitophagy in hTERT-RPE1-YFP-Parkin cells.

Scatter plot demonstrating the correlation between log2 (L-OPA1) and log2 (S-OPA1). Band intensities were normalised to actin and expressed as relative to the Mock T0 condition. Protein bands were measured using ImageStudio software. Note that the Mock T8 intensity of each blot is also included and is annotated according to the blot number. For example, B2 T8 represents the Mock T8 sample from blot 2. DUBs labelled in blue and red are 2 and 3 standard deviations from the average value of the total samples.

Therefore, MIRO, TIMM44 and S-OPA1 protein levels were all taken into consideration to identify DUBs for which depletion differentially affect the proteasomal and lysosomal degradation. Based on these criteria, I selected UCHL1, USP25, USP28 and USP31 for further investigation. Note that while the effect of UCHL1 is milder compared to the other DUB siRNAs, it was still selected for deconvolution as mutation of this DUB has been reported in Parkinson's Disease. While the cleavage of OPA1 in cells treated with these siRNAs was not affected, these cells accumulated higher levels of S-OPA1, TIMM44 but not MIRO levels compared to the mock-transfected cells.

It is also worth mentioning that siRNA depletion of PSMD7 and PSMD14 resulted in the accumulation of a 52kDa fragment of PINK1 (Figure 5.20). This fragment is normally constitutively degraded by the proteasome and is typically observed upon treatment of cells with proteasome inhibitor. On the other hand, S-OPA1 and TIMM44 degradation via the lysosomal pathway was not affected. These observations are consistent with the role of both PSMD7 and PSMD14 as subunits of the 19S regulatory particle of the proteasome (Yao and Cohen 2002, Wauer and Komander 2014). In fact, depletion of these two DUBs is the only condition for which an inhibition of the proteasomal but not the lysosomal degradation pathway is observed. O+A treatment in PSMD14-depleted cells also accumulated a distinct lower molecular weight species of MIRO that is not observed in other samples. Based on its approximate molecular weight, this fragment might represents a cleaved MIRO lacking its transmembrane domain.

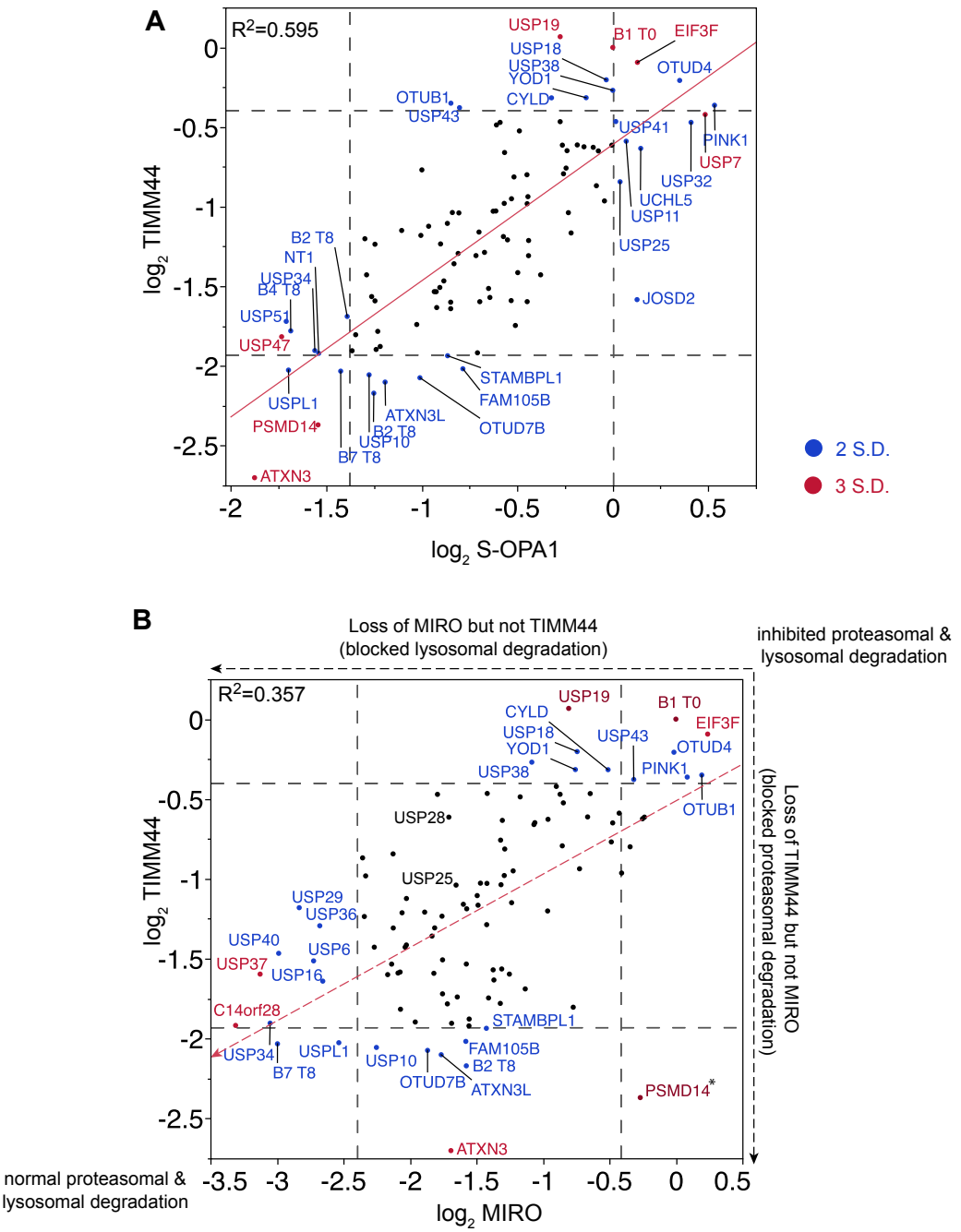

Figure 5.22 Statistical analysis of TIMM44, S-OPA1 and MIRO protein levels from DUB siRNA screen in hTERT-RPE1-YFP-Parkin cells.

(A) Scatter plot of $\log_2$ TIMM44 versus $\log_2$ S-OPA1. Protein bands were quantified using ImageStudio. Protein bands were normalised to actin and expressed as a relative value to the Mock T0 loading control at basal state. Proteins labeled in blue and red represent 2 and 3 standard deviations from the average value of the total samples. Note that the Mock T8 intensity of each blot is also included and is annotated according to the blot number. For example, B2 T8 represents the Mock T8 sample from blot 2. DUBs labelled in blue and red are 2 and 3 standard deviations from the average value of the total samples.

(B) Scatter plot of $\log_2$TIMM44 versus $\log_2$ MIRO. Asterisk: Quantitation for MIRO in PSMD14 siRNA trasfected cells were based on MIRO doublet that only exists in that sample.

5.3.1 Deconvolution of UCHL1, USP25, USP28 and USP31

I first deconvoluted the DUBs that I selected from the biochemical screen by measuring MIRO, TIMM44, L-OPA1 and S-OPA1 protein levels for each individual siRNA oligo after 8hr of O+A treatment.

Of the UCHL1 siRNAs, only oligo Q3 recapitulated the effect observed with the siRNA pool, namely normal degradation of MIRO but delayed degradation of TIMM44 whereas knockdown with oligo Q1 strongly inhibited both MIRO and TIMM44 degradation (Figure 5.23A). The residual two oligos did not affect either MIRO or TIMM44 degradation. Note that in the OPA1 blots for the UCHL1, USP25 and USP28 deconvolution, there is a non-specific band that is just above the L-OPA1 band. To avoid confusion, I marked that band with an asterisk sign.

With regards to USP25 knockdown, only oligo Q1 phenocopied the effects seen with the pool, whereas oligo Q3 showed mild inhibition of the induction of mitophagy, as evident from the partial cleavage of OPA1 and the higher levels of both MIRO and TIMM44 (Figure 5.23B). I did not assess the knockdown efficiency for either UCHL1 or USP25 deconvolution.

On the other hand, USP28 deconvolution revealed that knockdown with both oligos Q2 and Q3 inhibited TIMM44 degradation but not MIRO degradation, recapitulating the results observed with the pool. However, upon assessing the knockdown efficiency, it was clear that USP28 was not depleted in the cells transfected with oligo Q3, strongly suggesting that the effect seen with USP28 is also an off-target effect. Therefore, I did not follow up on these DUBs.

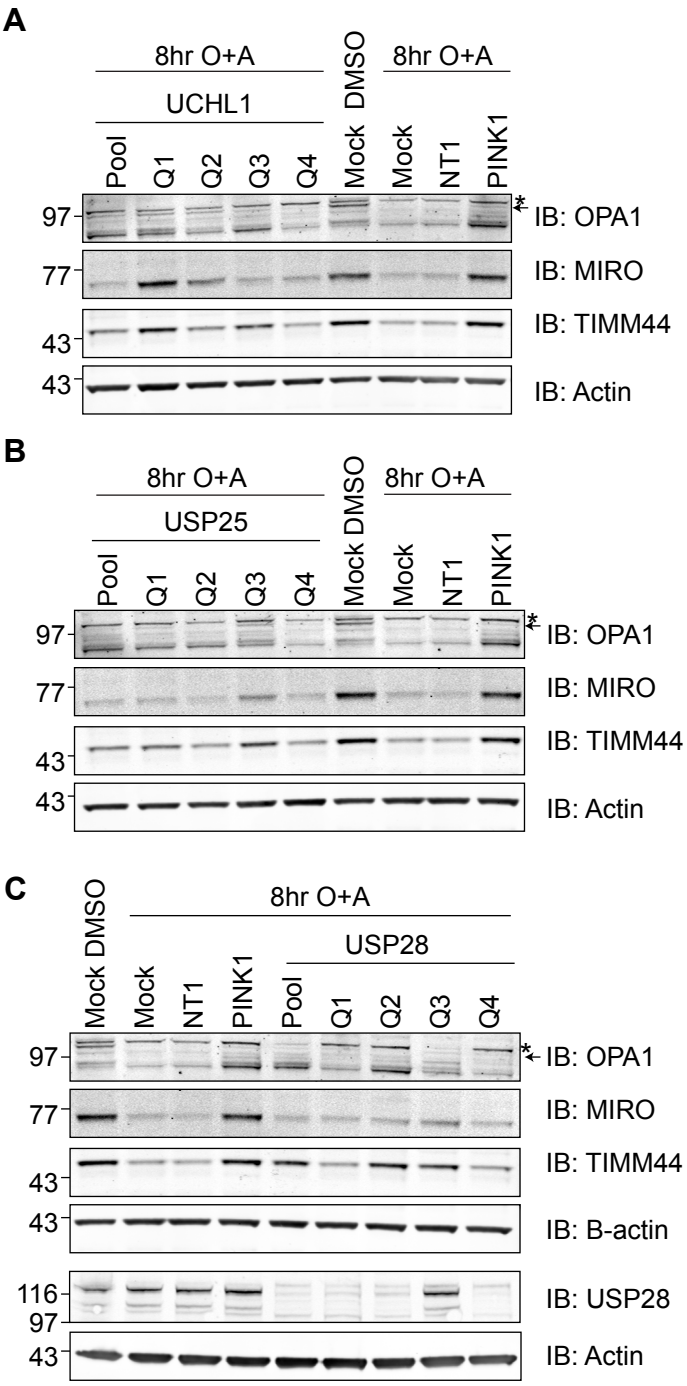

Figure 5.23 UCHL1, USP25 and USP28 deconvolution in hTERT-RPE1-YFP-Parkin cells.
(A-C) hTERT-RPE1-YFP-Parkin cells were transfected for 72hr with either mock (transfection reagent without siRNA oligo), non-targeting siRNA control (NT1), PINK1, or siRNA oligos targeting UCHL1, USP25, and USP28 (four siRNA oligos per DUB). Cells were then treated with oligomycin A and antimycin A (O+A, 1μM each) for 8hr. Cells were harvested in RIPA lysis buffer. 15μg of lysates were probed as indicated. Asterisk: non-specific band.

The most promising results were obtained with the USP31 deconvolution, with two oligos, Q2 and Q3, partially inhibiting TIMM44 but not MIRO degradation in response to O+A treatment. qRT-PCR analysis showed that oligos Q2, Q3 and Q5 knocked down USP31 (Figure 5.24B). I further investigated the effect of USP31 with or without O+A treatment. Before treatment with O+A, LC3-I levels were lower with USP31 Q2 and Q3 knockdown, suggesting a defect in the autophagic machinery (Figure 5.24C). This might explain the inhibition of TIMM44 and S-OPA1 degradation during mitophagy. After 8hr of O+A treatment, MIRO was degraded but residual S-OPA1 and TIMM44 levels were higher in cells transfected with oligos Q2 and Q3 compared to the two non-targeting controls, NT1 and Ctrl IX.

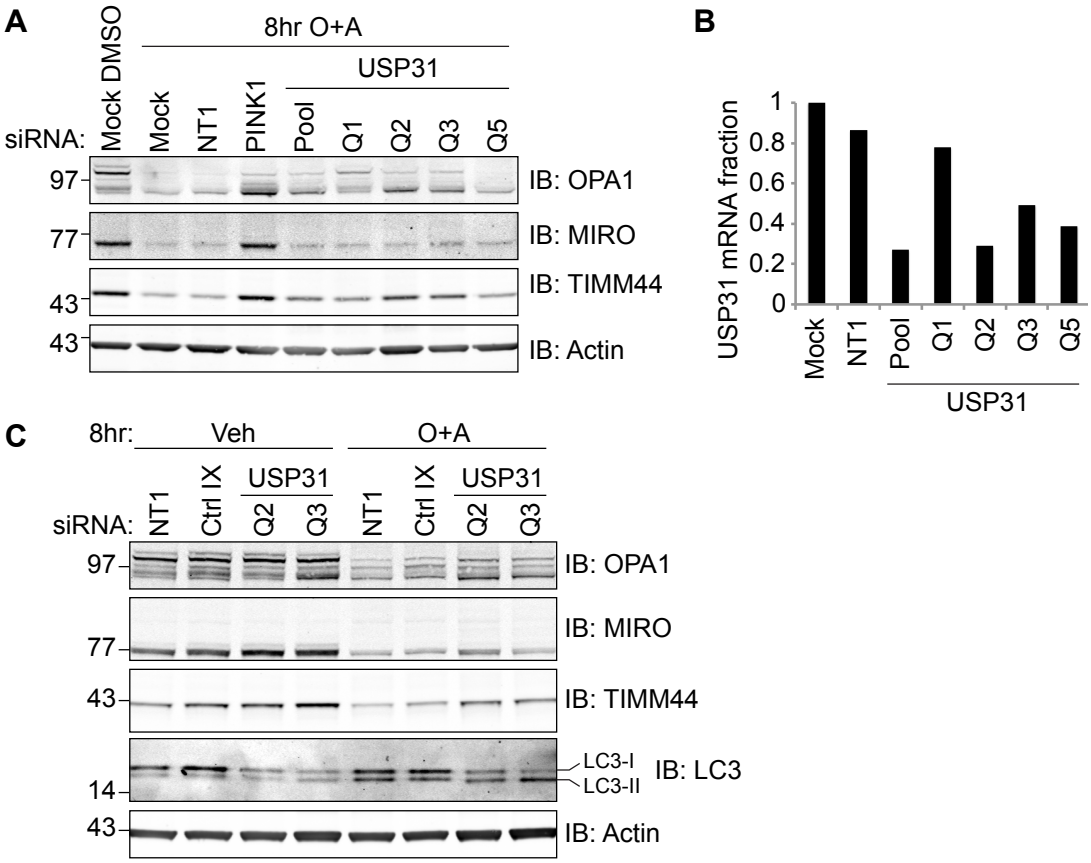

Figure 5.24 USP31 deconvolution in hTERT-RPE1-YFP-Parkin cells.

(A) hTERT-RPE1-YFP-Parkin cells were transfected for 72hr with either mock (transfection reagent without siRNA oligo), non-targeting siRNA control (NT1), PINK1, or USP31 (Q1, Q2, Q3 and Q5) siRNA oligos. Cells were then treated with oligomycin A and antimycin A (O+A, 1μM each) for 8hr. Cells were harvested in RIPA lysis buffer. 15μg of lysates were probed as indicated.
(B) hTERT-RPE1-YFP-Parkin cells were transfected for 24hr with either mock (transfection reagent without siRNA oligo), non-targeting siRNA control (NT1), or siRNA oligos targeting USP31 (Q1, Q2, Q3 and Q5). Cells were then harvested for RNA extraction, reverse transcription and qRT-PCR. cDNA level of USP31 were normalized to actin and expressed as relative fold change compared to mock control.
(C) hTERT-RPE1-YFP-Parkin cells were transfected for 72hr with either non-targeting controls, (Ctrl IX, NT1), or USP31 (Q1, Q2, Q3 and Q5) siRNA oligos. Cells were then treated with oligomycin A and antimycin A (O+A, 1μM each) for 8hr. Cells were harvested in RIPA lysis buffer. 15μg of lysates were probed as indicated.

5.4 Western blot screen for DUBs involved in Parkin-mediated mitophagy in SH-SY5Y cells

In neither the live-cell imaging screen, nor the western blot-based screen did I find a DUB for which the knockdown would enhance Parkin recruitment. This is most likely due to the high levels of Parkin that may mask the involvement of DUBs that may oppose Parkin-dependent mitophagy. Therefore, I decided to turn to SH-SY5Y cells, which express low endogenous Parkin and in which an enhancement of mitophagy might be easier to observe. In chapter 3, I showed that SH-SY5Y cells treated with either CCCP or O+A show mild ubiquitylation of MIRO. No bulk mitophagy was observed in these cells even after 24hr of treatment. I speculated that the low expression of endogenous Parkin coupled with the autoubiquitylation and degradation of Parkin during activation of mitophagy rapidly exhausts the small pool of endogenous Parkin. It is however, possible that this is further compounded by the deubiquitylating activity of an opposing DUB, weakening the effects of Parkin. I decided to perform a siRNA screen in these cells to determine if depletion of any of the DUBs promotes mitophagy in SH-SY5Y cells.

Prior to the actual siRNA screen, I compared the knockdown efficiencies of forward and reverse transfection using Lipofectamine RNAiMAX in SH-SY5Y cells. As shown in Figure 5.25, both methods knocked down USP33 to comparable levels. For simplicity, I decided to also use the same reverse transfection protocol as in hTERT-RPE1-YFP-Parkin cells.

The same DUB siRNA library from Qiagen was used to transfect SH-SY5Y cells. I also included the same non-targeting siRNAs (NT1 and NT3) and siRNA targeting PINK1 as negative and positive controls, respectively. Mock-transfected samples (transfection reagent without oligo) were also included for comparison across different blots. SH-SY5Y cells were also treated with 1μM of O+A but the treatment was extended to 24hrs to maximize the effects (see Chapter 3).

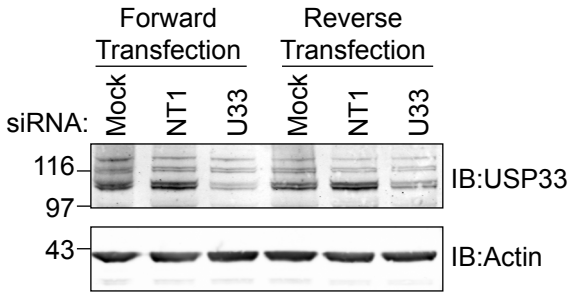

Figure 5.25 Comparison of Lipofectamine RNAiMAX forward and reverse transfection protocols in SH-SY5Y cells.

SH-SY5Y cells were transfected for 72hrs with 40nM of either mock (transfection reagent without siRNA oligo), non-targeting siRNA control oligo (NT1) or siRNA targeting USP33 (D6). Cells were harvested in RIPA lysis buffer and 10µg of lysates were probed with USP33 and actin antibodies.

One of the first issues I observed was the lack of PINK1 accumulation in mock-transfected cells as well as in cells transfected with six of the siRNA pools (OTUB6B, OTUB6A, OTUD5, OTUD1, BRCC3 and COPS5) after 24hr of O+A treatment. I also observed a slight decrease in the levels of MIRO and TIMM44 under these conditions compared to the O+A treated mock condition (Mock T8). These six transfections (on the same 6-well plate) as well as the mock-transfected cells had been very confluent on the day of mitophagy induction. Therefore, it is possible that the high cell density alters the accumulation of PINK1 and MIRO levels. Since these observations on the mock-transfected cells were not consistent with previous characterization work, the mock controls were not used as standards for comparison. Instead, comparisons were made based on the overall protein levels across all of the DUB depletions.

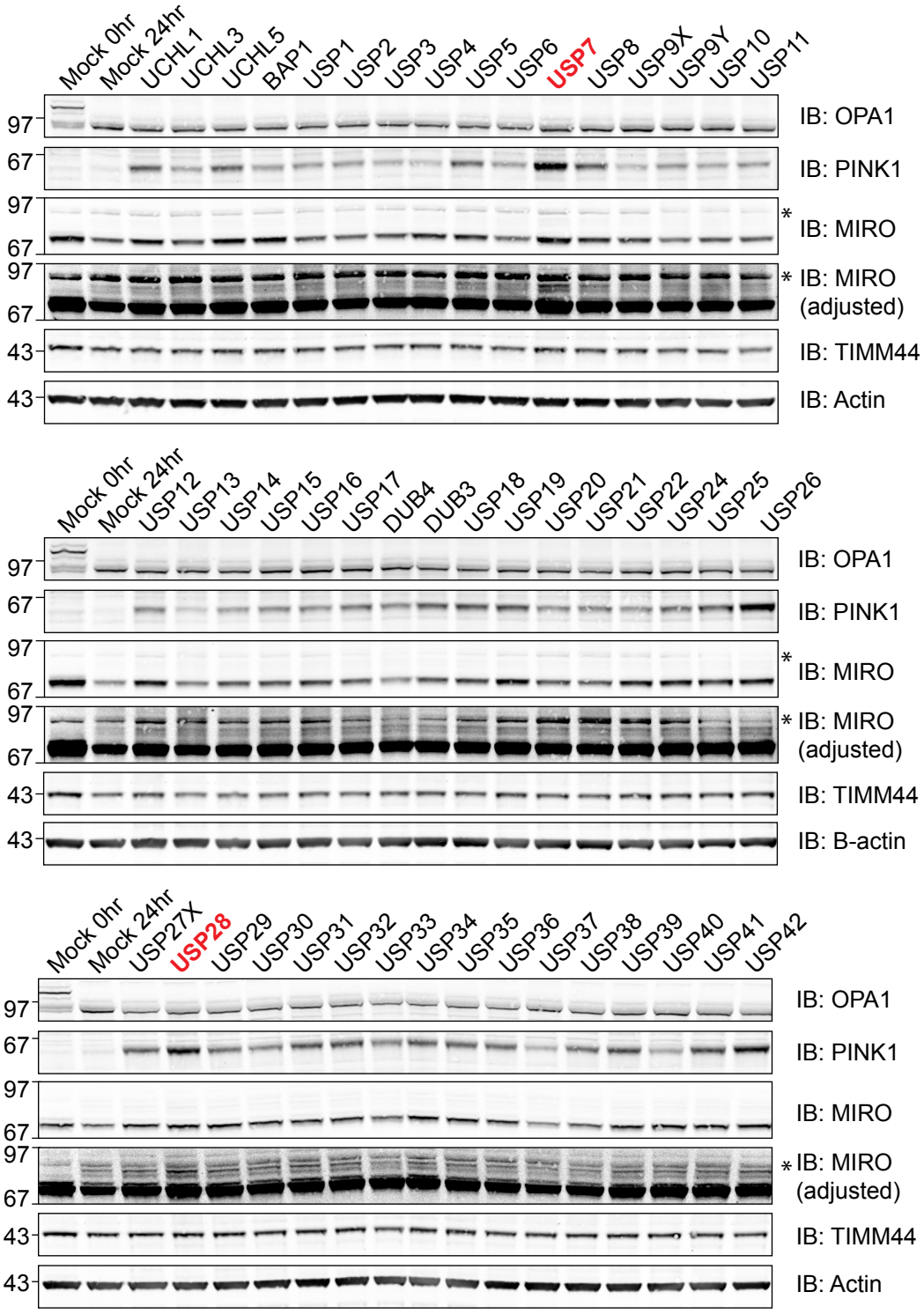

Figure 5.26 Biochemical screen for DUBs regulating Parkin-mediated mitophagy in SH-SY5Y cells.
SH-SY5Y cells were treated for 72hr with either mock (transfection reagent without siRNA oligo), non-targeting siRNA oligos (NT1 and NT3) or siRNA oligos targeting 94 DUBs (20nM). Cells were treated with oligomycin A and antimycin A (1μM each) for 8hr and harvested in RIPA lysis buffer. 10μg of lysates were probed as indicated. DUBs labeled in red: shortlisted DUBs. Asterisk: non-specific band.

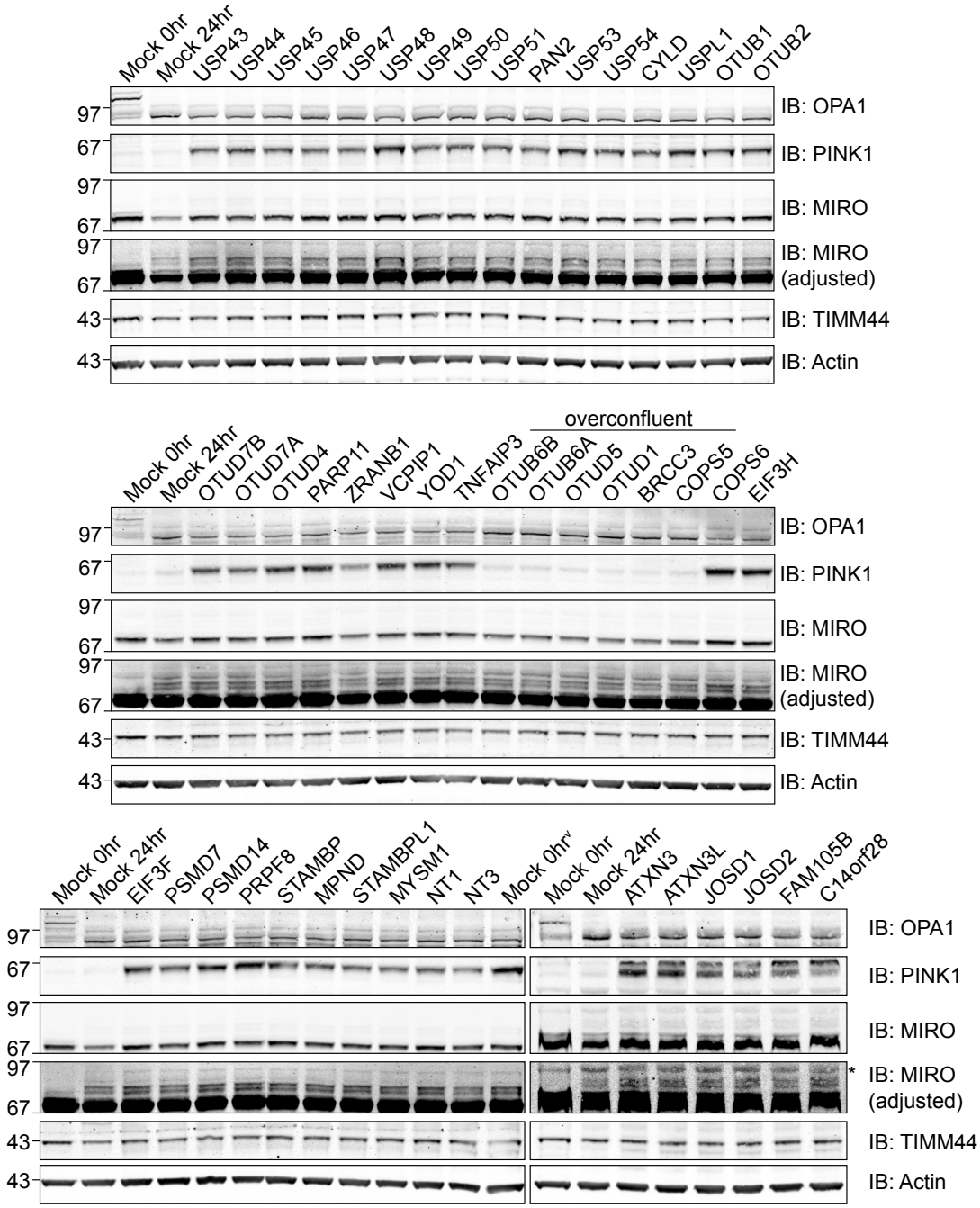

Figure 5.27 Biochemical screen for DUBs regulating Parkin-mediated mitophagy in SH-SY5Y cells (continued).
SH-SY5Y cells were treated for 72hr with either mock (transfection reagent without siRNA oligo), non-targeting siRNA oligos (NT1 and NT3) or siRNA oligos targeting 94 DUBs (20nM). Cells were treated with oligomycin A and antimycin A (1μM each) for 8hr and harvested in RIPA lysis buffer. 10μg of lysates were probed as indicated. Asterisk: non-specific band. §: Misloaded lane (Mock T0 sample was added instead on PINK1-depleted sample).

In contrast to the DUB siRNA screen in hTERT-RPE1-YFP-Parkin cells, SH-SY5Y cells underwent complete OPA1 cleavage upon O+A treatment. However, cells were treated for 24hr as opposed to 8hr in hTERT-RPE1-YFP-Parkin cells. It is also possible that the partial or inhibited OPA1 cleavage observed in hTERT-RPE1-YFP-Parkin cells is a cell-type dependent effect, as previously discussed.

Overall, most of the siRNA pools did not induce obvious changes in response to O+A treatment based on the proteins I assessed, except for an increase in PINK1 accumulation and MIRO ubiquitylation upon USP7 and USP28 depletion (Figure 5.26).

I wondered whether poor knockdown efficiency might be responsible for the lack of effects seen in this DUB screen. Therefore, I randomly selected a few DUB siRNA lysate samples from the western blot screen to assess the general siRNA transfection efficiency (Figure 5.28). While there is a visible decrease in the levels of PINK1, USP8 and USP33 upon treatment with their respective siRNA pools, depletion was not complete for either of these proteins. Knockdown of several other DUBs, including UCHL5, USP15, USP21 and USP28 did not significantly decrease the respective protein levels, which may be due to a combination of poor transfection efficiency and long half-lives of these DUBs.

Subsequent deconvolution of USP28, using the four Qiagen siRNA oligos and also additional Dharmacon and Ambion siRNA oligos did not yield any consistent effect on PINK1 accumulation and MIRO ubiquitylation (Figure 5.29). USP7 deconvolution demonstrated that siRNA oligo Q1, Q10, Q2, Q3 and D6 knocked down USP7 most efficiently compared to oligo D5, D7 and D8 (Figure 5.30). These oligos also seemed to induce higher accumulation of PINK1. However, subsequent experiments failed to reproduce this result.
In both USP28 and USP7 deconvolution, both DUBs were also only partially depleted, which may explain the lack of consistent changes in both cases, rendering these results inconclusive.

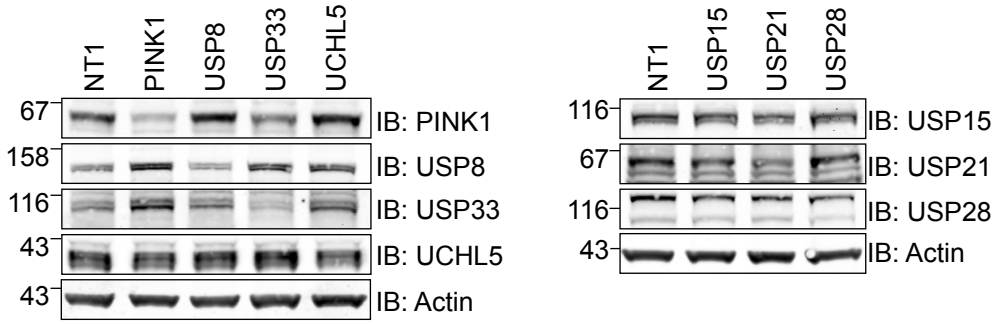

Figure 5.28 Assessment on the knockdown efficiency of DUB siRNA transfection.

Selected lysates from the same experiment in Figure 5.26 and Figure 5.27 were rerun to probe for the respective DUBs.

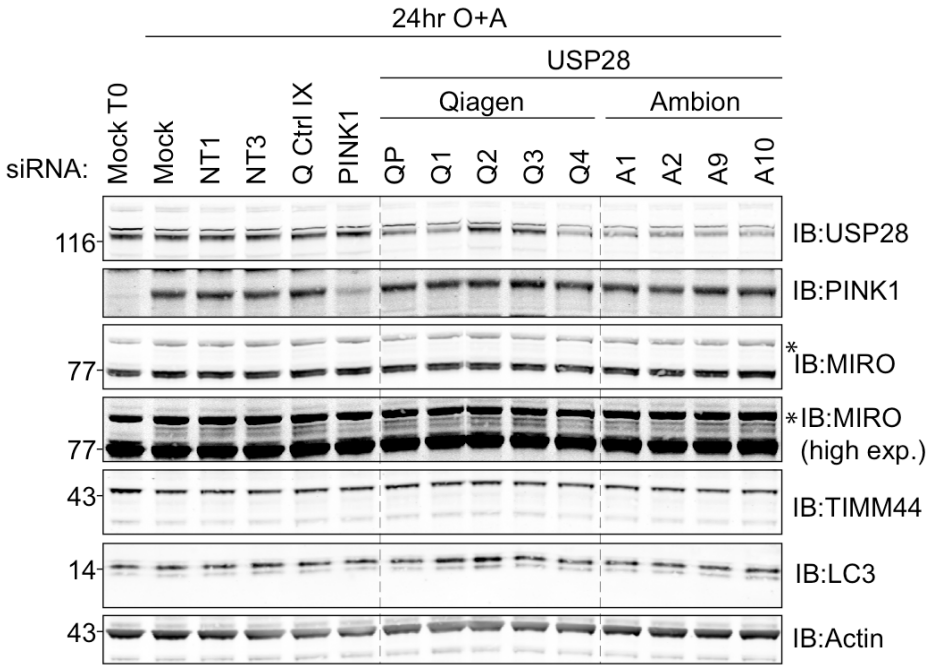

Figure 5.29 USP28 siRNA deconvolution in SH-SY5Y cells.

SH-SY5Y cells were transfected for 72hr with either mock (transfection reagent without siRNA oligo), non-targeting siRNA oligos (NT1, NT3 and Ctrl IX), siRNA oligos targeting PINK1 or USP28. The cells were then treated with oligomycin A and and antimycin A (O+A; 1μM each) for 24hr. The cells were harvested in RIPA lysis buffer and 15μg of lysates probed as indicated. Asterisk: non-specific band.

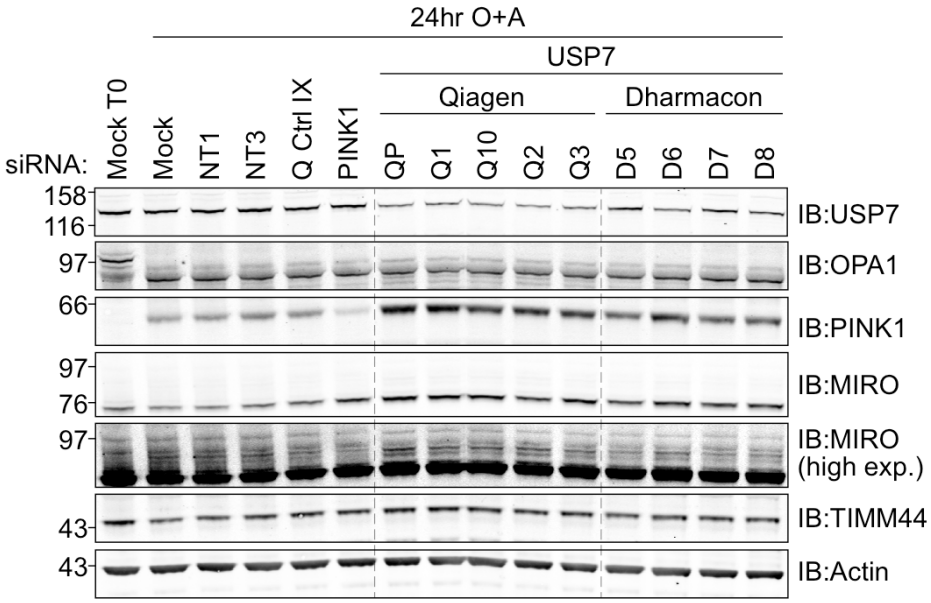

Figure 5.30 USP7 siRNA deconvolution in SH-SY5Y cells.

SH-SY5Y cells were transfected for 72hr with either mock (transfection reagent without siRNA oligo), non-targeting siRNA oligos (NT1, NT3 and Ctrl IX), siRNA oligos targeting PINK1 or USP7. The cells were then treated with oligomycin A and and antimycin A (O+A; 1μM each) for 24hr. The cells were harvested in RIPA lysis buffer and 15μg of lysates probed as indicated.

5.5 Discussion

Having characterised hTERT-RPE1-YFP-Parkin and SH-SY5Y cells in chapters 3 and chapter 4, I first carried out a DUB siRNA screen by live-cell imaging using the former cell line, followed by two western blotting screens with both of the cell lines to identify DUBs that are involved in mitophagy. However, the poor siRNA transfection efficiency in SH-5Y cells in the last DUB siRNA screen renders the results inconclusive. Therefore, the results from that screen will not be further discussed.

5.5.1 DUB knockdowns that inhibited OPA1 cleavage

From the live-cell imaging screen, I identified USP10, USP30, USP38, USP42, USP43, USP49, BAP1, OTUD4 and ZRANB1, for which depletion resulted in delayed Parkin recruitment but without any obvious effect on Parkin clearance. Further analysis of the top hits by western blotting revealed that the depletion of the DUB candidates induced partial or complete inhibition of OPA1 cleavage, and caused similar inhibition of the downstream PINK1 accumulation, Parkin autoubiquitylation and mitochondrial protein degradation. In addition, the second screen by western blotting revealed more DUB siRNAs that also caused either partial or complete inhibition of OPA1 cleavage. Shortlisted proteins and their functions are summarised in Table 5.2.

Based on the characterisation work performed on USP42 and USP43 depleted cells, I came to the conclusion that: (1) OPA1 cleavage inhibition is most likely a cell type-dependent effect as it was only observed in both parental and YFP-Parkin expressing hTERT-RPE1 cells but not in HEK293T cells; (2) The inhibition of OPA1 cleavage was not a CCCP-specific effect, but rather, is due to the decrease in cellular response towards mitochondrial depolarisation. This assumption is made based on the observation that OPA1 cleavage was inhibited not just upon CCCP but also upon O+A treatments and importantly could be overcome by doubling the concentration of CCCP. It still remains to be seen whether these observations can be

extrapolated to the other DUB siRNAs that showed a similar lack of OPA1 cleavage inhibition.

One hypothesis is that the depletion of these DUBs may upregulate the multidrug resistance-associated proteins (MRPs), a family of drug transporters that pump a wide range of anionic organic drugs out of the cells and have been proposed to contribute to unexplained cases of anticancer drug resistance (Borst et al. 2000). To assess whether the observed lack of OPA1 cleavage is truly due to a reduction in CCCP, oligomycin A and antimycin A being taken up and retained in the cells, one pivotal experiment that remains to be carried out in the future is to assess the mitochondrial membrane potential upon CCCP or O+A treatment. This can be achieved using tetramethylrhodamine (TMRE), a positively-charged, red-orange dye that accumulates in active mitochondria with a relative negative membrane potential. Cells that retain their membrane potential are stained with TMRE and can then be quantitatively assessed by fluorescence-activated cell sorting (FACS).

MacVicar and Lane (2014) recently reported that hTERT-RPE1-YFP-Parkin cells cultured in glucose-based media undergo Parkin-mediated mitophagy upon CCCP treatment but the same cells cultured in galactose switched to dependence on oxidative phosphorylation (OXPHOS) and were resistant to CCCP-induced mitophagy (MacVicar and Lane 2014). This effect is due to the suppression of OMA1, an inducible OPA1 protease that cleaves L-OPA1 to S-OPA1 in OXPHOS-dependent hTERT-RPE1 cells. Since I cultured hTERT-RPE1-YFP-Parkin cells in glucose rich medium (17.5mM of D-glucose), these cells should be more glycolytic and less dependent on OXPHOS for cellular energy production. However, it is possible that the depletion of a subset of DUBs reprogrammes the cells to be more OXPHOS dependent. This could be tested in the future by measuring the oxygen consumption rate (OCR) and extracellular acidification rate (ECAR) of the cells. Glycolytic cells have lower OCR and higher ECAR whereas OXPHOS-dependent cells have higher OCR and lower ECAR (Wu et al. 2007).

Interestingly, two of the DUBs, USP10 and USP42 for which depletion inhibited OPA1 cleavage were previously implicated in p53 regulation. Cytosolic and nuclear p53 pools have been shown to inhibit and promote autophagy, respectively (Levine and Abrams 2008, Morselli et al. 2008, Tasdemir et al. 2008a, Tasdemir et al. 2008b). Consistent with a role of p53 during autophagy, cytosolic p53 has also been shown to physically bind to and inhibit the activity of Parkin in pancreatic β-cell (Hoshino et al. 2014, Hoshino et al. 2013).

USP10 is a DUB that counteracts the nuclear export of ubiquitylated p53 (Yuan et al. 2010). In addition, Liu and colleagues showed that USP10 and USP13 form a complex with Beclin-1 and regulate the stability of each other, thereby inhibiting autophagy (Liu et al. 2011). However, USP13 depletion did not induce any visible change in either the live-cell imaging or western blotting screen.

USP42 has previously been reported to directly interact with and regulate the stability of p53 during DNA damage, allowing rapid accumulation of p53 to induce cell cycle arrest (Hock et al. 2011). While I did not assess the localization of p53, USP42 depletion with two siRNA oligos inhibited the accumulation of p53 during CCCP-induced mitophagy, which is observed in the control cells. Since the same two USP42 siRNA oligos also inhibited OPA1 cleavage and its subsequent mitophagic readouts, it is uncertain whether the p53 accumulation is a consequence of a failure to trigger OPA1 cleavage and mitophagy or more directly due to a proposed failure of CCCP to trigger depolarisation in these cells. A systematic proteomic interaction screen of DUBs performed by Sowa et al. identified a group of mitochondrial ribosomal protein subunits that were immunoprecipitated with HA-tagged USP42, suggesting that USP42 may also regulate general mitochondrial translation of genes encoded by the mitochondrial DNA (Figure 5.31A) (Sowa et al. 2009).

USP43 is a poorly characterized DUB. The same interaction screen described above by Sowa et al. identified VPS35 as an interactor of USP43

(Figure 5.31B) (Sowa et al. 2009). VPS35 is a core component of the retromer complex mediating endosome-to-Golgi transport of membrane proteins such as the cation-independent mannose 6-phosphate receptor (CIMPR) (Seaman 2012). Importantly, mutation in VPS35 (D620N), which causes reduced binding efficiency for the WASH complex to the endosome, has been reported in some cases of autosomal-dominant, late-onset Parkinsonism (Zimprich et al. 2011, Vilarino-Guell et al. 2011, Harbour et al. 2010, Jia et al. 2012, Zavodszky et al. 2014a, Zavodszky et al. 2014b). In addition, Zavodszky and colleagues reported that cells with a VPS35 (D620N) mutation or depleted of WASH complex also show defects in the trafficking of ATG9A to autophagosomal membrane, causing inhibition of autophagy (Zavodszky et al. 2014b). Although a link between VPS35 or WASH and mitophagy has not yet been established, I assessed the protein levels of VPS35 in USP43-depleted cells. While I did not observe any decrease in the levels of VPS35 upon USP43 knockdown, I cannot exclude possible changes in the localization of VPS35 upon USP43 depletion.

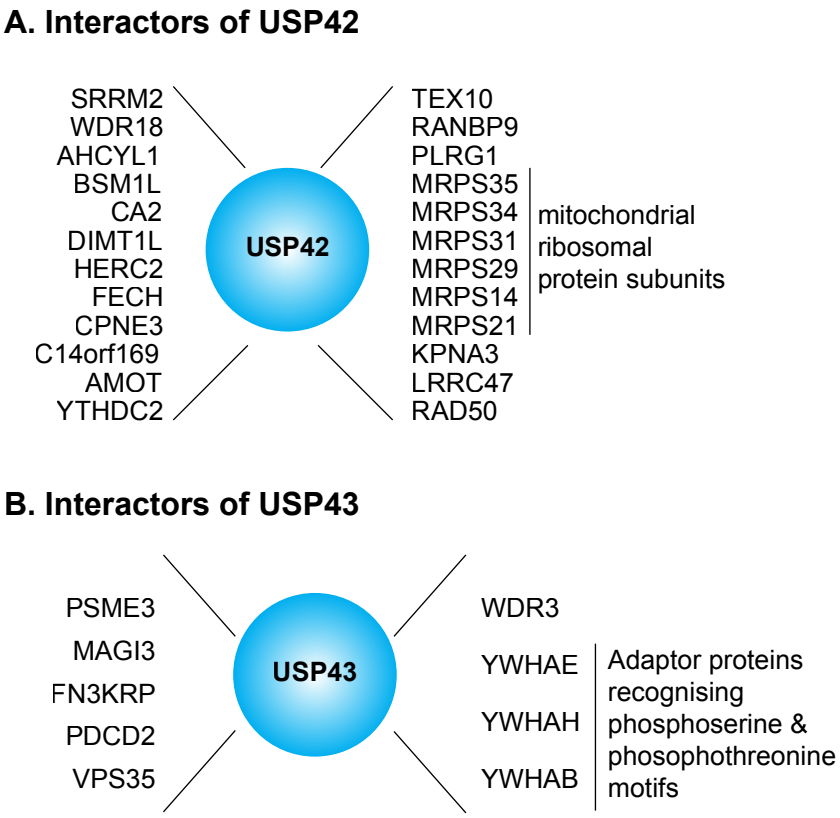

Figure 5.31 Reported interactors of USP42 and USP43.

Interactors of USP42 and USP43 are derived from the systematic proteomic interaction screen of DUBs carried out by Sowa et al. 2009.

BAP1 (BRCA1-Associated Protein 1) depletion also resulted in delayed Parkin recruitment and partial OPA1 cleavage. BAP1 localises to the nucleus and promotes the stability of HCF-1, a scaffolding protein that binds to different transcription factors such as Yin Yang 1 (YY1) (Yu et al. 2010, Machida et al. 2009). One of the genes that is transcribed by YY1 is *cox7c*, which encodes for a component involved in the mitochondria electron transport chain (Yu et al. 2010, Deng et al. 2010). In addition, BAP1 also regulates the stability of *O*-linked *N*-acetylglucosamine transferase (OGT), an interacting partner of HCF-1 (Dey et al. 2012). N-acetylglygosylation of peroxisome proliferator-activated receptor-γ co-activator 1α (PGC-1α; a key co-activator involved in gluconeogenesis and mitochondrial biogenesis) by the HCF-1/OGT complex confers recognition of PGC-1α by BAP1 to protect it from degradation, thereby promoting mitochondrial biogenesis (Ruan et al. 2012).

USP38 depletion also resulted in delayed Parkin recruitment upon CCCP treatment. USP38 has been shown in a proteomic interaction screen to interact with RPL7 and RPS12 both of which are components of the 60S and 40S ribosomes, respectively (Seshadri et al. 1993, Herault et al. 1991, Sowa et al. 2009). Other interacting partners include LGALS7 (a carbohydrate-binding protein implicated in cell adhesion and cell matrix interaction), HSPB1 (a chaperone protein that is upregulated during stress response) and HMX3 (a transcription factor involved in inner ear development and reproduction) (Wang et al. 1998, Seshadri et al. 1993, Herault et al. 1991, St-Pierre et al. 2012, Arrigo et al. 2007). A siRNA screen for DUBs that regulate E-cadherin levels performed by an ex-colleague in the laboratory, Jia Lih Wong, reported that USP38 depletion reduces the levels of E-cadherin in A549 and MCF7 cells (Wong 2012). However, further work so far failed to elucidate the mechanistic link between USP38 and E-cadherin.

ZRANB1-depleted cells demonstrated delayed Parkin recruitment followed by enhanced Parkin clearance whereas the western blot screen showed inhibition of OPA1 cleavage in ZRANB1-depleted cells. ZRANB1 (also known as TRABID) was reported to bind and deubiquitylate adenomatous polyposis coli (APC), an antagonist of the Wnt-β-catenin signaling pathway (Tran et al. 2008). Hyperubiquitylation of APC in TRABID-depleted cells leads to its hyperactivation and subsequently repression of Wnt target genes.

5.5.2 USP31, a DUB required for late stages of mitophagy

From the western blot screen, USP31 was the only DUB for which more than one oligo (two in this case) recapitulated the effect of the siRNA pool, namely selective inhibition of the lysosomal but not the proteasomal degradation of mitochondrial proteins during mitophagy. I also observed less LC3-I in untreated, USP31-depleted cells. Under steady state conditions, precursor LC3 (pro-LC3) is constitutively cleaved and converted to LC3-I by Atg4B (Kabeya et al. 2000). During autophagy, or in this case, mitophagy, LC3-I (upper band) is conjugated with phosphatidylethanolamide (PE), forming LC3-II (lower band), which then recruits autophagosomal membranes to the mitochondria (Mizushima and Yoshimori 2007, Klionsky et al. 2007). The

lower LC3-I at steady state suggests that there could be a defect in the expression of pro-LC3 or its proteolytic processing to form LC3-I. Subsequently, this may affect LC3-II conversion and the recruitment of autophagosomal membrane to the mitochondria during mitophagy induction.

To understand the effect of USP31 depletion on LC3-I, the mRNA levels of pro-LC3 need to be assessed by qRT-PCR. Immunofluorescence microscopy should also be performed to see if there is any difference in the abundance and distribution of LC3-punctae both at steady state and upon induction of mitophagy. USP31 depletion could also affect the acidification of the lysosome, a crucial step to activate lysosomal hydrolases for their optimal degradative capacity (Pillay et al. 2002). Immunofluorescence visualization of mitochondria and lysosomes using TOM20 antibody staining (for mitochondria) and either acridine orange dye or LAMP1 antibody staining (for lysosomes) may provide information on the targeting of mitochondria to the lysosomes. In addition, a coral-derived acid-stable fluorescent protein that displays pH-dependent changes in fluorescence emission (450nm at pH>6; 543nm at pH<6), conjugated with a mitochondria-targeting signal from the mitochondrial matrix protein COXVIII, called ‘mitoKeima’ could been used to monitor delivery of mitochondria into an acidic environment upon fusion of autophagosomes with lysosomes (Katayama et al. 2011). This has recently been used by Bingol and colleagues to show that USP30 overexpression antagonizes Parkin-mediated mitophagy in hippocampal neurons (Bingol et al. 2014).

5.5.3 Recent advances in the identification of DUBs regulating Parkin-mediated mitophagy

Recently, two papers have been published, identifying USP15 and USP30 respectively as DUBs that oppose Parkin-mediated mitophagy. Bingol and colleagues reported that the overexpression of USP30 opposes Parkin-mediated mitophagy in HEK293, HeLa and SH-SY5Y cells stably expressing Parkin. They further demonstrated that TOM20 and MIRO are *bona fide* substrates for USP30. Importantly, whole fly or dopaminergic neuron knockdown of dUSP30 rescued the climbing defect and the dopamine

depletion observed in PINK1 mutant and paraquat-treated flies, respectively, suggesting that USP30 inhibition may be a therapeutic target for Parkinson's disease by promoting mitochondrial clearance and quality control (Bingol et al. 2014).

Using tandem affinity purification coupled to mass spectrometry, Cornelissen and colleagues identified USP15 as an interactor of FLAG-Parkin in HEK293 cells (Cornelissen et al. 2014). They further demonstrated that co-expression of USP15 and Parkin in HeLa cells rescues cells from mitophagy. Interestingly, they reported that USP30 overexpression did not oppose Parkin-mediated mitophagy in their system. In my hTERT-RPE1-YFP-Parkin screens, USP30 depletion led to delayed Parkin recruitment and partial OPA1 cleavage in hTERT-RPE1-YFP-Parkin cells whereas USP15 depletion inhibited OPA1 cleavage.

In both the USP15 and USP30 studies, they used an overexpression system, similar to a 'gain-of-function' study to identify DUBs that oppose the ubiquitylating activity of Parkin. In my case, the use of a siRNA approach to study the loss-of-function effect of DUBs makes it difficult to identify such DUBs in a cell line that is already overexpressing high levels of Parkin. Indeed, Bingol and colleagues could only demonstrate the effect of USP30 depletion in SH-SY5Y cells expressing a mutant form of Parkin (G430D) that only has partial ubiquitylating ability. On the other hand, knockdown of USP15 was performed in cells expressing normal Parkin and assessed by immunofluorescence quantitation of HSP60 staining (an IMM protein) after 24hr of CCCP treatment. Considering that only 30% of the cells undergo complete mitophagy in the control cells and USP15 depletion only enhanced the loss of mitochondria by 15%, this effect may not be easily visible by western blotting.

During the course of writing up this thesis, another group reported that USP8 is also involved in Parkin-mediated mitophagy (Durcan et al. 2014). Durcan and colleagues reported that knockdown of USP8 delayed Parkin recruitment to mitochondria upon CCCP treatment in U2-OS cells expressing GFP-

Parkin. USP8 preferentially removes K6-linked ubiquitin chains from Parkin, which promotes efficient recruitment of Parkin to depolarised mitochondria, thereby serving as a positive regulator of Parkin activity in mitophagy. The delayed Parkin recruitment reported with USP8 depletion is reminiscent of the delayed Parkin recruitment observed with USP42, USP43 and possibly other DUBs reported in my DUB screen. In my initial visual screen, USP8 depletion affected cell growth and resulted in cell death at steady state. In my western blot screen, USP8 depletion affected OPA1 cleavage in hTERT-RPE1-YFP-Parkin cells. Therefore, its downstream effect on mitophagy was masked and USP8 was not further pursued in this study.

The current understanding of the regulation of DUBs on Parkin-mediated mitophagy (USP30, USP15, and USP8), together with the deconvoluted DUBs identified in my project and their proposed functions are summarised in Table 5.2 and Figure 5.32. My results concerning USP30 will be the focus of Chapter 6.

DUB family	DUB	Live-cell imaging Screen (RPE1-YFP-Parkin) Observations (no. of oligos)	Western blot screen (RPE1-YFP-Parkin) Observations (no. of oligos)	Western blot screen (SH-SY5Y) Observations (no. of oligos)	Literature	References
UCH	BAP1	Reduced response (2)	Partial OPA1 cleavage		Binds to BRCA1, tumour suppressor, interacts with AHCYL2	(Sowa et al. 2009)
	UCHL1	-	Inhibited lysosomal degradation (1)	-	Mutated in Familial Parkinson's Disease	(Maraganore et al. 2004)
OTU	OTUD4	Reduced response (2)	Normal	-	-	-
	ZRANB1	Reduced response (2)	Inhibited OPA1 cleavage	-	DUB for APC (Wnt pathway)	(Tran et al. 2008)
USP	USP3	Reduced response (1)	Inhibited OPA1 cleavage	-	DUB for H2A and H2B, involved in DNA damage response	(Nicassio et al. 2007)
	USP7	Reduced response (1)	Inhibited OPA1 cleavage	Higher Ub-MIRO levels (0)	Regulate p53 and Mdm2 levels	(Cummins and Vogelstein 2004, Li et al. 2004, Li et al. 2002)
	USP10	Reduced response (3)	Normal	-	Regulates p53 localisation & stability; regulates NEMO stability and suppresses NF-κB	(Yuan et al. 2010, Niu et al. 2013, Liu et al. 2011)
	USP25	-	Inhibited lysosomal degradation of TIMM44 and S-OPA1 (1)	-	Opposes HRD1 E3 ligase activity in ERAD pathway	(Blount et al. 2012)
	USP28	-	Inhibited lysosomal degradation of TIMM44 and S-OPA1 (1)	Higher Ub-MIRO levels (0)	Opposes FBX7 E3 ligase activity, regulates myc, LSD1 and HIF-1α stability; homolog of USP25	(Popov et al. 2007, Wu et al. 2013, Flugel et al. 2012, Valero et al. 2001)
	USP30	Reduced response, cell death (2)	Inhibited OPA1 cleavage	-	Regulates mitochondrial morphology	(Nakamura and Hirose 2008, Bingol et al. 2014)
	USP31	-	Inhibited lysosomal degradation of TIMM44 and S-OPA1 (2)	-	-	-
	USP38	Reduced response (2)	Inhibited OPA1 cleavage	-	Possible role in regulating with E-cadherin levels	(Wong 2012)
	USP42	Reduced response (2)	Inhibited OPA1 cleavage	-	Regulates p53 stability, interacts with AHCYL1	(Sowa et al. 2009, Hock et al. 2011)

	USP43	Reduced response (4)	Inhibited OPA1 cleavage	-	Interacts with VPS35, PSME3	(Sowa et al. 2009)
	USP49	Reduced response (3)	Partial OPA1 cleavage	-	Interacts with HUWE1	(Sowa et al. 2009)
MJD	ATXN3	Reduced response (1)	Normal	-	Binds and inhibits E3 ligase activity of Parkin	(Bai et al. 2013, Durcan et al. 2012)

Table 5.2 Overview of candidate DUBs that were selected for deconvolution in all three DUB siRNA screens. (number in bracket represents numbers of oligos that recapitulated the effect seen with the siRNA pool).

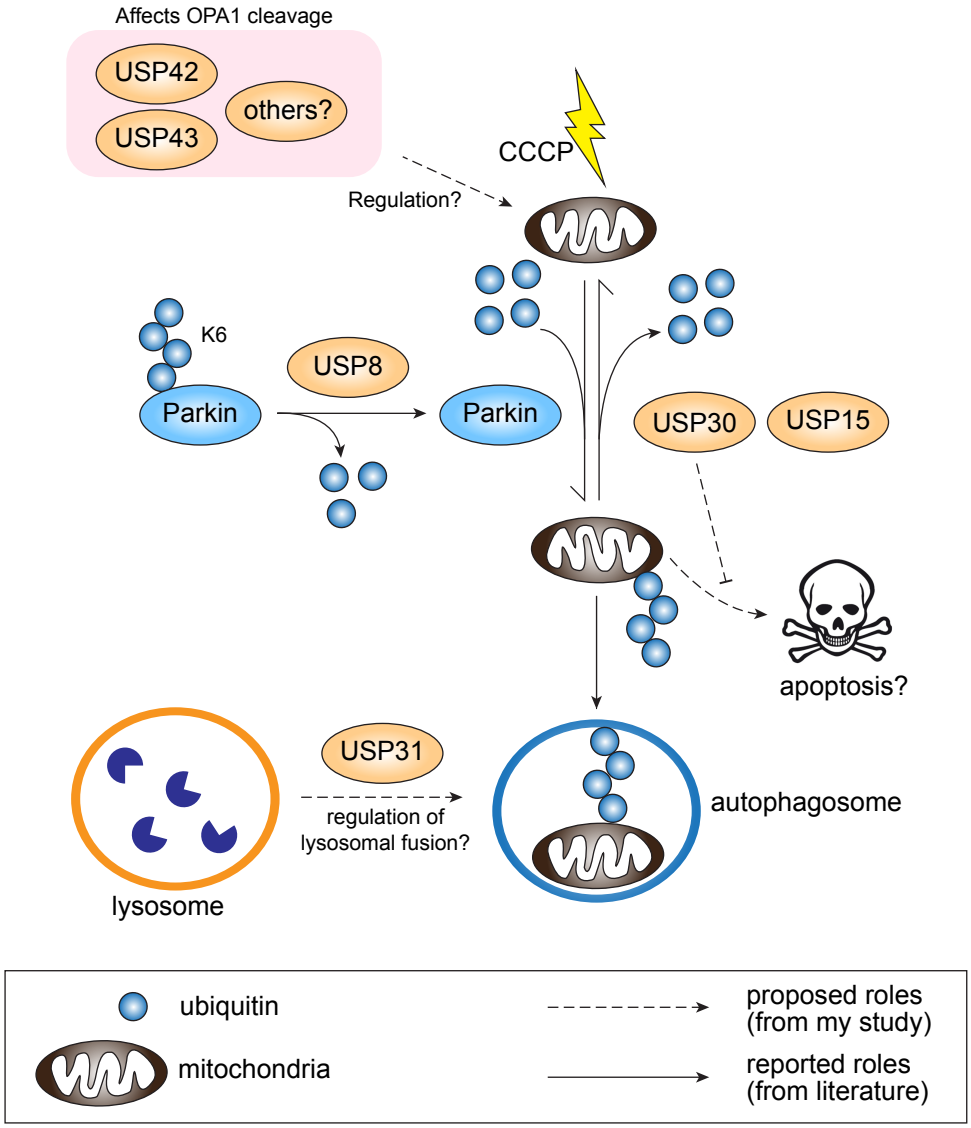

Figure 5.32 Schematic illustration of the current understanding of the role of DUBs in Parkin-mediated mitophagy.

USP8 has recently been reported to deubiquitylate K6-linked chains from Parkin, which promotes Parkin recruitment to the mitochondria during mitophagy (Durcan et al. 2014). Conversely, USP30 and USP15 are both reported to oppose Parkin-mediated mitophagy (Bingol et al. 2014, Cornelissen et al. 2014). In the case of USP30, two substrates have been identified as TOM20 and MIRO. In my screen, I found a subset of DUBs, for which depletion desensitized the hTERT-RPE1-YFP-Parkin cell response towards mitochondrial depolarisation by CCCP and O+A treatment. These DUBs include USP42 and USP43. USP30 might have a cytoprotective role during mitophagy as depletion of USP30 resulted in enhanced cell death during mitophagy (see Chapter 6). USP31 depletion resulted in delayed lysosomal degradation without affecting proteasomal degradation of mitochondrial proteins, suggesting that USP31 might be involved in the later stages of autophagosomal fusion with the lysosomes or the maturation of autolysosomes.

Chapter 6: Characterisation of USP30

6.1 Introduction

USP30 is 517 amino acids in length and belongs to the USP family of deubiquitylases (Figure 6.1). It is one of the two deubiquitylases that has a specific transmembrane domain, the other one being USP19, which localizes to the endoplasmic reticulum (Urbe et al. 2012, Hassink et al. 2009, Clague et al. 2013). Nakamura and Hirose (2008) showed that a hydrophobic region at the N-terminus (35-54 a.a.) confers its transmembrane (TM) domain. A series of positively charged amino acids following the TM domain serves as a 'signal-anchor' sequence that allows the translocation of USP30 from the endoplasmic reticulum to the mitochondria (Nakamura and Hirose 2008). The catalytic domain of USP30 consists of a catalytic triad (C77, H452 and S477) and spans most of the rest of the protein (69 to 499 a.a.) (Ye et al. 2009). Using mitochondria-enriched fraction, Nakamura and Hirose (2008) demonstrated that USP30 is inserted into the OMM such that its catalytic domain is facing the cytosol, making it susceptible to Proteinase K treatment. USP30 is conserved across multiple organisms, including cow, fish, mouse and fly (Figure 6.1B). In yeast, the only DUB that has a similar TM domain and localizes to the mitochondria is ubp16 (Kinner and Kolling 2003, Nakamura and Hirose 2008). However, there is only 16.4% identity similarity between ubp16 and human USP30, suggesting possible convergent evolution of two different genes that serve similar function in the mitochondria.

In this chapter, I summarize my findings on the role of USP30 at steady states as well as during mitophagy and other stimuli.

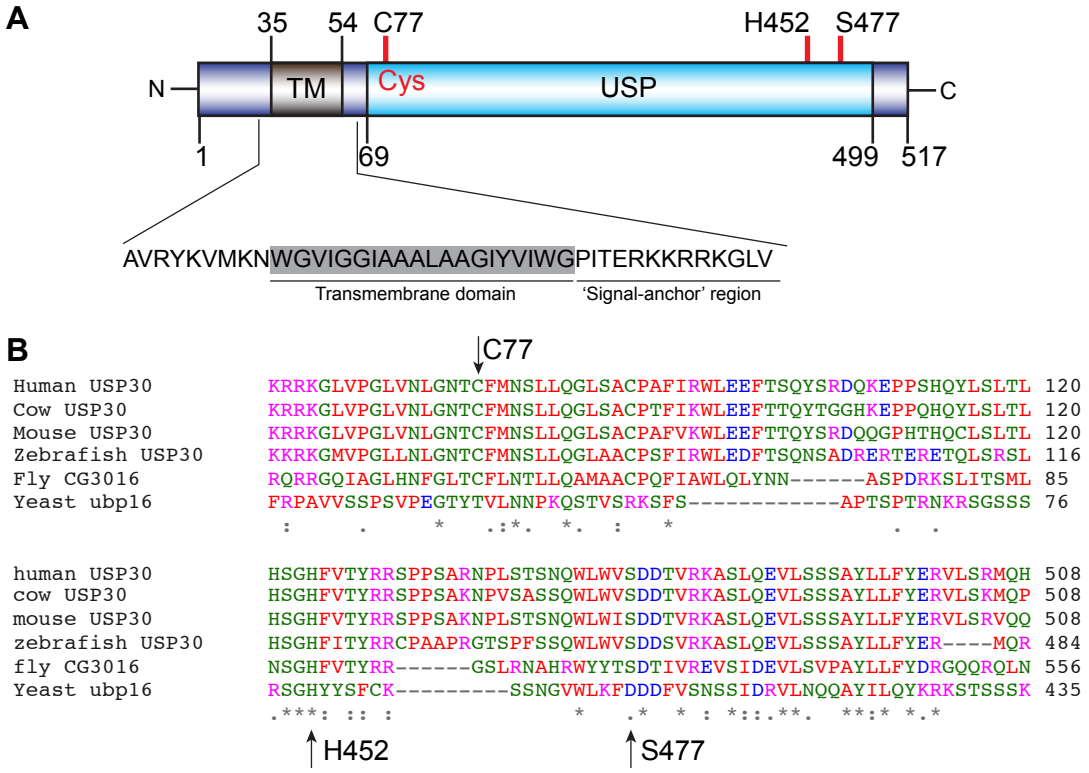

Figure 6.1 Protein domain architecture of USP30.

(A) USP30 has a transmembrane domain (TM) at the N-terminus. The catalytic triad consists of C77, H452 and an unconventional S452 instead of aspartate or asparagine.
(B) Clustalw alignment of human, cow, mouse, zebrafish, fly (CG3016) and yeast USP30 (ubp16). Arrows indicate the catalytic cysteine, histidine and serine, which in Ubp16 is an aspartic acid.

6.2 Understanding the role of USP30 in mitophagy

In the previous chapter, I identified USP30 as one of the DUBs that may regulate Parkin-mediated mitophagy in my live-cell imaging screen.

6.2.1 USP30 depletion exacerbates cell death during mitophagy

Knockdown of USP30 enhanced CCCP-mediated mitophagic cell death in hTERT-RPE1-YFP-Parkin cells as evident by the increase in DRAQ7-positive cells (see video 3 and Figure 6.2A). This observation is consistent with the preceding cleavage of PARP at 4hr (Figure 6.2B). As seen in Figure 6.3A, double knockdown of PINK1 and USP30 inhibited PARP cleavage, to the same extend as PINK1 knockdown. Furthermore, USP30 depletion in parental hTERT-RPE1 cells did not induce cell death during CCCP treatment (Figure 6.3B). These observations confirm that USP30 acts downstream of PINK1 and Parkin during mitophagic cell death.

At a later stage of my project, I obtained an USP30 antibody from Baris Bingol (Genentech, San Francisco). This allowed me to assess the knockdown efficiency of our array of siRNA oligos against USP30 (Figure 6.4A) (Bingol et al. 2014). Prior to obtaining that antibody, I had been assessing the knockdown efficiency using qRT-PCR. As shown in Figure 6.4B, all USP30 siRNA oligos depleted USP30 protein levels to less than 40% of the control (NT1) with the exception of oligo D8, which did not deplete USP30, as assessed by both western blotting and qRT-PCR. There is also a good correlation between USP30 mRNA and protein levels across the siRNA panel (R-squared value= 0.95).

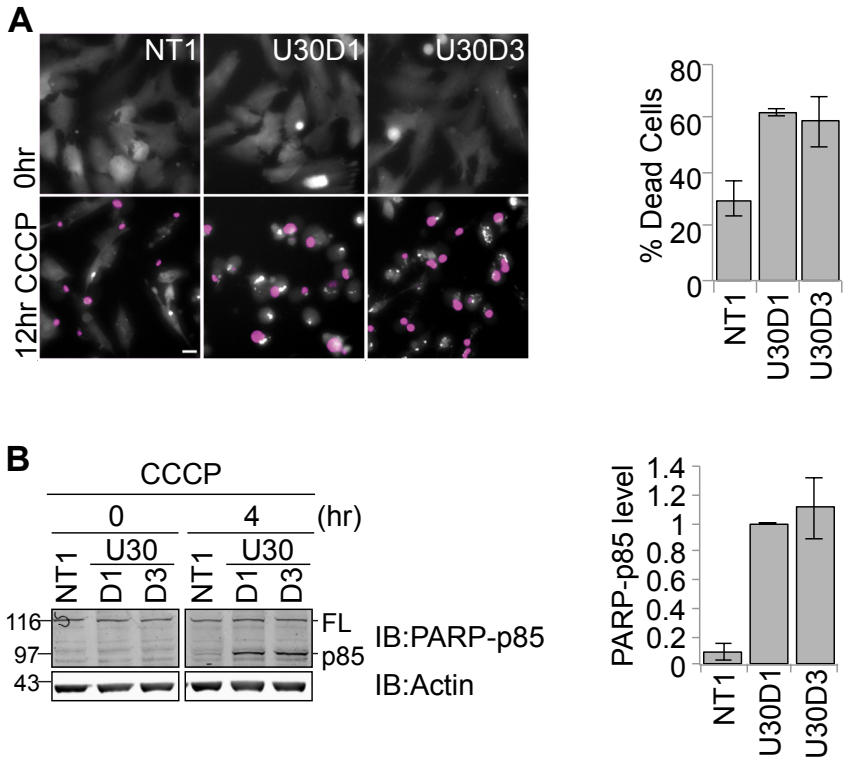

Figure 6.2 USP30 depletion in hTERT-RPE1-YFP-Parkin cells enhances cell death.

(A) hTERT-RPE1-YFP-Parkin cells were transfected with siRNA oligos against control (NT1) or USP30 (D1, D3) for 72hr. Cells were then treated with CCCP (10μM) for up to 24hrs. The progression of mitophagy was recorded by live-cell imaging in the presence of the membrane impermeable dye DRAQ7. Frames were captured at 15 min intervals. Shown is a cropped single frame from a representative video. YFP- Parkin is shown in grey, DRAQ7 in pink. Scale bar: 10 μm. The number of DRAQ7 positive cells (dead cells) at 12hr of CCCP treatment is shown as percentage of total cells at T=0. Error bars indicate SD; n= 4 imaged positions.
(B) hTERT-RPE1-YFP-Parkin cells were transfected as in (A) and treated with CCCP (10μM) for 4hr. Cells were lysed in NP40 lysis buffer and lysates were probed with indicated antibodies. FL: full length PARP. P85: PARP-p85 fragment. The band intensity of PARP-p85 (normalised to Actin) is shown as bar graph relative to the PARP-p85 level of USP30D1. Error bars indicate SD, n= 5 independent experiments.

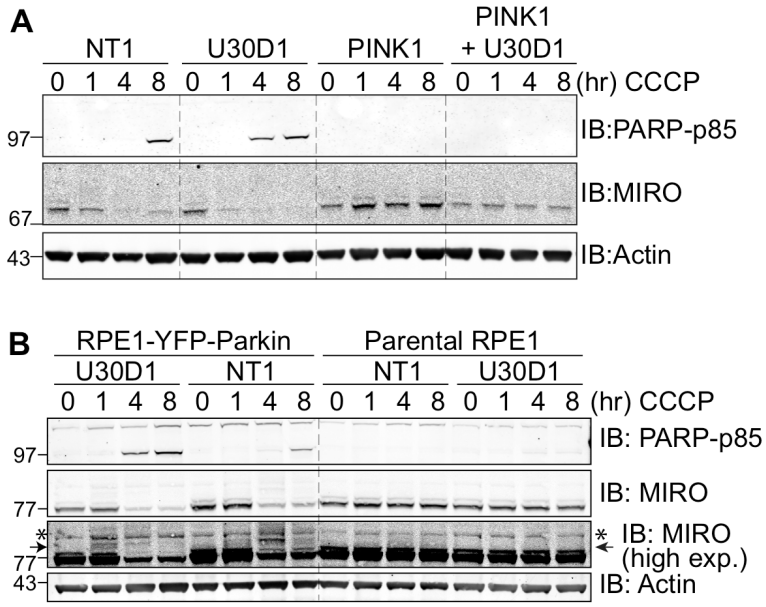

Figure 6.3 USP30 depletion enhances CCCP-induced cell death in a PINK1 and Parkin-dependent manner.

(A) hTERT-RPE1-YFP-Parkin cells were transfected as before with siRNA against control (NT1), PINK1 and USP30 (D1) and treated with CCCP (10μM) for 0, 1, 4 and 8hrs. Cells were lysed in RIPA lysis buffer.
(B) hTERT-RPE1-YFP-Parkin cells and parental hTERT-RPE1 cells were transfected and treated as in (A). Asterisk: non-specific band. Arrow: high molecular weight MIRO band.

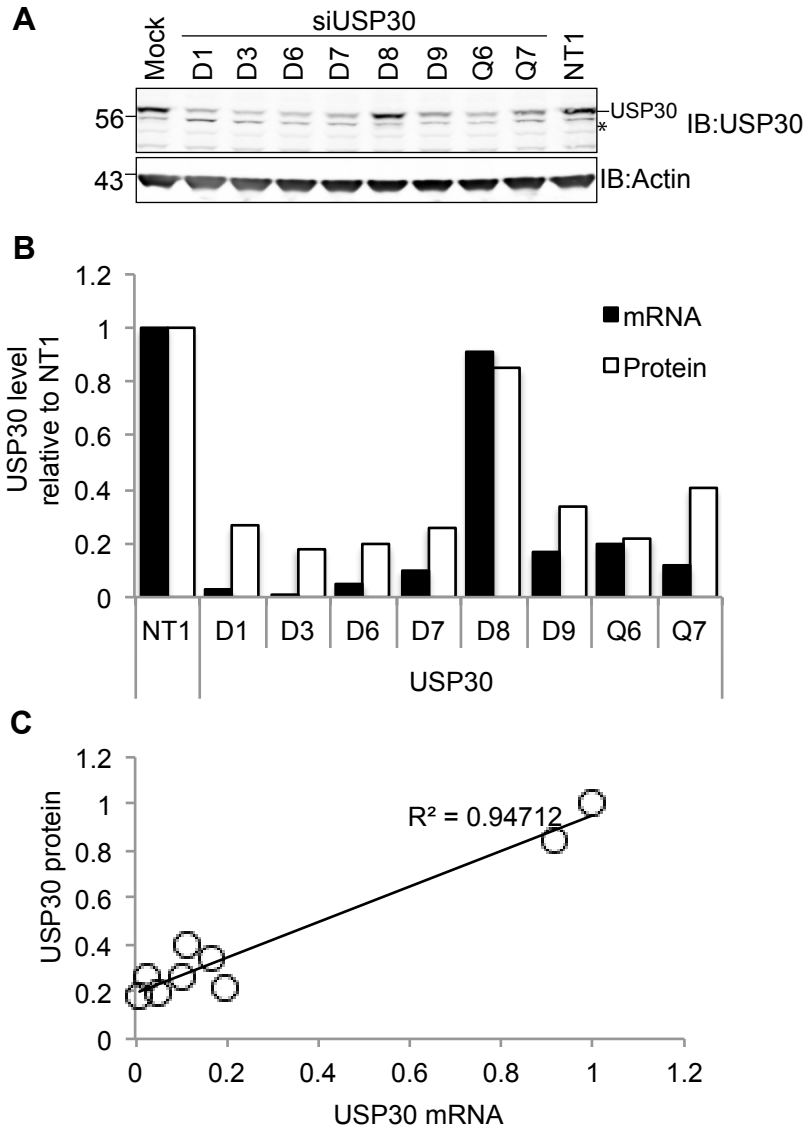

Figure 6.4 USP30 siRNA deconvolution.

(A) hTERT-RPE1-YFP-Parkin cells were transfected with siRNA oligos against USP30 (dharmacon oligos D1, D3, D6, D7, D8, D9; Qiagen oligos Q6, Q7) or control (NT1) and mock (transfected with RNAiMAX transfection reagent without siRNA oligo) for 72hr. Cells were then harvested in NP40 lysis buffer. Asterisk: non-specific band.
(B) Bar chart represents a comparison of USP30 protein levels and USP30 mRNA levels (24hr post-transfection) normalized to actin and expressed relative to NT1 control.
(C) Scatter plot illustrates correlation between relative USP30 protein and relative mRNA levels after siRNA oligo transfection.

6.2.2 USP30 localises to the mitochondria

A previous member of our laboratory, Richard Buus, had generated several different USP30 constructs. The constructs were: (1) full length USP30, (2) catalytically inactive (cysteine to serine modification at position 77) and (3) a truncated USP30 construct lacking the TM region (Δ1-53). Green fluorescent protein (GFP) tag was added to these constructs at the C-terminus instead of the N-terminus to avoid interference with the transmembrane signal at the N-terminus. As shown in Figure 6.5, both USP30-GFP and USP30-C77S-GFP localized to mitochondria, as evident by their co-localisation with TOM20. On the contrary, the N-terminal truncated USP30-Δ1-53 was distributed in the cytosol and nucleus, confirming the mitochondria-targeting function of the TM domain and 'signal-anchor' region.

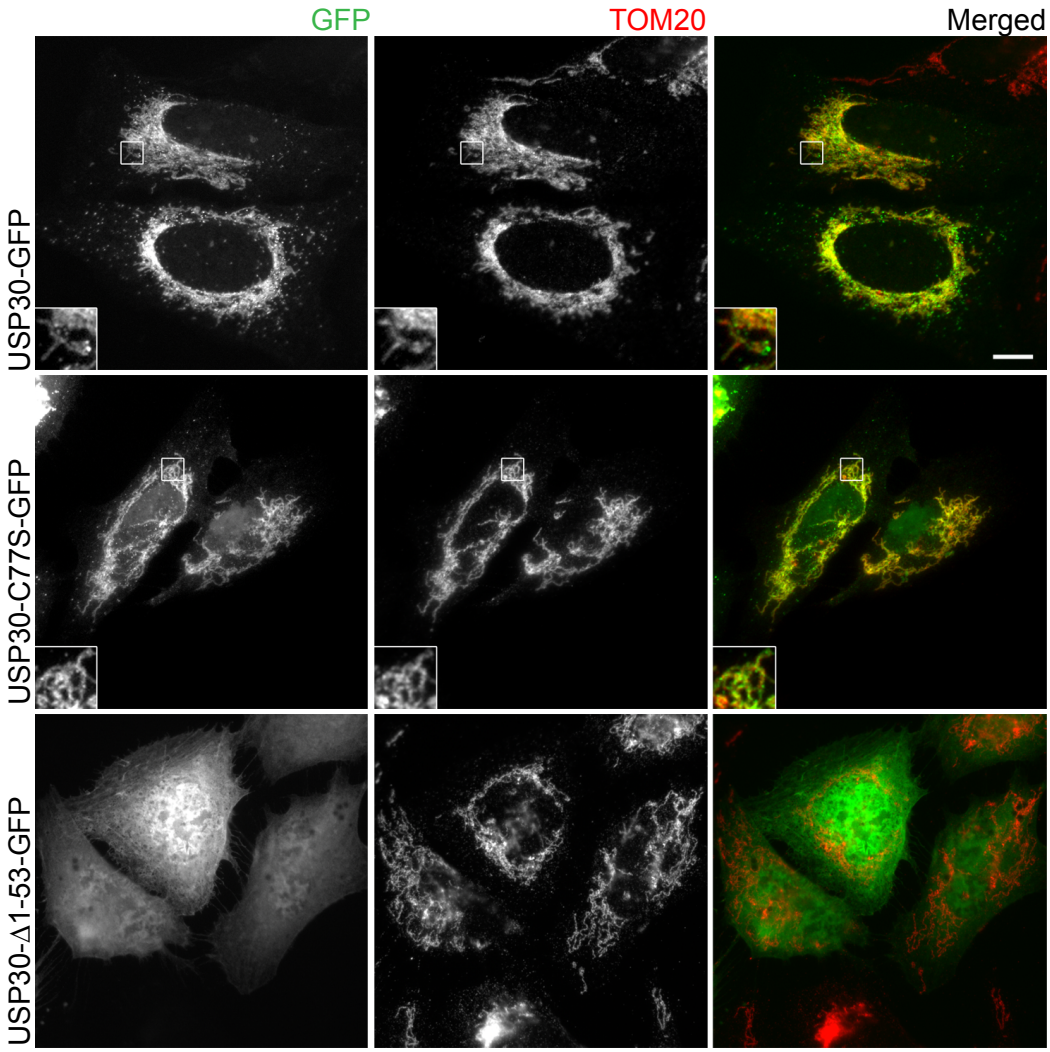

Figure 6.5 Localisation of USP30 in U2-OS cells.

U2-OS cells were transfected with 1µg of different USP30 plasmids for 24hr. Cells were then fixed in 4% PFA and permeabilised with 0.2% Triton-X100. Anti-TOM20 was used to visualize the mitochondria. Insets show 3-fold enlargement of the boxed area. Scale bar: 10µm.

6.2.3 Predicting the substrates and function of USP30

In *Drosophila* melanogaster, a large-scale yeast two-hybrid proteomic screen identified six interacting partners for CG3016 (fly USP30) (Giot et al. 2003). One of the proteins, Miro, was of particular interest as both Miro and USP30 are OMM proteins, with transmembrane domains that insert into the OMM and catalytic domains that face the cytosol (Frederick and Shaw 2007, Aspenstrom et al. 2004, Nakamura and Hirose 2008).

Symbol	Name	Function	Reference
CG3430	-	Uncharacterised	-
Miro	Mitochondrial Rho	Mitochondrion transport along microtubule	(Fransson et al. 2006)
Opa	Odd Paired	Transcription factor; essential for parasegmental subdivision of *Drosophila* embryo	(Benedyk et al. 1994)
CG12428	-	Carnitine O-octanoyltransferase activity (based on domain structure)	FlyBase
tna	tonalli	Interacts with Osa, a subunit of BHRAMA, a chromatin-remodeling complex, and UBC9, a SUMO E2 conjugating enzyme	(Gutierrez et al. 2003, Monribot-Villanueva et al. 2013)
Fd68A	Forkhead domain 68A	Transcription factor (prediction from domain)	FlyBase

Table 6.1 Interacting partners of CG3016 (fly USP30) and their known functions.

Data were obtained from yeast-two hybrid screen by Giot et al. (2003). Protein function annotation is based on FlyBase annotation (http://flybase.org/) and literature report.

6.2.4 USP30 depletion affects the levels of MIRO at steady state and during mitophagy

I first investigated the effect of USP30 depletion on MIRO protein stability at steady state. Upon USP30 depletion with two different oligos, USP30 D1 and D3 (Dharmacon siGenome oligos), MIRO protein levels decreased marginally but reproducibly (Figure 6.6A and B). I then questioned if the decrease in protein levels is due to transcriptional down-regulation of MIRO. qRT-PCR analysis of mRNA samples revealed no consistent effect of USP0 depletion on the levels of either MIRO1 or MIRO2; except USP30 oligo D1 decreased the mRNA levels of MIRO1 (Figure 6.1C).

Since MIRO1 and MIRO2 have high protein sequence similarity, we suspected the MIRO1 antibody that we used (Sigma, HPA010687) could bind to MIRO2 as well. ClustalW alignment revealed 60% protein sequence similarity across MIRO1 and MIRO2. The immunogen that was used to generate the antibody recognizes a region close to the N-terminus of MIRO1 that is highly similar in MIRO2 (Figure 6.6E). To verify the specificity of the MIRO1 antibody, I knocked down MIRO1 and MIRO2 individually or simultaneously (Figure 6.6D). Upon MIRO1 knockdown, there is still a considerable MIRO band observed on the western blot. On the contrary, MIRO2 knockdown dramatically reduced the intensity of the MIRO band, with a further reduction seen with a double knockdown of MIRO1 and MIRO2. This confirms that the antibody recognizes both forms of MIRO. In addition, it suggests that MIRO2 is the dominant form in hTERT-RPE1-YFP-Parkin cells.

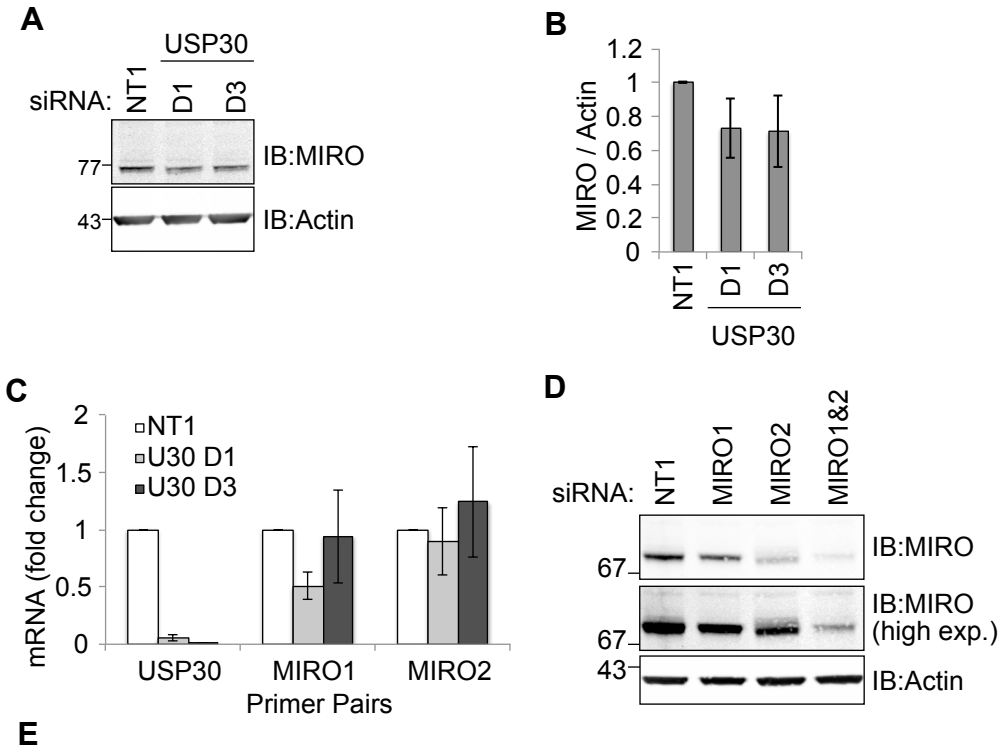

E

```
MIRO1           MKKDVRILLVGEPRVGKTSLIMSLVSEEFPEEVPPRAEEITIPADVTPERVPTHIVDYSE 60
MIROimmunogen   ------------------------------------------------THIVDYSE 8
MIRO2           MRRDVRILLLGEAQVGKTSLILSLVGEEFPEEVPPRAEEITIPADVTPEKVPTHIVDYSE 60
                                                                ********

MIRO1           AEQSDEQLHQEISQANVICIVYAVNNKHSIDKVTSRWIPLINERTDKDSRLPLILVGNKS 120
MIROimmunogen   AEQSDEQLHQEISQANVICIVYAVNNKHSIDKVTSRWIPLINERTDKDSRLPLILVGNKS 68
MIRO2           AEQTDEELREEIHKANVVCVVYDVSEEATIEKIRTKWIPLVNGGTTQGPRVPIILVGNKS 120
                ***:**:*::** :***:*:** *.:: :*:*: ::****:*  * :..*:*:*******

MIRO1           DLVEYSSMETILPIMNQYTEIETCVECSAKNLKNISELFYYAQKAVLHPTGPLYCPEEKE 180
MIROimmunogen   DLVEYSSMETILPIMNQYTEIE---------------------------------------- 90
MIRO2           DLRSGSSMEAVLPIMSQFPEIETCVECSAKNLRNISELFYYAQKAVLHPTAPLYDPEAKQ 180
                ** . ****::****.*:.***
```

Figure 6.6 USP30 depletion only marginally reduces the protein level of MIRO.

(A) hTERT-RPE1-YFP-Parkin cells were transfected with siRNA oligos against either control (NT1) or USP30 (oligo D1 and D3) for 72hr. Cells were harvested in RIPA lysis buffer.
(B) Bar graph represents MIRO protein levels normalised to actin and expressed as relative to NT1. Error bar represents standard deviation of 5 experimental repeats.
(C) hTERT-RPE1-YFP-Parkin cells were transfected with siRNA oligos against control (NT1), MIRO1 or MIRO2. Cells were harvested 24hr post-transfection for qRT-PCR analysis. mRNA level of USP30, MIRO1, and MIRO2 were normalized to B-actin and fold change is expressed in relative to NT1 level. Error bar represents standard deviation of 3 experimental repeats.
(D) hTERT-RPE1-YFP-Parkin cells were transfected with siRNA oligos against control (NT1), MIRO1 or/ and MIRO2 for 72hr. Cells were harvested in NP40 lysis buffer.
(E) ClustalW protein sequence alignment of MIRO1, MIRO2 and the immunogen sequence of MIRO1 antibody from Sigma (HPA010687).

6.2.5 USP30 physically interacts with MIRO

Next, I investigated the interaction of USP30 and MIRO at the protein level. Immunoprecipitation of either USP30-GFP or its catalytically inactive mutant, USP30-C77S-GFP in HEK293T cells demonstrated interaction with endogenous MIRO (Figure 6.7). This interaction is specific and is not observed with GFP alone. Intriguingly, the immunoprecipitated MIRO bands are higher molecular weight than that those observed in the total lysates. These higher molecular weight forms of MIRO may be due to post-translational modifications and suggest that MIRO recognition by USP30 may be regulated post-translationally. Equally interesting is the weaker interaction between USP30-C77S-GFP with endogenous MIRO compared to USP30-GFP. As negative controls, I reprobed for TIMM44 and actin, neither of which was pulled down in either of the immunoprecipitations. It is important to note that I have only performed this experiment once and more repeats are required to confirm these observations.

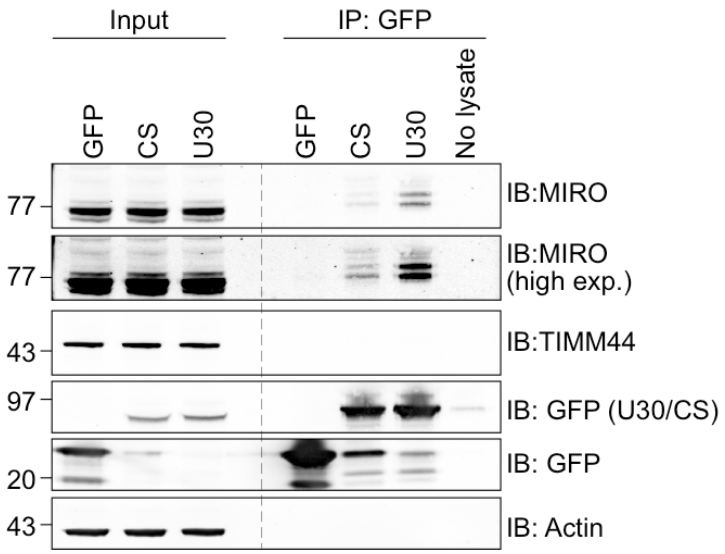

Figure 6.7 USP30 physically interacts with MIRO.

HEK293T cells were transfected with 3µg of plasmids for 24hr and 800µl of lysate (2µg/µl) of NP40 lysate were incubated with 30µl of 1:1 nanotrap slurry in the cold room for 2hr. Bound proteins were analysed alongside 1.8% of input sample. U30, USP30-GFP; CS, catalytically inactive mutant USP30-C77S-GFP; no lysate input: NP40 lysis buffer with nanotrap.

6.2.6 USP30 depletion alters the ubiquitylation of MIRO during mitophagy

During the early stages of mitophagy, activated Parkin ubiquitylates MIRO on the OMM surface for proteasomal degradation. Loss of MIRO dissociates mitochondria from the microtubules and impedes their movement, thereby segregating malfunctioning mitochondria from the healthy population. Upon CCCP treatment, USP30 knockdown induced the appearance of a higher molecular weight banding indicative of an ubiquitylated species (Figure 6.8). In control NT1-treated cells, the ubiquitylated MIRO bands (Ub-MIRO) peaked at 4hr after CCCP treatment. On the other hand, USP30 depletion promoted earlier ubiquitylation of MIRO (around 1hr). This observation suggests that MIRO is a substrate for USP30 and the loss of USP30 promotes the ubiquitylation and subsequent proteasomal degradation of MIRO.

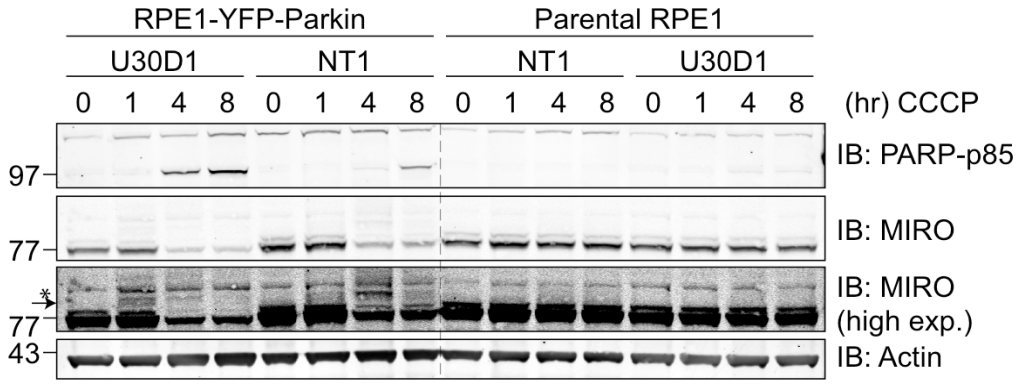

Figure 6.8 USP30 depletion alters the ubiquitylation of MIRO during mitophagy.

hTERT-RPE1-YFP-Parkin and parental hTERT-RPE1 cells were transfected with siRNA against control (NT1) or USP30 (oligo D1) for 72hr. Cells were then treated with CCCP (10μM). Cells were harvested in RIPA lysis buffer. The same figure as Figure 6.3B is shown again to show the MIRO blot.

6.2.7 siUSP30-mediated loss of MIRO is not restored with proteasomal inhibitors

I then proceeded to inhibit proteasomal degradation and lysosomal degradation in USP30-depleted cells with epoxomicin and folimycin, respectively. In theory, if USP30 depletion promotes MIRO ubiquitylation and proteasomal degradation, proteasome inhibition should be able to rescue MIRO from degradation.

Epoxomicin or folimycin treatment alone for 8hr did not accumulate more MIRO in either control NT1 or USP30-transfected cells. Simultaneous treatment of CCCP with epoxomicin for 8hr only marginally rescued the levels of MIRO and Ub-MIRO in the control NT1-transfected cells. There was also a slight accumulation of MIRO and Ub-MIRO in the NT1-transfected cells upon CCCP and folimycin treatment, suggesting that a small population of Ub-MIRO may be degraded via the lysosomal pathway. We observed little rescue of MIRO levels in USP30 knockdown cells in with either epoxomicin or folimycin treatment.

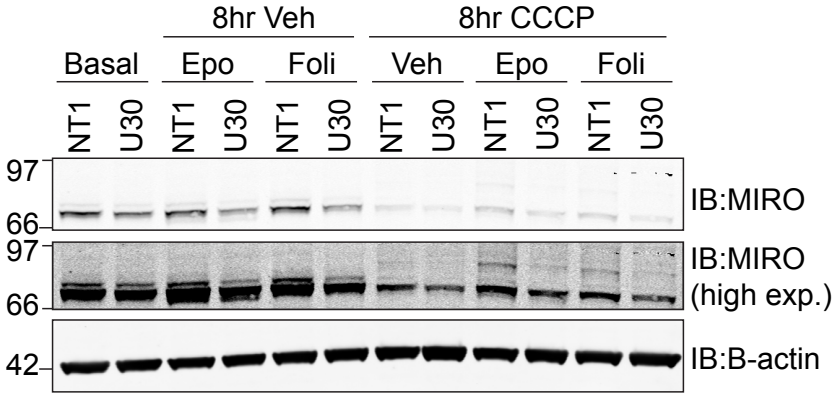

Figure 6.9 USP30 depletion-induced MIRO protein decrease is not rescued by proteasomal inhibition.

hTERT-RPE1-YFP-Parkin cells were transfected with siRNA against USP30 (oligo D1) and NT1 control for 72hr. Cells were then treated with CCCP (10μM), epoxomicin (100nM), and folimycin (100nM) for 8hr. Cells were lysed in NP40 lysis buffer. 20μg of lysates were probed as indicated.

6.2.8 MIRO2 depletion does not lead to enhanced cell death

Whilst the decrease in MIRO levels upon USP30 depletion was not dramatic, I wondered whether this might cause the enhanced cell death we observed during mitophagy. To investigate this, I knocked down MIRO2 in hTERT-RPE1-YFP-Parkin cells and treated the cells with CCCP for 8hr. As shown in Figure 6.10A, transfection with three out of four MIRO2 siRNA oligos (D9, D10 and D12) reduced the level of PARP-p85, suggesting that MIRO2 depletion is cytoprotective during mitophagy as opposed to the enhanced cell death observed in USP30 depleted cells. Double knockdown of both MIRO2 and USP30 did not rescue the apoptotic effect of USP30 depletion (Figure 6.10B). This suggests that the decrease in MIRO2 level in USP30 depleted cells is not the cause of enhanced cell death. It is worth noting that I did not get good depletion of MIRO2 with any of the MIRO2 siRNA oligos in these experiments. It is possible that MIRO2 has a long half-life and might require more than 72hr of siRNA transfection for complete depletion of protein level. Nevertheless, since USP30 depletion only marginally decreased MIRO protein levels (less than that observed with MIRO2 siRNA, see Figure 6.10B) but still enhanced mitophagic cell death, it is unlikely that MIRO2 depletion is responsible for the enhanced mitophagic cell death observed.

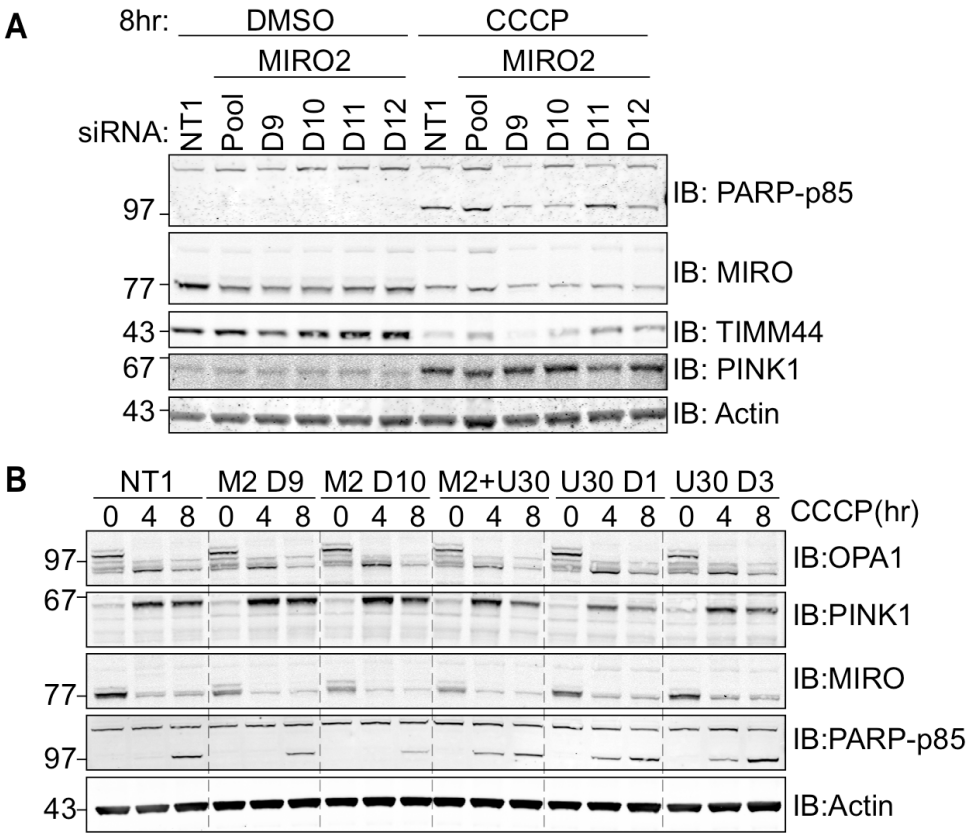

Figure 6.10 MIRO2 depletion does not enhance cell death during CCCP treatment.

(A) hTERT-RPE1-YFP-Parkin cells were transfected with siRNA oligos against either control (NT1), or MIRO2 (pool, D9, D10, D11 and D12) for 72hr. Cells were then treated with CCCP (10μM) for 8hr. Cells were lysed in RIPA lysis buffer and lysates (8μg) were immunoblotted as indicated.
(B) hTERT-RPE1-YFP-Parkin cells were transfected with siRNA oligos targeting Miro2 (M2, D9 and D10), or USP30 (D1 and D3), or with siRNAs targeting both Miro2 (D9 and D10) and USP30 (D1and D3), treated with CCCP and harvested in RIPA lysis buffer at indicated times. 10μg of lysates were immunoblotted as indicated.

6.3 TOM20 and TOM22 are substrates of USP30

6.3.1 USP30 depletion enhanced TOM20 and TOM22 turnover during mitophagy

During the investigation of the effect of USP30 on MIRO, I also probed the lysates for TOM20 as a marker for mitochondria and I followed TOM20 degradation as a readout for mitophagy. I discovered that TOM20 was degraded faster in USP30 depleted cells (Figure 6.11). In addition, more TOM20 appeared as higher molecular weight species, suggesting that it was di-ubiquitinated on one, or monoubiquitinated at two different lysine residues, when USP30 was depleted. Similar observations were seen with TOM22 as the protein was accumulated as a higher molecular weight species and was degraded faster when USP30 was depleted. All the above observations were reproducible with two USP30 siRNA oligos, D1 and D3. This strongly suggests that TOM20 and TOM22 are direct deubiquitylating substrates of USP30. This effect is not due to faster overall mitophagy as other OMM and IMM proteins, including MFN, TIMM44 and S-OPA1, were not affected with USP30 depletion. LC3 conversion from LC3-I to LC3-II was also not affected.

It is also noteworthy that USP30 itself seems to be ubiquitylated as well during CCCP treatment, suggesting that it may be a direct substrate of Parkin. The enhanced degradation of TOM20 was further validated with additional siRNA oligos and was found to correspond to the knockdown level of USP30 (Figure 6.11B). USP30 siRNA oligos D1, D3, D6, D7, D9 and Q6, which all depleted USP30, also enhanced TOM20 degradation during CCCP treatment whereas USP30 D8, and two controls (NT1, mock) did not affect USP30 or TOM20 degradation. Apart from USP30 oligo D1 and D3, I also observed higher levels of PARP-p85 accumulation during CCCP treatment with USP30 oligo Q6. Interestingly, the higher levels of PARP cleavage correlate with the strongest depletion of TOM20.

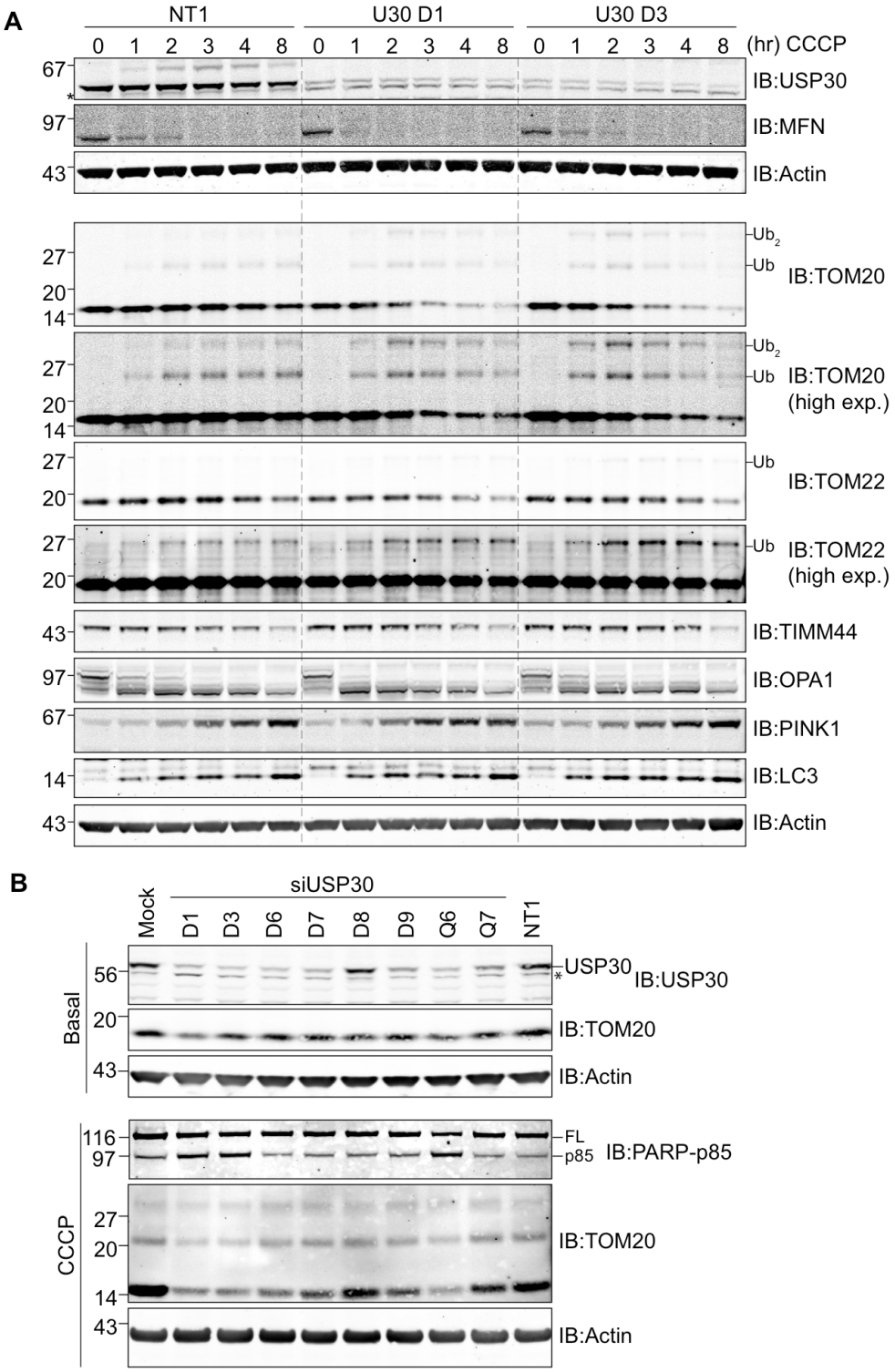

Figure 6.11 USP30 depletion enhanced TOM20 and TOM22 degradation.

(A) hTERT-RPE1-YFP-Parkin cells were transfected for 72hr with siRNA targeting USP30 (D1 and D3) or siRNA control oligo (NT1). Cells were then treated with CCCP (10μM) and harvested with RIPA lysis buffer at indicated times.
(B) The blots presented in Figure 6.4A were shown again to allow for direct comparison of degree of USP30 knockdown and TOM20 level. Cells treated with siRNA as indicated for 72hr. The cells were either harvested directly or further treated with CCCP (10μM) for 4hr. Cells were harvested in NP40 lysis buffer. Asterisk: non-specific band.

6.3.2 USP30 physically interacts with TOM20 and TOM22

I next investigated the physical interaction of USP30 with TOM20 and TOM22 by immunoprecipitation. Using GFP-tagged USP30 (USP30-GFP) and its catalytically inactive mutant (USP30-C77S-GFP) expressed in HEK293T cells, I could show that both TOM20 and TOM22 were immunoprecipitated together with both active and inactive USP30 (Figure 6.12B). On the other hand, TIMM44, the IMM protein and Actin were not immunoprecipitated.

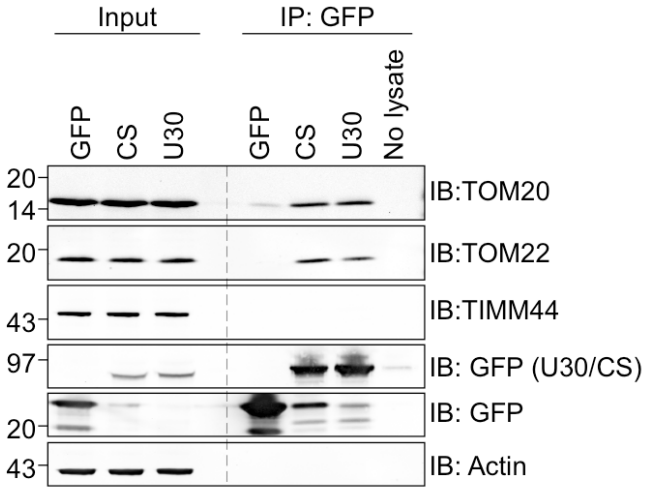

Figure 6.12 TOM20 is a substrate and interactor of USP30.

HEK293T cells expressing GFP-tagged USP30 were lysed in NP40 lysis buffer and subjected to immunoprecipitation (IP) with GFP-nanotrap and probed as indicated. Bound proteins were analysed alongside 1.8% of input sample. U30, USP30-GFP; CS, catalytically inactive mutant USP30-C77S-GFP; no lysate input: NP40 lysis buffer with nanotrap. Note that these samples were probed in parallel for MIRO shown in Figure 6.7.

6.3.3 Proteasomal inhibition rescues TOM20 levels in USP30 depleted cells

To further demonstrate that TOM20 is deubiquitylated and rescued from from proteasomal degradation by USP30 during CCCP treatment, I treated USP30 depleted hTERT-RPE1-YFP-Parkin cells with CCCP in the presence of epoxomicin and/or folimycin. As can be seen in Figure 6.13, CCCP treatment alone induced faster degradation of TOM20 in USP30 depleted cells. Simultaneous treatment of CCCP with epoxomicin delayed TOM20 degradation in NT1 and also USP30 D1 and D3 transfected cells. Interestingly, the ubiquitylated forms of TOM20 (Ub-TOM20) accumulated only in USP30 D1 and D3 transfected cells whereas Ub-TOM20 is not observed in NT1-transfected cells. Strikingly, this effect is only observed with epoxomicin but not with folimycin treatment. However, compared to CCCP treatment only, simultaneous treatment of CCCP with folimycin slightly delayed TOM20 degradation in both control and USP30-depleted cells, suggesting partial involvement of the lysosomal degradation in the degradation of TOM20. Simultaneous inhibition of both proteasomal and lysosomal pathways during CCCP treatment confers additive inhibitory effect on the degradation of TOM20. The accumulation of Ub-TOM20 in USP30-depleted cells is also more striking.

Since the background signal is very high in the TOM22 blot, no conclusive statement can be made. It seems like similar but less striking observations to that of TOM20 could be observed with TOM22 protein degradation during CCCP treatment in the presence of either epoxomicin or folimycin.

Consistent with observations from Figure 6.3 and Figure 6.11, USP30 depletion did not affect OPA1 cleavage or PINK1 accumulation but enhanced PARP cleavage. Proteasomal and lysosomal inhibitors did not affect OPA1 cleavage or PINK1 accumulation but especially when combined caused a slight accumulation. As described in chapter 4, inhibition of proteasomal but not lysosomal degradation inhibits PARP cleavage. This inhibitory effect overrides the enhanced cell death effect of USP30.

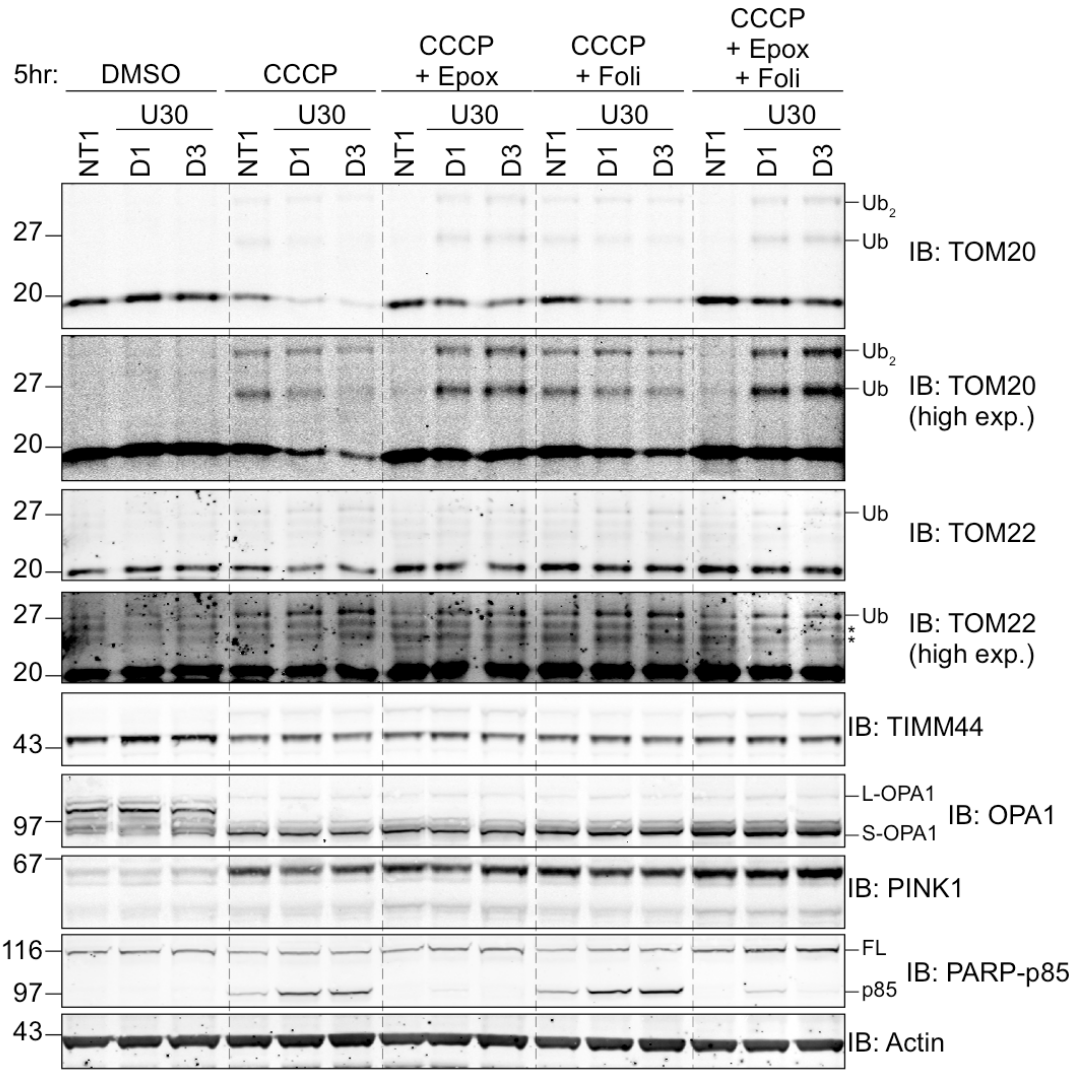

Figure 6.13 Proteasomal inhibition rescues TOM20 levels.

hTERT-RPE1-YFP-Parkin cells were transfected with either non-targeting siRNA (NT1) or siRNA against USP30 (D1, D3), then treated with CCCP (10 μM) together with either Epoxomicin (100 nM) or Folimycin (100 nM) for 5hrs. Lysates were probed with antibodies as indicated. Asterisk: non-specific band. Ub: ubiquitylated bands. FL: full length PARP. P85: PARP-p85 fragment.

6.3.4 Mouse USP30 (mUSP30) rescued TOM20 and mitophagic cell death in USP30 depleted cells

To further confirm that USP30 depletion causes enhanced cell death during mitophagy, I depleted it for 72hr and expressed mouse USP30 during the last 48hr of siRNA transfection. Subsequent treatment with CCCP showed that mouse USP30 expression partially protects the cells from PARP cleavage. This is most apparent in NT1 treated cells (Figure 6.14A; compare lane 1 and 2). In addition, the expression of mouse USP30 in USP30 depleted cells partially delayed the degradation of TOM20. Simultaneous treatment of CCCP with epoxomicin also showed a slight decrease in the ubiquitylated bands of TOM20 when mouse USP30 was expressed. However, these experiments will require further validation. Overall, these data support the hypothesis that USP30 deubiquitylates TOM20 and promotes cell death during mitophagy.

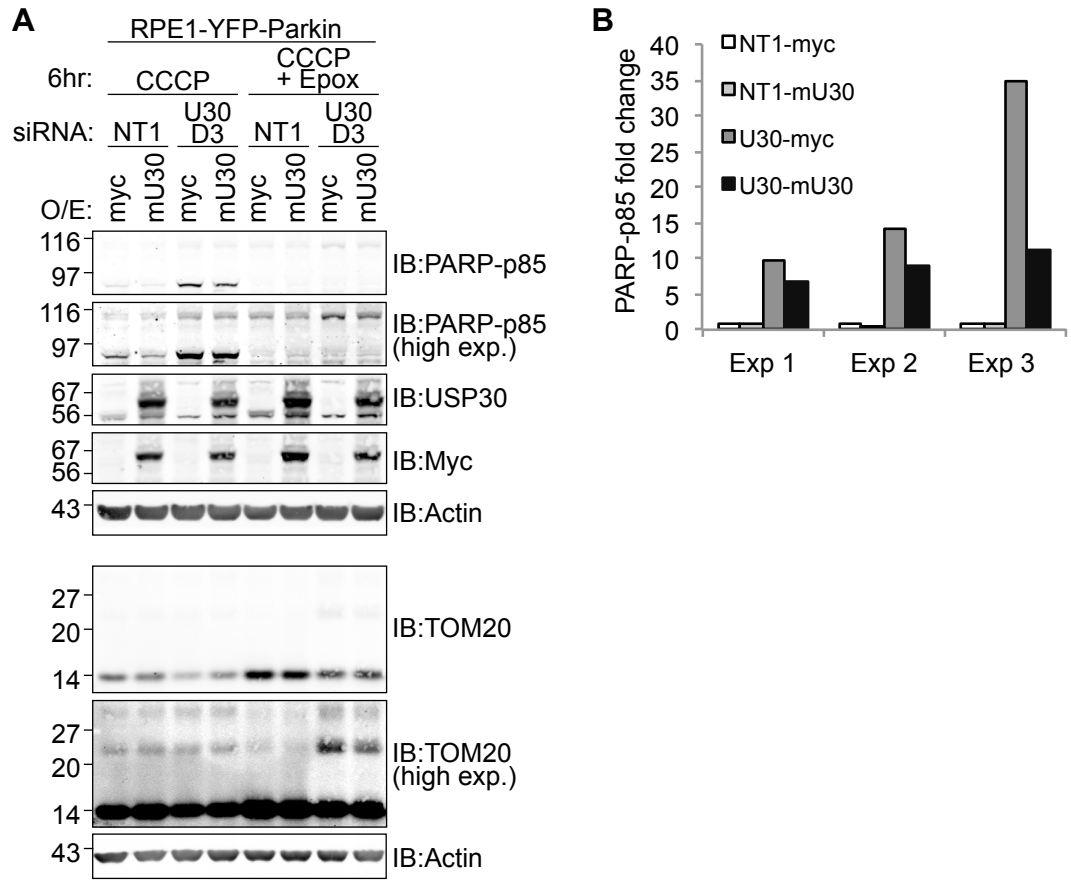

Figure 6.14 PARP cleavage can be rescued by overexpression of mouse USP30.

(A) hTERT-RPE1-YFP-Parkin cells were transfected with 40nM of either NT1 (control) or USP30 D3 oligo for 72hr. 24hr post-transfection, cells were transfected with 1µg of pCMV-myc or pCMV6-myc-ddk-mUSP30 plasmids for 48hr. Cells were then treated with 10µM of CCCP or 10µM of CCCP with 100nM of epoxomicin. 15µg of NP40 lysates were immunoblotted as indicated.
(B) Bar chart represents quantitation of PARP-p85 protein band intensities normalized to actin and expressed as relative to NT1-myc control samples from three independent experimental repeats. Data from Exp1 was obtained from the blots of Figure 6.14A.

6.4 Investigation of a cytoprotective role of USP30 in the face of other apoptotic stimuli

Given that mitochondria play a pivotal role during apoptosis and USP30 localises to the mitochondria, it is possible that USP30 has a more general role in regulating cell responses to other cell death stimuli. I first tested a list of apoptosis-triggering drugs including taxol, thapsigargin, TNF-α, tunicamycin, etoposide, ABT-737 and ABT-263. All of these drugs induce apoptosis by different mechanisms (summarized in Table 6.2). Due to the different timecourse of apoptotic response to different drugs, I carried out the initial analysis by live-cell imaging and judged cell death responses by the incorporation of the membrane-impermeable dye, DRAQ7 over 24hr. Most of the drugs did not induce apoptosis in hTERT-RPE1-YFP-Parkin cells. Taxol treatment caused the cells to round up but no DRAQ7 incorporation to the cells was observed. Only two drugs, ABT-737 and its orally bioavailable analog, ABT-263 induced apoptosis within 8-12hr of treatment.

Drug (working Concentration)	DRAQ7 staining	Observations	Description of Mechanism	References
TNF-alpha (10ng/ml)	Negative	-	Binds to TNF receptor 1/2, recruits TRADD and FADD, subsequently activates caspase 8	(Wallach et al. 1996)
Taxol (100nM)	Negative	Cells round up but are not DRAQ7 positive	Stabilizes microtubules, inhibits cell division	(Das et al. 2001)
Thapsigargin (10μM)	Negative	-	SERCA Ca2+ ATPase inhibitor (induce Ca2+ overload)	(Brayden et al. 1989, Foder et al. 1989)
Tunicamycin (10μM)	Negative	-	inhibits N-linked gylcosylation (ER stress, triggers UPR)	(Leavitt et al. 1977)
Etoposide (10μM)	Negative	-	topoisomerase inhibitor (promote DNA double strand breakage)	(Onishi et al. 1993)
ABT-737(10μM)	Positive	Cell death at 8-12hr	BH3 mimetic small molecule inhibitor, binds and removes inhibitory function of anti-apoptotic BCL2 family members (Bcl2, BCL-xL, Bcl-w)	(M. F. van Delft et al. 2006, Vogler et al. 2008)
ABT-263 (10μM)	Positive	Cell death at 8-12hr	Orally bioavailable analog of ABT-737	(Tse et al. 2008)

Table 6.2 Different apoptotic stimuli tested on hTERT-RPE1-YFP-Parkin cells. Cell death was recorded by live-cell imaging at every 30min intervals up to 24hr. The membrane-impermeable dye, DRAQ7 (0.3μM) was used to assess cell death response.

6.4.1 USP30 depletion exacerbates cell death induced by ABT-263 and ABT-737

ABT-737 and its orally bioavailable analog, ABT-263 belong to the group of Bad-like BH3 mimetics (Oltersdorf et al. 2005). ABT-737 and ABT-263 induced some cell death in hTERT-RPE1-YFP-Parkin cells within 8-12hr of treatment, as demonstrated by the incorporation of DRAQ7 into the cells (see video 4 and 5; Figure 6.15). USP30 depletion (siRNA by U30D1 and D3) induced more cell death compared to the control (NT1). In addition, I also observed that ABT-737 was more potent than ABT-263 in inducing cell death in hTERT-RPE1-YFP-Parkin cells.

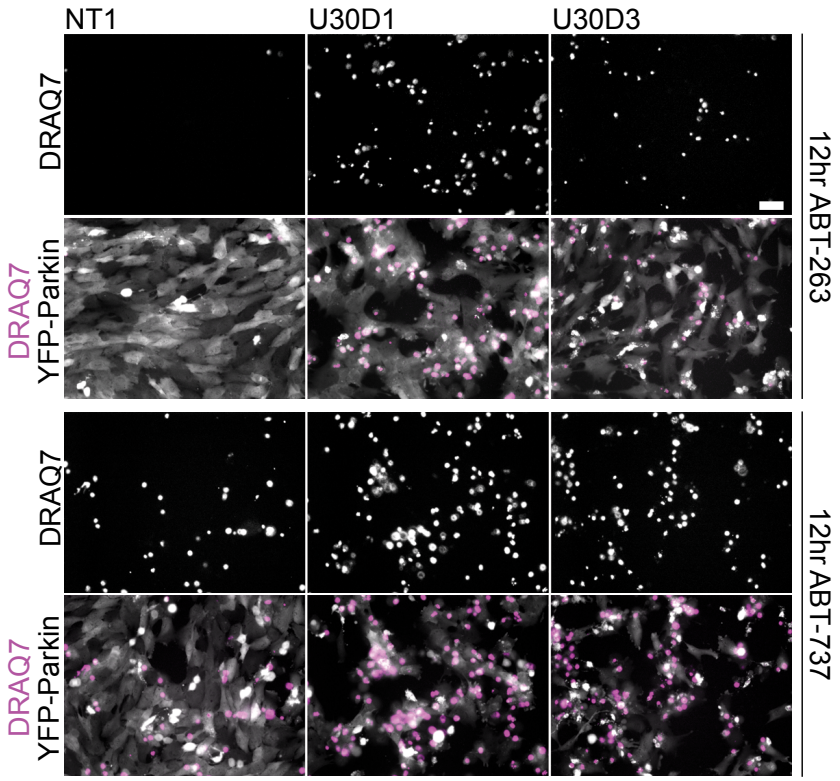

Figure 6.15 USP30 depletion sensitizes hTERT-RPE1-YFP-Parkin cells to ABT-737 and ABT263 induced cell death.

hTERT-RPE1-YFP- Parkin cells were transfected for 72 hrs with either non-targeting siRNA (NT1) or siRNA targeting USP30 (D1 and D3). Cells were then treated either with CCCP, ABT-263 or ABT-737 (all 10 μM). Cells were imaged at 30 min intervals in the presence of the membrane impermeable dye DRAQ7 and a single frame corresponding to the 12hr time point is shown (see also video 4 and 5). Top rows show the isolated DRAQ7 staining (dead cells, white on black). Bottom rows show YFP-Parkin in grey and DRAQ7 in pink. Scale bar 40 μm.

I further characterized the cell death triggered by ABT-737 and ABT-263 using western blotting (Figure 6.16). USP30-depleted cells showed more PARP and caspase 3 cleavage compared to NT1. It is noteworthy that there is a slight difference in the cleaved caspase 3 fragments between USP30 D1 and USP30 D3 siRNA-transfected cells. ABT-263 and ABT-737 treatment in USP30 D1-transfected cells seemed to accumulate more of the p15 fragment compared to USP30 D3-transfected cells. In contrast to CCCP-induced cell death, ABT-737 and ABT-263-induced cell death occurs independently of mitophagy as evidenced by the lack of PINK1 accumulation and Parkin autoubiquitylation. TOM20, MIRO, MFN and TIMM44 were also not degraded during ABT-737 and ABT263 treatments. This indicates that ABT-737 and ABT-263 trigger cell death via a different mechanism than CCCP.

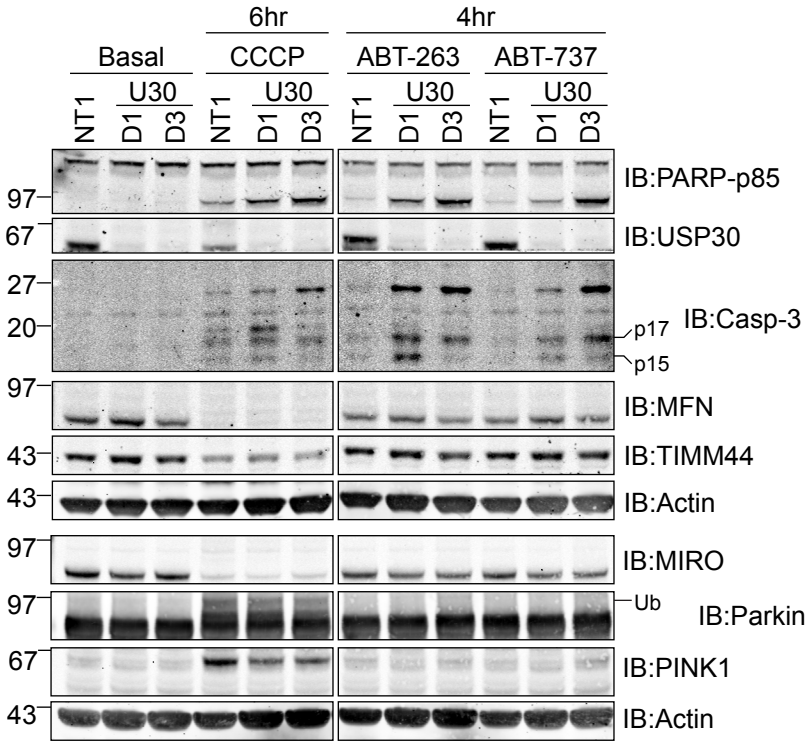

Figure 6.16 USP30 depletion sensitises cells to ABT-737 and ABT-263 induced cell death in a Parkin-independent manner.

hTERT-RPE1-YFP-Parkin cells were transfected for 72hr with either 40nM of non-targeting control siRNA (NT1) or siRNA targeting USP30 (D1 and D3). Cells were treated either with CCCP, ABT-263 or ABT- 737 (all 10 μM). CCCP-treated cells were harvested after 6hr and ABT-263 and ABT-737-treated cells after 4hr of treatment, using “hot lysis” buffer, and samples were probed with antibodies as indicated. Basal: untreated.

6.4.2 USP30 depletion increases the levels of BAK and BCL2

ABT-737 and ABT263 are BH3 only-mimetics (BAD-like) that show high affinity to the pro-survival BCL2 family members, BCL2, BCL-xL and Bcl-W (*Ki* <1nM) but not MCL1 (*Ki*>1μM). (Mark F. van Delft et al. 2006, Vogler et al. 2009a, Vogler et al. 2009b, Vogler et al. 2008). Binding of ABT-737 and ABT-263 sequesters these proteins away from the pro-apoptotic BAK and BAX. This allows BAK and BAX to either homo-oligomerise or hetero-oligomerise on the OMM to induce mitochondrial outer membrane permeabilization (MOMP) and cytochrome C release.

Therefore, I decided to measure the levels of both pro-survival and pro-apoptotic BCL2 family members, including BCL2, BCL-xL, MCL1, BAK and BAX. Under basal condition, USP30 depletion induced an increase in BAK and BCL2 but not BAX and BCL-xL (Figure 6.17A and B). The effect of USP30 on MCL1 is less clear as transfection with USP30 D3 but not USP30 D1 siRNA oligo decreased MCL1, suggesting a potential off-target effect of either of the siRNA oligos on MCL1 expression. Intriguingly, CCCP treatment increased MCL1 levels independent of transfection conditions. It is known that MCL1 levels are tightly regulated by several E3 ligases, including HUWE1, FBXW7 and TRIM17 (Ren et al. 2013, Inuzuka et al. 2011, Pandya et al. 2010, Magiera et al. 2013). We speculate that the elevated MCL1 levels observed during mitophagy might account for newly synthesized protein that cannot be translocated to depolarised mitochondria and are therefore protected from degradation.

On the other hand, CCCP treatment promoted the accumulation of higher molecular weight forms of BAK that is indicative of ubiquitylated BAK, which is consistent with the observation by Chan et al. (2011) that it can be ubiquitylated by Parkin during mitophagy (Chan et al. 2011). ABT-263 and ABT-737 treatment did not induce ubiquitylation of BAK.

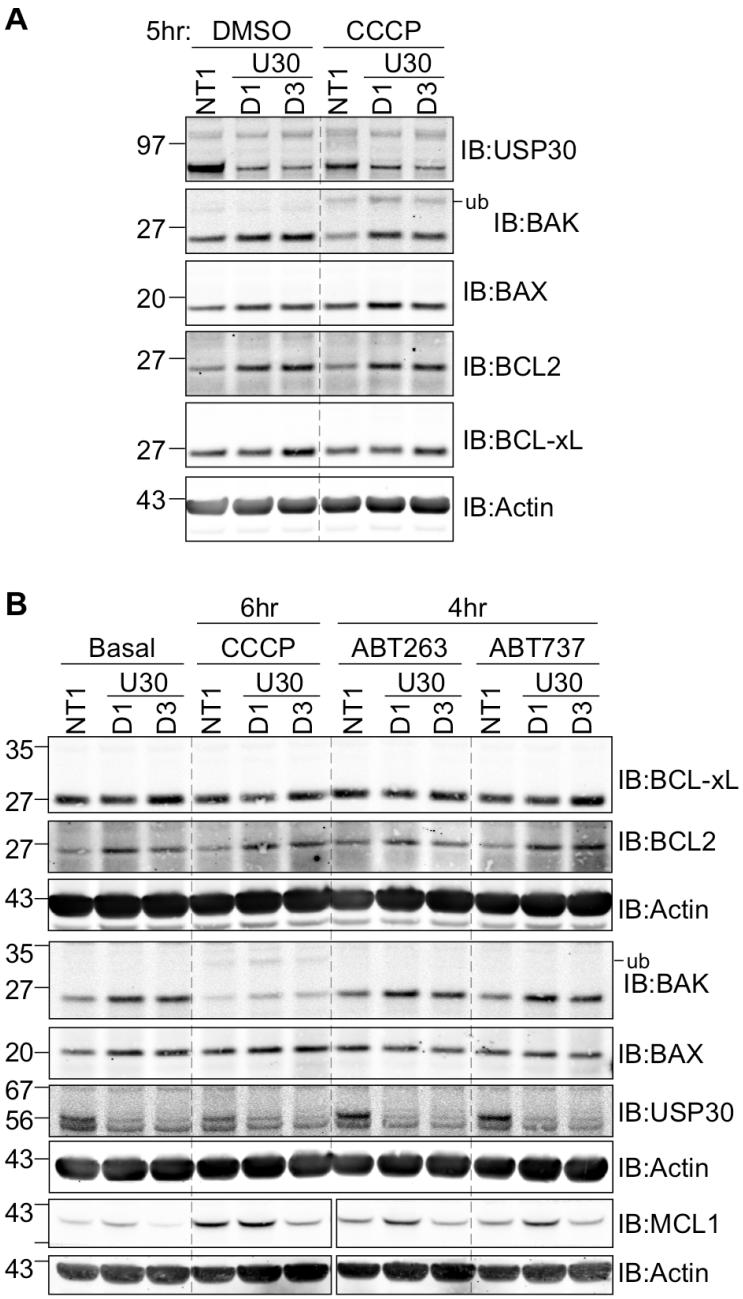

Figure 6.17 USP30 depletion increases BAK and BCL2 protein levels

(A) hTERT-RPE1-YFP-Parkin cells were transfected for 72hr with either non-targeting control siRNA oligo (NT1) or USP30 (D1 and D3). Cells were treated with CCCP (10μM) for 5hr and harvested in RIPA lysis buffer. 15μg of lysates were immunoblotted as indicated.
(B) Samples described in Figure 6.16 were re-run and re-probed for the indicated proteins.

6.4.3 BAK and BAX are required for ABT-737-induced cell death but not mitophagy-induced cell death

Since there is an upregulation of BAK upon USP30 depletion, I wanted to investigate the involvement of BAK and BAX in CCCP and ABT-737-induced cell death. I co-depleted either BAK or BAX together with USP30. Independently of BAX levels, USP30-depletion increased the levels of BAK (Figure 6.18A). In the context of CCCP induced cell death, BAK and BAX depletion did not affect the enhanced accumulation of PARP-p85 seen upon USP30 knockdown. In ABT-737-treated cells, in contrast, BAX-depletion, fully and BAK depletion partially, rescued cell death mediated by USP30 depletion (Figure 6.18A and B). In Figure 6.18B, I also observed the appearance of a lower molecular weight species in both BAX and BAK that are indicative of cleaved BAK and BAX by activated caspases and calpains during apoptosis induction (Meng et al. 2003, Cao et al. 2003, Choi et al. 2001, Yanase et al. 2000, Itoh et al. 2000, Wood and Newcomb 2000, Wood et al. 1998). These observations suggest that USP30-depletion induced cell death via two different mechanisms in response to CCCP and ABT-737.

6.4.4 USP30 depletion also enhances ABT-737 induced cell death in MCF7 and U2-OS cells

Since the USP30-depletion mediated, ABT-737-induced cell death is independent of mitophagy, I decided to test the effect of USP30 depletion on other cell lines. Both U2-OS and MCF7 cells responded rapidly to ABT-737 treatment and I observed some cell death within 1-2hr of ABT-737 treatment as evident by annexin V and DRAQ7 staining during live-cell imaging (Figure 6.19A). The cell death was compounded by USP30 depletion with both USP30 D1 and D3 siRNA oligos. In agreement with this, I observed enhanced PARP-p85 accumulation upon USP30 depletion in both cell lines. I also observed an increase in BAK expression levels upon USP30 depletion as well as lower levels of MCL1 in USP30 D3 transfected cells but not in USP30 D1 transfected cells, in both cell lines.

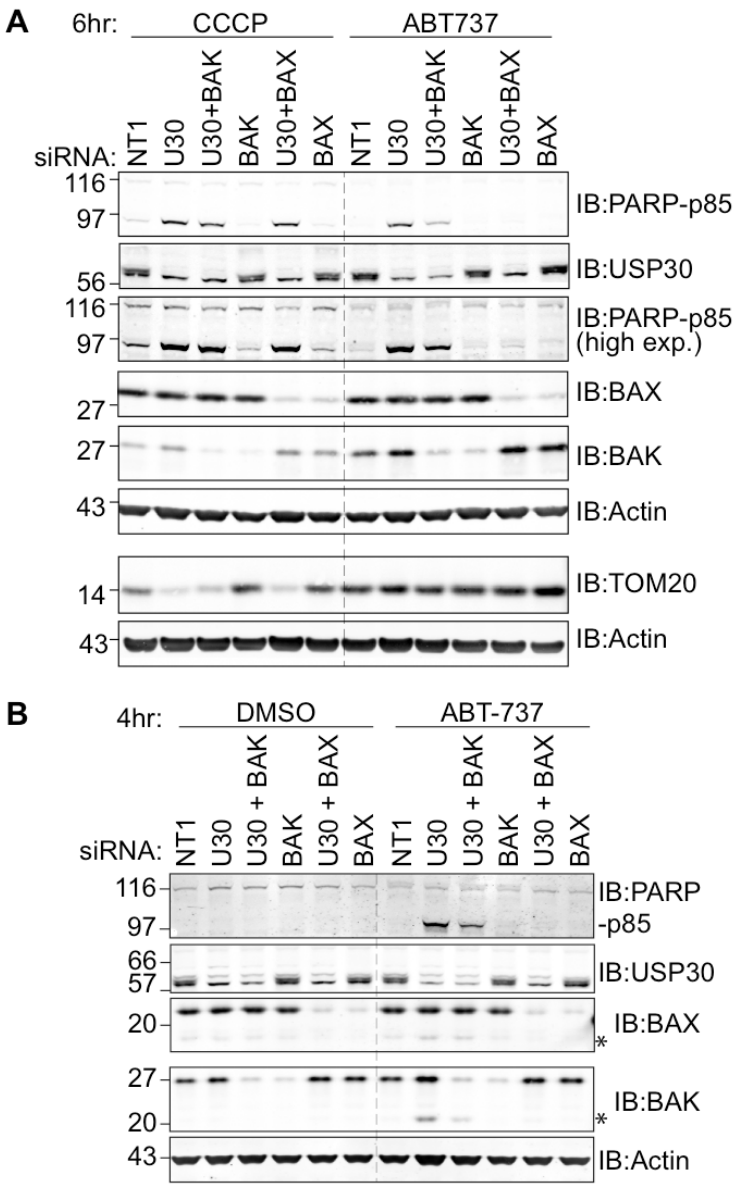

Figure 6.18 BAK and BAX are required for ABT-737-induced cell death but not mitophagy-induced cell death.

hTERT-RPE1-YFP-Parkin cells were transfected for 72hr with non-targeting siRNA oligo (NT1), USP30 (D3), BAK and BAX. Cells were then treated with ABT-737 or CCCP (all 10μM) for 6hr (A) and 4hr (B). Cells were harvested in NP40 lysis buffer. 15μg of lysates were probed as indicated. Asterisk: possible cleaved forms of BAX and BAK.

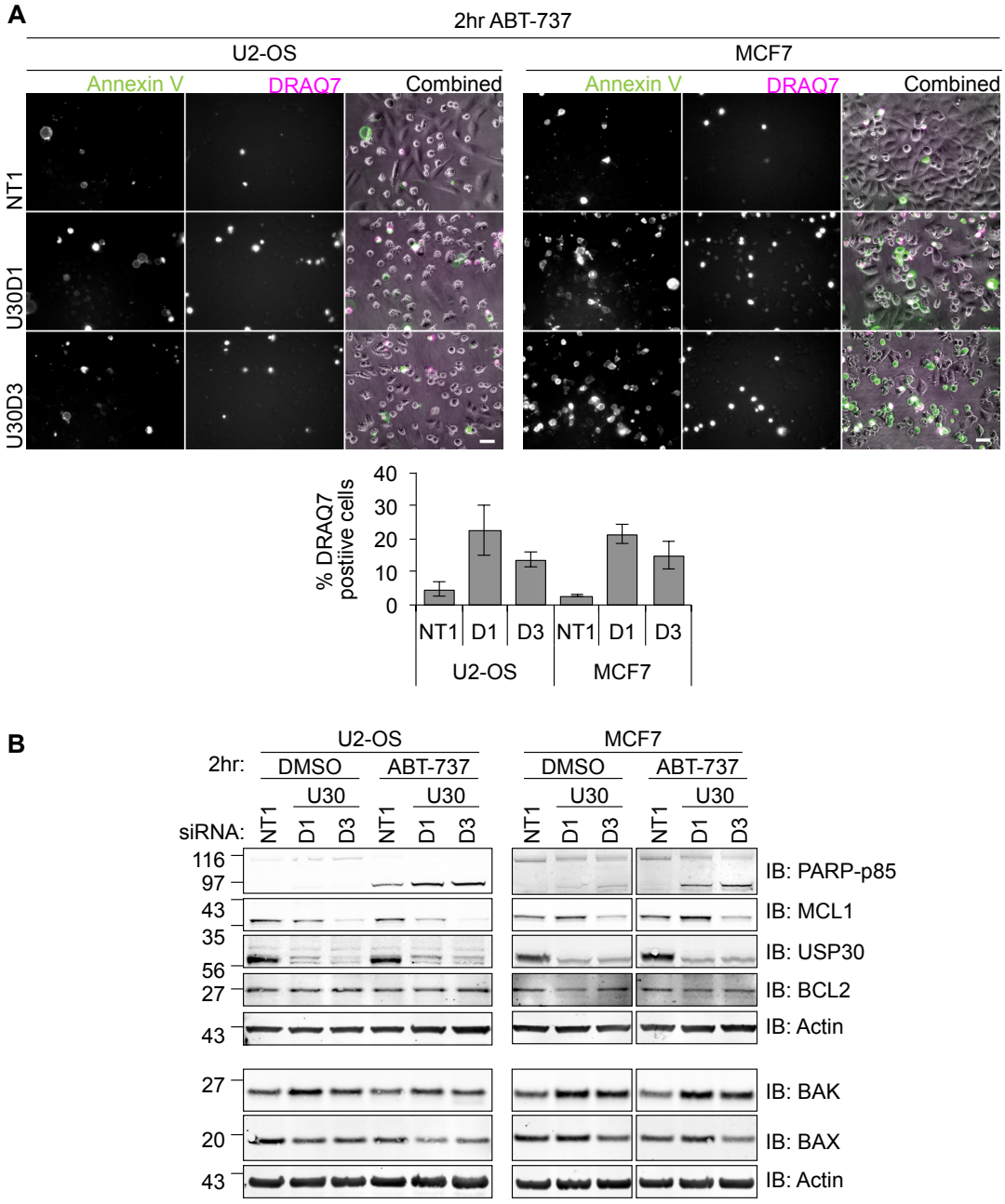

Figure 6.19 USP30 depletion enhances apoptosis tirggered by BH3-mimetics in U2-OS and MCF7 cells.

(A) U2-OS and MCF7 cells were transfected for 72hr with either non-targeting siRNA oligo (NT1) or siRNA targeting USP30 (D1 and D3). Cells were treated with ABT-737 (10μM) for 2hr. Progression of apoptosis was recorded using live-cell video microscopy imaged at 15min interval. Cells were visualised by phase contrast (pseudocoloured in grey), apoptotic cells were visualised with annexin V-AF350 (pseudocoloured in green), and dead cells were visualised with DRAQ7 (pseudocoloured in pink). Representative still frames after 2hr of ABT-737 treatment from the live-cell imaging are shown. Scale bar: 40μm. Bar chart shows the average percentage of DRAQ7 positive cells at T=2hr of ABT-737 treatment from 4 different positions of the same well. Error bars represent standard deviation.

(B) U2-OS and MCF7 cells were transfected and treated as in (A). Cells were harvested in NP40 lysis buffer after 2hr of ABT-737 treatment. 10μg of lysates were immunoblotted as indicated.

6.5 Discussion

6.5.1 USP30 depletion enhances cell death during Parkin-mediated mitophagy

USP30 is the only DUB with a signal-anchor sequence and a transmembrane domain that is targeted to the mitochondrial outer membrane. It was previously reported that depletion of USP30 induces mitochondrial elongation in HeLa and COS7 cells (Nakamura and Hirose 2008). While the exact mechanism and substrate of USP30 have not been identified, it was proposed that it might regulate the stability of proteins involved in the mitochondrial fusion and fission machineries. Nonetheless, previous characterization work carried out in our laboratory by another colleague, Richard Buus reported only a mild collapse of the mitochondrial network around the perinuclear region but no elongated mitochondria in USP30 depleted cells (Buus 2008).

In Chapter 4, I characterised a novel observation of PINK1 and Parkin-mediated mitophagic cell death. In an effort to identify DUBs that oppose Parkin, USP30 turned up as one of the top hits in my Parkin-mediated mitophagy screen. Upon USP30 depletion, I observed that more cells die during CCCP treatment. Since mitochondria play a pivotal role in the activation of apoptosis, this observation is particularly interesting and suggests that USP30 might play an anti-apoptotic role during mitophagy.

Considering that USP30 is a DUB, it is likely that USP30 regulates the stability of a mitochondrial protein that normally serves an anti-apoptotic role. I first focused on investigating the effect of USP30 depletion on MIRO, a mitochondrial Rho-like GTPase that was previously reported by Giot et al. (2003) to be one of the interactors of *Drosophila* USP30 (CG3016) in a large-scale yeast two hybrid screen (Giot et al. 2003). MIRO has a C-terminal transmembrane domain, which confers localization to the outer mitochondria membrane (Fransson et al. 2006). Under normal conditions, Milton, an

adaptor protein, links MIRO to the heavy chain of kinesin (KHC) to facilitate anterograde mitochondrial transport along the microtubule. MIRO contains two EF-hand Ca^{2+}-binding domains. In the presence of high intracellular Ca^{2+} concentration, Ca^{2+} binds to the EF-hands and causes conformational change of MIRO. MIRO then pulls and disengages Milton from KHC, thereby arresting mitochondria movement (Cai and Sheng 2009). The ability of MIRO to respond to Ca^{2+} flux has been reported to be crucial in the delivery and re-localization of mitochondria to regions of high energy demand within neurons, for example, at the synapse region where high calcium arrests and accumulates mitochondria to provide ATP energy for the exocytosis of synaptic vesicles (MacAskill and Kittler 2010). Intriguingly, loss of *Drosophila* MIRO (dMIRO) affects both anterograde and retrograde mitochondrial transport (Russo et al. 2009). Exactly how MIRO regulates the bi-directional movement of mitochondria is unclear but it is likely that this could be due to the interdependency of kinesin and dynein along the microtubule. Alternatively, MIRO might have a more direct interaction with dynein, thereby facilitating retrograde mitochondrial transport as well. Consistent with this, Morlino et al. recently demonstrated MIRO1 plays a role in lymphocyte migration and polarity. In response to the presence of integrin, MIRO1 directly interacts with dynein and redistributes mitochondria to the microtubule-organizing center (MTOC) at the adhesion zone to promote lymphocyte migration (Morlino et al. 2014).

During mitophagy, MIRO is one of the OMM proteins that is phosphorylated by PINK1 for Parkin ubiquitylation and subsequently degraded by the proteasome (Wang et al. 2011). There are two MIROs in human, MIRO1 and MIRO2. Selective depletion of MIRO1 and MIRO2 revealed that MIRO2 is the dominant form in hTERT-RPE1-YFP-Parkin cells. Fransson et al. (2006) previously showed that while overexpression of constitutively active forms of both MIRO1 and MIRO2 caused aggregation of mitochondria, only constitutively active form of MIRO1 induced elongation of mitochondria, suggesting overlapping but not redundant functions of the two MIROs (Fransson et al. 2006).

Under basal condition, I found that USP30 depletion marginally but consistently reduces MIRO protein levels with two individual siRNA oligos but did not affect its mRNA levels, suggesting that USP30 post-translationally regulates MIRO. During CCCP treatment, MIRO was ubiquitylated earlier (1hr after CCCP treatment compared to 4hrs in the control cells) and degraded faster in USP30-depleted cells, suggesting that USP30 deubiquitylates and rescues MIRO from proteasomal degradation. However, inhibition of the proteasome using epoxomicin (8hr) did not rescue MIRO levels in USP30 depleted cells. I speculate that MIRO might have a long half-life and/ or a low expression rate. Therefore, the marginal decrease in MIRO levels observed with USP30 depletion might be a cumulative effect observed over the 72hr of transfection. Consistent with this speculation, MIRO2 siRNA transfection for 72hr did not deplete MIRO2 completely.

Immunoprecipitation of USP30-GFP showed interaction with endogenous MIRO in HEK293T cells under basal condition. This interaction seemed to be dependent on the catalytic activity of USP30 as the use of catalytically inactive USP30 weakened the interaction with MIRO. It is possible that the interaction between USP30 and MIRO may be enhanced with CCCP treatment, as Parkin-ubiquitylated MIRO is more likely to be recognised by USP30.

Direct depletion of MIRO2 by siRNA interference did not exacerbate CCCP-induced cell death. Instead, three, out of four MIRO2 siRNA oligos tested, reduced PARP cleavage. Furthermore, simultaneous depletion of MIRO2 and USP30 did not induce additional cell death. Considering that MIRO2 siRNA transfection reduces MIRO2 level more than that by USP30 depletion, it is unlikely that the depletion of MIRO2 is responsible for the enhanced cell death observed. Instead, I speculate that the decrease of MIRO levels in MIRO2 siRNA-treated cells translates into an overall decrease in the OMM proteins that can be ubiquitylated by Parkin, thereby protecting the integrity of the outer mitochondrial membrane.

I found that during CCCP treatment, USP30 depletion induced higher accumulation of ubiquitylated TOM20 and TOM22, which were degraded faster than in control cells. TOM20 and TOM22 are subunits of the TOM complex, which provides a platform for PINK1 and Parkin recruitment to the mitochondria during mitochondrial depolarization (Jin et al. 2010). TOM20 and TOM22 are likely substrates for USP30 as they have also been previously shown to be ubiquitylated by Parkin (Yoshii et al. 2011, Chan et al. 2011, S. A. Sarraf et al. 2013). USP30 depletion resulted in the accumulation of possible diubiquitylated or doubly-monoubiquitylated species whereas NT1 transfected cells preferentially accumulated monoubiquitylated TOM20. It is possible that the differential ubiquitylation status of TOM20 determines the stability of the protein. IMM proteins such as TIMM44 and OPA1 were not differentially turned over upon USP30 degradation, suggesting that USP30 specifically regulates the stability of TOM20 and TOM22 but does not regulate the degradation of IMM proteins by mitophagy. Strikingly, simultaneous treatment of CCCP and epoxomicin (proteasome inhibitor) accumulated the ubiquitylated form of TOM20 (Ub-TOM20) in USP30 depleted cells but not in control cells. In the control cells, it appears that the TOM20 is deubiquitylated by USP30 and accumulates as an unmodified form of TOM20, whereas in USP30-depleted cells, Ub-TOM20 cannot be deubiquitylated and accumulates in the ubiquitylated form. This strongly suggests that TOM20 is a *bona fide* substrate of USP30. Consistent with my finding, Bingol et al. (2014) demonstrated by immunoprecipitation of HA-tagged ubiquitin that ubiquitylated MIRO and TOM20 can be deubiquitylated by USP30 (Bingol et al. 2014).

It is not possible to knockdown TOM20 to assess its link with cell death as TOM20 depletion would disrupt the TOM complex and affect the import and insertion of proteins into the mitochondria, thereby severely affecting their normal physiology. I showed that the effect of USP30 depletion on TOM20 and PARP cleavage could be partially rescued by transfecting the USP30-depleted cells with mouse USP30. The partial rescue effect might be due to the fact that only approximately 40% of the cells were transfected.

While I only observed the degradation of MIRO2, TOM20 and TOM22 to be differentially regulated with USP30 depletion, it is possible that the Parkin-mediated ubiquitylation and degradation of other OMM proteins is also affected. Using affinity enrichment of ubiquitinated peptides with ubiquitin branch-specific (K-GG) antibodies followed by mass spectrometry, Bingol et al. recently identified a list of other mitochondrial proteins, including VDAC1/2/3, MUL1, FKBP8, TOM70, PRDX3, MAT2B, PTH2 and IDE that show increased ubiquitylation upon USP30 depletion in HEK293 cells.

While my observation that USP30 opposes Parkin-mediated mitophagy is consistent with Bingol et al. (2014), they reported that USP30 depletion rescues the defect in mitophagy by pathogenic mutants of Parkin (G430D and K161D) in SH-SY5Y. They further demonstrated in PINK1 and Parkin mutant (loss-of-function) flies that depletion of USP30 helped to restore normal mitochondrial morphology. Importantly, depletion of USP30 also conferred protection against paraquat-induced dopamine depletion and promotes fly survival.

The key reason between the opposing cell survival roles of USP30 reported by Bingol et al. (2014) and our group is most likely due to the different type and the levels of Parkin expressed and the levels of Parkin expression. In Bingol's case. the use of a Parkin mutant with partial defect in ubiquitylating ability provides a preceding scenario where defective mitochondria are unable to be efficiently turned over by mitophagy. In that case, further deubiquitylation of mitochondrial proteins by USP30 promotes the accumulation of damaged mitochondria in the cells. Therefore, it is unsurprising that the depletion of USP30 plays a cytoprotective role in that setting.

In our study, we used fully functional Parkin that is highly efficient at ubiquitylating OMM proteins. As discussed in chapter 4, acute ubiquitylation of OMM proteins by Parkin induces their extraction and degradation by the proteasome (Yoshii et al. 2011). The extraction of OMM proteins during that process can damage the outer mitochondrial membrane, which can lead to

the activation of apoptosis. We speculate that during Parkin-mediated mitophagy, USP30 opposes Parkin-mediated ubiquitylation of OMM proteins, serving as a 'brake' to keep proteasomal and lysosomal degradations in balance. Upon USP30 depletion, the balance is tipped, leading to increased rates of hazardous proteasomal degradation at the expense of 'safe' lysosomal degradation, allowing release of cytochrome c from damaged mitochondria (refer to Figure 6.20).

Therefore, we suggest a direct protective effect of USP30 on the maintenance of outer mitochondrial membrane integrity whereas Bingol and colleagues described USP30 function on the overall quality control of the mitochondria population and the subsequent effect on the well being of cells and organism as a whole.

Consistent with our observation, in a systemic knockdown of DUBs in *Drosophila*, Tsou and colleagues reported that CG3016 (*drosophila* USP30; dUSP30) knockdown throughout the fly resulted in early death whereas pan-neuronal knockdown of dUSP30 resulted in slower growth of adult flies (Tsou et al. 2012). On the other hand, Bingol and colleagues reported that dUSP30 depletion in Parkin-mutant flies protects against mitochondrial oxidative stress and restores mitochondria morphology as well as improves climbing index (Bingol et al. 2014). While the knockdown of dUSP30 in flies expressing mutant Parkin might rescue the mitochondria morphology as reported by Bingol and colleagues, the knockdown of dUSP30 in normal flies may be detrimental to neuronal development and/or regulation.

6.5.2 USP30 depletion enhances cell death induced by BH3-mimetics

Given the pivotal role of mitochondria in the activation of apoptosis, we asked whether USP30 plays a general moderating role in other forms of cell death. I discovered that hTERT-RPE1-YFP-Parkin cells were resistant to apoptosis induced by a series of commonly used apoptosis-inducing compounds, including DNA topoisomerase inhibitor (etoposide), microtubule depolymerisation inhibitor (taxol), sarco/endoplasmic reticulum Ca^{2+}-ATPase inhibitor (thapsigargin), N-gylcosylation inhibitor (tunicamycin) and activation

of the TNF receptor-mediated extrinsic apoptotic pathway via TNF-α. Eventually, I found that hTERT-RPE1-YFP-Parkin cells responded to ABT-737 and its orally bioavailable analog, ABT263 (Navitoclax)-induced apoptosis (Vogler et al. 2009b). In addition, USP30 depletion compounded the apoptotic response. This effect is not dependent on mitophagy and was observed not only in hTERT-RPE1-YFP-Parkin cells but also in U2-OS and MCF7 cells.

It is worth noting that PARP cleavage occurs around 8-12hr of ABT-737 treatment in hTERT-RPE1-YFP-Parkin cells whereas the similar observation takes 1-2hr in U2-OS and MCF7 cells. Whilst the levels of BCL2 family members have not been compared across the different cell types, the relative abundance and dependency towards different BCL2 pro-survival members have been reported to affect the apoptotic response towards ABT-737 and ABT-263 in different cell types. This is because ABT-737 and ABT-263 have higher affinity to BCL2 and BCL-xL than other BCL2 prosurvival family members, especially MCL1. For instance, depletion of another DUB, USP9X, has previously been shown to promote polyubiquitylation and degradation of MCL1 and enhance ABT-737-mediated cell death in human follicular lymphomas and diffuse large B-cell lymphomas (Schwickart et al. 2010). Several different groups have also shown that down-regulation of MCL1 sensitizes different cancer cell types including leukemia, melanoma and neuroblastoma cells to ABT-737-mediated apoptosis (Keuling et al. 2009, Lestini et al. 2009, Chen et al. 2007). Furthermore, in acute myeloid leukemia cells that have elevated expression of MCL1, simultaneous treatment with ABT-737 and Maritoclax, a small molecule inhibitor MCL1, has a synergistic effect in inducing cell death (Doi et al. 2014).

Intriguingly, USP30 D3 transfection consistently decreased MCL1 protein level in all three cell-lines tested. While it is currently uncertain whether this effect is truly due to USP30 depletion, it is likely that the depletion of MCL1 confers additional toxicity to the cells in response to BH3-mimetics. A USP30 rescue experiment will need to be performed to investigate if USP30 truly regulates MCL1 levels.

Further investigation into the level of the pro-survival and pro-apoptotic BCL2 family members suggest that there is a trend of elevated BAK but not BAX in all three cell lines upon USP30 depletion while there is a mild elevation of BCL2 in hTERT-RPE1-YFP-Parkin cells. Since BCL2 is inhibited during ABT-737 and ABT-263 treatment, the elevated levels of BCL2 are less likely to be a contributing factor to the cell death observed. Normally, the pro-survival and pro-apoptotic BCL2 family members exist in equilibrium to counteract the effect of each other. Elevation of BAK levels could explain the sensitisation of USP30 depletion cells towards ABT-737 treatment. The elevated BAK levels can either be transcriptionally or post-translationally regulated by USP30. One of the hypotheses is that USP30 might regulate an E3 ubiquitin ligase that ubiquitylates BAK for degradation. Considering the localization of both USP30 and BAK, it is most likely that USP30 regulates the stability or activity of a mitochondrial E3 ubiquitin ligase, for example, MARCH5/MITOL, MAPL/GIDE/MULAN, IBRDC2 or RNF185 (Benard et al. 2010, Karbowski et al. 2007, Tang et al. 2011, Zemirli et al. 2014). Among these, IBRDC2 is particularly interesting as it has been demonstrated to ubiquitylate BAX for degradation and suppress spontaneous apoptosis (Benard et al. 2010). It is possible that BAK could be regulated in a similar manner by IBRDC2 or an alternative E3 ligase.

6.5.3 USP30 depletion sensitises cells to mitophagic cell death and BH3-mimetics-induced cell death via different mechanisms

During CCCP treatment, both BAK and BAX have been reported to be ubiquitylated by Parkin (Chan et al. 2011, Shireen A. Sarraf et al. 2013). Consistent with this, I observed ubiquitylation of BAK in hTERT-RPE1-YFP-Parkin cells during CCCP treatment.

However, BAX was not apparently ubiquitylated. USP30-depletion mediated BAK upregulation is unlikely to be the cause of enhanced mitophagic cell death as ubiquitylated BAK will be degraded together with other OMM proteins such as MIRO and TOM20. Indeed, depletion of BAK and BAX did

not visibly affect CCCP induced cell death enhanced by USP30 depletion. As discussed before, it is more likely that the loss of USP30 promoted aberrant ubiquitylation and extraction of OMM proteins by Parkin, which affect the integrity of the outer mitochondrial membrane and cause cell death (Figure 6.20).

On the other hand, elevated levels of BAK may explain the sensitized cell death of USP30-depleted cells towards ABT-737 treatment, as more BAK is able to either homo-oligomerise or hetero-oligomerise with BAX readily in response to the inhibition of BCL2 and BCL-xL (Chandra et al. 2005, Upreti et al. 2008). Consistent with this, BAK knockdown partially and BAX knockdown fully inhibited the enhanced PARP cleavage caused by USP30 depletion during ABT-737 treatment. It is possible that BAK and BAX could compensate each other to induce apoptosis during ABT-737 treatment and this hypothesis could be tested in the future with a double knockdown of BAK and BAX (Figure 6.20).

It is also worth mentioning that ABT-737 treatment induced accumulation of lower molecular weight species for both BAK and BAX that are indicative of cleaved products and that correlate with PARP cleavage. This is consistent with previous report of BAK and BAX cleavage by both caspases and calpains during apoptosis (Wood et al. 1998, Meng et al. 2003). Whilst the effect of cleaved BAK is relatively understudied, cleaved BAX has been demonstrated to be more potent than full length BAX in inducing apoptosis (Toyota et al. 2003, Cao et al. 2003).

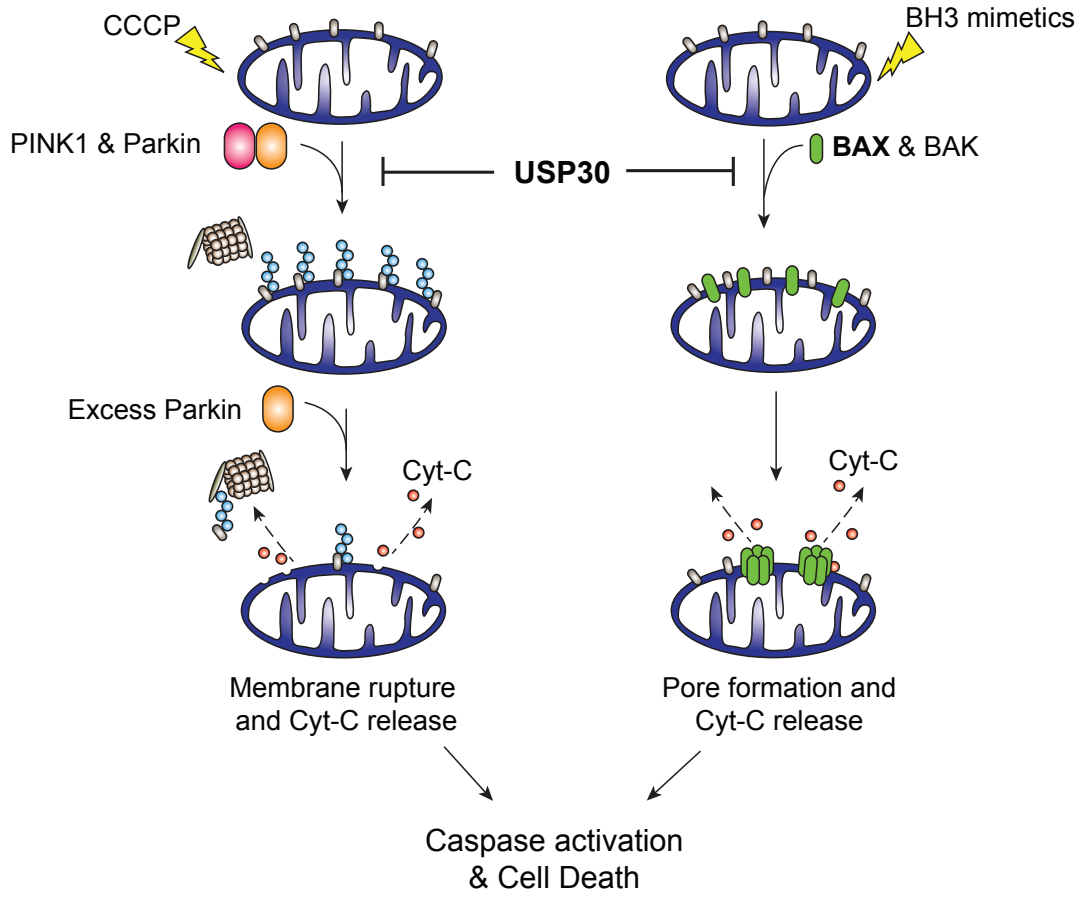

Figure 6.20 Illustration of CCCP-induced mitophagic cell death and ABT-737-induced cell death under normal and USP30-depleted conditions.

During CCCP treatment, high Parkin expression resulted in acute ubiquitylation and extraction of OMM proteins for proteasomal degradation. This can affect the OMM integrity and cause Cytochrome-C to be released into the cytosol, causing caspase activation and apoptosis. USP30 acts as a 'brake' to oppose the ubiquitylation of OMM proteins, thereby promoting cell survival.
During BH3-mimetic treatment, BCL2 pro-survival proteins are inactivated, leading to the activation and oligomerisation of BAK and BAX on the outer mitochondrial membrane and promote cytochrome C release. We showed that USP30 depletion induces higher protein levels of BAK, which might exacerbate BH3-mimetic induced cell death.

Chapter 7: Identification of USP30 Substrates by Mass Spectrometry

7.1 Introduction

One important role of deubiquitylation is to rescue ubiquitylated proteins from proteasomal degradation. Therefore, the loss of a DUB with such a function will promote the ubiquitylation and degradation of its substrate(s). Quantitative proteomics with the use of mass spectrometry (MS) provides an unbiased approach to analyse various changes in the property of a protein (e.g. protein abundance, ubiquitylation and phosphorylation) in response to a specific stimulus, be it drug/inhibitor treatment, growth factor administration or mutation/depletion of a protein of interest. Such a discovery-based study allows the identification of proteins that are involved in a common pathway and could open up new biology.

Quantitative MS analysis can be achieved using Stable Isotope Labelling by Amino acids in Cell culture (SILAC). Stable 'heavy' and 'light' isotopes (introduced in the form of lysine and arginine) are metabolically incorporated into separate sets of cells for different treatment conditions. The two isotopically labeled samples can then be combined at equal amounts for MS analysis. 'Heavy' and 'light' peptides can be distinguished based on the relative shift in mass of the 'heavy' peptide compared to the 'light' peptide. A heavy-to-light ratio can then be quantified for each peptide based on the relative MS signal intensities (Ong et al. 2002, Ong and Mann 2006). This ratio informs on the relative abundance of the parent protein in each sample.

Alongside the work described in chapter 6 to characterise the effect of USP30 depletion on mitophagic and BH3-mimetics-induced cell death, a separate strand of my project focused on investigating the effects of USP30

depletion at steady state. While depletion of USP30 has been reported to induce elongated and interconnected mitochondrial networks in HeLa and COS7 cells, the underlying mechanism and the substrate of USP30 that regulates this process were not identified (Nakamura and Hirose 2008).

Therefore, I decided to use the SILAC-MS approach to identify proteins with altered abundance upon siRNA-mediated USP30 depletion.

In this chapter, the following work will be presented:

(1) Quality control and optimization of SILAC labeling for HeLa S3 cells, mitochondria enrichment protocol and siRNA transfection.
(2) Analysis of four biological replicates of SILAC MS experiments to identify proteins with altered abundance upon USP30 depletion.
(3) Deconvolution and functional characterisation of the shortlisted proteins.

7.2 Quality control and optimization of SILAC MS experiment

7.2.1 Workflow of SILAC MS Analysis

HeLa S3 cells were selected for this study as this cell line is routinely used in the laboratory to perform SILAC-based experiments and isotope labeling efficiency is assessed regularly. The SILAC workflow for the identification of USP30 substrates is described in Figure 7.1A. Briefly, HeLa S3 cells were cultured in 'light' (Arg0, Lys0- 'L') or 'heavy' (Arg10, Lys8- 'H') media. 'Light'-cells were transfected using Oligofectamine with non-targeting siRNA control oligo (NT1; 40nM) whereas 'heavy'-cells were transfected with a siRNA pool targeting USP30 (oligo D1, D3 and D4, total 40nM). Light and heavy cells were then harvested and combined at a 1:1 ratio (w/w) for mitochondria enrichment using the mitochondria isolation kit (Details described in the next section and in Chapter 2 Section 2.3.4.1). The lysate was then resolved on a NU-PAGE and protein bands were processed for in-gel digestion followed by liquid chromatography and tandem mass spectrometry analysis (LC-MS/MS). The H/L protein intensity ratio reflects the change in protein abundance upon USP30 depletion.

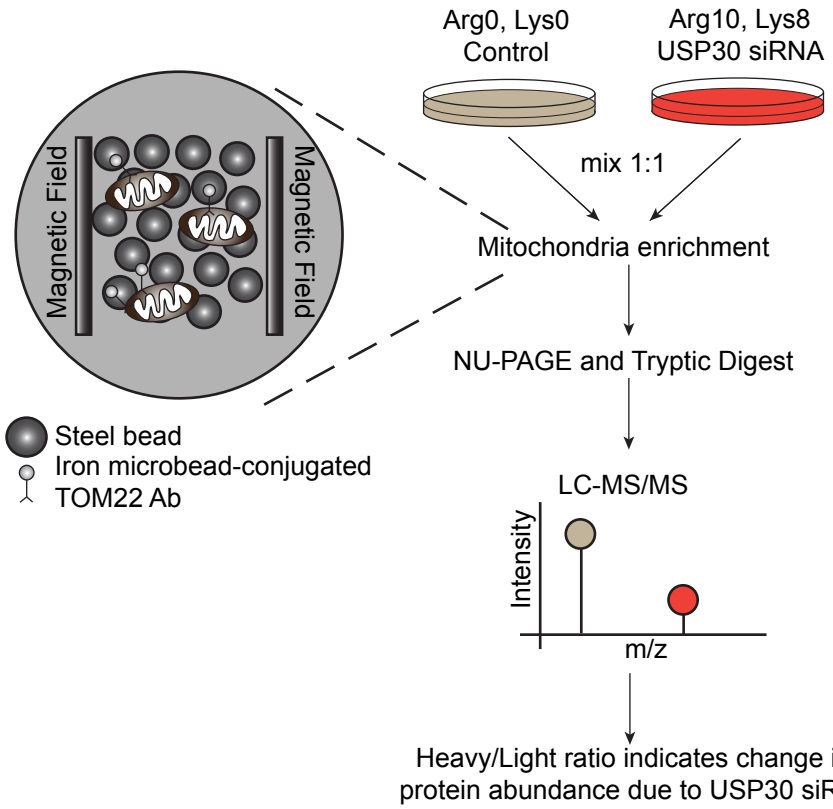

Figure 7.1 Workflow of SILAC experiment and quality control for SILAC labeling of cells and siRNA transfection efficiency.

Illustration of the SILAC workflow with mitochondria enrichment. HeLa S3 cells were cultured in ‘light’ (Arg0, Lys0- ‘L’) or ‘heavy’ (Arg10, Lys8- ‘H’) media. L-cells were transfected for 72hr with non-targeting siRNA control oligo (NT1; 40nM) whereas H-cells were transfected with siRNA pool oligo targeting USP30 (oligo D1, D3 and D4, total 40nM). L and H cells were then harvested and combined at 1:1 (weight: weight) for mitochondria enrichment using the mitochondria isolation kit. The lysate was then resolved on a NU-PAGE and protein bands were processed for in-gel digestion with trypsin and LC-MS/MS analysis. The H/L protein intensity ratio reflects the change in protein abundance upon USP30 depletion.

7.2.2 Quality control of SILAC incorporation and siRNA transfection

HeLa S3 cells were cultured in SILAC media containing either 'light' amino acids (Arg0 and Lys0- 'L') or 'heavy' amino acids (Arg10, Lys8- 'H') for at least 5 passages to ensure maximal labeling efficiency. H and L cells were then harvested and resolved on a NU-PAGE. Three protein bands from each condition were excised for in-gel digestion and liquid chromatography and tandem mass spectrometry analysis (LC-MS/MS). As shown in Figure 7.2A, HeLa S3 cells cultured in heavy medium (right graph) incorporated 98.6% each of Arg10 and Lys8.

Next, I assessed the siRNA transfection efficiency in HeLa S3 cells. Transfection using Oligofectamine with siRNA oligo targeting USP33 (oligo 6, 40nM) efficiently depleted USP33 in these cells as evident from the western blot probed with anti-USP33 antibody (Figure 7.2B). As described in previous chapters, USP33 knockdown is used to assess the knockdown efficiency as this protein has been extensively studied in our laboratory and the antibody we routinely use is specific and sensitive (Thorne et al. 2011). In addition, I also tested the knockdown efficiency of USP30 siRNA oligos (D1, D3 and D4) that were used later for the actual experiment. Since a working USP30 antibody was not available at that time, I assessed the knockdown efficiency by qRT-PCR (Figure 7.2C; Chapter 2, section 2.1.9). siRNA transfection for 24hrs reduced the mRNA level of USP30 by more than 80% compared to the mock control (Figure 7.2C).

A

Incorporation efficiency	Light label	Heavy Label
Arginine	98.0%	98.6%
Lysine	98.6%	98.6%

B

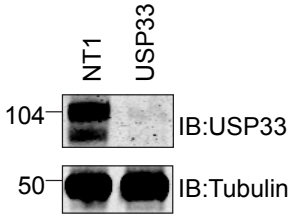

C

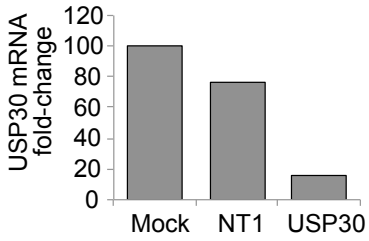

Figure 7.2 Quality control for SILAC labeling and transfection efficiency in HeLa S3 cells.

(A) HeLa S3 cells cultured in 'light' (Arg0, Lys0) or 'heavy' (Arg10, Lys8) media for 5 passages were lysed in NP40 lysis buffer. Cells were resolved on a NU-PAGE and protein identification and isotope incorporation efficiencies were analysed by LC-MS/MS and MaxQuant.
(B) HeLa S3 cells were transfected for 72hr with either non-targeting siRNA control oligo (NT1) or siRNA targeting USP33 (oligo D6). Cells were then harvested in NP40 lysis buffer and probed for USP33 and Tubulin.
(C) HeLA S3 cells were either transfected with mock (transfection reagent without siRNA), non-targeting siRNA control oligo (NT1), or siRNA pool oligo targeting USP30 (D1, D3 and D4). RNA extraction was performed 24hr post-transfection for qRT-PCR analysis. USP30 mRNA levels were normalized to β-actin mRNA levels.

7.2.3 Quality control of mitochondria enrichment protocol

USP30 is a DUB with an N-terminal transmembrane domain which localizes it to the OMM, with the catalytic domain facing the cytosol (Nakamura and Hirose 2008). Therefore, it is likely that USP30 deubiquitylates mitochondrial substrates. To increase the probability of identifying mitochondrial substrates, I decided to enrich mitochondria from the cell lysate prior to LC-MS/MS analysis. Mitochondria enrichment was carried out using the mitochondria isolation kit (MACS Miltenyi Biotech) according to the manufacturer's instruction but with slight modifications as described in Chapter 2, section 2.3.4.1). The mitochondria isolation kit relies on the use of anti-TOM22 antibody conjugated to microbeads (Hornig-Do et al. 2009). The antibody recognises a cytoplasmic region of the OMM protein, TOM22, while the microbeads consist of a colloidal suspension of extremely small (50nm) superparamagnetic particles that can be magnetically isolated upon passing through an iron-bead filled column attached to a MACS magnetic separator (Figure 7.3). These mitochondria-enriched fractions were subjected to gel electrophoresis and gel slices were processed for LC-MS/MS analysis.

I first performed a test experiment to assess the mitochondria-enrichment efficiency of the kit. I annotated the subcellular localisation of the list of proteins identified from the LC-MS/MS analysis using the Database for Annotation, Visualization and Integrated Discovery (DAVID; http://david.abcc.ncifcrf.gov/) and MitoCarta (Figure 7.4A). DAVID is an integrated database that collates available literature to annotate Gene Ontology (GO) based on different classifications, such as metabolic processes, biochemical pathways, subcellular localization and protein domains (Dennis et al. 2003). On the other hand, MitoCarta is an inventory of over 1000 mouse proteins and their human homologs. These genes were originally identified from MS analysis of mouse mitochondria enriched fractions using Percoll density gradient separation from fourteen different tissues. Human homologs of those genes that had previously not been reported as associated with mitochondria were GFP-tagged at the C-

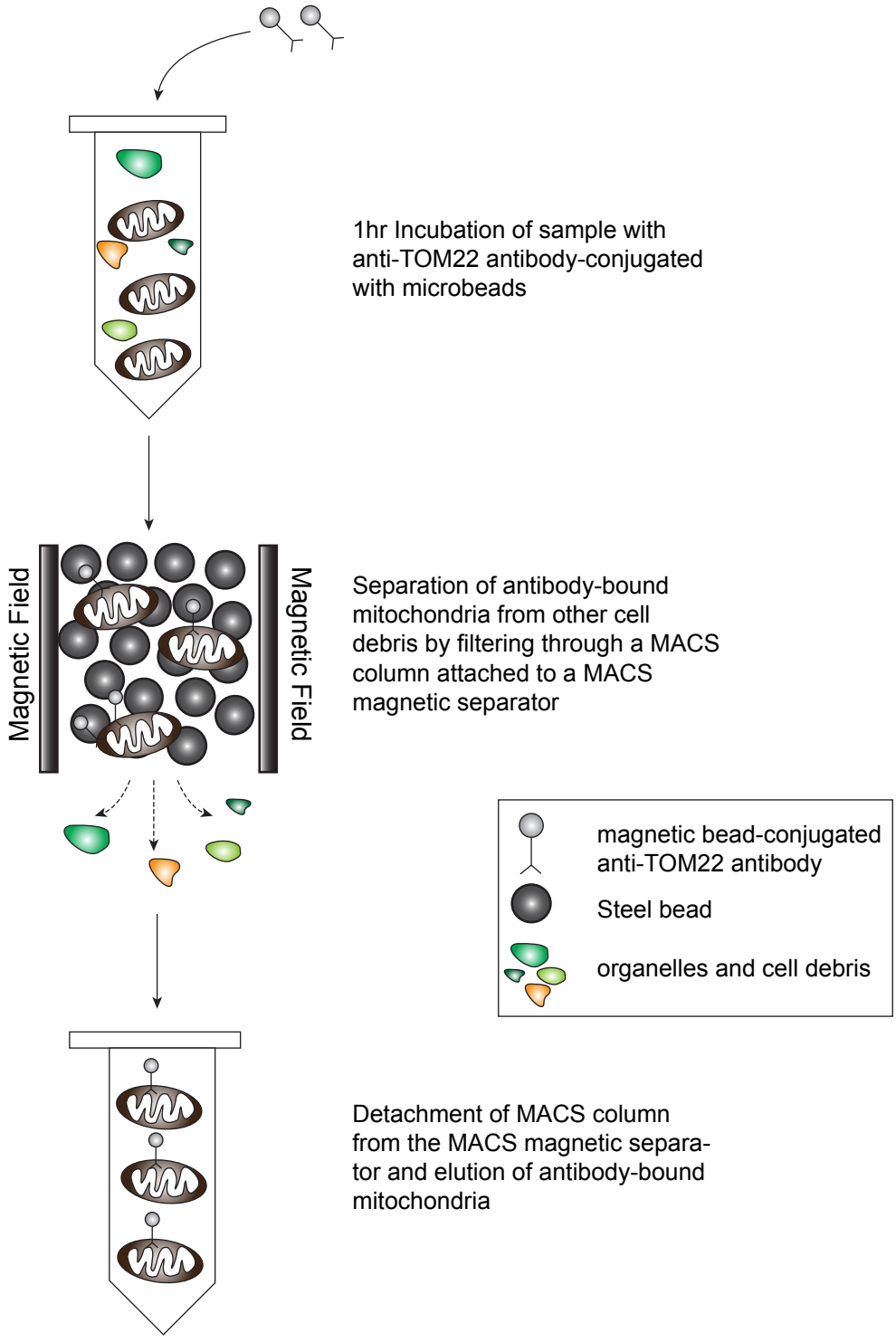

Figure 7.3 Schematic illustration of the mitochondria enrichment protocol.

HeLa S3 cells were homogenised using a 23G syringe and nuclei were removed by centrifugation. The post-nuclear supernatant was further centrifuged to enrich for mitochondria. The mitochondria fraction was then incubated with anti-TOM22 antibody conjugated with microbeads for 1hr. The antibody-bound mitochondria were enriched according to the mitochondria isolation protocol (Hornig-Do et al. 2009).

terminus to visualise their subcellular localization in HeLa cells using fluorescence microscopy (Pagliarini et al. 2008).

Analysis of the list of proteins identified in my MS experiment using these two databases revealed that 37% of the total proteins identified were known mitochondrial proteins, among which, 26% were exclusively mitochondrial proteins whereas 5% were annotated as mitochondrial and nuclear, and 6% as mitochondrial and cytoplasmic proteins. The next largest group of proteins from the mitochondria-enriched sample was endoplasmic reticulum (ER) proteins. This is unsurprising and expected as the mitochondrial network is tightly tethering with the ER network (Rowland and Voeltz 2012).

I next compared the mitochondria-enriched samples from my four actual experiments with the lists of proteins identified from total lysate samples reported by the groups of Angus Lamond and Mattias Mann in their comprehensive proteomic studies (Cambridge et al. 2011, Boisvert et al. 2012). While the total number of proteins that I identified using the mitochondria isolation kit was approximately 6 to 8-fold lower than that by the two studies, I found that mitochondrial proteins made up approximately 15% of the total proteins in both of the studies (Figure 7.4B). In my case, the use of the mitochondria isolation kit increased the percentage of mitochondrial proteins for about two-fold.

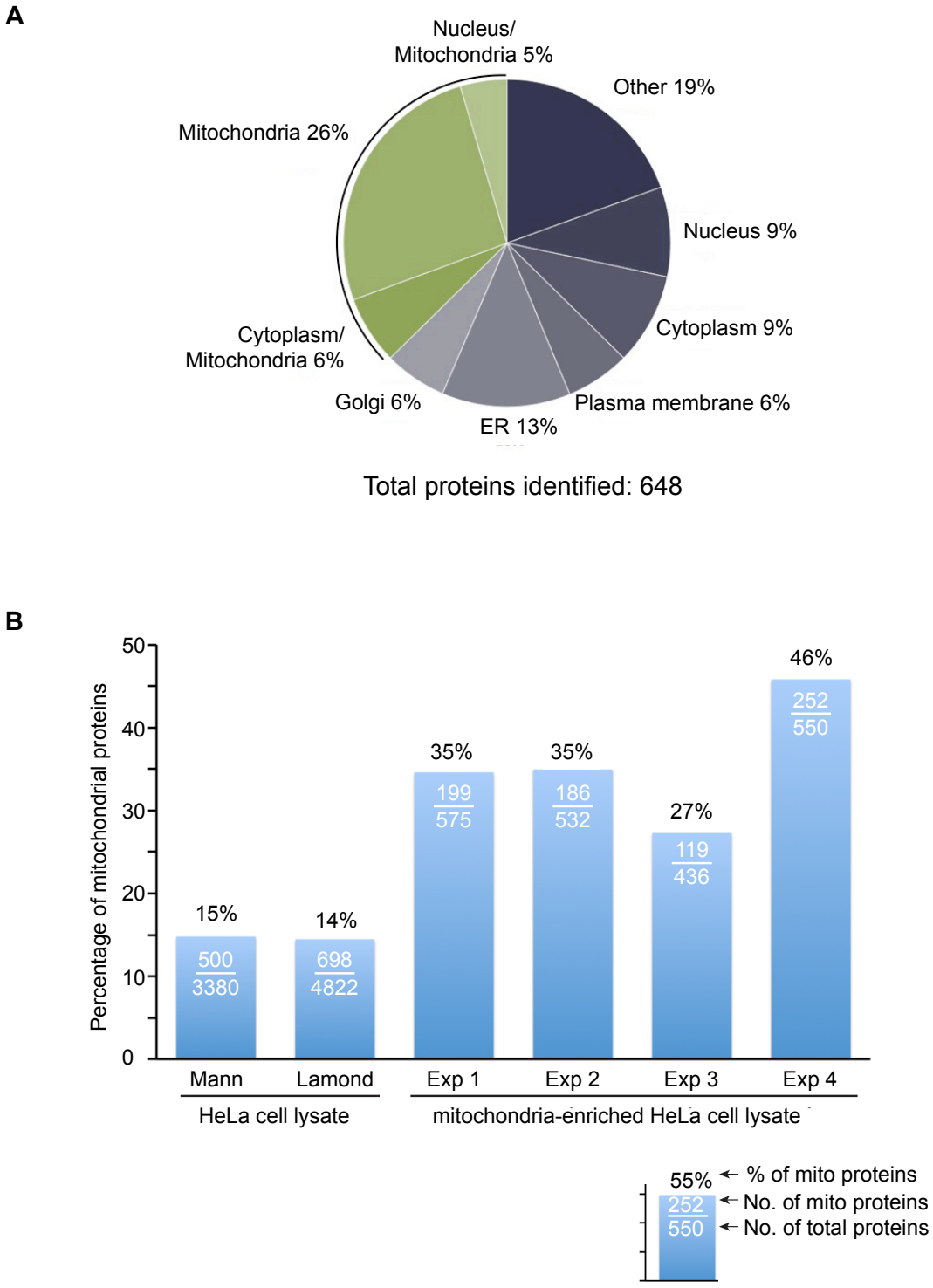

Figure 7.4 Analysis of the mitochondria-enriched samples.

(A) Pie diagram illustrates the different subcellular localisation of proteins identified in the test mitochondria-enrichment experiment.
(B) Bar chart shows the percentage of mitochondrial proteins in total lysates identified by the groups of Mattias Mann and Angus Lamond compared with the relative enrichment of mitochondria proteins in the mitochondria-enriched fractions from the four independent experiments that I performed (Cambridge et al. 2011, Boisvert et al. 2012).

7.3 Analysis of the LC-MS/MS datasets

I carried out four independent SILAC experiments according to the workflow described in Figure 7.1. In experiments 1 to 3, 'light'-cells were transfected with non-targeting siRNA control oligo (NT1) whereas 'heavy'-cells were transfected with siRNA pool targeting USP30. In experiment 4, the transfection conditions were inversed, therefore, 'heavy'-cells were transfected with the non-targeting siRNA control oligo (NT1) whereas 'light'-cells were transfected with siRNA oligo targeting USP30.

Overall, I managed to identify 810 unique proteins across all four experiments, out of which, 309 of the proteins were annotated as mitochondrial proteins based on Mitocarta and DAVID analysis. The distribution and overlap in number of total proteins and mitochondrial proteins is shown in Figure 7.5A. In general, there is a good overlap of proteins identified across the four experiments. 29% of the total proteins were identified in all four experiments, whereas and additional 22% and 26% of the total proteins were only identified in 3 and 2 sets of experiments, respectively (Figure 7.5B and C). Only proteins that were found in at least two experiments were selected for further analysis.

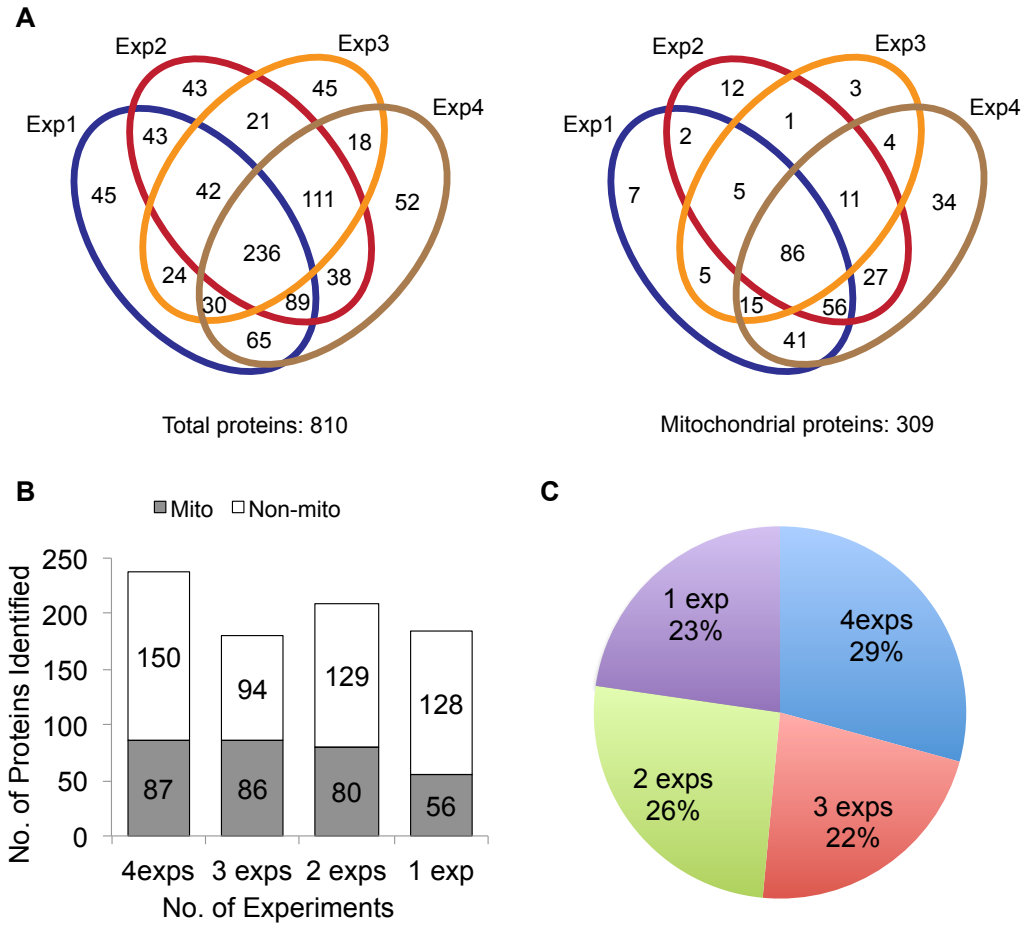

Figure 7.5 Analysis of the proteins identified by LC-MS/MS in each experimental repeats.

(A) Diagrams represent the number of total proteins (left) and mitochondrial proteins (right) identified in each category and overlap between each experiment.
(B) Bar chart shows non-mitochondrial and mitochondrial proteins identified in 4, 3, 2 or 1 of the experiments.
(C) Pie diagram illustrates the overlap of proteins (both mitochondrial and non-mitochondrial proteins) identified in HeLa S3 cells in 4, 3, 2 or 1 of the experiments.

7.3.1 Scatter plot analysis of changes in protein abundance upon USP30 knockdown

For experiments 1 to 3, the data were expressed as Heavy-to-light protein abundance ratio (H/L ratio or USP30/NT1 knockdown ratio). Since I purposely inversed the transfection protocol for experiment 4, such that L-cells were now transfected with USP30 siRNA oligos and H-cells were transfected with control NT1 siRNA oligos, the protein ratios from experiment 4 were expressed as an L/H.

I then log_2-transformed the USP30/NT1 knockdown ratios and expressed them as a scatter plot relative to the log_{10}(Intensity) of the proteins, which is proportional to the abundance of the protein (Figure 7.6). A positive log_2-ratio (right side of the plot) reflects relative enrichment whereas a negative log_2-ratio (left side of the plot) reflects relative loss upon USP30 depletion compared to the NT1 control. Proteins with unchanged abundance between control and USP30-depleted samples have a log-ratio value of zero. To aid with visualization, mitochondrial proteins were labeled in blue and non-mitochondrial proteins in grey. Proteins with significantly altered abundance upon USP30 depletion were determined by their significance A score as analysed using Perseus software (a data analysis and presentation software that is part of MaxQuant). Proteins with significance A score of $p<0.05$ were labeled with solid circle and protein names annotated whereas proteins with a significance A score of $p>0.05$ were labeled with hollow circles (Cox and Mann 2012). I further plotted the protein ratios in pairs to compare the ratios that were altered in the same trend across the four experiments (Figure 7.7).

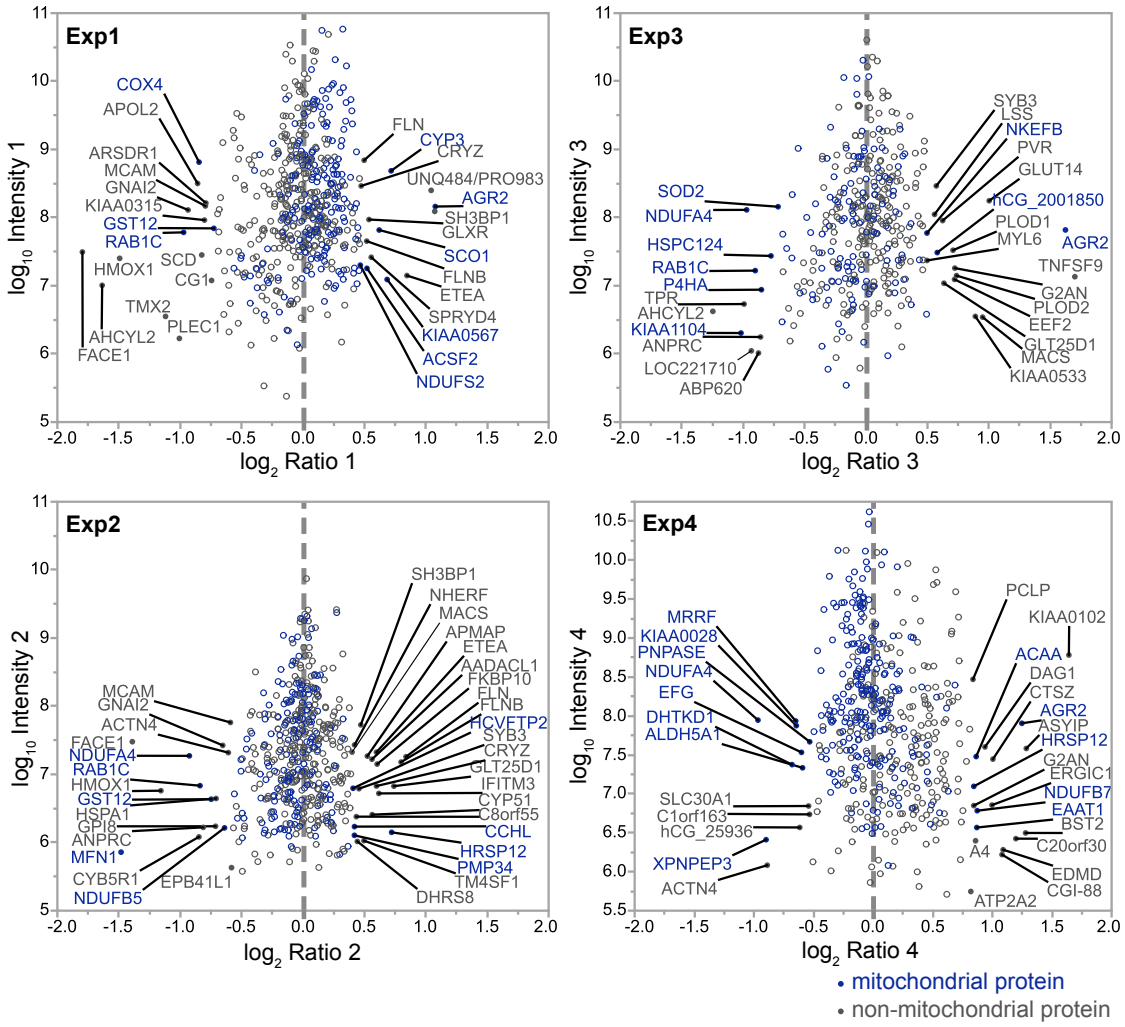

Figure 7.6 Scatter plots showing the logarithmic ratio of protein intensities versus the logarithmic ratio of USP30/NT1 knockdown for all four experiments.

Proteins labeled in blue are mitochondrial proteins where as proteins labeled in grey are non-mitochondrial proteins. Proteins with solid circles have a significance A score of $p<0.05$ whereas proteins with hollow circles have a significance A score of $p>0.05$.

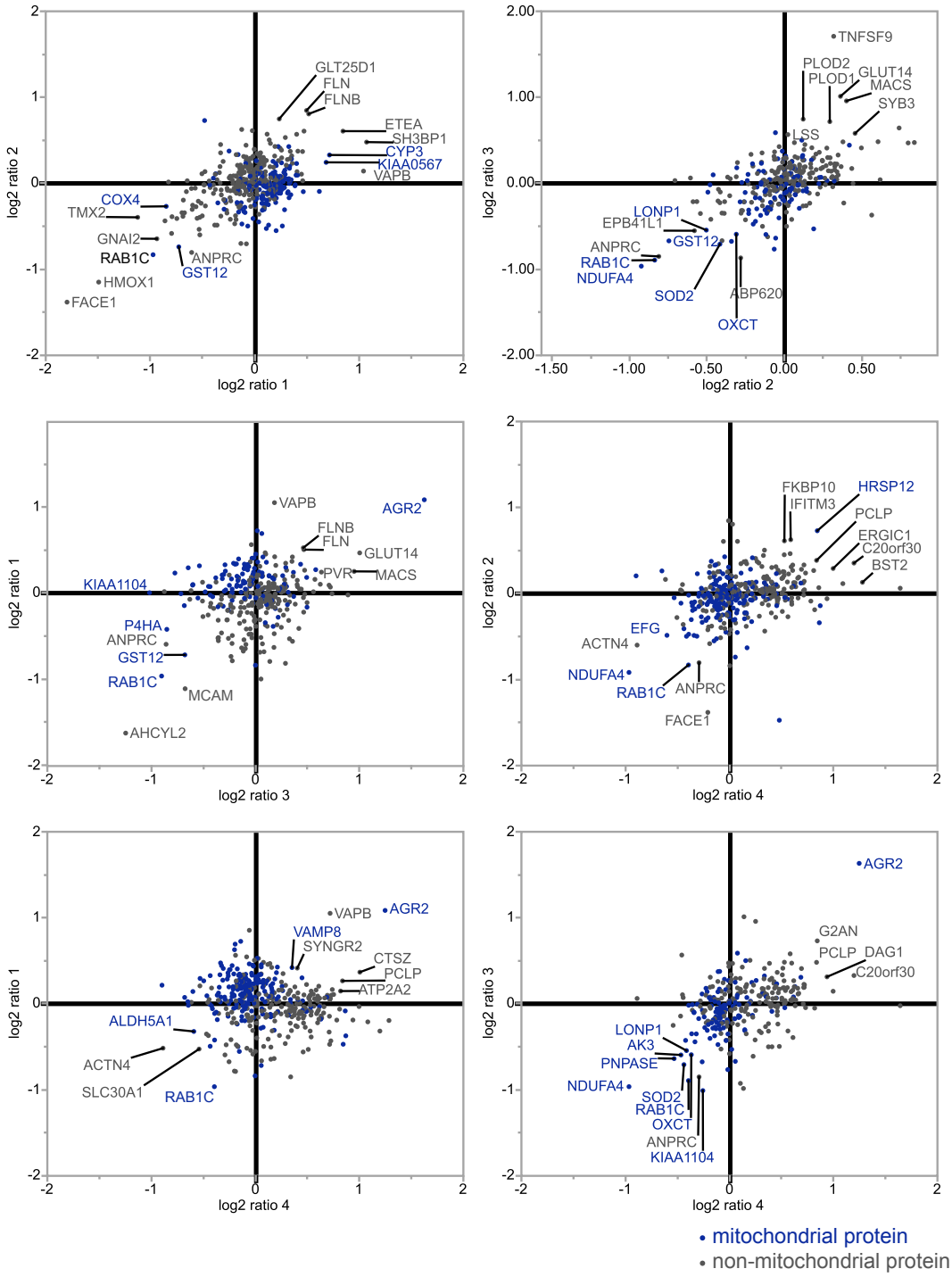

Figure 7.7 Comparison of (USP30/NT1 ratio) across all four experiments.

Proteins labeled in blue are mitochondrial proteins where as proteins labeled in grey are non-mitochondrial proteins

7.3.2 Shortlisting and functional annotation of top hits

I further filtered the list of proteins using Perseus, based on the significance A score of each protein in each experiment. Proteins with significance A scores of less than 0.05 in at least two experiments were shortlisted. The list of top hits was presented as a heat map to help visualize the trend of each protein across all four experiments (Figure 7.8). Proteins labeled with shades of green represent low USP30/NT1 ratios (i.e. are de-enriched upon USP30 depletion) whereas proteins labeled with shades of red represent high USP30/NT1 ratios (i.e. are enriched upon USP30 depletion). In experiments where a particular protein is not identified, a grey box was assigned. A total of 21 proteins were selected, of which, 5 of the proteins were mitochondrial proteins (labeled in bold), including GST12, AGR2, NDUFA4, RAB1C and HRSP12. Note that RAB1C is also known as RAB35 and GST12 is also known as MGST1.

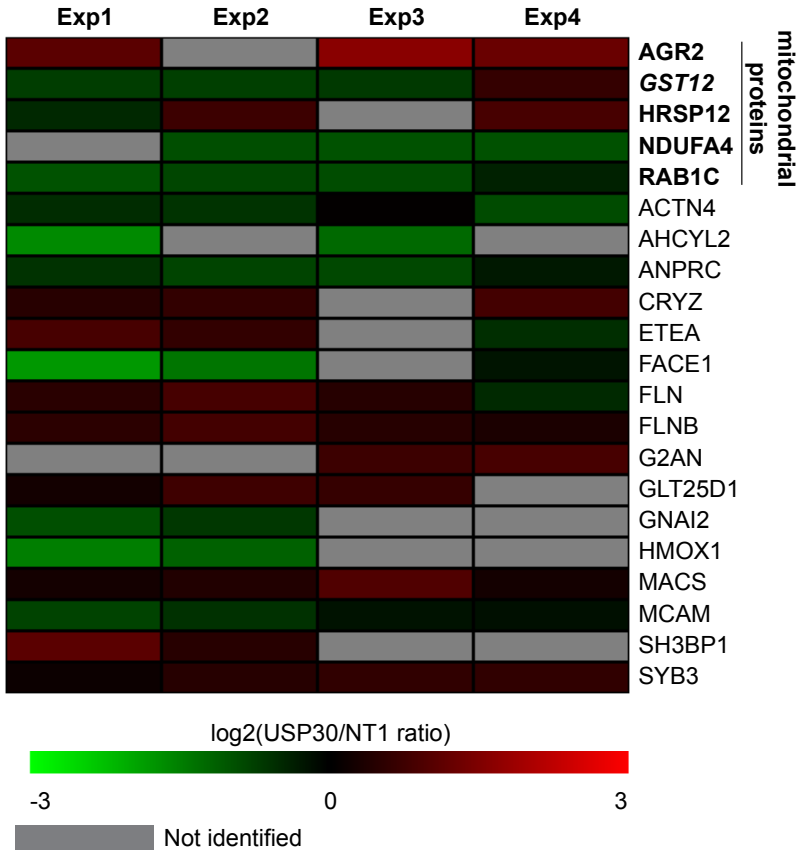

Figure 7.8 Statistical analysis and functional annotation of the shortlisted proteins.

Heatmap illustrates relative change in protein level upon USP30 knockdown. Top hits were selected based on identification in at least two experiments with significance A scores of $p<0.05$. Proteins in bold represents mitochondrial proteins compared with DAVID and Mitocarta databases. Boxes in shades of green represent protein de-enrichment upon USP30 knockdown. Boxes in shades of red represent protein enrichment upon USP30 knockdown. Boxes in grey represents protein not identified in that particular experiment.

7.3.3 Verification and deconvolution of top hits in post-nuclear supernatant and mitochondrial fraction

To confirm the mass spectrometry data, I assessed the protein levels of the shortlisted proteins by western blotting. Based on the availability of antibodies, I checked the protein levels of RAB1C (RAB35), AHCYL2, ACTN4, AGR2 and GST12 (MGST1) (Figure 7.9A). USP30 depletion marginally reduced the levels of RAB35, ACNT4 and MGST1. On the other hand, the levels of AGR2 increased upon USP30 depletion. AHCYL2 levels were not visibly changed upon USP30 depletion. While the changes were mild between USP30 depleted and the control samples, the preliminary work revealed that the results were largely consistent with the trend observed from the mass spectrometry data. Since MS analysis provides a highly sensitive quantitative analysis whereas western blot only provides semi-quantitative analysis, it is not surprising that some of the changes reported by MS might not be as easily observed by western blotting.

In the end, I decided to follow up on RAB35, AGR2 and ACTN4. To eliminate the possibility of off-target effects, I first assessed the levels of these proteins with individual USP30 siRNA transfections (USP30 D1, D3 and D4 siRNA oligos). As shown in Figure 7.10, all three siRNA oligos efficiently reduced the mRNA level of USP30 as assessed by qRT-PCR. However, there was no consistent change in the protein levels of RAB35, AGR2 and ACTN4 that correspond to the degree of USP30 depletion. Instead, I found that the elevated AGR2 levels observed with the pool USP30 siRNA transfection was only recapitulated by USP30 D1 oligo. The changes in protein levels of RAB35 and ACTN4 were variable and inconsistent across the different USP30 siRNA transfections.

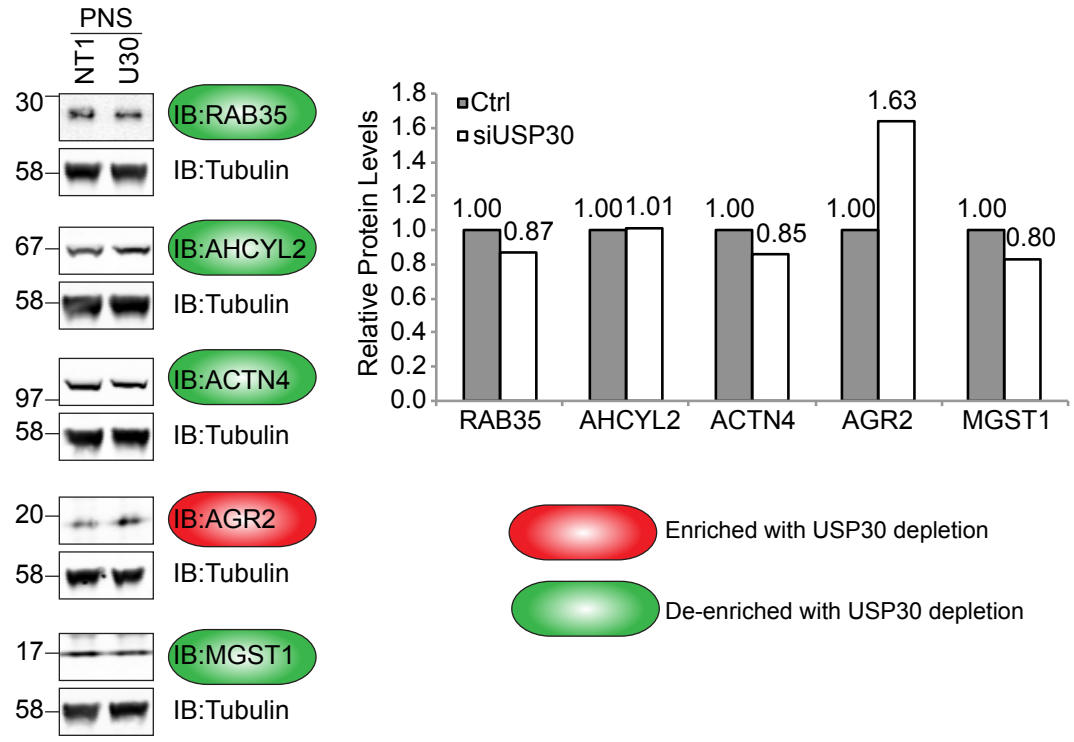

Figure 7.9 Verification of protein change by western blotting.

(A) HeLa S3 cells were transfected for 72hr with either non-targeting siRNA control oligo (NT1) or a siRNA oligo pool targeting USP30 (D1, D3 and D4). Cells were then harvested in HIM buffer. Post-nuclear supernatant (PNS) was obtained by homogenization using a 26G needle and centrifugation at 700 x g. Colour codes correspond to trends observed by mass spectrometry. RAB35= RAB1C.

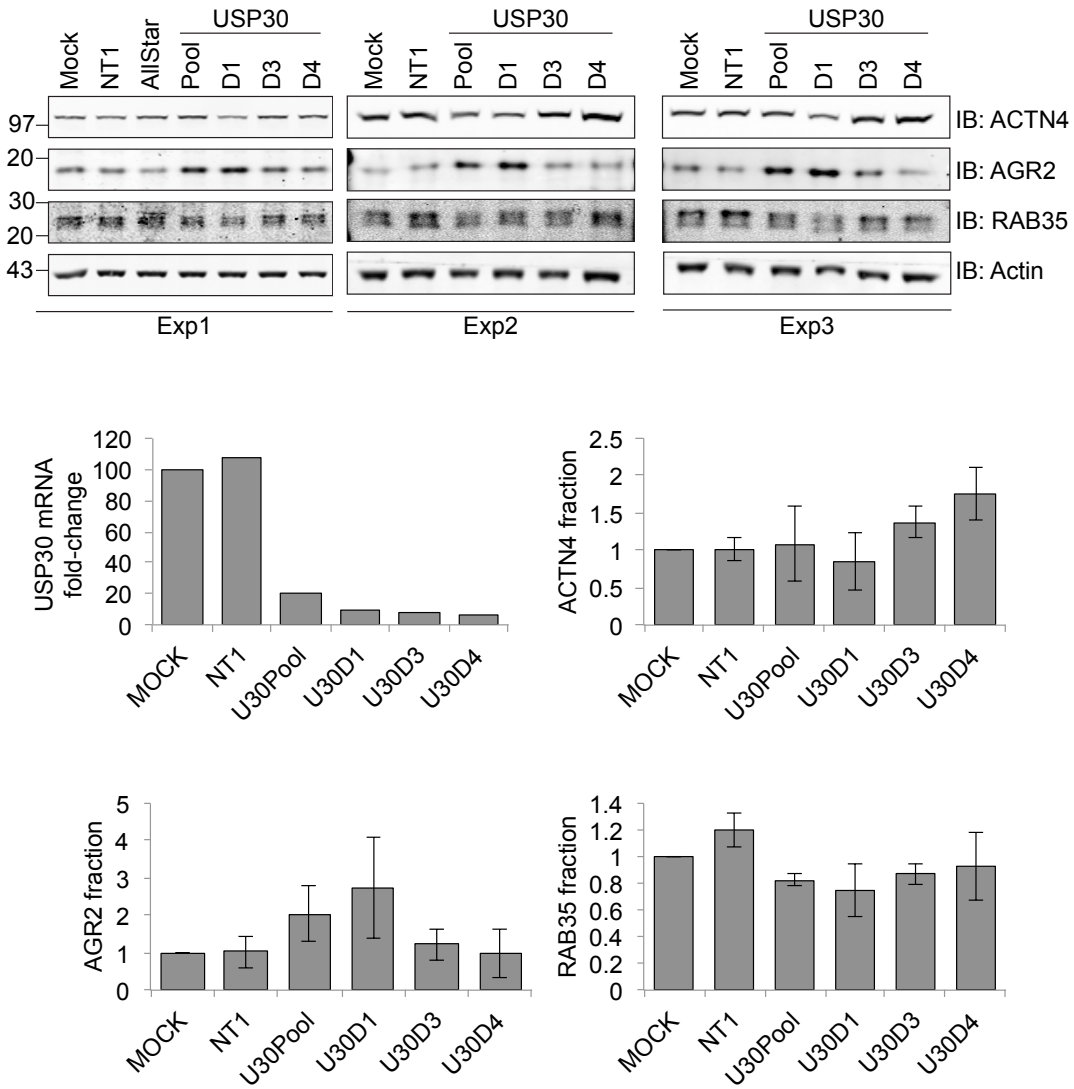

Figure 7.10 USP30 siRNA deconvolution.

HeLa S3 cells were transfected for 72hr with either mock (transfection reagent without siRNA oligo), non-targeting siRNA controls (NT1 or AllStar), or siRNA oligos targeting USP30 (pool, D1, D3 and D4). Cells were then harvested in NP40 lysis buffer and probed as indicated. Error bars represent standard deviations of the three independent experiments. For the assessment of USP30 knockdown efficiency, RNA (from experiment 2) was harvested 24hr post-transfection for qRT-PCR analysis. USP30 mRNA levels were normalized to the β-actin mRNA levels.

7.4 Discussion

7.4.1 Functional characterisations of proteins with altered abundance upon USP30 depletion

In this chapter, I summarized the work carried out to identify substrates of USP30 under steady state conditions using a SILAC-based mass spectrometry approach. Since USP30 is a mitochondrial DUB, it is most likely that it regulates the stability of mitochondrial proteins as well. Therefore, I enriched for mitochondrial proteins using the mitochondria isolation kit prior to mass spectrometry analysis to increase the probability of identifying mitochondrial proteins. Overall, I performed four independent experiments and shortlisted 21 proteins that were significantly altered in protein abundance upon USP30 depletion based on Significance A analysis using Perseus software (Cox and Mann 2012).

Out of these 21 proteins, 5 were known mitochondrial proteins based on the MitoCarta and DAVID database (Pagliarini et al. 2008, Dennis et al. 2003). One of the mitochondrial proteins that was de-enriched upon USP30 knockdown is GST12. GST12 belongs to the MAPEG (Membrane Associated Proteins in Eicosanoid and Glutathione metabolism) family of glutathione transferases that conjugate gluthathione to electrophiles and confer protection against accumulation of ROS (Morgenstern et al. 2011, Morgenstern et al. 1985). Interestingly, GST12 is also found on the outer mitochondrial membrane, making it a likely substrate of USP30 (Morgenstern et al. 1985, Morgenstern 2005). If depletion of USP30 indeed decreases the levels of GST12, then this could lead to increased oxidative stress. However, Bingol et al. recently reported that depletion of USP30 in hippocampal neurons reduces the relative oxidative index in the cells as assessed using mito-roGFP, a mitochondrial redox potential sensor, suggesting that USP30 depletion may reduce oxidative stress in the cells. However, this remains to be validated.

Another mitochondrial protein that is de-enriched upon USP30 knockdown is NDUFA4, a core component of the electron transport chain complex IV

(cytochrome C oxidase) found in the inner mitochondrial membrane (Balsa et al. 2012). siRNA depletion of NDUFA4 affects the assembly and function of complex IV, which significantly impairs cell proliferation in OXPHOS-dependent cells (Balsa et al. 2012). USP30 and NDUFA4 are not localized within the same compartment. However, since NDUFA4 is a nuclear encoded protein, one hypothesis is that nascent NDUFA4 may be regulated by USP30 prior to import into the mitochondria to ensure proper folding and insertion of the protein or appropriate protein abundance.

HRSP12/UK114/L-PSP is a heat responsive endoribonuclease that is upregulated upon heat shock in mouse tissues (Drabek et al. 2014, Samuel et al. 1997). It has been shown to form a homodimer and inhibit the translation of mRNA by dissociating the polysome in an *in vitro* rabbit reticulocyte lysate system (Samuel et al. 1997, Morishita et al. 1999, Oka et al. 1995). Based on the MitoCarta database, HRSP12 is annotated as a mitochondrial protein (Mootha et al. 2003). However, the exact sub-mitochondrial localisation of HRSP12 is unknown. In my proteomic study, USP30 depletion elevated HRSP12 protein levels. Based on the literature on HRSP12, the upregulation of HRSP12 seen in my study is most likely a secondary effect of cell stress upon USP30 depletion.

The MitoCarta database reported that GFP-tagged AGR2 and RAB35 colocalise with Mitotracker (Mootha et al. 2003). However, both of these proteins have not been functionally related to the mitochondria. AGR2 (anterior gradient protein 2 homolog) is upregulated in multiple cancers, including breast, pancreatic, lung, ovarian, oesophageal, and prostate cancers, and is generally associated with the metastatic phenotype and poor prognosis (Patel et al. 2013, Barraclough et al. 2009, Zhang et al. 2007, Pohler et al. 2004, Armes et al. 2013, Park et al. 2011, Fritzsche et al. 2007). A functional study of AGR2 linked it to the post-translational modification of MUC2 in the ER for secretion into the gastrointestinal mucus (Park et al. 2009). Dunmartin and colleagues reported that while AGR2 is mostly found in the ER, it has also been detected on the plasma membrane surface and is secreted into the media. Loss of its KTEL motif (a variant of the ER-targeting

KDEL motif) or mutation of a cysteine residue (C81S) further promotes extracellular secretion of AGR2 (Bergstrom et al. 2014, Gupta et al. 2012). In my proteomic study, AGR2 levels were consistently upregulated upon USP30 depletion. However, only oligo D1 recapitulated the AGR2 effect observed with the siRNA pool and this effect did not correlate with the knockdown efficiency of each of the siRNA oligo. Therefore, this is most likely an off target effect.

RAB35 is involved in the endocytic recycling pathway and is required for the transport of cadherin to adherens junctions. (Charrasse et al. 2013). Knockdown of RAB35 relocalises N-, M- and E-cadherin to transferrin- and clathrin-positive vesicles, suggesting a defect in the recycling pathway. (Charrasse et al. 2013). RAB35 knockdown also promoted cell migration and proliferation via the hyperactivation of Arf6-mediated recycling of β1-integrin and EGF receptors, a mechanism that is consistent with epithelial-to-mesenchymal transition observed in invasive cancer cells (Allaire et al. 2013). Based on the reported effects of RAB35 knockdown on cell migration and proliferation, the decrease in RAB35 protein levels upon USP30 knockdown may also cause similar phenotypes.

While shortlisted proteins that are localized to the outer mitochondrial membrane are more likely to be regulated by USP30, proteins of other localisations such as cytoplasmic or cytoskeletal proteins could also be regulated by USP30, either via direct transient interaction or as an indirect result of an upstream substrate regulated by USP30. In fact, USP30 depletion also altered the protein abundance of a subset of ER proteins including AHCYL2, ETEA, FACE1, G2AN, GLT25D1 and HMOX1. Membrane contact sites between ER and mitochondria, known as ER-mitochondria junctions have been extensively described in the past (Rowland and Voeltz 2012). These contact sites have been proposed to be important for lipid and Ca^{2+} exchange as well as maintenance of mitochondrial dynamics (Schlattner et al. 2014, Tatsuta et al. 2014, Friedman et al. 2011). Therefore, it is possible that USP30 can also regulate ER proteins.

Based on preexisting data in the literature, I further categorized the proteins of interest into several functional groups including vesicular transport, actin assembly and arrangement, cell adhesion and motility and oxidative stress response (Figure 7.11). These functional groups are not mutually exclusive since actin assembly and remodeling also play important roles in both the trafficking of vesicles and also cell motility. The detailed function and subcellular localisation of all the shortlisted proteins are summarized in Table 7.1.

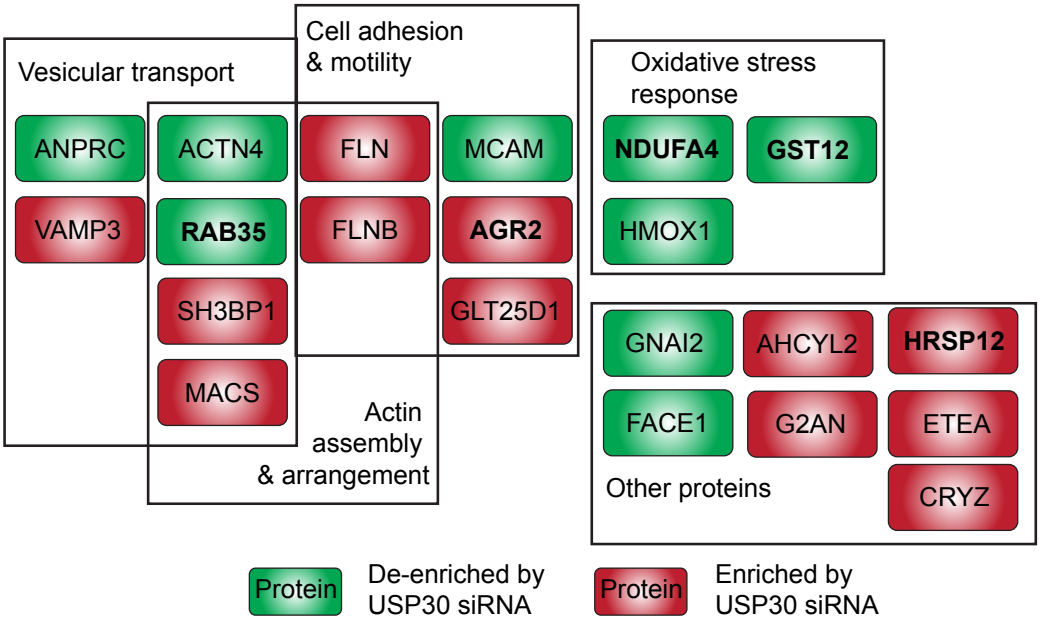

Figure 7.11 Functional annotations of shortlisted proteins.

Categorisation of the top-hits based on functional annotations from literature search. Color-coding reflects either protein enrichment (red) or de-enrichment (green). Proteins in bold represents mitochondrial proteins.

Gene Symbol	Full Name	Localisation	Function	Reference
AGR2 ↑	Anterior gradient protein 2 homolog	mitochondria, endoplasmic reticulum	Involved in MUC2 post-translational synthesis and secretion; promotes cell survival, motility and invasion	(Bergstrom et al. 2014, Di Maro et al. 2014)
GST12 (MGST1) ↓	Microsomal glutathione S-transferase 1	mitochondria, endoplasmic reticulum	Conjugates reduced glutathione to hydrophobic electrophiles; cellular detoxification and protection against ROS	(Morgenstern et al. 2011, Morgenstern et al. 1985)
HRSP12	Heat	mitochondria,	Potentially Inhibits	(Lambrecht et

(UK114) ↓	responsive protein 12	cytoplasm, nucleus	phosphoribosylamine synthesis	al. 2010)
NDUFA4 ↓	NADH dehydrogenase 1α subunit 4	mitochondria	Subunit of ETC complex IV	(Balsa et al. 2012)
RAB1C (RAB35) ↓	Ras-related protein Rab-35	mitochondria, cytoplasm	Involved in recycling endosome trafficking and neurite outgrowth	(Kobayashi et al. 2014b, Kobayashi et al. 2014a)
ACTN4 ↓	α-actinin-4	cytoskeleton	Binds to actin, regulates cell motility; transcriptional co-activator of RelA/p65 sub-unit of NF-kB	(Aksenova et al. 2013, Hamill et al. 2013)
AHCYL2 ↓	Adenosylhomocysteinase 3	endoplasmic reticulum	Potential regulator of sodium bicarbonate cotransporter NBCe1-B	(Yamaguchi and Ishikawa 2014)
ANPRC (NPR3) ↓	Atrial natriuretic peptide receptor 3	plasma membrane	Indirectly involved in TORC1 inactivation and autophagy activation via GTP hydrolysis of the RAG family proteins, Gtr1 and Gtr2	(Kira et al. 2014)
CRYZ ↑	zeta-Crystallin	cytoplasm	Binds to AU rich region of Bcl2 mRNA and promote overexpression of Bcl2	(Lapucci et al. 2010)
ETEA (UBXD8) ↑	FAS-associated factor 2	endoplasmic reticulum	Contains UBA and UBX domains, binds to mis-folded proteins and recruits p97 to ER for protein degradation; also shown to negatively regulates Ira2 and neurofibromin	(Ernst et al. 2009, Phan et al. 2010)
FACE1 (ZMPSTE24) ↓	CAAX prenyl protease 1 homolog	endoplasmic reticulum, Golgi	Recognizes and cleaves C-terminal CAAX-farnesylated prelamin A to form mature lamin A	(Young et al. 2005)
FLN (FLNA) ↑	Filamin A	plasma membrane, cytoskeleton	FLN and FLNB forms homo- and heterodimers, bind to actin and promotes orthogonal branching of actin filaments and links actin filaments to membrane glycoproteins	(Sheen et al. 2002, van der Flier and Sonnenberg 2001)
FLNB ↑	Filamin B	plasma membrane, cytoskeleton		
G2AN (GANAB) ↑	Neutral α-glucosidase AB	endoplasmic reticulum, Golgi	Cleaves N-linked glucose residues from precursor of immature glycoproteins	(Trombetta et al. 1996)
GLT25D1 (COLGALT1) ↑	Procollagen galactosyltransferase	endoplasmic reticulum	Transfers beta-galactose to hydroxylysine residues of collagen	(Perrin-Tricaud et al. 2011)

	1			
GNAI2 ↓	Guanine nucleotide-binding protein G(i) subunit α2	cytoplasm, nucleus	Binds and inhibits the activity of adenylate cyclase, leading to decrease in cAMP level	(Dhanasekaran et al. 1998, Gudermann 2001)
HMOX1 ↓	Heme oxygenase 1	cytoplasm, endoplasmic reticulum	Cleaves heme ring at α-methene bridge, forms biliverdin, iron and carbon monoxide; involves in iron efflux, confers cytoprotection	(Chen 2014)
MACS (MARCKS) ↑	Myristoylated alanine-rich C-kinase substrate	cytoskeleton, cytoplasm	Actin cross-linking protein; substrate of protein kinase C, involved in cell motility, mitosis and exocytosis	(Blackshear 1993, Tsaadon et al. 2008, Li et al. 2008)
MCAM ↓	Melanoma cell adhesion molecule	plasma membrane	Surface receptor expressed on 70% of metastatic melanoma cells; inducibly upregulated by endothelin-1, proposed to play a role in metastasis	(Mangahas et al. 2004)
SH3BP1 ↑	SH3 domain-binding protein 1	cytoplasm, nucleus	Rac1 GAP, inactivates Rac1 to promote cell motility	(Parrini et al. 2011)
SYB3 (VAMP3) ↑	Vesicle-associated membrane protein 3	cytoplasm	A small R-SNARE protein involved in recycling and retrograde transport of vesicles; regulates recycling of integrins, transferrin and the transferrin receptor to the plasma membrane	(McMahon et al. 1993, Galli et al. 1994)

Table 7.1 GO terms and functional annotations of shortlisted proteins.

Arrow represents the change in protein abundance upon USP30 depletion. An upward pointing arrow represents an increase in protein abundance and a downward pointing arrow represents a decrease in protein abundance.

Interestingly, I found that several proteins that promote cell motility, including FLN, FLNB, SH3BP1 and MACS were enriched whereas RAB35, a protein that promotes cell-cell adhesion and inhibits cell migration, was de-enriched upon USP30 depletion (Di Maro et al. 2014, Wang et al. 2008, Zhang et al. 2005, Allaire et al. 2013). However proteins such as ACTN4, which regulate vesicular trafficking as well as cell motility and MCAM, its upregulation of which correlates with metastatic melanoma, were downregulated upon USP30 knockdown (Aksenova et al. 2013, Hamill et al. 2013, Mangahas et al. 2004).

Interestingly, a previous PhD student in our laboratory reported that USP30 knockdown hepatocyte growth factor (HGF)-induced cell scattering in A549 cells (Buus et al. 2009). The HGF-induced cell scattering response involves a complex orchestration of the loss of cell-cell contact, change in cell morphology followed by increase cell motility, all of which recapitulates the epithelial-to-mesenchymal phenotype of metastatic cancer cells. While the exact interplay and the downstream effects of the shortlisted proteins in my proteomic study remained to be elucidated, the general trend indicates that USP30 depletion affects actin assembly, vesicular trafficking and subsequently cell motility, all of which, are key processes that are involved in the metastatic behaviors of cancer cells.

7.4.2 Deconvolution of shortlisted proteins by western blotting

The western blot verification of the shortlisted proteins revealed a marginal decrease in the protein levels of RAB35, GST12 and ACTN4, and elevated AGR2 protein levels upon USP30 knockdown. Whilst the effects were mild, they were consistent with the change in ratio reported from the MS analysis. However, further deconvolution of USP30 also revealed marginal changes and inconsistency between the knockdown efficiency and the change in levels of RAB35, AGR2 and ACTN4. In the case of AGR2, the increase in protein levels observed with USP30 pool knockdown was only recapitulated with one oligo, strongly indication that the effect observed with AGR2 is an off-target effect. On the other hand, the mild effect of USP30 knockdown on

RAB35 and ACTN4 might be due to incomplete depletion of USP30. Importantly, it should also be taken into consideration that the mass spectrometry experiments were performed using mitochondrial-enriched samples whereas the subsequent western blotting analyses were performed using NP-40 lysates. If UPS30 depletion affects the recruitment of a protein to the mitochondria rather than its degradation, this effect will not be visible using the NP-40 lysates.

Proteomic analysis of immunoaffinity-purified K-GG peptides performed by Bingol and colleagues reported a list of proteins in which the ubiquitylation statuses were changed upon CCCP treatment with either USP30 depletion or Parkin overexpression (Bingol et al. 2014). Among them, TOM20 and MIRO1 were highlighted and further verified to be *bona fide* substrates of USP30. Other mitochondrial proteins that were reported include FKBP8, MUL1, TOM70, VDAC1/2/3, MAT2B, PRDX3, PTH2 and IDE. These proteins were not shortlisted in my experiment but this is unsurprising as the aims and experimental settings of our proteomic studies were different (summarised in Table 7.2). Firstly, they set out to identify mitochondrial proteins that can be deubiquitylated by USP30 during mitophagy. Therefore, they used HEK293 cells, which express low endogenous levels of Parkin and depolarise the cells using CCCP to activate Parkin-mediated ubiquitylation of OMM proteins. Since my aim was to characterise the role of USP30 at steady state, HeLa S3 cells were used (which do not express endogenous Parkin; see Chapter 3, Figure 3.1) and I did not induce mitochondrial depolarisation in the cells. Sample-wise, I enriched for mitochondria proteins whereas Bingol et al. immunoprecipitated ubiquitylated peptides to compare the change in abundance of ubiquitylated proteins between control and USP30 depleted cells.

	My Proteomic Study	Bingol et al. (2014)
Cell types	HeLa S3	HEK293
Parkin expressions	No Parkin expression	Low endogenous Parkin
Treatments	Steady state	CCCP treatment
Sample types	Mitochondria-enriched sample	Immunoprecipitation using K-GG antibody for ubiquitylated peptides

Table 7.2 Comparison of the experimental settings of my proteomic study with Bingol et al. (2014).

7.5 Future work

Due to time constraints, I was unable to allocate more time to investigate the other proteins of interest from this SILAC-MS study as the other part of my project on the role of USP30 in Parkin-mediated mitophagy (described in Chapter 6) was showing promising results. The MS data are therefore deposited for future use in the laboratory.

If given more time, it will be worthwhile to use other methods to either further deplete USP30 or inhibit its activity. For example, the use of new technology such as the CRISPR-Cas9 gene editing method allows one to fully deplete a targeted protein as it directly alters the DNA rather than the mRNA (reviewed in (Zhang et al. 2014)). Alternatively, Yue et al. recently identified a small molecule inhibitor of USP30, 15-oxospiramilactone (S3), which inhibits the deubiquitylating activity of USP30 on Mitofusin 1 and 2 (MFN1/2). This promotes the accumulation of MFN1/2 that are ubiquitylated in a non-degradative manner, resulting in mitochondria hyperfusion (Yue et al. 2014). However, the authors did no demonstrate whether the inhibitor could also affect other DUBs, thus casting doubt on the specificity of the inhibitor (Yue et al. 2014). If proven specific, this inhibitor could be used in my SILAC MS study to understand the function of USP30. In addition, it would be worth performing pulse chase dynamic SILAC to compare the synthesis and turnover rates of proteins between control and USP30 depleted cells.

Chapter 8: Conclusion

The past decade witnessed the exponential growth in our understanding of Parkinson's Disease (PD) and its complex etiology involving the interplay between environmental and genetic factors. In particular, the identification of two mutated genes, *PINK1* and *Parkin*, which are functionally linked to the quality control of mitochondria, has opened up an entirely new biology on mitophagy. While it is known that Parkin ubiquitylates outer mitochondrial membrane proteins to target mitochondria for mitophagy, the deubiquitylases that oppose this process remained relatively unexplored at the start of my PhD. My study was focused on the identification of deubiquitylases that are involved in this pathway.

8.1 Different Parkin expression levels promote mitophagy or cell death

From the characterisation work that I performed, I found that cells expressing low endogenous Parkin levels do not undergo global mitophagy. On the other hand, while cells that overexpress high levels of Parkin can undergo global mitophagy, a small population of the cells also undergoes apoptosis. This observation is in contrast to the general understanding of a cytoprotective role of Parkin. I speculate that high levels of Parkin may cause acute ubiquitylation of OMM proteins, targeting them for proteasomal degradation and thereby disrupting the outer mitochondrial membrane integrity. However, it remains to be seen whether this effect can also be observed in other cell lines that overexpress Parkin or whether this is specific to non-transformed hTERT-RPE1 cells. It may be useful perform a titration of Parkin expression levels using inducible promoter to assess whether there is a specific threshold beyond which high levels of Parkin induce cell death. Electron microscopy studies of the structure of the outer mitochondrial membrane may also help to provide further clues for the mechanism of cell death.

Other forms of Parkin-independent mitophagic pathways, namely GP78 and cardiolipin-mediated mitophagy, have been recently described (Fu et al. 2013). GP78 is an E3 ligase previously implicated in endoplasmic reticulum-

associated degradation (ERAD), mitochondrial antiviral signaling (MAVS) and mitophagy (Jacobs et al. 2014, Chen et al. 2014, Liu et al. 2014, Fu et al. 2013). Chu et al. recently reported that rotenone induces cardiolipid redistribution from the inner to outer mitochondrial membrane surface, which directly recruits LC3 to promote mitophagy in rat cortical neurons (Chu et al. 2014, Chu et al. 2013). It will be interesting to investigate the involvement of ubiquitylation, in particular, the roles of DUBs in these mitophagic pathways as well. For example, USP13 has been reported to oppose GP78-mediated ERAD but it is unclear whether it also antagonizes GP78-mediated mitophagy (Liu et al. 2014).

8.2 USP30 depletion enhances cell death in two scenarios

I originally discovered that USP30 depletion enhances Parkin-mediated mitophagic cell death in hTERT-RPE1-YFP-Parkin cells. I further demonstrated that TOM20 is a *bona fide* substrate of USP30. At a later stage of my project, I found that USP30 depletion also enhances cell death induced by the BH3-memetics, ABT-737 and ABT-263. Importantly, CCCP-induced, Parkin-mediated cell death occurs via a BAK and BAX independent fashion whereas the latter depends on both of the BCL2 pro-apoptotic members, suggesting that USP30 may regulate more than just TOM20.

While I shortlisted several proteins that might be regulated by USP30 in my SILAC MS study, I was unable to fully validate and characterise these proteins due to time constraint. Other alternatives to identify DUB substrates have previously been reported. For example, Bingol et al. compared the ubiquitome of USP30 depleted cells with Parkin overexpressing cells after CCCP treatment (Bingol et al. 2014). Sowa and colleagues also previously characterised the interactome of 75 HA-tagged DUBs, including USP30, using affinity purification coupled with mass spectrometry analysis (Sowa et al. 2009). However, the HA-tag was attached to the N-terminus of USP30, which disrupted the N-terminal mitochondrial targeting signal and transmembrane domain crucial for its mitochondrial localisation, rendering the interactome inconclusive. Alternatively, a yeast-two hybrid screen may also reveal interacting partners and potential substrates of USP30.

8.3 USP31 depletion affects the later stages of mitophagy

From the western blot screen, I identified USP31 as a DUB for which depletion results in the partial inhibition of the lysosomal degradation of mitochondrial proteins during mitophagy. Further investigation revealed that LC3-I levels were lower at steady state upon USP31 depletion, suggesting that it might regulate autophagy. However, this result requires further validation. For example, it remains to be answered whether USP31 regulates LC3-I at a post-transcriptional or post-translational level. Fluorescence microscopy study will also be required to assess the abundance and distribution of LC3-I and LC3-II at steady state and during mitophagy. In addition, the effect of USP31 depletion on the acidification of the lysosome and general lysosomal degradation pathways should also be assessed.

8.4 Other DUBs that influence Parkin-mediated mitophagy

Recently, USP30, USP15 and USP8 have been implicated in Parkin-mediated mitophagy. While my results on USP30 agree with Bingol and colleagues, and I have obtained convincing results that USP30 opposes Parkin dependent ubiquitylation and proteasomal degradation of its substrate TOM20, I have not obtained any data suggesting that USP15 or USP8 may be involved.

It is worth mentioning that the major function of USP8 lies in the deubiquitylation of endosomal cargos, including growth factor receptors and the stabilization of the endosomal ESCRT-0 machinery (Clague and Urbe 2006, Clague et al. 2012). Depletion of USP8 has been shown to affect multiple trafficking pathways (Row et al. 2006, Row et al. 2007, Bowers et al. 2006, MacDonald et al. 2014). In particular, Macdonald and colleagues recently showed that lysosomal enzymes are mis-sorted in USP8 depleted cells, leading to their secretion instead of deposition in the lysosomes. Therefore, it is possible that USP8 depletion may affect autophagic degradation by affecting the biogenesis and functionality of lysosomes (MacDonald et al. 2014).

Overall, my data suggest that high levels of Parkin may be just as bad as not having enough Parkin. This should be taken into consideration in future therapeutic approaches to treat PD. The identification of USP30 as a DUB that opposes the degradation of Parkin-mediated substrates as well as its anti-apoptotic role suggest that USP30 may be a potential drug target not only for PD, but also for combinatorial anti-cancer therapies.

References

Aguilera, M., Oliveros, M., Martinez-Padron, M., Barbas, J. A. and Ferrus, A. (2000) 'Ariadne-1: a vital Drosophila gene is required in development and defines a new conserved family of ring-finger proteins', *Genetics,* 155(3), 1231-44.

Akhtar, R. S., Geng, Y., Klocke, B. J., Latham, C. B., Villunger, A., Michalak, E. M., Strasser, A., Carroll, S. L. and Roth, K. A. (2006) 'BH3-only proapoptotic Bcl-2 family members Noxa and Puma mediate neural precursor cell death', *The Journal of neuroscience : the official journal of the Society for Neuroscience,* 26(27), 7257-64.

Al-Hakim, A. K., Zagorska, A., Chapman, L., Deak, M., Peggie, M. and Alessi, D. R. (2008) 'Control of AMPK-related kinases by USP9X and atypical Lys(29)/Lys(33)-linked polyubiquitin chains', *The Biochemical journal,* 411(2), 249-60.

Alam, M. and Schmidt, W. J. (2002) 'Rotenone destroys dopaminergic neurons and induces parkinsonian symptoms in rats', *Behavioural brain research,* 136(1), 317-24.

Allen, G. F., Toth, R., James, J. and Ganley, I. G. (2013) 'Loss of iron triggers PINK1/Parkin-independent mitophagy', *EMBO reports,* 14(12), 1127-35.

Almeida, A., Almeida, J., Bolanos, J. P. and Moncada, S. (2001) 'Different responses of astrocytes and neurons to nitric oxide: the role of glycolytically generated ATP in astrocyte protection', *Proceedings of the National Academy of Sciences of the United States of America,* 98(26), 15294-9.

Amerik, A., Swaminathan, S., Krantz, B. A., Wilkinson, K. D. and Hochstrasser, M. (1997) 'In vivo disassembly of free polyubiquitin chains by yeast Ubp14 modulates rates of protein degradation by the proteasome', *The EMBO journal,* 16(16), 4826-38.

Ashkenazi, A. and Dixit, V. M. (1998) 'Death receptors: signaling and modulation', *Science,* 281(5381), 1305-8.

Axe, E. L., Walker, S. A., Manifava, M., Chandra, P., Roderick, H. L., Habermann, A., Griffiths, G. and Ktistakis, N. T. (2008) 'Autophagosome formation from membrane compartments enriched in phosphatidylinositol 3-phosphate and dynamically connected to the endoplasmic reticulum', *The Journal of cell biology,* 182(4), 685-701.

Baboshina, O. V. and Haas, A. L. (1996) 'Novel multiubiquitin chain linkages catalyzed by the conjugating enzymes E2EPF and RAD6 are recognized by 26 S proteasome subunit 5', *The Journal of biological chemistry,* 271(5), 2823-31.

Bailly, V., Lauder, S., Prakash, S. and Prakash, L. (1997) 'Yeast DNA repair proteins Rad6 and Rad18 form a heterodimer that has ubiquitin conjugating, DNA binding, and ATP hydrolytic activities', *The Journal of biological chemistry,* 272(37), 23360-5.

Baker, R. T. and Board, P. G. (1991) 'The human ubiquitin-52 amino acid fusion protein gene shares several structural features with mammalian ribosomal protein genes', *Nucleic acids research,* 19(5), 1035-40.

Baliga, B. C., Read, S. H. and Kumar, S. (2004) 'The biochemical mechanism of caspase-2 activation', *Cell death and differentiation,* 11(11), 1234-41.

Basanez, G., Sharpe, J. C., Galanis, J., Brandt, T. B., Hardwick, J. M. and Zimmerberg, J. (2002) 'Bax-type apoptotic proteins porate pure lipid bilayers through a mechanism sensitive to intrinsic monolayer curvature', *The Journal of biological chemistry,* 277(51), 49360-5.

Bedford, L., Layfield, R., Mayer, R. J., Peng, J. and Xu, P. (2011) 'Diverse polyubiquitin chains accumulate following 26S proteasomal dysfunction in mammalian neurones', *Neuroscience letters,* 491(1), 44-7.

Beites, C. L., Xie, H., Bowser, R. and Trimble, W. S. (1999) 'The septin CDCrel-1 binds syntaxin and inhibits exocytosis', *Nature neuroscience,* 2(5), 434-9.

Ben-Saadon, R., Zaaroor, D., Ziv, T. and Ciechanover, A. (2006) 'The polycomb protein Ring1B generates self atypical mixed ubiquitin chains required for its in vitro histone H2A ligase activity', *Molecular cell,* 24(5), 701-11.

Bendall, S. C., Hughes, C., Stewart, M. H., Doble, B., Bhatia, M. and Lajoie, G. A. (2008) 'Prevention of amino acid conversion in SILAC experiments with embryonic stem cells', *Molecular & cellular proteomics : MCP,* 7(9), 1587-97.

Berndsen, C. E. and Wolberger, C. (2014) 'New insights into ubiquitin E3 ligase mechanism', *Nature structural & molecular biology,* 21(4), 301-7.

Betarbet, R., Sherer, T. B., Di Monte, D. A. and Greenamyre, J. T. (2002) 'Mechanistic approaches to Parkinson's disease pathogenesis', *Brain pathology,* 12(4), 499-510.

Betarbet, R., Sherer, T. B., MacKenzie, G., Garcia-Osuna, M., Panov, A. V. and Greenamyre, J. T. (2000) 'Chronic systemic pesticide exposure reproduces features of Parkinson's disease', *Nature neuroscience,* 3(12), 1301-6.

Birgisdottir, A. B., Lamark, T. and Johansen, T. (2013) 'The LIR motif - crucial for selective autophagy', *Journal of cell science,* 126(Pt 15), 3237-47.

Boatright, K. M. and Salvesen, G. S. (2003) 'Mechanisms of caspase activation', *Current opinion in cell biology,* 15(6), 725-31.

Boname, J. M., Thomas, M., Stagg, H. R., Xu, P., Peng, J. and Lehner, P. J. (2010) 'Efficient internalization of MHC I requires lysine-11 and lysine-63 mixed linkage polyubiquitin chains', *Traffic,* 11(2), 210-20.

Bonnet, J., Romier, C., Tora, L. and Devys, D. (2008) 'Zinc-finger UBPs: regulators of deubiquitylation', *Trends in biochemical sciences,* 33(8), 369-75.

Bove, J., Prou, D., Perier, C. and Przedborski, S. (2005) 'Toxin-induced models of Parkinson's disease', *NeuroRx : the journal of the American Society for Experimental NeuroTherapeutics,* 2(3), 484-94.

Bremm, A., Freund, S. M. and Komander, D. (2010) 'Lys11-linked ubiquitin chains adopt compact conformations and are preferentially hydrolyzed by the deubiquitinase Cezanne', *Nature structural & molecular biology,* 17(8), 939-47.

Brinkmann, K., Zigrino, P., Witt, A., Schell, M., Ackermann, L., Broxtermann, P., Schull, S., Andree, M., Coutelle, O., Yazdanpanah, B., Seeger, J. M., Klubertz, D., Drebber, U., Hacker, U. T., Kronke, M., Mauch, C., Hoppe, T. and Kashkar, H. (2013) 'Ubiquitin C-terminal hydrolase-L1 potentiates cancer chemosensitivity by stabilizing NOXA', *Cell reports,* 3(3), 881-91.

Budhavarapu, V. N., White, E. D., Mahanic, C. S., Chen, L., Lin, F. T. and Lin, W. C. (2012) 'Regulation of E2F1 by APC/C Cdh1 via K11 linkage-specific ubiquitin chain formation', *Cell cycle,* 11(10), 2030-8.

Burchell, V. S., Nelson, D. E., Sanchez-Martinez, A., Delgado-Camprubi, M., Ivatt, R. M., Pogson, J. H., Randle, S. J., Wray, S., Lewis, P. A., Houlden, H., Abramov, A. Y., Hardy, J., Wood, N. W., Whitworth, A. J., Laman, H. and Plun-Favreau, H. (2013) 'The Parkinson's disease-linked proteins Fbxo7 and Parkin interact to mediate mitophagy', *Nature neuroscience,* 16(9), 1257-65.

Burlacu, A. (2003) 'Regulation of apoptosis by Bcl-2 family proteins', *Journal of cellular and molecular medicine,* 7(3), 249-57.

Burnett, B., Li, F. and Pittman, R. N. (2003) 'The polyglutamine neurodegenerative protein ataxin-3 binds polyubiquitylated proteins and has ubiquitin protease activity', *Human molecular genetics,* 12(23), 3195-205.

Burnette, W. N. (1981) '"Western blotting": electrophoretic transfer of proteins from sodium dodecyl sulfate--polyacrylamide gels to unmodified nitrocellulose and radiographic detection with antibody and radioiodinated protein A', *Analytical biochemistry,* 112(2), 195-203.

Cao, J. and Yan, Q. (2012) 'Histone ubiquitination and deubiquitination in transcription, DNA damage response, and cancer', *Frontiers in oncology,* 2, 26.

Castino, R., Davies, J., Beaucourt, S., Isidoro, C. and Murphy, D. (2005) 'Autophagy is a prosurvival mechanism in cells expressing an autosomal dominant familial neurohypophyseal diabetes insipidus mutant vasopressin transgene', *FASEB journal : official publication of the Federation of American Societies for Experimental Biology,* 19(8), 1021-3.

Catic, A., Fiebiger, E., Korbel, G. A., Blom, D., Galardy, P. J. and Ploegh, H. L. (2007) 'Screen for ISG15-crossreactive deubiquitinases', *PloS one,* 2(7), e679.

Cha, G. H., Kim, S., Park, J., Lee, E., Kim, M., Lee, S. B., Kim, J. M., Chung, J. and Cho, K. S. (2005) 'Parkin negatively regulates JNK pathway in the dopaminergic neurons of Drosophila', *Proceedings of the National Academy of Sciences of the United States of America,* 102(29), 10345-50.

Chan, E. Y. and Tooze, S. A. (2009) 'Evolution of Atg1 function and regulation', *Autophagy,* 5(6), 758-65.

Chan, N. C., Salazar, A. M., Pham, A. H., Sweredoski, M. J., Kolawa, N. J., Graham, R. L., Hess, S. and Chan, D. C. (2011) 'Broad activation of the ubiquitin-proteasome system by Parkin is critical for mitophagy', *Human molecular genetics,* 20(9), 1726-37.

Chastagner, P., Israel, A. and Brou, C. (2006) 'Itch/AIP4 mediates Deltex degradation through the formation of K29-linked polyubiquitin chains', *EMBO reports,* 7(11), 1147-53.

Chau, V., Tobias, J. W., Bachmair, A., Marriott, D., Ecker, D. J., Gonda, D. K. and Varshavsky, A. (1989) 'A multiubiquitin chain is confined to specific lysine in a targeted short-lived protein', *Science,* 243(4898), 1576-83.

Chen, H., Detmer, S. A., Ewald, A. J., Griffin, E. E., Fraser, S. E. and Chan, D. C. (2003) 'Mitofusins Mfn1 and Mfn2 coordinately regulate mitochondrial fusion and are essential for embryonic development', *The Journal of cell biology,* 160(2), 189-200.

Chen, L. and Madura, K. (2002) 'Rad23 promotes the targeting of proteolytic substrates to the proteasome', *Molecular and cellular biology,* 22(13), 4902-13.

Chen, Y. and Dorn, G. W., 2nd (2013) 'PINK1-phosphorylated mitofusin 2 is a Parkin receptor for culling damaged mitochondria', *Science,* 340(6131), 471-5.

Chiang, H. L., Terlecky, S. R., Plant, C. P. and Dice, J. F. (1989) 'A role for a 70-kilodalton heat shock protein in lysosomal degradation of intracellular proteins', *Science,* 246(4928), 382-5.

Chin, L. S., Olzmann, J. A. and Li, L. (2010) 'Parkin-mediated ubiquitin signalling in aggresome formation and autophagy', *Biochemical Society transactions,* 38(Pt 1), 144-9.

Chipuk, J. E., Bouchier-Hayes, L., Kuwana, T., Newmeyer, D. D. and Green, D. R. (2005) 'PUMA couples the nuclear and cytoplasmic proapoptotic function of p53', *Science,* 309(5741), 1732-5.

Chong, C. L., Huang, S. F., Hu, C. P., Chen, Y. L., Chou, H. Y., Chau, G. Y., Shew, J. Y., Tsai, Y. L., Chen, C. T., Chang, C. and Chen, M. L. (2008) 'Decreased expression of UK114 is related to the differentiation status of human hepatocellular carcinoma', *Cancer epidemiology, biomarkers & prevention : a publication of the American Association for Cancer Research, cosponsored by the American Society of Preventive Oncology,* 17(3), 535-42.

Chou, T.-F. F., Brown, S. J., Minond, D., Nordin, B. E., Li, K., Jones, A. C., Chase, P., Porubsky, P. R., Stoltz, B. M., Schoenen, F. J., Patricelli, M. P., Hodder, P., Rosen, H. and Deshaies, R. J. (2011) 'Reversible inhibitor of p97, DBeQ, impairs both ubiquitin-dependent and autophagic protein clearance pathways', *Proceedings of the National Academy of Sciences of the United States of America,* 108(12), 4834-4839.

Chu, C. T., Bayir, H. and Kagan, V. E. (2014) 'LC3 binds externalized cardiolipin on injured mitochondria to signal mitophagy in neurons: implications for Parkinson disease', *Autophagy,* 10(2), 376-378.

Chu, C. T., Ji, J., Dagda, R. K., Jiang, J. F., Tyurina, Y. Y., Kapralov, A. A., Tyurin, V. A., Yanamala, N., Shrivastava, I. H., Mohammadyani, D., Qiang Wang, K. Z., Zhu, J., Klein-Seetharaman, J., Balasubramanian, K., Amoscato, A. A., Borisenko, G., Huang, Z., Gusdon, A. M., Cheikhi, A., Steer, E. K., Wang, R., Baty, C., Watkins, S., Bahar, I., Bay*ƒ*±r, H. I. and Kagan, V. E. (2013) 'Cardiolipin externalization to the outer mitochondrial membrane acts as an elimination signal for mitophagy in neuronal cells', *Nature cell biology,* 15(10), 1197-1205.

Chung, K. K., Zhang, Y., Lim, K. L., Tanaka, Y., Huang, H., Gao, J., Ross, C. A., Dawson, V. L. and Dawson, T. M. (2001) 'Parkin ubiquitinates the alpha-synuclein-interacting protein, synphilin-1: implications for Lewy-body formation in Parkinson disease', *Nature medicine,* 7(10), 1144-50.

Ciechanover, A. (2005) 'Proteolysis: from the lysosome to ubiquitin and the proteasome', *Nature reviews. Molecular cell biology,* 6(1), 79-87.

Ciechanover, A., Elias, S., Heller, H. and Hershko, A. (1982) '"Covalent affinity" purification of ubiquitin-activating enzyme', *The Journal of biological chemistry,* 257(5), 2537-42.

Ciechanover, A., Hod, Y. and Hershko, A. (2012) 'A heat-stable polypeptide component of an ATP-dependent proteolytic system from reticulocytes. 1978', *Biochemical and biophysical research communications,* 425(3), 565-570.

Clague, M. J., Barsukov, I., Coulson, J. M., Liu, H., Rigden, D. J. and Urb√©, S. (2013) 'Deubiquitylases from genes to organism', *Physiological reviews,* 93(3), 1289-1315.

Clague, M. J., Coulson, J. M. and Urbe, S. (2012) 'Cellular functions of the DUBs', *Journal of cell science,* 125(Pt 2), 277-86.

Clague, M. J. and Urbe, S. (2006) 'Endocytosis: the DUB version', *Trends in cell biology,* 16(11), 551-9.

Clague, M. J. and Urbé, S. (2010) 'Ubiquitin: same molecule, different degradation pathways', *Cell,* 143(5), 682-685.

Clark, I. E., Dodson, M. W., Jiang, C., Cao, J. H., Huh, J. R., Seol, J. H., Yoo, S. J., Hay, B. A. and Guo, M. (2006) 'Drosophila pink1 is required for mitochondrial function and interacts genetically with parkin', *Nature,* 441(7097), 1162-6.

Conze, D. B., Wu, C. J., Thomas, J. A., Landstrom, A. and Ashwell, J. D. (2008) 'Lys63-linked polyubiquitination of IRAK-1 is required for interleukin-1 receptor- and toll-like receptor-mediated NF-kappaB activation', *Molecular and cellular biology,* 28(10), 3538-47.

Cooper, E. M., Cutcliffe, C., Kristiansen, T. Z., Pandey, A., Pickart, C. M. and Cohen, R. E. (2009) 'K63-specific deubiquitination by two JAMM/MPN+ complexes: BRISC-associated Brcc36 and proteasomal Poh1', *The EMBO journal,* 28(6), 621-31.

Cope, G. A., Suh, G. S., Aravind, L., Schwarz, S. E., Zipursky, S. L., Koonin, E. V. and Deshaies, R. J. (2002) 'Role of predicted metalloprotease motif of Jab1/Csn5 in cleavage of Nedd8 from Cul1', *Science,* 298(5593), 608-11.

Cory, S. and Adams, J. M. (2002) 'The Bcl2 family: regulators of the cellular life-or-death switch', *Nature reviews. Cancer,* 2(9), 647-56.

Cox, J. and Mann, M. (2008) 'MaxQuant enables high peptide identification rates, individualized p.p.b.-range mass accuracies and proteome-wide protein quantification', *Nature biotechnology,* 26(12), 1367-72.

Cox, J. and Mann, M. (2012) '1D and 2D annotation enrichment: a statistical method integrating quantitative proteomics with complementary high-throughput data', *BMC bioinformatics,* 13 Suppl 16, S12.

Cox, J., Matic, I., Hilger, M., Nagaraj, N., Selbach, M., Olsen, J. V. and Mann, M. (2009) 'A practical guide to the MaxQuant computational platform for SILAC-based quantitative proteomics', *Nature protocols,* 4(5), 698-705.

Cuervo, A. M. and Dice, J. F. (1996) 'A receptor for the selective uptake and degradation of proteins by lysosomes', *Science,* 273(5274), 501-3.

Czabotar, P. E., Lessene, G., Strasser, A. and Adams, J. M. (2014) 'Control of apoptosis by the BCL-2 protein family: implications for physiology and therapy', *Nature reviews. Molecular cell biology,* 15(1), 49-63.

Dammer, E. B., Na, C. H., Xu, P., Seyfried, N. T., Duong, D. M., Cheng, D., Gearing, M., Rees, H., Lah, J. J., Levey, A. I., Rush, J. and Peng, J. (2011) 'Polyubiquitin linkage profiles in three models of proteolytic stress suggest the etiology of Alzheimer disease', *The Journal of biological chemistry,* 286(12), 10457-65.

Das, C., Hoang, Q. Q., Kreinbring, C. A., Luchansky, S. J., Meray, R. K., Ray, S. S., Lansbury, P. T., Ringe, D. and Petsko, G. A. (2006) 'Structural basis for conformational plasticity of the Parkinson's disease-associated ubiquitin hydrolase UCH-L1', *Proceedings of the National Academy of Sciences of the United States of America,* 103(12), 4675-80.

Datta, S. R., Brunet, A. and Greenberg, M. E. (1999) 'Cellular survival: a play in three Akts', *Genes & development,* 13(22), 2905-27.

Dawson, T. M. and Dawson, V. L. (2010) 'The role of parkin in familial and sporadic Parkinson's disease', *Movement disorders : official journal of the Movement Disorder Society,* 25 Suppl 1, S32-9.

De Duve, C. and Wattiaux, R. (1966) 'Functions of lysosomes', *Annual review of physiology,* 28, 435-92.

Deas, E., Plun-Favreau, H., Gandhi, S., Desmond, H., Kjaer, S., Loh, S. H., Renton, A. E., Harvey, R. J., Whitworth, A. J., Martins, L. M., Abramov, A. Y. and Wood, N. W. (2011) 'PINK1 cleavage at position A103 by the mitochondrial protease PARL', *Human molecular genetics,* 20(5), 867-879.

Del Bello, B., Valentini, M. A., Comporti, M. and Maellaro, E. (2003) 'Cisplatin-induced apoptosis in melanoma cells: role of caspase-3 and caspase-7 in Apaf-1 proteolytic cleavage and in execution of the degradative phases', *Annals of the New York Academy of Sciences,* 1010, 200-4.

Dennis, G., Jr., Sherman, B. T., Hosack, D. A., Yang, J., Gao, W., Lane, H. C. and Lempicki, R. A. (2003) 'DAVID: Database for Annotation, Visualization, and Integrated Discovery', *Genome biology,* 4(5), P3.

Deshaies, R. J. and Joazeiro, C. A. (2009) 'RING domain E3 ubiquitin ligases', *Annual review of biochemistry,* 78, 399-434.

Di Bartolomeo, S., Corazzari, M., Nazio, F., Oliverio, S., Lisi, G., Antonioli, M., Pagliarini, V., Matteoni, S., Fuoco, C., Giunta, L., D'Amelio, M., Nardacci, R., Romagnoli, A., Piacentini, M., Cecconi, F. and Fimia, G. M. (2010) 'The dynamic interaction of AMBRA1 with the dynein motor complex regulates mammalian autophagy', *The Journal of cell biology,* 191(1), 155-68.

Diaz, C. and Schroit, A. J. (1996) 'Role of translocases in the generation of phosphatidylserine asymmetry', *The Journal of membrane biology,* 151(1), 1-9.

Dice, J. F. (1990) 'Peptide sequences that target cytosolic proteins for lysosomal proteolysis', *Trends in biochemical sciences,* 15(8), 305-9.

Ding, W.-X. X., Ni, H.-M. M., Li, M., Liao, Y., Chen, X., Stolz, D. B., Dorn, G. W. and Yin, X.-M. M. (2010) 'Nix is critical to two distinct phases of mitophagy, reactive oxygen species-mediated autophagy induction and Parkin-ubiquitin-p62-mediated mitochondrial priming', *The Journal of biological chemistry,* 285(36), 27879-27890.

Ding, W. X., Ni, H. M., Li, M., Liao, Y., Chen, X., Stolz, D. B., Dorn, G. W., 2nd and Yin, X. M. (2010) 'Nix is critical to two distinct phases of mitophagy, reactive oxygen species-mediated autophagy induction and Parkin-ubiquitin-p62-mediated mitochondrial priming', *The Journal of biological chemistry,* 285(36), 27879-90.

Dooley, H. C., Razi, M., Polson, H. E., Girardin, S. E., Wilson, M. I. and Tooze, S. A. (2014) 'WIPI2 links LC3 conjugation with PI3P, autophagosome formation, and pathogen clearance by recruiting Atg12-5-16L1', *Molecular cell,* 55(2), 238-52.

Dove, K. K. and Klevit, R. E. (2013) 'Structural Biology: Parkin's Serpentine Shape Revealed in the Year of the Snake', *Current biology : CB,* 23(16), R691-3.

Du, C., Fang, M., Li, Y., Li, L. and Wang, X. (2000) 'Smac, a mitochondrial protein that promotes cytochrome c-dependent caspase activation by eliminating IAP inhibition', *Cell,* 102(1), 33-42.

Duda, D. M., Borg, L. A., Scott, D. C., Hunt, H. W., Hammel, M. and Schulman, B. A. (2008) 'Structural insights into NEDD8 activation of cullin-RING ligases: conformational control of conjugation', *Cell,* 134(6), 995-1006.

Duncan, L. M., Piper, S., Dodd, R. B., Saville, M. K., Sanderson, C. M., Luzio, J. P. and Lehner, P. J. (2006) 'Lysine-63-linked ubiquitination is required for endolysosomal degradation of class I molecules', *The EMBO journal,* 25(8), 1635-45.

Durcan, T. M., Tang, M. Y., Perusse, J. R., Dashti, E. A., Aguileta, M. A., McLelland, G. L., Gros, P., Shaler, T. A., Faubert, D., Coulombe, B. and Fon, E. A. (2014) 'USP8 regulates mitophagy by removing K6-linked ubiquitin conjugates from parkin', *The EMBO journal*.

Duve, C. D., Gianetto, R., Appelmans, F. and Wattiaux, R. (1953) 'Enzymic Content of the Mitochondria Fraction', *Nature,* 172(4390), 1143-1144.

Edelmann, M. J., Iphofer, A., Akutsu, M., Altun, M., di Gleria, K., Kramer, H. B., Fiebiger, E., Dhe-Paganon, S. and Kessler, B. M. (2009) 'Structural basis and specificity of human otubain 1-mediated deubiquitination', *The Biochemical journal,* 418(2), 379-90.

Eguchi, Y., Srinivasan, A., Tomaselli, K. J., Shimizu, S. and Tsujimoto, Y. (1999) 'ATP-dependent steps in apoptotic signal transduction', *Cancer research,* 59(9), 2174-81.

Eisenberg-Lerner, A., Bialik, S., Simon, H. U. and Kimchi, A. (2009) 'Life and death partners: apoptosis, autophagy and the cross-talk between them', *Cell death and differentiation,* 16(7), 966-75.

Ekholm-Reed, S., Goldberg, M. S., Schlossmacher, M. G. and Reed, S. I. (2013) 'Parkin-dependent degradation of the F-box protein Fbw7beta promotes neuronal survival in response to oxidative stress by stabilizing Mcl-1', *Molecular and cellular biology,* 33(18), 3627-43.

Elliott, P. R., Liu, H., Pastok, M. W., Grossmann, G. J., Rigden, D. J., Clague, M. J., Urbe, S. and Barsukov, I. L. (2011) 'Structural variability of the ubiquitin specific protease DUSP-UBL double domains', *FEBS letters,* 585(21), 3385-90.

Elsasser, S., Chandler-Militello, D., Muller, B., Hanna, J. and Finley, D. (2004) 'Rad23 and Rpn10 serve as alternative ubiquitin receptors for the proteasome', *The Journal of biological chemistry,* 279(26), 26817-22.

Emoto, K., Toyama-Sorimachi, N., Karasuyama, H., Inoue, K. and Umeda, M. (1997) 'Exposure of phosphatidylethanolamine on the surface of apoptotic cells', *Experimental cell research,* 232(2), 430-4.

Enesa, K., Ito, K., Luong le, A., Thorbjornsen, I., Phua, C., To, Y., Dean, J., Haskard, D. O., Boyle, J., Adcock, I. and Evans, P. C. (2008) 'Hydrogen peroxide prolongs nuclear localization of NF-kappaB in activated cells by suppressing negative regulatory mechanisms', *The Journal of biological chemistry,* 283(27), 18582-90.

Essner, E. and Novikoff, A. B. (1961) 'Localization of acid phosphatase activity in hepatic lysosomes by means of electron microscopy', *The Journal of biophysical and biochemical cytology,* 9, 773-84.

Etlinger, J. D. and Goldberg, A. L. (1977) 'A soluble ATP-dependent proteolytic system responsible for the degradation of abnormal proteins in reticulocytes', *Proceedings of the National Academy of Sciences,* 74(1), 54-58.

Fadok, V. A., Voelker, D. R., Campbell, P. A., Cohen, J. J., Bratton, D. L. and Henson, P. M. (1992) 'Exposure of phosphatidylserine on the surface of apoptotic lymphocytes triggers specific recognition and removal by macrophages', *Journal of immunology,* 148(7), 2207-16.

Faesen, A. C., Dirac, A. M., Shanmugham, A., Ovaa, H., Perrakis, A. and Sixma, T. K. (2011a) 'Mechanism of USP7/HAUSP activation by its C-terminal ubiquitin-like domain and allosteric regulation by GMP-synthetase', *Molecular cell,* 44(1), 147-59.

Faesen, A. C., Luna-Vargas, M. P., Geurink, P. P., Clerici, M., Merkx, R., van Dijk, W. J., Hameed, D. S., El Oualid, F., Ovaa, H. and Sixma, T. K. (2011b) 'The differential modulation of USP activity by internal regulatory domains, interactors and eight ubiquitin chain types', *Chemistry & biology,* 18(12), 1550-61.

Faesen, A. C., Luna-Vargas, M. P. and Sixma, T. K. (2012) 'The role of UBL domains in ubiquitin-specific proteases', *Biochemical Society transactions,* 40(3), 539-45.

Fang, S., Ferrone, M., Yang, C., Jensen, J. P., Tiwari, S. and Weissman, A. M. (2001) 'The tumor autocrine motility factor receptor, gp78, is a ubiquitin protein ligase implicated in degradation from the endoplasmic reticulum', *Proceedings of the National Academy of Sciences of the United States of America,* 98(25), 14422-7.

Feng, Z., Zhang, H., Levine, A. J. and Jin, S. (2005) 'The coordinate regulation of the p53 and mTOR pathways in cells', *Proceedings of the National Academy of Sciences of the United States of America,* 102(23), 8204-9.

Ferreira, K. S., Kreutz, C., Macnelly, S., Neubert, K., Haber, A., Bogyo, M., Timmer, J. and Borner, C. (2012) 'Caspase-3 feeds back on caspase-8, Bid and XIAP in type I Fas signaling in primary mouse hepatocytes', *Apoptosis : an international journal on programmed cell death,* 17(5), 503-15.

Finley, D. (2009) 'Recognition and processing of ubiquitin-protein conjugates by the proteasome', *Annual review of biochemistry,* 78, 477-513.

Finney, N., Walther, F., Mantel, P. Y., Stauffer, D., Rovelli, G. and Dev, K. K. (2003) 'The cellular protein level of parkin is regulated by its ubiquitin-like domain', *The Journal of biological chemistry,* 278(18), 16054-8.

Foster, F. M., Traer, C. J., Abraham, S. M. and Fry, M. J. (2003) 'The phosphoinositide (PI) 3-kinase family', *Journal of cell science,* 116(Pt 15), 3037-40.

Fransson, A., Ruusala, A. and Aspenstrom, P. (2003) 'Atypical Rho GTPases have roles in mitochondrial homeostasis and apoptosis', *The Journal of biological chemistry,* 278(8), 6495-502.

Fransson, S., Ruusala, A. and Aspenstrom, P. (2006) 'The atypical Rho GTPases Miro-1 and Miro-2 have essential roles in mitochondrial trafficking', *Biochemical and biophysical research communications,* 344(2), 500-10.

Freemont, P. S., Hanson, I. M. and Trowsdale, J. (1991) 'A novel cysteine-rich sequence motif', *Cell,* 64(3), 483-4.

French, M., Swanson, K., Shih, S. C., Radhakrishnan, I. and Hicke, L. (2005) 'Identification and characterization of modular domains that bind ubiquitin', *Methods in enzymology,* 399, 135-57.

Frias, M. A., Thoreen, C. C., Jaffe, J. D., Schroder, W., Sculley, T., Carr, S. A. and Sabatini, D. M. (2006) 'mSin1 is necessary for Akt/PKB phosphorylation, and its isoforms define three distinct mTORC2s', *Current biology : CB,* 16(18), 1865-70.

Fuchs, G. and Oren, M. (2014) 'Writing and reading H2B monoubiquitylation', *Biochimica et biophysica acta,* 1839(8), 694-701.

Fujita, N., Itoh, T., Omori, H., Fukuda, M., Noda, T. and Yoshimori, T. (2008) 'The Atg16L complex specifies the site of LC3 lipidation for membrane biogenesis in autophagy', *Molecular biology of the cell,* 19(5), 2092-100.

Galan, J. M. and Haguenauer-Tsapis, R. (1997) 'Ubiquitin lys63 is involved in ubiquitination of a yeast plasma membrane protein', *The EMBO journal,* 16(19), 5847-54.

Ganley, I. G., Lam du, H., Wang, J., Ding, X., Chen, S. and Jiang, X. (2009) 'ULK1.ATG13.FIP200 complex mediates mTOR signaling and is essential for autophagy', *The Journal of biological chemistry,* 284(18), 12297-305.

Geetha, T. and Wooten, M. W. (2008) 'TrkA receptor endolysosomal degradation is both ubiquitin and proteasome dependent', *Traffic,* 9(7), 1146-56.

Gegg, M. E., Cooper, J. M., Chau, K. Y., Rojo, M., Schapira, A. H. and Taanman, J. W. (2010) 'Mitofusin 1 and mitofusin 2 are ubiquitinated in a PINK1/parkin-dependent manner upon induction of mitophagy', *Human molecular genetics,* 19(24), 4861-70.

Geiger, T., Wehner, A., Schaab, C., Cox, J. and Mann, M. (2012) 'Comparative proteomic analysis of eleven common cell lines reveals ubiquitous but varying expression of most proteins', *Molecular & cellular proteomics : MCP,* 11(3), M111 014050.

Geisler, S., Holmstrom, K. M., Skujat, D., Fiesel, F. C., Rothfuss, O. C., Kahle, P. J. and Springer, W. (2010) 'PINK1/Parkin-mediated mitophagy is dependent on VDAC1 and p62/SQSTM1', *Nature cell biology,* 12(2), 119-31.

Goldberg, A. L. (2012) 'Development of proteasome inhibitors as research tools and cancer drugs', *The Journal of cell biology,* 199(4), 583-8.

Goldknopf, I. L. and Busch, H. (1977) 'Isopeptide linkage between nonhistone and histone 2A polypeptides of chromosomal conjugate-protein A24', *Proceedings of the National Academy of Sciences of the United States of America,* 74(3), 864-8.

Goldknopf, I. L., Taylor, C. W., Baum, R. M., Yeoman, L. C., Olson, M. O., Prestayko, A. W. and Busch, H. (1975) 'Isolation and characterization of protein A24, a "histone-like" non-histone chromosomal protein', *The Journal of biological chemistry,* 250(18), 7182-7.

Goldstein, G., Scheid, M., Hammerling, U., Schlesinger, D. H., Niall, H. D. and Boyse, E. A. (1975) 'Isolation of a polypeptide that has lymphocyte-differentiating properties and is probably represented universally in living cells', *Proceedings of the National Academy of Sciences of the United States of America,* 72(1), 11-5.

Gong, L., Kamitani, T., Millas, S. and Yeh, E. T. (2000) 'Identification of a novel isopeptidase with dual specificity for ubiquitin- and NEDD8-conjugated proteins', *The Journal of biological chemistry,* 275(19), 14212-6.

Gorell, J. M., Johnson, C. C., Rybicki, B. A., Peterson, E. L. and Richardson, R. J. (1998) 'The risk of Parkinson's disease with exposure to pesticides, farming, well water, and rural living', *Neurology,* 50(5), 1346-50.

Greene, A. W., Grenier, K., Aguileta, M. A., Muise, S., Farazifard, R., Haque, M. E., McBride, H. M., Park, D. S. and Fon, E. A. (2012) 'Mitochondrial processing peptidase regulates PINK1 processing, import and Parkin recruitment', *EMBO reports,* 13(4), 378-85.

Greene, J. C., Whitworth, A. J., Kuo, I., Andrews, L. A., Feany, M. B. and Pallanck, L. J. (2003) 'Mitochondrial pathology and apoptotic muscle degeneration in Drosophila parkin mutants', *Proceedings of the National Academy of Sciences of the United States of America,* 100(7), 4078-83.

Grenier, K., McLelland, G. L. and Fon, E. A. (2013) 'Parkin- and PINK1-Dependent Mitophagy in Neurons: Will the Real Pathway Please Stand Up?', *Frontiers in neurology,* 4, 100.

Griffiths, G. J., Dubrez, L., Morgan, C. P., Jones, N. A., Whitehouse, J., Corfe, B. M., Dive, C. and Hickman, J. A. (1999) 'Cell damage-induced conformational changes of the pro-apoptotic protein Bak in vivo precede the onset of apoptosis', *The Journal of cell biology,* 144(5), 903-14.

Groll, M., Bajorek, M., Kohler, A., Moroder, L., Rubin, D. M., Huber, R., Glickman, M. H. and Finley, D. (2000) 'A gated channel into the proteasome core particle', *Nature structural biology,* 7(11), 1062-7.

Groll, M. and Clausen, T. (2003) 'Molecular shredders: how proteasomes fulfill their role', *Current opinion in structural biology,* 13(6), 665-73.

Haglund, K., Sigismund, S., Polo, S., Szymkiewicz, I., Di Fiore, P. P. and Dikic, I. (2003) 'Multiple monoubiquitination of RTKs is sufficient for their endocytosis and degradation', *Nature cell biology,* 5(5), 461-6.

Hailey, D. W., Rambold, A. S., Satpute-Krishnan, P., Mitra, K., Sougrat, R., Kim, P. K. and Lippincott-Schwartz, J. (2010) 'Mitochondria supply membranes for autophagosome biogenesis during starvation', *Cell,* 141(4), 656-67.

Hamasaki, M., Furuta, N., Matsuda, A., Nezu, A., Yamamoto, A., Fujita, N., Oomori, H., Noda, T., Haraguchi, T., Hiraoka, Y., Amano, A. and Yoshimori, T. (2013) 'Autophagosomes form at ER-mitochondria contact sites', *Nature,* 495(7441), 389-93.

Hamazaki, J., Iemura, S., Natsume, T., Yashiroda, H., Tanaka, K. and Murata, S. (2006) 'A novel proteasome interacting protein recruits the deubiquitinating enzyme UCH37 to 26S proteasomes', *The EMBO journal,* 25(19), 4524-36.

Hanada, T., Noda, N. N., Satomi, Y., Ichimura, Y., Fujioka, Y., Takao, T., Inagaki, F. and Ohsumi, Y. (2007) 'The Atg12-Atg5 conjugate has a novel E3-like activity for protein lipidation in autophagy', *The Journal of biological chemistry,* 282(52), 37298-302.

Harding, T. M., Morano, K. A., Scott, S. V. and Klionsky, D. J. (1995) 'Isolation and characterization of yeast mutants in the cytoplasm to vacuole protein targeting pathway', *The Journal of cell biology,* 131(3), 591-602.

Hardy, J., Cookson, M. R. and Singleton, A. (2003) 'Genes and parkinsonism', *The Lancet. Neurology,* 2(4), 221-8.

Hartley, A., Stone, J. M., Heron, C., Cooper, J. M. and Schapira, A. H. (1994) 'Complex I inhibitors induce dose-dependent apoptosis in PC12 cells: relevance to Parkinson's disease', *Journal of neurochemistry,* 63(5), 1987-90.

Hassink, G. C., Zhao, B., Sompallae, R., Altun, M., Gastaldello, S., Zinin, N. V., Masucci, M. G. and Lindsten, K. (2009) 'The ER-resident ubiquitin-specific protease 19 participates in the UPR and rescues ERAD substrates', *EMBO reports,* 10(7), 755-761.

Hayes, S. D., Liu, H., MacDonald, E., Sanderson, C. M., Coulson, J. M., Clague, M. J. and Urbe, S. (2012) 'Direct and indirect control of mitogen-activated protein kinase pathway-associated components, BRAP/IMP E3 ubiquitin ligase and CRAF/RAF1 kinase, by the deubiquitylating enzyme USP15', *The Journal of biological chemistry,* 287(51), 43007-18.

He, C. and Klionsky, D. J. (2009) 'Regulation mechanisms and signaling pathways of autophagy', *Annual review of genetics,* 43, 67-93.

Henn, I. H., Bouman, L., Schlehe, J. S., Schlierf, A., Schramm, J. E., Wegener, E., Nakaso, K., Culmsee, C., Berninger, B., Krappmann, D., Tatzelt,

J. and Winklhofer, K. F. (2007) 'Parkin mediates neuroprotection through activation of IkappaB kinase/nuclear factor-kappaB signaling', *The Journal of neuroscience : the official journal of the Society for Neuroscience,* 27(8), 1868-78.

Heride, C., Urbe, S. and Clague, M. J. (2014) 'Ubiquitin code assembly and disassembly', *Current biology : CB,* 24(6), R215-20.

Hershko, A., Ciechanover, A. and Rose, I. A. (1979) 'Resolution of the ATP-dependent proteolytic system from reticulocytes: a component that interacts with ATP', *Proceedings of the National Academy of Sciences of the United States of America,* 76(7), 3107-10.

Hershko, A., Heller, H., Elias, S. and Ciechanover, A. (1983) 'Components of ubiquitin-protein ligase system. Resolution, affinity purification, and role in protein breakdown', *The Journal of biological chemistry,* 258(13), 8206-14.

Heyninck, K. and Beyaert, R. (2005) 'A20 inhibits NF-kappaB activation by dual ubiquitin-editing functions', *Trends in biochemical sciences,* 30(1), 1-4.

Hicke, L., Schubert, H. L. and Hill, C. P. (2005) 'Ubiquitin-binding domains', *Nature reviews. Molecular cell biology,* 6(8), 610-21.

Higuchi, R., Dollinger, G., Walsh, P. S. and Griffith, R. (1992) 'Simultaneous amplification and detection of specific DNA sequences', *Bio/technology,* 10(4), 413-7.

Hochstrasser, M. (2009) 'Origin and function of ubiquitin-like proteins', *Nature,* 458(7237), 422-9.

Hofmann, K. and Falquet, L. (2001) 'A ubiquitin-interacting motif conserved in components of the proteasomal and lysosomal protein degradation systems', *Trends in biochemical sciences,* 26(6), 347-50.

Hollville, E., Carroll, R. G., Cullen, S. P. and Martin, S. J. (2014) 'Bcl-2 Family Proteins Participate in Mitochondrial Quality Control by Regulating Parkin/PINK1-Dependent Mitophagy', *Molecular cell*.

Hough, R., Pratt, G. and Rechsteiner, M. (1986) 'Ubiquitin-lysozyme conjugates. Identification and characterization of an ATP-dependent protease from rabbit reticulocyte lysates', *The Journal of biological chemistry,* 261(5), 2400-8.

Hough, R. and Rechsteiner, M. (1986) 'Ubiquitin-lysozyme conjugates. Purification and susceptibility to proteolysis', *The Journal of biological chemistry,* 261(5), 2391-9.

Hristova, V. A., Beasley, S. A., Rylett, R. J. and Shaw, G. S. (2009) 'Identification of a novel Zn2+-binding domain in the autosomal recessive

juvenile Parkinson-related E3 ligase parkin', *The Journal of biological chemistry,* 284(22), 14978-86.

Hu, M., Li, P., Li, M., Li, W., Yao, T., Wu, J. W., Gu, W., Cohen, R. E. and Shi, Y. (2002) 'Crystal structure of a UBP-family deubiquitinating enzyme in isolation and in complex with ubiquitin aldehyde', *Cell,* 111(7), 1041-54.

Hu, M., Li, P., Song, L., Jeffrey, P. D., Chenova, T. A., Wilkinson, K. D., Cohen, R. E. and Shi, Y. (2005) 'Structure and mechanisms of the proteasome-associated deubiquitinating enzyme USP14', *The EMBO journal,* 24(21), 3747-56.

Huang, H., Jeon, M. S., Liao, L., Yang, C., Elly, C., Yates, J. R., 3rd and Liu, Y. C. (2010) 'K33-linked polyubiquitination of T cell receptor-zeta regulates proteolysis-independent T cell signaling', *Immunity,* 33(1), 60-70.

Huang, J. and Manning, B. D. (2008) 'The TSC1-TSC2 complex: a molecular switchboard controlling cell growth', *The Biochemical journal,* 412(2), 179-90.

Huang, M. and D'Andrea, A. D. (2010) 'A new nuclease member of the FAN club', *Nature structural & molecular biology,* 17(8), 926-8.

Hunt, L. T. and Dayhoff, M. O. (1977) 'Amino-terminal sequence identity of ubiquitin and the nonhistone component of nuclear protein A24', *Biochemical and biophysical research communications,* 74(2), 650-5.

Hurley, J. H., Lee, S. and Prag, G. (2006) 'Ubiquitin-binding domains', *The Biochemical journal,* 399(3), 361-72.

Hurley, J. H. and Stenmark, H. (2011) 'Molecular mechanisms of ubiquitin-dependent membrane traffic', *Annual review of biophysics,* 40, 119-42.

Husnjak, K., Elsasser, S., Zhang, N., Chen, X., Randles, L., Shi, Y., Hofmann, K., Walters, K. J., Finley, D. and Dikic, I. (2008) 'Proteasome subunit Rpn13 is a novel ubiquitin receptor', *Nature,* 453(7194), 481-8.

Hwang, S., Kim, D., Choi, G., An, S. W., Hong, Y. K., Suh, Y. S., Lee, M. J. and Cho, K. S. (2010) 'Parkin suppresses c-Jun N-terminal kinase-induced cell death via transcriptional regulation in Drosophila', *Molecules and cells,* 29(6), 575-80.

Ichimura, Y., Kirisako, T., Takao, T., Satomi, Y., Shimonishi, Y., Ishihara, N., Mizushima, N., Tanida, I., Kominami, E., Ohsumi, M., Noda, T. and Ohsumi, Y. (2000) 'A ubiquitin-like system mediates protein lipidation', *Nature,* 408(6811), 488-92.

Ikeda, F. and Dikic, I. (2008) 'Atypical ubiquitin chains: new molecular signals. 'Protein Modifications: Beyond the Usual Suspects' review series', *EMBO reports,* 9(6), 536-42.

Imai, Y., Soda, M., Inoue, H., Hattori, N., Mizuno, Y. and Takahashi, R. (2001) 'An unfolded putative transmembrane polypeptide, which can lead to endoplasmic reticulum stress, is a substrate of Parkin', *Cell,* 105(7), 891-902.

Inbal, B., Bialik, S., Sabanay, I., Shani, G. and Kimchi, A. (2002) 'DAP kinase and DRP-1 mediate membrane blebbing and the formation of autophagic vesicles during programmed cell death', *The Journal of cell biology,* 157(3), 455-468.

Inuzuka, H., Shaik, S., Onoyama, I., Gao, D., Tseng, A., Maser, R. S., Zhai, B., Wan, L., Gutierrez, A., Lau, A. W., Xiao, Y., Christie, A. L., Aster, J., Settleman, J., Gygi, S. P., Kung, A. L., Look, T., Nakayama, K. I., DePinho, R. A. and Wei, W. (2011) 'SCF(FBW7) regulates cellular apoptosis by targeting MCL1 for ubiquitylation and destruction', *Nature,* 471(7336), 104-109.

Ishihara, N., Fujita, Y., Oka, T. and Mihara, K. (2006) 'Regulation of mitochondrial morphology through proteolytic cleavage of OPA1', *The EMBO journal,* 25(13), 2966-77.

Itakura, E., Kishi, C., Inoue, K. and Mizushima, N. (2008) 'Beclin 1 forms two distinct phosphatidylinositol 3-kinase complexes with mammalian Atg14 and UVRAG', *Molecular biology of the cell,* 19(12), 5360-72.

Ito, H., Daido, S., Kanzawa, T., Kondo, S. and Kondo, Y. (2005) 'Radiation-induced autophagy is associated with LC3 and its inhibition sensitizes malignant glioma cells', *International journal of oncology,* 26(5), 1401-10.

Jankowski, A., Kim, J. H., Collins, R. F., Daneman, R., Walton, P. and Grinstein, S. (2001) 'In situ measurements of the pH of mammalian peroxisomes using the fluorescent protein pHluorin', *The Journal of biological chemistry,* 276(52), 48748-53.

Jiang, X. and Wang, X. (2000) 'Cytochrome c promotes caspase-9 activation by inducing nucleotide binding to Apaf-1', *The Journal of biological chemistry,* 275(40), 31199-203.

Jin, L., Williamson, A., Banerjee, S., Philipp, I. and Rape, M. (2008) 'Mechanism of ubiquitin-chain formation by the human anaphase-promoting complex', *Cell,* 133(4), 653-65.

Jin, M. and Klionsky, D. (2013) 'The Core Molecular Machinery of Autophagosome Formation' in Wang, H.-G., ed. *Autophagy and Cancer*, Springer New York, 25-45.

Jin, S. M., Lazarou, M., Wang, C., Kane, L. A., Narendra, D. P. and Youle, R. J. (2010) 'Mitochondrial membrane potential regulates PINK1 import and proteolytic destabilization by PARL', *The Journal of cell biology,* 191(5), 933-942.

Jin, S. M., Lazarou, M., Wang, C., Kane, L. A., Narendra, D. P. and Youle, R. J. (2010) 'Mitochondrial membrane potential regulates PINK1 import and proteolytic destabilization by PARL', *The Journal of cell biology,* 191(5), 933-42.

Jin, S. M. and Youle, R. J. (2013) 'The accumulation of misfolded proteins in the mitochondrial matrix is sensed by PINK1 to induce PARK2/Parkin-mediated mitophagy of polarized mitochondria', *Autophagy,* 9(11), 1750-7.

Jin, Z. and El-Deiry, W. S. (2005) 'Overview of cell death signaling pathways', *Cancer biology & therapy,* 4(2), 139-63.

Johnson, B. N., Berger, A. K., Cortese, G. P. and Lavoie, M. J. (2012) 'The ubiquitin E3 ligase parkin regulates the proapoptotic function of Bax', *Proceedings of the National Academy of Sciences of the United States of America,* 109(16), 6283-8.

Johnson, E. S., Ma, P. C., Ota, I. M. and Varshavsky, A. (1995) 'A proteolytic pathway that recognizes ubiquitin as a degradation signal', *The Journal of biological chemistry,* 270(29), 17442-56.

Johnston, S. C., Larsen, C. N., Cook, W. J., Wilkinson, K. D. and Hill, C. P. (1997) 'Crystal structure of a deubiquitinating enzyme (human UCH-L3) at 1.8 A resolution', *The EMBO journal,* 16(13), 3787-96.

Johnston, S. C., Riddle, S. M., Cohen, R. E. and Hill, C. P. (1999) 'Structural basis for the specificity of ubiquitin C-terminal hydrolases', *The EMBO journal,* 18(14), 3877-87.

Johri, A. and Beal, M. F. (2012) 'Mitochondrial dysfunction in neurodegenerative diseases', *The Journal of pharmacology and experimental therapeutics,* 342(3), 619-30.

Kaiser, S. E., Riley, B. E., Shaler, T. A., Trevino, R. S., Becker, C. H., Schulman, H. and Kopito, R. R. (2011) 'Protein standard absolute quantification (PSAQ) method for the measurement of cellular ubiquitin pools', *Nature methods,* 8(8), 691-6.

Kamada, Y., Yoshino, K., Kondo, C., Kawamata, T., Oshiro, N., Yonezawa, K. and Ohsumi, Y. (2010) 'Tor directly controls the Atg1 kinase complex to regulate autophagy', *Molecular and cellular biology,* 30(4), 1049-58.

Kane, L. A., Lazarou, M., Fogel, A. I., Li, Y., Yamano, K., Sarraf, S. A., Banerjee, S. and Youle, R. J. (2014) 'PINK1 phosphorylates ubiquitin to activate Parkin E3 ubiquitin ligase activity', *The Journal of cell biology,* 205(2), 143-53.

Kane, L. A. and Youle, R. J. (2011) 'PINK1 and Parkin flag Miro to direct mitochondrial traffic', *Cell,* 147(4), 721-3.

Kanki, T. and Klionsky, D. J. (2008) 'Mitophagy in yeast occurs through a selective mechanism', *The Journal of biological chemistry,* 283(47), 32386-93.

Kasianowicz, J., Benz, R. and McLaughlin, S. (1984) 'The kinetic mechanism by which CCCP (carbonyl cyanide m-chlorophenylhydrazone) transports protons across membranes', *The Journal of membrane biology,* 82(2), 179-90.

Kaushik, S. and Cuervo, A. M. (2012) 'Chaperone-mediated autophagy: a unique way to enter the lysosome world', *Trends in cell biology,* 22(8), 407-17.

Kayagaki, N., Phung, Q., Chan, S., Chaudhari, R., Quan, C., O'Rourke, K. M., Eby, M., Pietras, E., Cheng, G., Bazan, J. F., Zhang, Z., Arnott, D. and Dixit, V. M. (2007) 'DUBA: a deubiquitinase that regulates type I interferon production', *Science,* 318(5856), 1628-32.

Kazlauskaite, A., Kondapalli, C., Gourlay, R., Campbell, D. G., Ritorto, M. S., Hofmann, K., Alessi, D. R., Knebel, A., Trost, M. and Muqit, M. M. (2014) 'Parkin is activated by PINK1-dependent phosphorylation of ubiquitin at Ser65', *The Biochemical journal,* 460(1), 127-39.

Kerr, J. F. (1971) 'Shrinkage necrosis: a distinct mode of cellular death', *The Journal of pathology,* 105(1), 13-20.

Kerr, J. F., Wyllie, A. H. and Currie, A. R. (1972) 'Apoptosis: a basic biological phenomenon with wide-ranging implications in tissue kinetics', *British journal of cancer,* 26(4), 239-257.

Keusekotten, K., Elliott, P. R., Glockner, L., Fiil, B. K., Damgaard, R. B., Kulathu, Y., Wauer, T., Hospenthal, M. K., Gyrd-Hansen, M., Krappmann, D., Hofmann, K. and Komander, D. (2013) 'OTULIN antagonizes LUBAC signaling by specifically hydrolyzing Met1-linked polyubiquitin', *Cell,* 153(6), 1312-26.

Kihara, A., Noda, T., Ishihara, N. and Ohsumi, Y. (2001) 'Two distinct Vps34 phosphatidylinositol 3-kinase complexes function in autophagy and carboxypeptidase Y sorting in Saccharomyces cerevisiae', *The Journal of cell biology,* 152(3), 519-30.

Kim, E., Goraksha-Hicks, P., Li, L., Neufeld, T. P. and Guan, K. L. (2008) 'Regulation of TORC1 by Rag GTPases in nutrient response', *Nature cell biology,* 10(8), 935-45.

Kim, H., Chen, J. and Yu, X. (2007) 'Ubiquitin-binding protein RAP80 mediates BRCA1-dependent DNA damage response', *Science,* 316(5828), 1202-5.

Kim, H. C. and Huibregtse, J. M. (2009) 'Polyubiquitination by HECT E3s and the determinants of chain type specificity', *Molecular and cellular biology,* 29(12), 3307-18.

Kim, H. T., Kim, K. P., Lledias, F., Kisselev, A. F., Scaglione, K. M., Skowyra, D., Gygi, S. P. and Goldberg, A. L. (2007) 'Certain pairs of ubiquitin-conjugating enzymes (E2s) and ubiquitin-protein ligases (E3s) synthesize nondegradable forked ubiquitin chains containing all possible isopeptide linkages', *The Journal of biological chemistry,* 282(24), 17375-86.

Kim, I., Rodriguez-Enriquez, S. and Lemasters, J. J. (2007) 'Selective degradation of mitochondria by mitophagy', *Archives of biochemistry and biophysics,* 462(2), 245-53.

Kim, J., Kundu, M., Viollet, B. and Guan, K. L. (2011) 'AMPK and mTOR regulate autophagy through direct phosphorylation of Ulk1', *Nature cell biology,* 13(2), 132-41.

Kirisako, T., Ichimura, Y., Okada, H., Kabeya, Y., Mizushima, N., Yoshimori, T., Ohsumi, M., Takao, T., Noda, T. and Ohsumi, Y. (2000) 'The reversible modification regulates the membrane-binding state of Apg8/Aut7 essential for autophagy and the cytoplasm to vacuole targeting pathway', *The Journal of cell biology,* 151(2), 263-76.

Kirisako, T., Kamei, K., Murata, S., Kato, M., Fukumoto, H., Kanie, M., Sano, S., Tokunaga, F., Tanaka, K. and Iwai, K. (2006) 'A ubiquitin ligase complex assembles linear polyubiquitin chains', *The EMBO journal,* 25(20), 4877-87.

Kirkin, V. and Dikic, I. (2007) 'Role of ubiquitin- and Ubl-binding proteins in cell signaling', *Current opinion in cell biology,* 19(2), 199-205.

Klionsky, D. J. (2005) 'The molecular machinery of autophagy: unanswered questions', *Journal of cell science,* 118(Pt 1), 7-18.

Klionsky, D. J. (2008) 'Autophagy revisited: a conversation with Christian de Duve', *Autophagy,* 4(6), 740-3.

Klionsky, D. J., Abeliovich, H., Agostinis, P., Agrawal, D. K., Aliev, G., Askew, D. S., Baba, M., Baehrecke, E. H., Bahr, B. A., Ballabio, A., Bamber, B. A., Bassham, D. C., Bergamini, E., Bi, X., Biard-Piechaczyk, M., Blum, J. S., Bredesen, D. E., Brodsky, J. L., Brumell, J. H., Brunk, U. T., Bursch, W., Camougrand, N., Cebollero, E., Cecconi, F., Chen, Y., Chin, L. S., Choi, A., Chu, C. T., Chung, J., Clarke, P. G., Clark, R. S., Clarke, S. G., Clave, C., Cleveland, J. L., Codogno, P., Colombo, M. I., Coto-Montes, A., Cregg, J. M., Cuervo, A. M., Debnath, J., Demarchi, F., Dennis, P. B., Dennis, P. A., Deretic, V., Devenish, R. J., Di Sano, F., Dice, J. F., Difiglia, M., Dinesh-Kumar, S., Distelhorst, C. W., Djavaheri-Mergny, M., Dorsey, F. C., Droge, W., Dron, M., Dunn, W. A., Jr., Duszenko, M., Eissa, N. T., Elazar, Z., Esclatine, A., Eskelinen, E. L., Fesus, L., Finley, K. D., Fuentes, J. M., Fueyo, J., Fujisaki, K., Galliot, B., Gao, F. B., Gewirtz, D. A., Gibson, S. B., Gohla, A., Goldberg, A. L., Gonzalez, R., Gonzalez-Estevez, C., Gorski, S., Gottlieb, R. A., Haussinger, D., He, Y. W., Heidenreich, K., Hill, J. A., Hoyer-Hansen, M., Hu, X., Huang, W. P., Iwasaki, A., Jaattela, M., Jackson, W. T., Jiang, X., Jin,

S., Johansen, T., Jung, J. U., Kadowaki, M., Kang, C., Kelekar, A., Kessel, D. H., Kiel, J. A., Kim, H. P., Kimchi, A., Kinsella, T. J., Kiselyov, K., Kitamoto, K., Knecht, E., et al. (2008) 'Guidelines for the use and interpretation of assays for monitoring autophagy in higher eukaryotes', *Autophagy,* 4(2), 151-75.

Klionsky, D. J., Cregg, J. M., Dunn, W. A., Jr., Emr, S. D., Sakai, Y., Sandoval, I. V., Sibirny, A., Subramani, S., Thumm, M., Veenhuis, M. and Ohsumi, Y. (2003) 'A unified nomenclature for yeast autophagy-related genes', *Developmental cell,* 5(4), 539-45.

Klionsky, D. J. and Emr, S. D. (2000) 'Autophagy as a regulated pathway of cellular degradation', *Science,* 290(5497), 1717-21.

Kluck, R. M., Bossy-Wetzel, E., Green, D. R. and Newmeyer, D. D. (1997) 'The release of cytochrome c from mitochondria: a primary site for Bcl-2 regulation of apoptosis', *Science,* 275(5303), 1132-6.

Knipscheer, P., Raschle, M., Smogorzewska, A., Enoiu, M., Ho, T. V., Scharer, O. D., Elledge, S. J. and Walter, J. C. (2009) 'The Fanconi anemia pathway promotes replication-dependent DNA interstrand cross-link repair', *Science,* 326(5960), 1698-701.

Komander, D. (2009) 'The emerging complexity of protein ubiquitination', *Biochemical Society transactions,* 37(Pt 5), 937-53.

Komander, D. (2010) 'Mechanism, specificity and structure of the deubiquitinases', *Sub-cellular biochemistry,* 54, 69-87.

Komander, D. (2010) 'Mechanism, Specificity and Structure of the Deubiquitinases' in Groettrup, M., ed. *Conjugation and Deconjugation of Ubiquitin Family Modifiers*, Springer New York, 69-87.

Komander, D. and Barford, D. (2008) 'Structure of the A20 OTU domain and mechanistic insights into deubiquitination', *The Biochemical journal,* 409(1), 77-85.

Komander, D., Clague, M. J. and Urbe, S. (2009a) 'Breaking the chains: structure and function of the deubiquitinases', *Nature reviews. Molecular cell biology,* 10(8), 550-63.

Komander, D., Lord, C. J., Scheel, H., Swift, S., Hofmann, K., Ashworth, A. and Barford, D. (2008) 'The structure of the CYLD USP domain explains its specificity for Lys63-linked polyubiquitin and reveals a B box module', *Molecular cell,* 29(4), 451-64.

Komander, D. and Rape, M. (2012) 'The ubiquitin code', *Annual review of biochemistry,* 81, 203-29.

Komander, D., Reyes-Turcu, F., Licchesi, J. D., Odenwaelder, P., Wilkinson, K. D. and Barford, D. (2009b) 'Molecular discrimination of structurally

equivalent Lys 63-linked and linear polyubiquitin chains', *EMBO reports,* 10(5), 466-73.

Korolchuk, V. I., Menzies, F. M. and Rubinsztein, D. C. (2010) 'Mechanisms of cross-talk between the ubiquitin-proteasome and autophagy-lysosome systems', *FEBS letters,* 584(7), 1393-8.

Koyano, F., Okatsu, K., Kosako, H., Tamura, Y., Go, E., Kimura, M., Kimura, Y., Tsuchiya, H., Yoshihara, H., Hirokawa, T., Endo, T., Fon, E. A., Trempe, J. F., Saeki, Y., Tanaka, K. and Matsuda, N. (2014) 'Ubiquitin is phosphorylated by PINK1 to activate parkin', *Nature,* 510(7503), 162-6.

Kubbutat, M. H., Jones, S. N. and Vousden, K. H. (1997) 'Regulation of p53 stability by Mdm2', *Nature,* 387(6630), 299-303.

Kuwana, T., Mackey, M. R., Perkins, G., Ellisman, M. H., Latterich, M., Schneiter, R., Green, D. R. and Newmeyer, D. D. (2002) 'Bid, Bax, and lipids cooperate to form supramolecular openings in the outer mitochondrial membrane', *Cell,* 111(3), 331-42.

Lamark, T., Kirkin, V., Dikic, I. and Johansen, T. (2009) 'NBR1 and p62 as cargo receptors for selective autophagy of ubiquitinated targets', *Cell cycle,* 8(13), 1986-90.

Landers, J. E., Cassel, S. L. and George, D. L. (1997) 'Translational enhancement of mdm2 oncogene expression in human tumor cells containing a stabilized wild-type p53 protein', *Cancer research,* 57(16), 3562-8.

Lazarou, M., Jin, S. M., Kane, L. A. and Youle, R. J. (2012) 'Role of PINK1 Binding to the TOM Complex and Alternate Intracellular Membranes in Recruitment and Activation of the E3 Ligase Parkin', *Developmental cell,* 22(2), 320-333.

Lee, J. G., Kim, W., Gygi, S. and Ye, Y. (2014) 'Characterization of the deubiquitinating activity of USP19 and its role in endoplasmic reticulum-associated degradation', *The Journal of biological chemistry,* 289(6), 3510-7.

Leroy, E., Boyer, R., Auburger, G., Leube, B., Ulm, G., Mezey, E., Harta, G., Brownstein, M. J., Jonnalagada, S., Chernova, T., Dehejia, A., Lavedan, C., Gasser, T., Steinbach, P. J., Wilkinson, K. D. and Polymeropoulos, M. H. (1998) 'The ubiquitin pathway in Parkinson's disease', *Nature,* 395(6701), 451-2.

Levine, B. and Klionsky, D. J. (2004) 'Development by self-digestion: molecular mechanisms and biological functions of autophagy', *Developmental cell,* 6(4), 463-77.

Li, M., Brooks, C. L., Wu-Baer, F., Chen, D., Baer, R. and Gu, W. (2003) 'Mono- versus polyubiquitination: differential control of p53 fate by Mdm2', *Science,* 302(5652), 1972-5.

Li, N., Ragheb, K., Lawler, G., Sturgis, J., Rajwa, B., Melendez, J. A. and Robinson, J. P. (2003) 'Mitochondrial complex I inhibitor rotenone induces apoptosis through enhancing mitochondrial reactive oxygen species production', *The Journal of biological chemistry,* 278(10), 8516-25.

Li, P., Nijhawan, D., Budihardjo, I., Srinivasula, S. M., Ahmad, M., Alnemri, E. S. and Wang, X. (1997) 'Cytochrome c and dATP-dependent formation of Apaf-1/caspase-9 complex initiates an apoptotic protease cascade', *Cell,* 91(4), 479-89.

Li, W., Bengtson, M. H., Ulbrich, A., Matsuda, A., Reddy, V. A., Orth, A., Chanda, S. K., Batalov, S. and Joazeiro, C. A. (2008) 'Genome-wide and functional annotation of human E3 ubiquitin ligases identifies MULAN, a mitochondrial E3 that regulates the organelle's dynamics and signaling', *PloS one,* 3(1), e1487.

Liao, Y. and Hung, M. C. (2010) 'Physiological regulation of Akt activity and stability', *American journal of translational research,* 2(1), 19-42.

Lim, G. G., Chew, K. C., Ng, X. H., Henry-Basil, A., Sim, R. W., Tan, J. M., Chai, C. and Lim, K. L. (2013) 'Proteasome inhibition promotes Parkin-Ubc13 interaction and lysine 63-linked ubiquitination', *PloS one,* 8(9), e73235.

Lin, W. and Kang, U. J. (2008) 'Characterization of PINK1 processing, stability, and subcellular localization', *Journal of neurochemistry,* 106(1), 464-74.

Liu, W., Shang, Y., Zeng, Y., Liu, C., Li, Y., Zhai, L., Wang, P., Lou, J., Xu, P., Ye, Y. and Li, W. (2014) 'Dimeric Ube2g2 simultaneously engages donor and acceptor ubiquitins to form Lys48-linked ubiquitin chains', *The EMBO journal,* 33(1), 46-61.

Lockshin, R. A. and Zakeri, Z. (2001) 'Programmed cell death and apoptosis: origins of the theory', *Nature reviews. Molecular cell biology,* 2(7), 545-550.

Loewith, R., Jacinto, E., Wullschleger, S., Lorberg, A., Crespo, J. L., Bonenfant, D., Oppliger, W., Jenoe, P. and Hall, M. N. (2002) 'Two TOR complexes, only one of which is rapamycin sensitive, have distinct roles in cell growth control', *Molecular cell,* 10(3), 457-68.

Longatti, A. and Tooze, S. A. (2009) 'Vesicular trafficking and autophagosome formation', *Cell death and differentiation,* 16(7), 956-65.

Longatti, A. and Tooze, S. A. (2012) 'Recycling endosomes contribute to autophagosome formation', *Autophagy,* 8(11), 1682-3.

MacVicar, T. D. and Lane, J. D. (2014) 'Impaired OMA1-dependent cleavage of OPA1 and reduced DRP1 fission activity combine to prevent mitophagy in

cells that are dependent on oxidative phosphorylation', *Journal of cell science,* 127(Pt 10), 2313-25.

Mao, Y., Senic-Matuglia, F., Di Fiore, P. P., Polo, S., Hodsdon, M. E. and De Camilli, P. (2005) 'Deubiquitinating function of ataxin-3: insights from the solution structure of the Josephin domain', *Proceedings of the National Academy of Sciences of the United States of America,* 102(36), 12700-5.

Martin, S. J., Reutelingsperger, C. P., McGahon, A. J., Rader, J. A., van Schie, R. C., LaFace, D. M. and Green, D. R. (1995) 'Early redistribution of plasma membrane phosphatidylserine is a general feature of apoptosis regardless of the initiating stimulus: inhibition by overexpression of Bcl-2 and Abl', *The Journal of experimental medicine,* 182(5), 1545-56.

Martins, L. M. (2002) 'The serine protease Omi/HtrA2: a second mammalian protein with a Reaper-like function', *Cell death and differentiation,* 9(7), 699-701.

Martins, L. M., Iaccarino, I., Tenev, T., Gschmeissner, S., Totty, N. F., Lemoine, N. R., Savopoulos, J., Gray, C. W., Creasy, C. L., Dingwall, C. and Downward, J. (2002) 'The serine protease Omi/HtrA2 regulates apoptosis by binding XIAP through a reaper-like motif', *The Journal of biological chemistry,* 277(1), 439-44.

Maspero, E., Mari, S., Valentini, E., Musacchio, A., Fish, A., Pasqualato, S. and Polo, S. (2011) 'Structure of the HECT:ubiquitin complex and its role in ubiquitin chain elongation', *EMBO reports,* 12(4), 342-9.

Massey, A., Kiffin, R. and Cuervo, A. M. (2004) 'Pathophysiology of chaperone-mediated autophagy', *The international journal of biochemistry & cell biology,* 36(12), 2420-34.

Mastrandrea, L. D., You, J., Niles, E. G. and Pickart, C. M. (1999) 'E2/E3-mediated assembly of lysine 29-linked polyubiquitin chains', *The Journal of biological chemistry,* 274(38), 27299-306.

Matsumoto, M. L., Wickliffe, K. E., Dong, K. C., Yu, C., Bosanac, I., Bustos, D., Phu, L., Kirkpatrick, D. S., Hymowitz, S. G., Rape, M., Kelley, R. F. and Dixit, V. M. (2010) 'K11-linked polyubiquitination in cell cycle control revealed by a K11 linkage-specific antibody', *Molecular cell,* 39(3), 477-84.

Matsunaga, K., Saitoh, T., Tabata, K., Omori, H., Satoh, T., Kurotori, N., Maejima, I., Shirahama-Noda, K., Ichimura, T., Isobe, T., Akira, S., Noda, T. and Yoshimori, T. (2009) 'Two Beclin 1-binding proteins, Atg14L and Rubicon, reciprocally regulate autophagy at different stages', *Nature cell biology,* 11(4), 385-96.

Mauthe, M., Jacob, A., Freiberger, S., Hentschel, K., Stierhof, Y. D., Codogno, P. and Proikas-Cezanne, T. (2011) 'Resveratrol-mediated autophagy requires

WIPI-1-regulated LC3 lipidation in the absence of induced phagophore formation', *Autophagy,* 7(12), 1448-61.

Maytal-Kivity, V., Reis, N., Hofmann, K. and Glickman, M. H. (2002) 'MPN+, a putative catalytic motif found in a subset of MPN domain proteins from eukaryotes and prokaryotes, is critical for Rpn11 function', *BMC biochemistry,* 3, 28.

McCullough, J., Clague, M. J. and Urbe, S. (2004) 'AMSH is an endosome-associated ubiquitin isopeptidase', *The Journal of cell biology,* 166(4), 487-92.

McCullough, J., Row, P. E., Lorenzo, O., Doherty, M., Beynon, R., Clague, M. J. and Urbe, S. (2006) 'Activation of the endosome-associated ubiquitin isopeptidase AMSH by STAM, a component of the multivesicular body-sorting machinery', *Current biology : CB,* 16(2), 160-5.

Meissner, C., Lorenz, H., Weihofen, A., Selkoe, D. J. and Lemberg, M. K. (2011) 'The mitochondrial intramembrane protease PARL cleaves human Pink1 to regulate Pink1 trafficking', *Journal of neurochemistry,* 117(5), 856-67.

Menegon, A., Board, P. G., Blackburn, A. C., Mellick, G. D. and Le Couteur, D. G. (1998) 'Parkinson's disease, pesticides, and glutathione transferase polymorphisms', *Lancet,* 352(9137), 1344-6.

Metzger, M. B., Hristova, V. A. and Weissman, A. M. (2012) 'HECT and RING finger families of E3 ubiquitin ligases at a glance', *Journal of cell science,* 125(Pt 3), 531-7.

Mevissen, T. E., Hospenthal, M. K., Geurink, P. P., Elliott, P. R., Akutsu, M., Arnaudo, N., Ekkebus, R., Kulathu, Y., Wauer, T., El Oualid, F., Freund, S. M., Ovaa, H. and Komander, D. (2013) 'OTU deubiquitinases reveal mechanisms of linkage specificity and enable ubiquitin chain restriction analysis', *Cell,* 154(1), 169-84.

Meyer, H., Bug, M. and Bremer, S. (2012) 'Emerging functions of the VCP/p97 AAA-ATPase in the ubiquitin system', *Nature cell biology,* 14(2), 117-123.

Mihara, M., Erster, S., Zaika, A., Petrenko, O., Chittenden, T., Pancoska, P. and Moll, U. M. (2003) 'p53 has a direct apoptogenic role at the mitochondria', *Molecular cell,* 11(3), 577-90.

Mikhailov, V., Mikhailova, M., Degenhardt, K., Venkatachalam, M. A., White, E. and Saikumar, P. (2003) 'Association of Bax and Bak homo-oligomers in mitochondria. Bax requirement for Bak reorganization and cytochrome c release', *The Journal of biological chemistry,* 278(7), 5367-76.

Misaghi, S., Galardy, P. J., Meester, W. J., Ovaa, H., Ploegh, H. L. and Gaudet, R. (2005) 'Structure of the ubiquitin hydrolase UCH-L3 complexed with a suicide substrate', *The Journal of biological chemistry,* 280(2), 1512-20.

Mizushima, N., Kuma, A., Kobayashi, Y., Yamamoto, A., Matsubae, M., Takao, T., Natsume, T., Ohsumi, Y. and Yoshimori, T. (2003) 'Mouse Apg16L, a novel WD-repeat protein, targets to the autophagic isolation membrane with the Apg12-Apg5 conjugate', *Journal of cell science,* 116(Pt 9), 1679-88.

Mizushima, N., Yoshimori, T. and Ohsumi, Y. (2011) 'The role of Atg proteins in autophagosome formation', *Annual review of cell and developmental biology,* 27, 107-32.

Moore, S. F., Hunter, R. W. and Hers, I. (2011) 'mTORC2 protein complex-mediated Akt (Protein Kinase B) Serine 473 Phosphorylation is not required for Akt1 activity in human platelets [corrected]', *The Journal of biological chemistry,* 286(28), 24553-60.

Morris, J. R. and Solomon, E. (2004) 'BRCA1 : BARD1 induces the formation of conjugated ubiquitin structures, dependent on K6 of ubiquitin, in cells during DNA replication and repair', *Human molecular genetics,* 13(8), 807-17.

Morrison, K. E. (2003) 'Parkin mutations and early onset parkinsonism', *Brain : a journal of neurology,* 126(Pt 6), 1250-1.

Mosesson, Y., Shtiegman, K., Katz, M., Zwang, Y., Vereb, G., Szollosi, J. and Yarden, Y. (2003) 'Endocytosis of receptor tyrosine kinases is driven by monoubiquitylation, not polyubiquitylation', *The Journal of biological chemistry,* 278(24), 21323-6.

Mukhopadhyay, S., Panda, P. K., Sinha, N., Das, D. N. and Bhutia, S. K. (2014) 'Autophagy and apoptosis: where do they meet?', *Apoptosis : an international journal on programmed cell death,* 19(4), 555-566.

Muller-Rischart, A. K., Pilsl, A., Beaudette, P., Patra, M., Hadian, K., Funke, M., Peis, R., Deinlein, A., Schweimer, C., Kuhn, P. H., Lichtenthaler, S. F., Motori, E., Hrelia, S., Wurst, W., Trumbach, D., Langer, T., Krappmann, D., Dittmar, G., Tatzelt, J. and Winklhofer, K. F. (2013) 'The E3 ligase parkin maintains mitochondrial integrity by increasing linear ubiquitination of NEMO', *Molecular cell,* 49(5), 908-21.

Mullis, K., Faloona, F., Scharf, S., Saiki, R., Horn, G. and Erlich, H. (1992) 'Specific enzymatic amplification of DNA in vitro: the polymerase chain reaction. 1986', *Biotechnology,* 24, 17-27.

Munz, C. (2006) 'Autophagy and antigen presentation', *Cellular microbiology,* 8(6), 891-8.

Murakami, T., Shoji, M., Imai, Y., Inoue, H., Kawarabayashi, T., Matsubara, E., Harigaya, Y., Sasaki, A., Takahashi, R. and Abe, K. (2004) 'Pael-R is accumulated in Lewy bodies of Parkinson's disease', *Annals of neurology,* 55(3), 439-42.

Nakamura, N. and Hirose, S. (2008) 'Regulation of mitochondrial morphology by USP30, a deubiquitinating enzyme present in the mitochondrial outer membrane', *Molecular biology of the cell,* 19(5), 1903-1911.

Narendra, D., Kane, L. A., Hauser, D. N., Fearnley, I. M. and Youle, R. J. (2010) 'p62/SQSTM1 is required for Parkin-induced mitochondrial clustering but not mitophagy; VDAC1 is dispensable for both', *Autophagy,* 6(8), 1090-1106.

Narendra, D., Tanaka, A., Suen, D. F. and Youle, R. J. (2008) 'Parkin is recruited selectively to impaired mitochondria and promotes their autophagy', *The Journal of cell biology,* 183(5), 795-803.

Narendra, D., Tanaka, A., Suen, D. F. and Youle, R. J. (2009) 'Parkin-induced mitophagy in the pathogenesis of Parkinson disease', *Autophagy,* 5(5), 706-8.

Narendra, D. P., Jin, S. M., Tanaka, A., Suen, D. F., Gautier, C. A., Shen, J., Cookson, M. R. and Youle, R. J. (2010) 'PINK1 is selectively stabilized on impaired mitochondria to activate Parkin', *PLoS biology,* 8(1), e1000298.

Nicassio, F., Corrado, N., Vissers, J. H., Areces, L. B., Bergink, S., Marteijn, J. A., Geverts, B., Houtsmuller, A. B., Vermeulen, W., Di Fiore, P. P. and Citterio, E. (2007) 'Human USP3 is a chromatin modifier required for S phase progression and genome stability', *Current biology : CB,* 17(22), 1972-7.

Nicastro, G., Habeck, M., Masino, L., Svergun, D. I. and Pastore, A. (2006) 'Structure validation of the Josephin domain of ataxin-3: conclusive evidence for an open conformation', *Journal of biomolecular NMR,* 36(4), 267-77.

Nicastro, G., Menon, R. P., Masino, L., Knowles, P. P., McDonald, N. Q. and Pastore, A. (2005) 'The solution structure of the Josephin domain of ataxin-3: structural determinants for molecular recognition', *Proceedings of the National Academy of Sciences of the United States of America,* 102(30), 10493-8.

Nuytemans, K., Theuns, J., Cruts, M. and Van Broeckhoven, C. (2010) 'Genetic etiology of Parkinson disease associated with mutations in the SNCA, PARK2, PINK1, PARK7, and LRRK2 genes: a mutation update', *Human mutation,* 31(7), 763-80.

Ogata, M., Hino, S., Saito, A., Morikawa, K., Kondo, S., Kanemoto, S., Murakami, T., Taniguchi, M., Tanii, I., Yoshinaga, K., Shiosaka, S., Hammarback, J. A., Urano, F. and Imaizumi, K. (2006) 'Autophagy is activated for cell survival after endoplasmic reticulum stress', *Molecular and cellular biology,* 26(24), 9220-31.

Okatsu, K., Oka, T., Iguchi, M., Imamura, K., Kosako, H., Tani, N., Kimura, M., Go, E., Koyano, F., Funayama, M., Shiba-Fukushima, K., Sato, S., Shimizu, H., Fukunaga, Y., Taniguchi, H., Komatsu, M., Hattori, N., Mihara, K., Tanaka, K. and Matsuda, N. (2012) 'PINK1 autophosphorylation upon membrane

potential dissipation is essential for Parkin recruitment to damaged mitochondria', *Nature communications,* 3, 1016.

Okatsu, K., Saisho, K., Shimanuki, M., Nakada, K., Shitara, H., Sou, Y.-S. S., Kimura, M., Sato, S., Hattori, N., Komatsu, M., Tanaka, K. and Matsuda, N. (2010) 'p62/SQSTM1 cooperates with Parkin for perinuclear clustering of depolarized mitochondria', *Genes to cells : devoted to molecular & cellular mechanisms,* 15(8), 887-900.

Ola, M. S., Nawaz, M. and Ahsan, H. (2011) 'Role of Bcl-2 family proteins and caspases in the regulation of apoptosis', *Molecular and cellular biochemistry,* 351(1-2), 41-58.

Opresko, L. K., Chang, C. P., Will, B. H., Burke, P. M., Gill, G. N. and Wiley, H. S. (1995) 'Endocytosis and lysosomal targeting of epidermal growth factor receptors are mediated by distinct sequences independent of the tyrosine kinase domain', *The Journal of biological chemistry,* 270(9), 4325-33.

Orsi, A., Razi, M., Dooley, H. C., Robinson, D., Weston, A. E., Collinson, L. M. and Tooze, S. A. (2012) 'Dynamic and transient interactions of Atg9 with autophagosomes, but not membrane integration, are required for autophagy', *Molecular biology of the cell,* 23(10), 1860-73.

Padman, B. S., Bach, M., Lucarelli, G., Prescott, M. and Ramm, G. (2013) 'The protonophore CCCP interferes with lysosomal degradation of autophagic cargo in yeast and mammalian cells', *Autophagy,* 9(11), 1862-75.

Padmanabhan, J., Park, D. S., Greene, L. A. and Shelanski, M. L. (1999) 'Role of cell cycle regulatory proteins in cerebellar granule neuron apoptosis', *The Journal of neuroscience : the official journal of the Society for Neuroscience,* 19(20), 8747-56.

Pagliarini, D. J., Calvo, S. E., Chang, B., Sheth, S. A., Vafai, S. B., Ong, S. E., Walford, G. A., Sugiana, C., Boneh, A., Chen, W. K., Hill, D. E., Vidal, M., Evans, J. G., Thorburn, D. R., Carr, S. A. and Mootha, V. K. (2008) 'A mitochondrial protein compendium elucidates complex I disease biology', *Cell,* 134(1), 112-23.

Pai, M. T., Tzeng, S. R., Kovacs, J. J., Keaton, M. A., Li, S. S., Yao, T. P. and Zhou, P. (2007) 'Solution structure of the Ubp-M BUZ domain, a highly specific protein module that recognizes the C-terminal tail of free ubiquitin', *Journal of molecular biology,* 370(2), 290-302.

Park, J., Lee, S. B., Lee, S., Kim, Y., Song, S., Kim, S., Bae, E., Kim, J., Shong, M., Kim, J. M. and Chung, J. (2006) 'Mitochondrial dysfunction in Drosophila PINK1 mutants is complemented by parkin', *Nature,* 441(7097), 1157-61.

Park, K. J., Lee, S. H., Kim, T. I., Lee, H. W., Lee, C. H., Kim, E. H., Jang, J. Y., Choi, K. S., Kwon, M. H. and Kim, Y. S. (2007) 'A human scFv antibody

against TRAIL receptor 2 induces autophagic cell death in both TRAIL-sensitive and TRAIL-resistant cancer cells', *Cancer research,* 67(15), 7327-34.

Parrish, A. B., Freel, C. D. and Kornbluth, S. (2013) 'Cellular mechanisms controlling caspase activation and function', *Cold Spring Harbor perspectives in biology,* 5(6).

Pattingre, S., Bauvy, C., Carpentier, S., Levade, T., Levine, B. and Codogno, P. (2009) 'Role of JNK1-dependent Bcl-2 phosphorylation in ceramide-induced macroautophagy', *The Journal of biological chemistry,* 284(5), 2719-28.

Paul, P. K. and Kumar, A. (2011) 'TRAF6 coordinates the activation of autophagy and ubiquitin-proteasome systems in atrophying skeletal muscle', *Autophagy,* 7(5), 555-6.

Peng, J., Schwartz, D., Elias, J. E., Thoreen, C. C., Cheng, D., Marsischky, G., Roelofs, J., Finley, D. and Gygi, S. P. (2003) 'A proteomics approach to understanding protein ubiquitination', *Nature biotechnology,* 21(8), 921-6.

Peters, J.-M., Cejka, Z., Harris, R. J., Kleinschmidt, J. A. and Baumeister, W. (1993) 'Structural features of the 26 S proteasome complex', *Journal of molecular biology,* 234(4), 932-937.

Petroski, M. D. and Deshaies, R. J. (2005) 'Function and regulation of cullin-RING ubiquitin ligases', *Nature reviews. Molecular cell biology,* 6(1), 9-20.

Pickart, C. M. and Cohen, R. E. (2004) 'Proteasomes and their kin: proteases in the machine age', *Nature reviews. Molecular cell biology,* 5(3), 177-87.

Pierzynska-Mach, A., Janowski, P. A. and Dobrucki, J. W. (2014) 'Evaluation of acridine orange, LysoTracker Red, and quinacrine as fluorescent probes for long-term tracking of acidic vesicles', *Cytometry. Part A : the journal of the International Society for Analytical Cytology,* 85(8), 729-37.

Pillay, C. S., Elliott, E. and Dennison, C. (2002) 'Endolysosomal proteolysis and its regulation', *The Biochemical journal,* 363(Pt 3), 417-29.

Polson, H. E., de Lartigue, J., Rigden, D. J., Reedijk, M., Urbe, S., Clague, M. J. and Tooze, S. A. (2010) 'Mammalian Atg18 (WIPI2) localizes to omegasome-anchored phagophores and positively regulates LC3 lipidation', *Autophagy,* 6(4), 506-22.

Poole, B., Ohkuma, S. and Warburton, M. J. (1977) 'The accumulation of weakly basic substances in lysosomes and the inhibition of intracellular protein degradation', *Acta biologica et medica Germanica,* 36(11-12), 1777-88.

Proikas-Cezanne, T. and Pfisterer, S. G. (2009) 'Assessing mammalian autophagy by WIPI-1/Atg18 puncta formation', *Methods in enzymology,* 452, 247-60.

Pykett, M. J., Landers, J. and George, D. L. (1997) 'Expression patterns of the p53 tumor suppressor gene and the mdm2 proto-oncogene in human meningiomas', *Journal of neuro-oncology,* 32(1), 39-44.

Qiu, X. B., Ouyang, S. Y., Li, C. J., Miao, S., Wang, L. and Goldberg, A. L. (2006) 'hRpn13/ADRM1/GP110 is a novel proteasome subunit that binds the deubiquitinating enzyme, UCH37', *The EMBO journal,* 25(24), 5742-53.

Raasi, S., Varadan, R., Fushman, D. and Pickart, C. M. (2005) 'Diverse polyubiquitin interaction properties of ubiquitin-associated domains', *Nature structural & molecular biology,* 12(8), 708-14.

Rabinovitz, M. and Fisher, J. M. (1964) 'Characteristics of the Inhibition of Hemoglobin Synthesis in Rabbit Reticulocytes by Threo-Alpha-Amino-Beta-Chlorobutyric Acid', *Biochimica et biophysica acta,* 91, 313-22.

Rakovic, A., Shurkewitsch, K., Seibler, P., Grunewald, A., Zanon, A., Hagenah, J., Krainc, D. and Klein, C. (2013) 'Phosphatase and tensin homolog (PTEN)-induced putative kinase 1 (PINK1)-dependent ubiquitination of endogenous Parkin attenuates mitophagy: study in human primary fibroblasts and induced pluripotent stem cell-derived neurons', *The Journal of biological chemistry,* 288(4), 2223-37.

Rakovic, A., Shurkewitsch, K., Seibler, P., Grünewald, A., Zanon, A., Hagenah, J., Krainc, D. and Klein, C. (2013) 'Phosphatase and Tensin Homolog (PTEN)-induced Putative Kinase 1 (PINK1)-dependent Ubiquitination of Endogenous Parkin Attenuates Mitophagy: STUDY IN HUMAN PRIMARY FIBROBLASTS AND INDUCED PLURIPOTENT STEM CELL-DERIVED NEURONS', *The Journal of biological chemistry,* 288(4), 2223-2237.

Ramonet, D., Perier, C., Recasens, A., Dehay, B., Bove, J., Costa, V., Scorrano, L. and Vila, M. (2013) 'Optic atrophy 1 mediates mitochondria remodeling and dopaminergic neurodegeneration linked to complex I deficiency', *Cell death and differentiation,* 20(1), 77-85.

Rana, A., Rera, M. and Walker, D. W. (2013) 'Parkin overexpression during aging reduces proteotoxicity, alters mitochondrial dynamics, and extends lifespan', *Proceedings of the National Academy of Sciences of the United States of America,* 110(21), 8638-43.

Rana, A., Rera, M. and Walker, D. W. (2013) 'Parkin overexpression during aging reduces proteotoxicity, alters mitochondrial dynamics, and extends lifespan', *Proceedings of the National Academy of Sciences of the United States of America,* 110(21), 8638-8643.

Ravikumar, B., Moreau, K., Jahreiss, L., Puri, C. and Rubinsztein, D. C. (2010a) 'Plasma membrane contributes to the formation of pre-autophagosomal structures', *Nature cell biology,* 12(8), 747-57.

Ravikumar, B., Moreau, K. and Rubinsztein, D. C. (2010b) 'Plasma membrane helps autophagosomes grow', *Autophagy,* 6(8), 1184-6.

Reggiori, F., Shintani, T., Nair, U. and Klionsky, D. J. (2005) 'Atg9 cycles between mitochondria and the pre-autophagosomal structure in yeasts', *Autophagy,* 1(2), 101-9.

Reggiori, F. and Tooze, S. A. (2012) 'Autophagy regulation through Atg9 traffic', *The Journal of cell biology,* 198(2), 151-3.

Ren, Y., Zhao, J. and Feng, J. (2003) 'Parkin binds to alpha/beta tubulin and increases their ubiquitination and degradation', *The Journal of neuroscience : the official journal of the Society for Neuroscience,* 23(8), 3316-24.

Reyes-Turcu, F. E., Horton, J. R., Mullally, J. E., Heroux, A., Cheng, X. and Wilkinson, K. D. (2006) 'The ubiquitin binding domain ZnF UBP recognizes the C-terminal diglycine motif of unanchored ubiquitin', *Cell,* 124(6), 1197-208.

Riedl, S. J. and Salvesen, G. S. (2007) 'The apoptosome: signalling platform of cell death', *Nature reviews. Molecular cell biology,* 8(5), 405-13.

Riess, O., Rub, U., Pastore, A., Bauer, P. and Schols, L. (2008) 'SCA3: neurological features, pathogenesis and animal models', *Cerebellum,* 7(2), 125-37.

Riley, B. E., Lougheed, J. C., Callaway, K., Velasquez, M., Brecht, E., Nguyen, L., Shaler, T., Walker, D., Yang, Y., Regnstrom, K., Diep, L., Zhang, Z., Chiou, S., Bova, M., Artis, D. R., Yao, N., Baker, J., Yednock, T. and Johnston, J. A. (2013) 'Structure and function of Parkin E3 ubiquitin ligase reveals aspects of RING and HECT ligases', *Nature communications,* 4, 1982.

Robzyk, K., Recht, J. and Osley, M. A. (2000) 'Rad6-dependent ubiquitination of histone H2B in yeast', *Science,* 287(5452), 501-4.

Rothbauer, U., Zolghadr, K., Muyldermans, S., Schepers, A., Cardoso, M. C. and Leonhardt, H. (2008) 'A versatile nanotrap for biochemical and functional studies with fluorescent fusion proteins', *Molecular & cellular proteomics : MCP,* 7(2), 282-289.

Russell, R. C., Tian, Y., Yuan, H., Park, H. W., Chang, Y. Y., Kim, J., Kim, H., Neufeld, T. P., Dillin, A. and Guan, K. L. (2013) 'ULK1 induces autophagy by phosphorylating Beclin-1 and activating VPS34 lipid kinase', *Nature cell biology,* 15(7), 741-50.

Sacco, J. J., Yau, T. Y., Darling, S., Patel, V., Liu, H., Urbe, S., Clague, M. J. and Coulson, J. M. (2014) 'The deubiquitylase Ataxin-3 restricts PTEN transcription in lung cancer cells', *Oncogene,* 33(33), 4265-72.

Saha, A. and Deshaies, R. J. (2008) 'Multimodal activation of the ubiquitin ligase SCF by Nedd8 conjugation', *Molecular cell,* 32(1), 21-31.

Saito, M., Maruyama, M., Ikeuchi, K., Kondo, H., Ishikawa, A., Yuasa, T. and Tsuji, S. (2000) 'Autosomal recessive juvenile parkinsonism', *Brain & development,* 22 Suppl 1, S115-7.

Sancak, Y., Bar-Peled, L., Zoncu, R., Markhard, A. L., Nada, S. and Sabatini, D. M. (2010) 'Ragulator-Rag complex targets mTORC1 to the lysosomal surface and is necessary for its activation by amino acids', *Cell,* 141(2), 290-303.

Sancak, Y., Peterson, T. R., Shaul, Y. D., Lindquist, R. A., Thoreen, C. C., Bar-Peled, L. and Sabatini, D. M. (2008) 'The Rag GTPases bind raptor and mediate amino acid signaling to mTORC1', *Science,* 320(5882), 1496-501.

Sancak, Y. and Sabatini, D. M. (2009) 'Rag proteins regulate amino-acid-induced mTORC1 signalling', *Biochemical Society transactions,* 37(Pt 1), 289-90.

Sarbassov, D. D., Ali, S. M., Sengupta, S., Sheen, J. H., Hsu, P. P., Bagley, A. F., Markhard, A. L. and Sabatini, D. M. (2006) 'Prolonged rapamycin treatment inhibits mTORC2 assembly and Akt/PKB', *Molecular cell,* 22(2), 159-68.

Sarraf, S. A., Raman, M., Guarani-Pereira, V., Sowa, M. E., Huttlin, E. L., Gygi, S. P. and Harper, J. W. (2013) 'Landscape of the PARKIN-dependent ubiquitylome in response to mitochondrial depolarization', *Nature,* 496(7445), 372-376.

Sarraf, S. A., Raman, M., Guarani-Pereira, V., Sowa, M. E., Huttlin, E. L., Gygi, S. P. and Harper, J. W. (2013) 'Landscape of the PARKIN-dependent ubiquitylome in response to mitochondrial depolarization', *Nature,* 496(7445), 372-6.

Sato, Y., Yoshikawa, A., Yamagata, A., Mimura, H., Yamashita, M., Ookata, K., Nureki, O., Iwai, K., Komada, M. and Fukai, S. (2008) 'Structural basis for specific cleavage of Lys 63-linked polyubiquitin chains', *Nature,* 455(7211), 358-62.

Sawai, H. (2013) 'Differential effects of caspase inhibitors on TNF-induced necroptosis', *Biochemical and biophysical research communications,* 432(3), 451-5.

Schauber, C., Chen, L., Tongaonkar, P., Vega, I., Lambertson, D., Potts, W. and Madura, K. (1998) 'Rad23 links DNA repair to the ubiquitin/proteasome pathway', *Nature,* 391(6668), 715-8.

Scheuermann, J. C., de Ayala Alonso, A. G., Oktaba, K., Ly-Hartig, N., McGinty, R. K., Fraterman, S., Wilm, M., Muir, T. W. and Muller, J. (2010) 'Histone H2A deubiquitinase activity of the Polycomb repressive complex PR-DUB', *Nature,* 465(7295), 243-7.

Schlesinger, D. H. and Goldstein, G. (1975) 'Molecular conservation of 74 amino acid sequence of ubiquitin between cattle and man', *Nature,* 255(5507), 423-4.

Schlesinger, D. H., Goldstein, G. and Niall, H. D. (1975) 'The complete amino acid sequence of ubiquitin, an adenylate cyclase stimulating polypeptide probably universal in living cells', *Biochemistry,* 14(10), 2214-8.

Schoenheimer, R., Ratner, S. and Rittenberg, D. (1939) 'The Process of Continuous Deamination and Reamination of Amino Acids in the Proteins of Normal Animals', *Science,* 89(2308), 272-3.

Schwanhausser, B., Busse, D., Li, N., Dittmar, G., Schuchhardt, J., Wolf, J., Chen, W. and Selbach, M. (2011) 'Global quantification of mammalian gene expression control', *Nature,* 473(7347), 337-42.

Scialpi, F., Malatesta, M., Peschiaroli, A., Rossi, M., Melino, G. and Bernassola, F. (2008) 'Itch self-polyubiquitylation occurs through lysine-63 linkages', *Biochemical pharmacology,* 76(11), 1515-21.

Seki, T., Gong, L., Williams, A. J., Sakai, N., Todi, S. V. and Paulson, H. L. (2013) 'JosD1, a membrane-targeted deubiquitinating enzyme, is activated by ubiquitination and regulates membrane dynamics, cell motility, and endocytosis', *The Journal of biological chemistry,* 288(24), 17145-55.

Sha, D., Chin, L. S. and Li, L. (2010) 'Phosphorylation of parkin by Parkinson disease-linked kinase PINK1 activates parkin E3 ligase function and NF-kappaB signaling', *Human molecular genetics,* 19(2), 352-63.

Shackelford, D. B. and Shaw, R. J. (2009) 'The LKB1-AMPK pathway: metabolism and growth control in tumour suppression', *Nature reviews. Cancer,* 9(8), 563-75.

Shao, G., Lilli, D. R., Patterson-Fortin, J., Coleman, K. A., Morrissey, D. E. and Greenberg, R. A. (2009) 'The Rap80-BRCC36 de-ubiquitinating enzyme complex antagonizes RNF8-Ubc13-dependent ubiquitination events at DNA double strand breaks', *Proceedings of the National Academy of Sciences of the United States of America,* 106(9), 3166-71.

Shembade, N., Ma, A. and Harhaj, E. W. (2010) 'Inhibition of NF-kappaB signaling by A20 through disruption of ubiquitin enzyme complexes', *Science,* 327(5969), 1135-9.

Sherer, T. B., Betarbet, R. and Greenamyre, J. T. (2002a) 'Environment, mitochondria, and Parkinson's disease', *The Neuroscientist : a review journal bringing neurobiology, neurology and psychiatry,* 8(3), 192-7.

Sherer, T. B., Betarbet, R., Stout, A. K., Lund, S., Baptista, M., Panov, A. V., Cookson, M. R. and Greenamyre, J. T. (2002b) 'An in vitro model of Parkinson's disease: linking mitochondrial impairment to altered alpha-synuclein metabolism and oxidative damage', *The Journal of neuroscience : the official journal of the Society for Neuroscience,* 22(16), 7006-15.

Sherer, T. B., Betarbet, R., Testa, C. M., Seo, B. B., Richardson, J. R., Kim, J. H., Miller, G. W., Yagi, T., Matsuno-Yagi, A. and Greenamyre, J. T. (2003a) 'Mechanism of toxicity in rotenone models of Parkinson's disease', *The Journal of neuroscience : the official journal of the Society for Neuroscience,* 23(34), 10756-64.

Sherer, T. B., Kim, J. H., Betarbet, R. and Greenamyre, J. T. (2003b) 'Subcutaneous rotenone exposure causes highly selective dopaminergic degeneration and alpha-synuclein aggregation', *Experimental neurology,* 179(1), 9-16.

Shiba-Fukushima, K., Imai, Y., Yoshida, S., Ishihama, Y., Kanao, T., Sato, S. and Hattori, N. (2012) 'PINK1-mediated phosphorylation of the Parkin ubiquitin-like domain primes mitochondrial translocation of Parkin and regulates mitophagy', *Scientific reports,* 2, 1002.

Shimura, H., Schlossmacher, M. G., Hattori, N., Frosch, M. P., Trockenbacher, A., Schneider, R., Mizuno, Y., Kosik, K. S. and Selkoe, D. J. (2001) 'Ubiquitination of a new form of alpha-synuclein by parkin from human brain: implications for Parkinson's disease', *Science,* 293(5528), 263-9.

Shin, J. H., Ko, H. S., Kang, H., Lee, Y., Lee, Y. I., Pletinkova, O., Troconso, J. C., Dawson, V. L. and Dawson, T. M. (2011) 'PARIS (ZNF746) repression of PGC-1alpha contributes to neurodegeneration in Parkinson's disease', *Cell,* 144(5), 689-702.

Shintani, T. and Klionsky, D. J. (2004) 'Autophagy in health and disease: a double-edged sword', *Science,* 306(5698), 990-5.

Sims, J. J. and Cohen, R. E. (2009) 'Linkage-specific avidity defines the lysine 63-linked polyubiquitin-binding preference of rap80', *Molecular cell,* 33(6), 775-83.

Sledz, P., Forster, F. and Baumeister, W. (2013a) 'Allosteric effects in the regulation of 26S proteasome activities', *Journal of molecular biology,* 425(9), 1415-23.

Sledz, P., Unverdorben, P., Beck, F., Pfeifer, G., Schweitzer, A., Forster, F. and Baumeister, W. (2013b) 'Structure of the 26S proteasome with ATP-gammaS bound provides insights into the mechanism of nucleotide-dependent substrate translocation', *Proceedings of the National Academy of Sciences of the United States of America,* 110(18), 7264-9.

Slee, E. A., Adrain, C. and Martin, S. J. (2001) 'Executioner caspase-3, -6, and -7 perform distinct, non-redundant roles during the demolition phase of apoptosis', *The Journal of biological chemistry,* 276(10), 7320-6.

Slee, E. A., Zhu, H., Chow, S. C., MacFarlane, M., Nicholson, D. W. and Cohen, G. M. (1996) 'Benzyloxycarbonyl-Val-Ala-Asp (OMe) fluoromethylketone (Z-VAD.FMK) inhibits apoptosis by blocking the processing of CPP32', *The Biochemical journal,* 315 (Pt 1), 21-24.

Smogorzewska, A., Matsuoka, S., Vinciguerra, P., McDonald, E. R., 3rd, Hurov, K. E., Luo, J., Ballif, B. A., Gygi, S. P., Hofmann, K., D'Andrea, A. D. and Elledge, S. J. (2007) 'Identification of the FANCI protein, a monoubiquitinated FANCD2 paralog required for DNA repair', *Cell,* 129(2), 289-301.

Sobhian, B., Shao, G., Lilli, D. R., Culhane, A. C., Moreau, L. A., Xia, B., Livingston, D. M. and Greenberg, R. A. (2007) 'RAP80 targets BRCA1 to specific ubiquitin structures at DNA damage sites', *Science,* 316(5828), 1198-202.

Sohn, D., Schulze-Osthoff, K. and Janicke, R. U. (2005) 'Caspase-8 can be activated by interchain proteolysis without receptor-triggered dimerization during drug-induced apoptosis', *The Journal of biological chemistry,* 280(7), 5267-73.

Spratt, D. E., Martinez-Torres, R. J., Noh, Y. J., Mercier, P., Manczyk, N., Barber, K. R., Aguirre, J. D., Burchell, L., Purkiss, A., Walden, H. and Shaw, G. S. (2013) 'A molecular explanation for the recessive nature of parkin-linked Parkinson's disease', *Nature communications,* 4, 1983.

Srivastava, D. and Chakrabarti, O. (2014) 'Mahogunin-mediated alpha-tubulin ubiquitination via noncanonical K6 linkage regulates microtubule stability and mitotic spindle orientation', *Cell death & disease,* 5, e1064.

St-Pierre, J., Drori, S., Uldry, M., Silvaggi, J. M., Rhee, J., Jager, S., Handschin, C., Zheng, K., Lin, J., Yang, W., Simon, D. K., Bachoo, R. and Spiegelman, B. M. (2006) 'Suppression of reactive oxygen species and neurodegeneration by the PGC-1 transcriptional coactivators', *Cell,* 127(2), 397-408.

Stack, J. H., Horazdovsky, B. and Emr, S. D. (1995) 'Receptor-mediated protein sorting to the vacuole in yeast: roles for a protein kinase, a lipid kinase

and GTP-binding proteins', *Annual review of cell and developmental biology,* 11, 1-33.

Storer, A. C. and Menard, R. (1994) 'Catalytic mechanism in papain family of cysteine peptidases', *Methods in enzymology,* 244, 486-500.

Su, W. C., Chao, T. C., Huang, Y. L., Weng, S. C., Jeng, K. S. and Lai, M. M. (2011) 'Rab5 and class III phosphoinositide 3-kinase Vps34 are involved in hepatitis C virus NS4B-induced autophagy', *Journal of virology,* 85(20), 10561-71.

Sulston, J. E. and Horvitz, H. R. (1977) 'Post-embryonic cell lineages of the nematode, Caenorhabditis elegans', *Developmental biology,* 56(1), 110-156.

Sulston, J. E., Schierenberg, E., White, J. G. and Thomson, J. N. (1983) 'The embryonic cell lineage of the nematode Caenorhabditis elegans', *Developmental biology,* 100(1), 64-119.

Sun, Q., Fan, W., Chen, K., Ding, X., Chen, S. and Zhong, Q. (2008) 'Identification of Barkor as a mammalian autophagy-specific factor for Beclin 1 and class III phosphatidylinositol 3-kinase', *Proceedings of the National Academy of Sciences of the United States of America,* 105(49), 19211-6.

Sun, X. M., MacFarlane, M., Zhuang, J., Wolf, B. B., Green, D. R. and Cohen, G. M. (1999) 'Distinct caspase cascades are initiated in receptor-mediated and chemical-induced apoptosis', *The Journal of biological chemistry,* 274(8), 5053-5060.

Sun, Y., Vashisht, A. A., Tchieu, J., Wohlschlegel, J. A. and Dreier, L. (2012) 'Voltage-dependent anion channels (VDACs) recruit Parkin to defective mitochondria to promote mitochondrial autophagy', *The Journal of biological chemistry,* 287(48), 40652-60.

Suzuki, M., Youle, R. J. and Tjandra, N. (2000) 'Structure of Bax: coregulation of dimer formation and intracellular localization', *Cell,* 103(4), 645-54.

Takahashi, Y., Coppola, D., Matsushita, N., Cualing, H. D., Sun, M., Sato, Y., Liang, C., Jung, J. U., Cheng, J. Q., Mule, J. J., Pledger, W. J. and Wang, H. G. (2007) 'Bif-1 interacts with Beclin 1 through UVRAG and regulates autophagy and tumorigenesis', *Nature cell biology,* 9(10), 1142-51.

Takahashi, Y., Meyerkord, C. L., Hori, T., Runkle, K., Fox, T. E., Kester, M., Loughran, T. P. and Wang, H. G. (2011) 'Bif-1 regulates Atg9 trafficking by mediating the fission of Golgi membranes during autophagy', *Autophagy,* 7(1), 61-73.

Tanaka, A., Cleland, M. M., Xu, S., Narendra, D. P., Suen, D. F., Karbowski, M. and Youle, R. J. (2010) 'Proteasome and p97 mediate mitophagy and degradation of mitofusins induced by Parkin', *The Journal of cell biology,* 191(7), 1367-80.

Tanaka, K., Waxman, L. and Goldberg, A. L. (1983) 'ATP serves two distinct roles in protein degradation in reticulocytes, one requiring and one independent of ubiquitin', *The Journal of cell biology,* 96(6), 1580-1585.

Tanner, C. M., Kamel, F., Ross, G. W., Hoppin, J. A., Goldman, S. M., Korell, M., Marras, C., Bhudhikanok, G. S., Kasten, M., Chade, A. R., Comyns, K., Richards, M. B., Meng, C., Priestley, B., Fernandez, H. H., Cambi, F., Umbach, D. M., Blair, A., Sandler, D. P. and Langston, J. W. (2011) 'Rotenone, paraquat, and Parkinson's disease', *Environmental health perspectives,* 119(6), 866-72.

Tauriello, D. V., Haegebarth, A., Kuper, I., Edelmann, M. J., Henraat, M., Canninga-van Dijk, M. R., Kessler, B. M., Clevers, H. and Maurice, M. M. (2010) 'Loss of the tumor suppressor CYLD enhances Wnt/beta-catenin signaling through K63-linked ubiquitination of Dvl', *Molecular cell,* 37(5), 607-19.

Terrell, J., Shih, S., Dunn, R. and Hicke, L. (1998) 'A function for monoubiquitination in the internalization of a G protein-coupled receptor', *Molecular cell,* 1(2), 193-202.

Tewari, M., Quan, L. T., O'Rourke, K., Desnoyers, S., Zeng, Z., Beidler, D. R., Poirier, G. G., Salvesen, G. S. and Dixit, V. M. (1995) 'Yama/CPP32 beta, a mammalian homolog of CED-3, is a CrmA-inhibitable protease that cleaves the death substrate poly(ADP-ribose) polymerase', *Cell,* 81(5), 801-9.

Thumm, M., Egner, R., Koch, B., Schlumpberger, M., Straub, M., Veenhuis, M. and Wolf, D. H. (1994) 'Isolation of autophagocytosis mutants of Saccharomyces cerevisiae', *FEBS letters,* 349(2), 275-80.

Tokunaga, F. and Iwai, K. (2009) '[Involvement of LUBAC-mediated linear polyubiquitination of NEMO in NF-kappaB activation]', *Tanpakushitsu kakusan koso. Protein, nucleic acid, enzyme,* 54(5), 635-42.

Tokunaga, F., Sakata, S., Saeki, Y., Satomi, Y., Kirisako, T., Kamei, K., Nakagawa, T., Kato, M., Murata, S., Yamaoka, S., Yamamoto, M., Akira, S., Takao, T., Tanaka, K. and Iwai, K. (2009) 'Involvement of linear polyubiquitylation of NEMO in NF-kappaB activation', *Nature cell biology,* 11(2), 123-32.

Tran, H., Hamada, F., Schwarz-Romond, T. and Bienz, M. (2008) 'Trabid, a new positive regulator of Wnt-induced transcription with preference for binding and cleaving K63-linked ubiquitin chains', *Genes & development,* 22(4), 528-42.

Trempe, J. F., Sauve, V., Grenier, K., Seirafi, M., Tang, M. Y., Menade, M., Al-Abdul-Wahid, S., Krett, J., Wong, K., Kozlov, G., Nagar, B., Fon, E. A. and Gehring, K. (2013) 'Structure of parkin reveals mechanisms for ubiquitin ligase activation', *Science,* 340(6139), 1451-5.

Trencia, A., Fiory, F., Maitan, M. A., Vito, P., Barbagallo, A. P., Perfetti, A., Miele, C., Ungaro, P., Oriente, F., Cilenti, L., Zervos, A. S., Formisano, P. and Beguinot, F. (2004) 'Omi/HtrA2 promotes cell death by binding and degrading the anti-apoptotic protein ped/pea-15', *The Journal of biological chemistry,* 279(45), 46566-72.

Trompouki, E., Hatzivassiliou, E., Tsichritzis, T., Farmer, H., Ashworth, A. and Mosialos, G. (2003) 'CYLD is a deubiquitinating enzyme that negatively regulates NF-kappaB activation by TNFR family members', *Nature,* 424(6950), 793-6.

Trump, B. F. and Berezesky, I. K. (1995) 'Calcium-mediated cell injury and cell death', *FASEB journal : official publication of the Federation of American Societies for Experimental Biology,* 9(2), 219-228.

Tsukada, M. and Ohsumi, Y. (1993) 'Isolation and characterization of autophagy-defective mutants of Saccharomyces cerevisiae', *FEBS letters,* 333(1-2), 169-74.

Van Humbeeck, C., Cornelissen, T., Hofkens, H., Mandemakers, W., Gevaert, K., De Strooper, B. and Vandenberghe, W. (2011a) 'Parkin interacts with Ambra1 to induce mitophagy', *The Journal of neuroscience : the official journal of the Society for Neuroscience,* 31(28), 10249-10261.

Van Humbeeck, C., Cornelissen, T. and Vandenberghe, W. (2011b) 'Ambra1: a Parkin-binding protein involved in mitophagy', *Autophagy,* 7(12), 1555-1556.

van Nocker, S., Sadis, S., Rubin, D. M., Glickman, M., Fu, H., Coux, O., Wefes, I., Finley, D. and Vierstra, R. D. (1996) 'The multiubiquitin-chain-binding protein Mcb1 is a component of the 26S proteasome in Saccharomyces cerevisiae and plays a nonessential, substrate-specific role in protein turnover', *Molecular and cellular biology,* 16(11), 6020-8.

Vanhaesebroeck, B. and Waterfield, M. D. (1999) 'Signaling by distinct classes of phosphoinositide 3-kinases', *Experimental cell research,* 253(1), 239-54.

Verhagen, A. M., Ekert, P. G., Pakusch, M., Silke, J., Connolly, L. M., Reid, G. E., Moritz, R. L., Simpson, R. J. and Vaux, D. L. (2000) 'Identification of DIABLO, a mammalian protein that promotes apoptosis by binding to and antagonizing IAP proteins', *Cell,* 102(1), 43-53.

Verma, R., Oania, R., Graumann, J. and Deshaies, R. J. (2004) 'Multiubiquitin chain receptors define a layer of substrate selectivity in the ubiquitin-proteasome system', *Cell,* 118(1), 99-110.

Vijay-Kumar, S., Bugg, C. E. and Cook, W. J. (1987) 'Structure of ubiquitin refined at 1.8 A resolution', *Journal of molecular biology,* 194(3), 531-44.

Virdee, S., Ye, Y., Nguyen, D. P., Komander, D. and Chin, J. W. (2010) 'Engineered diubiquitin synthesis reveals Lys29-isopeptide specificity of an OTU deubiquitinase', *Nature chemical biology,* 6(10), 750-7.

Viswanath, V., Wu, Y., Boonplueang, R., Chen, S., Stevenson, F. F., Yantiri, F., Yang, L., Beal, M. F. and Andersen, J. K. (2001) 'Caspase-9 activation results in downstream caspase-8 activation and bid cleavage in 1-methyl-4-phenyl-1,2,3,6-tetrahydropyridine-induced Parkinson's disease', *The Journal of neuroscience : the official journal of the Society for Neuroscience,* 21(24), 9519-28.

Vives-Bauza, C., de Vries, R. L., Tocilescu, M. and Przedborski, S. (2010a) 'PINK1/Parkin direct mitochondria to autophagy', *Autophagy,* 6(2), 315-6.

Vives-Bauza, C., Zhou, C., Huang, Y., Cui, M., de Vries, R. L., Kim, J., May, J., Tocilescu, M. A., Liu, W., Ko, H. S., Magrane, J., Moore, D. J., Dawson, V. L., Grailhe, R., Dawson, T. M., Li, C., Tieu, K. and Przedborski, S. (2010b) 'PINK1-dependent recruitment of Parkin to mitochondria in mitophagy', *Proceedings of the National Academy of Sciences of the United States of America,* 107(1), 378-83.

Voges, D., Zwickl, P. and Baumeister, W. (1999) 'The 26S proteasome: a molecular machine designed for controlled proteolysis', *Annual review of biochemistry,* 68, 1015-68.

Wachmann, K., Pop, C., van Raam, B. J., Drag, M., Mace, P. D., Snipas, S. J., Zmasek, C., Schwarzenbacher, R., Salvesen, G. S. and Riedl, S. J. (2010) 'Activation and specificity of human caspase-10', *Biochemistry,* 49(38), 8307-15.

Wang, B., Matsuoka, S., Ballif, B. A., Zhang, D., Smogorzewska, A., Gygi, S. P. and Elledge, S. J. (2007) 'Abraxas and RAP80 form a BRCA1 protein complex required for the DNA damage response', *Science,* 316(5828), 1194-8.

Wang, C. W. and Klionsky, D. J. (2003) 'The molecular mechanism of autophagy', *Molecular medicine,* 9(3-4), 65-76.

Wang, L., Narasaki, R., Kitano, Y. and Hasumi, K. (2009) 'Ascorbic acid conversion to erythroascorbic acid, mediated by ubiquitin', *Biochemical and biophysical research communications,* 384(2), 210-4.

Wang, L., Yokoyama, K., Miyaji, M. and Nishimura, K. (2000) 'Mitochondrial cytochrome b gene analysis of Aspergillus fumigatus and related species', *Journal of clinical microbiology,* 38(4), 1352-8.

Wang, P., Yu, J. and Zhang, L. (2007) 'The nuclear function of p53 is required for PUMA-mediated apoptosis induced by DNA damage', *Proceedings of the National Academy of Sciences of the United States of America,* 104(10), 4054-9.

Wang, T., Yin, L., Cooper, E. M., Lai, M. Y., Dickey, S., Pickart, C. M., Fushman, D., Wilkinson, K. D., Cohen, R. E. and Wolberger, C. (2009) 'Evidence for bidentate substrate binding as the basis for the K48 linkage specificity of otubain 1', *Journal of molecular biology,* 386(4), 1011-23.

Wang, X., Winter, D., Ashrafi, G., Schlehe, J., Wong, Y. L., Selkoe, D., Rice, S., Steen, J., LaVoie, M. J. and Schwarz, T. L. (2011) 'PINK1 and Parkin target Miro for phosphorylation and degradation to arrest mitochondrial motility', *Cell,* 147(4), 893-906.

Wauer, T. and Komander, D. (2013) 'Structure of the human Parkin ligase domain in an autoinhibited state', *The EMBO journal,* 32(15), 2099-112.

Wei, M. C., Lindsten, T., Mootha, V. K., Weiler, S., Gross, A., Ashiya, M., Thompson, C. B. and Korsmeyer, S. J. (2000) 'tBID, a membrane-targeted death ligand, oligomerizes BAK to release cytochrome c', *Genes & development,* 14(16), 2060-71.

Wenzel, D. M., Lissounov, A., Brzovic, P. S. and Klevit, R. E. (2011a) 'UBCH7 reactivity profile reveals parkin and HHARI to be RING/HECT hybrids', *Nature,* 474(7349), 105-8.

Wenzel, D. M., Stoll, K. E. and Klevit, R. E. (2011b) 'E2s: structurally economical and functionally replete', *The Biochemical journal,* 433(1), 31-42.

Wertz, I. E., O'Rourke, K. M., Zhou, H., Eby, M., Aravind, L., Seshagiri, S., Wu, P., Wiesmann, C., Baker, R., Boone, D. L., Ma, A., Koonin, E. V. and Dixit, V. M. (2004) 'De-ubiquitination and ubiquitin ligase domains of A20 downregulate NF-kappaB signalling', *Nature,* 430(7000), 694-9.

Whitby, F. G., Masters, E. I., Kramer, L., Knowlton, J. R., Yao, Y., Wang, C. C. and Hill, C. P. (2000) 'Structural basis for the activation of 20S proteasomes by 11S regulators', *Nature,* 408(6808), 115-20.

White, M. F. (1998) 'The IRS-signalling system: a network of docking proteins that mediate insulin action', *Molecular and cellular biochemistry,* 182(1-2), 3-11.

Whitworth, A. J., Lee, J. R., Ho, V. M., Flick, R., Chowdhury, R. and McQuibban, G. A. (2008) 'Rhomboid-7 and HtrA2/Omi act in a common pathway with the Parkinson's disease factors Pink1 and Parkin', *Disease models & mechanisms,* 1(2-3), 168-74; discussion 173.

Wiborg, O., Pedersen, M. S., Wind, A., Berglund, L. E., Marcker, K. A. and Vuust, J. (1985) 'The human ubiquitin multigene family: some genes contain multiple directly repeated ubiquitin coding sequences', *The EMBO journal,* 4(3), 755-9.

Wilkinson, K. D., Urban, M. K. and Haas, A. L. (1980) 'Ubiquitin is the ATP-dependent proteolysis factor I of rabbit reticulocytes', *The Journal of biological chemistry,* 255(16), 7529-32.

Williams, A. J. and Paulson, H. L. (2008) 'Polyglutamine neurodegeneration: protein misfolding revisited', *Trends in neurosciences,* 31(10), 521-8.

Williams, R. L. and Urbe, S. (2007) 'The emerging shape of the ESCRT machinery', *Nature reviews. Molecular cell biology,* 8(5), 355-68.

Winborn, B. J., Travis, S. M., Todi, S. V., Scaglione, K. M., Xu, P., Williams, A. J., Cohen, R. E., Peng, J. and Paulson, H. L. (2008) 'The deubiquitinating enzyme ataxin-3, a polyglutamine disease protein, edits Lys63 linkages in mixed linkage ubiquitin chains', *The Journal of biological chemistry,* 283(39), 26436-43.

Winklhofer, K. F. (2014) 'Parkin and mitochondrial quality control: toward assembling the puzzle', *Trends in cell biology,* 24(6), 332-41.

Wong, E. and Cuervo, A. M. (2010) 'Integration of clearance mechanisms: the proteasome and autophagy', *Cold Spring Harbor perspectives in biology,* 2(12), a006734.

Woodroof, H. I., Pogson, J. H., Begley, M., Cantley, L. C., Deak, M., Campbell, D. G., van Aalten, D. M., Whitworth, A. J., Alessi, D. R. and Muqit, M. M. (2011) 'Discovery of catalytically active orthologues of the Parkinson's disease kinase PINK1: analysis of substrate specificity and impact of mutations', *Open biology,* 1(3), 110012.

Xie, H. R., Hu, L. S. and Li, G. Y. (2010) 'SH-SY5Y human neuroblastoma cell line: in vitro cell model of dopaminergic neurons in Parkinson's disease', *Chinese medical journal,* 123(8), 1086-92.

Xu, P., Duong, D. M., Seyfried, N. T., Cheng, D., Xie, Y., Robert, J., Rush, J., Hochstrasser, M., Finley, D. and Peng, J. (2009) 'Quantitative proteomics reveals the function of unconventional ubiquitin chains in proteasomal degradation', *Cell,* 137(1), 133-45.

Xu, S., Peng, G., Wang, Y., Fang, S. and Karbowski, M. (2011) 'The AAA-ATPase p97 is essential for outer mitochondrial membrane protein turnover', *Molecular biology of the cell,* 22(3), 291-300.

Yamano, K. and Youle, R. J. (2013) 'PINK1 is degraded through the N-end rule pathway', *Autophagy,* 9(11), 1758-1769.

Yang, J., Liu, X., Bhalla, K., Kim, C. N., Ibrado, A. M., Cai, J., Peng, T. I., Jones, D. P. and Wang, X. (1997) 'Prevention of apoptosis by Bcl-2: release of cytochrome c from mitochondria blocked', *Science,* 275(5303), 1129-32.

Yang, Q., Inoki, K., Kim, E. and Guan, K. L. (2006) 'TSC1/TSC2 and Rheb have different effects on TORC1 and TORC2 activity', *Proceedings of the National Academy of Sciences of the United States of America,* 103(18), 6811-6.

Yang, Y., Gehrke, S., Imai, Y., Huang, Z., Ouyang, Y., Wang, J. W., Yang, L., Beal, M. F., Vogel, H. and Lu, B. (2006) 'Mitochondrial pathology and muscle and dopaminergic neuron degeneration caused by inactivation of Drosophila Pink1 is rescued by Parkin', *Proceedings of the National Academy of Sciences of the United States of America,* 103(28), 10793-8.

Yang, Z. and Klionsky, D. J. (2010) 'Eaten alive: a history of macroautophagy', *Nature cell biology,* 12(9), 814-22.

Yao, T. and Cohen, R. E. (2002) 'A cryptic protease couples deubiquitination and degradation by the proteasome', *Nature,* 419(6905), 403-7.

Yao, T., Song, L., Xu, W., DeMartino, G. N., Florens, L., Swanson, S. K., Washburn, M. P., Conaway, R. C., Conaway, J. W. and Cohen, R. E. (2006) 'Proteasome recruitment and activation of the Uch37 deubiquitinating enzyme by Adrm1', *Nature cell biology,* 8(9), 994-1002.

Ye, Y., Akutsu, M., Reyes-Turcu, F., Enchev, R. I., Wilkinson, K. D. and Komander, D. (2011) 'Polyubiquitin binding and cross-reactivity in the USP domain deubiquitinase USP21', *EMBO reports,* 12(4), 350-7.

Yee, K. S. and Vousden, K. H. (2008) 'Contribution of membrane localization to the apoptotic activity of PUMA', *Apoptosis : an international journal on programmed cell death,* 13(1), 87-95.

Yoshii, S. R., Kishi, C., Ishihara, N. and Mizushima, N. (2011) 'Parkin mediates proteasome-dependent protein degradation and rupture of the outer mitochondrial membrane', *The Journal of biological chemistry,* 286(22), 19630-19640.

You, J. and Pickart, C. M. (2001) 'A HECT domain E3 enzyme assembles novel polyubiquitin chains', *The Journal of biological chemistry,* 276(23), 19871-8.

Young, A. R., Chan, E. Y., Hu, X. W., Kochl, R., Crawshaw, S. G., High, S., Hailey, D. W., Lippincott-Schwartz, J. and Tooze, S. A. (2006) 'Starvation and ULK1-dependent cycling of mammalian Atg9 between the TGN and endosomes', *Journal of cell science,* 119(Pt 18), 3888-900.

Young, P., Deveraux, Q., Beal, R. E., Pickart, C. M. and Rechsteiner, M. (1998) 'Characterization of two polyubiquitin binding sites in the 26 S protease subunit 5a', *The Journal of biological chemistry,* 273(10), 5461-7.

Yu, J., Zhang, Y., McIlroy, J., Rordorf-Nikolic, T., Orr, G. A. and Backer, J. M. (1998) 'Regulation of the p85/p110 phosphatidylinositol 3'-kinase: stabilization

and inhibition of the p110alpha catalytic subunit by the p85 regulatory subunit', *Molecular and cellular biology,* 18(3), 1379-87.

Zamaraeva, M. V., Sabirov, R. Z., Maeno, E., Ando-Akatsuka, Y., Bessonova, S. V. and Okada, Y. (2005) 'Cells die with increased cytosolic ATP during apoptosis: a bioluminescence study with intracellular luciferase', *Cell death and differentiation,* 12(11), 1390-7.

Zhang, C., Lee, S., Peng, Y., Bunker, E., Giaime, E., Shen, J., Zhou, Z. and Liu, X. (2014) 'PINK1 Triggers Autocatalytic Activation of Parkin to Specify Cell Fate Decisions', *Current biology : CB,* 24(16), 1854-65.

Zhang, D., Chen, T., Ziv, I., Rosenzweig, R., Matiuhin, Y., Bronner, V., Glickman, M. H. and Fushman, D. (2009) 'Together, Rpn10 and Dsk2 can serve as a polyubiquitin chain-length sensor', *Molecular cell,* 36(6), 1018-33.

Zhang, Y., Gao, J., Chung, K. K., Huang, H., Dawson, V. L. and Dawson, T. M. (2000) 'Parkin functions as an E2-dependent ubiquitin- protein ligase and promotes the degradation of the synaptic vesicle-associated protein, CDCrel-1', *Proceedings of the National Academy of Sciences of the United States of America,* 97(24), 13354-9.

Zhao, J., Ren, Y., Jiang, Q. and Feng, J. (2003) 'Parkin is recruited to the centrosome in response to inhibition of proteasomes', *Journal of cell science,* 116(Pt 19), 4011-9.

Zheng, N., Schulman, B. A., Song, L., Miller, J. J., Jeffrey, P. D., Wang, P., Chu, C., Koepp, D. M., Elledge, S. J., Pagano, M., Conaway, R. C., Conaway, J. W., Harper, J. W. and Pavletich, N. P. (2002) 'Structure of the Cul1-Rbx1-Skp1-F boxSkp2 SCF ubiquitin ligase complex', *Nature,* 416(6882), 703-9.

Zhong, Y., Wang, Q. J., Li, X., Yan, Y., Backer, J. M., Chait, B. T., Heintz, N. and Yue, Z. (2009) 'Distinct regulation of autophagic activity by Atg14L and Rubicon associated with Beclin 1-phosphatidylinositol-3-kinase complex', *Nature cell biology,* 11(4), 468-76.

Zhou, Q., Zhao, J., Stout, J. G., Luhm, R. A., Wiedmer, T. and Sims, P. J. (1997) 'Molecular cloning of human plasma membrane phospholipid scramblase. A protein mediating transbilayer movement of plasma membrane phospholipids', *The Journal of biological chemistry,* 272(29), 18240-4.

Zhou, Z. R., Zhang, Y. H., Liu, S., Song, A. X. and Hu, H. Y. (2012) 'Length of the active-site crossover loop defines the substrate specificity of ubiquitin C-terminal hydrolases for ubiquitin chains', *The Biochemical journal,* 441(1), 143-9.

Zhu, P., Zhou, W., Wang, J., Puc, J., Ohgi, K. A., Erdjument-Bromage, H., Tempst, P., Glass, C. K. and Rosenfeld, M. G. (2007) 'A histone H2A deubiquitinase complex coordinating histone acetylation and H1 dissociation in transcriptional regulation', *Molecular cell,* 27(4), 609-21.

Zhu, X., Ménard, R. and Sulea, T. (2007) 'High incidence of ubiquitin-like domains in human ubiquitin-specific proteases', *Proteins: Structure, Function, and Bioinformatics,* 69(1), 1-7.

Ziviani, E., Tao, R. N. and Whitworth, A. J. (2010) 'Drosophila parkin requires PINK1 for mitochondrial translocation and ubiquitinates mitofusin', *Proceedings of the National Academy of Sciences of the United States of America,* 107(11), 5018-23.

Ziviani, E. and Whitworth, A. J. (2010) 'How could Parkin-mediated ubiquitination of mitofusin promote mitophagy?', *Autophagy,* 6(5), 660-2.

Zoncu, R., Bar-Peled, L., Efeyan, A., Wang, S., Sancak, Y. and Sabatini, D. M. (2011a) 'mTORC1 senses lysosomal amino acids through an inside-out mechanism that requires the vacuolar H(+)-ATPase', *Science,* 334(6056), 678-83.

Zoncu, R., Efeyan, A. and Sabatini, D. M. (2011b) 'mTOR: from growth signal integration to cancer, diabetes and ageing', *Nature reviews. Molecular cell biology,* 12(1), 21-35.

Zou, H., Yang, R., Hao, J., Wang, J., Sun, C., Fesik, S. W., Wu, J. C., Tomaselli, K. J. and Armstrong, R. C. (2003) 'Regulation of the Apaf-1/caspase-9 apoptosome by caspase-3 and XIAP', *The Journal of biological chemistry,* 278(10), 8091-8.

Appendices

Supplementary table 1 DUB siRNA oligo sequences used for DUB screen.

Gene	Plate Id	Product Id	siRNA Target Sequence	Row	Col
ATXN3	oligo 1	SI00071113	TACGATGGGATCATTATTTCA	H	5
ATXN3	oligo 2	SI00071134	TGCGTCGGTTGTAGGACTAAA	H	5
ATXN3	oligo 3	SI05185068	CTGCTGCAGGTAAACTCTATA	H	5
ATXN3	oligo 4	SI05185075	ATGGATATATATGTGACCCTA	H	5
ATXN3L	oligo 1	SI05002795	CAAGGAGACATTCAGCAATTA	H	6
ATXN3L	oligo 2	SI05002802	CTGTGTGATTATACTGTAGGA	H	6
ATXN3L	oligo 3	SI03027290	AACAAGTTCGAGAGCAATTGA	H	6
ATXN3L	oligo 4	SI03052833	CAACACTGGTTTACTATTAGA	H	6
BAP1	oligo 1	SI00066696	CAGCAGCTGATAAGAGTAACA	A	4
BAP1	oligo 2	SI00066703	CTCAATTCCTCTGTCCATCAA	A	4
BAP1	oligo 3	SI00066710	CCCGCTGGTGCTGGAAGCAAA	A	4
BAP1	oligo 4	SI03036390	AAGGTGAACCGTCAGACAGTA	A	4
BRCC3	oligo 1	SI03109456	TACGACGTTCTGATAAGAGGA	G	5
BRCC3	oligo 2	SI00136136	TACGATGTTGATTATAACATT	G	5
BRCC3	oligo 3	SI00136143	CAGATTGAGATGAATTTGCAA	G	5
BRCC3	oligo 4	SI00136150	CAGCATTTGCAGGAATTACAA	G	5
C14orf28	oligo 1	SI00319739	AAGAGATCAAAGCATCAATTA	H	10
C14orf28	oligo 2	SI04230786	CACCTGATTGCATGAACTGAA	H	10
C14orf28	oligo 3	SI04305301	AGCAGCGCACAATTAATATAA	H	10
C14orf28	oligo 4	SI04333497	CCCTACCTCACTATAATCCAA	H	10
COPS5	oligo 1	SI05031488	AAGGTGCTCTGAAGTGTCCTA	G	6
COPS5	oligo 2	SI05031495	CTGAGAAGTACTTTACCTGAA	G	6
COPS5	oligo 3	SI00092274	TAGGACATACCCAAAGGGCTA	G	6
COPS5	oligo 4	SI03030832	AAGAACAATATCCGCAGGGAA	G	6
COPS6	oligo 1	SI00092204	CCCAACCTTATAAACATGATA	G	7
COPS6	oligo 2	SI05079354	AAACATGATAATTGACTACTT	G	7
COPS6	oligo 3	SI00092225	CCCGGTGCTCAGCACAGACAA	G	7
COPS6	oligo 4	SI03081169	CCGCGTCAAGCTCATCTTGGA	G	7
CYLD	oligo 1	SI00110082	AAGGGTAGAACCTTTGCTAAA	F	1
CYLD	oligo 2	SI00110089	AAAGAACGATGTAGAATATTA	F	1
CYLD	oligo 3	SI00110096	AAGGTTCATCCAGTCATAATA	F	1
CYLD	oligo 4	SI03056949	CACCAAGATGCCCAATACCAA	F	1
EIF3F	oligo 1	SI05017635	CAGTTGTGTGTGACTCTAATA	G	9
EIF3F	oligo 2	SI05017642	CACACTGAGATAGTCAGTTGT	G	9
EIF3F	oligo 3	SI00055482	TACGCGTACTACGACACTGAA	G	9
EIF3F	oligo 4	SI02631811	CACAATGAGTCAGAAGATGAA	G	9
EIF3H	oligo 1	SI00300111	GCGGAGCCTTCGCCATGTAAA	G	8
EIF3H	oligo 2	SI05062911	AACAGTGTCTTTCTAGCCATA	G	8
EIF3H	oligo 3	SI05062918	CACAGAGGATTTCTTTAGTGT	G	8
EIF3H	oligo 4	SI04341379	ATGCGGAGCCTTCGCCATGTA	G	8
FAM105B	oligo 1	SI03130897	AAGCGGAAGCATACGGGAATA	H	9
FAM105B	oligo 2	SI04193392	GGGCATCAGAACCGAGATTAA	H	9
FAM105B	oligo 3	SI04221196	CTGAGGACGATCGGCACTATA	H	9
FAM105B	oligo 4	SI04330046	AACATCGATCAGTACAAGGAA	H	9
JOSD1	oligo 1	SI03099908	CTGGTGGTACCAGAAGAGGTA	H	7
JOSD1	oligo 2	SI05098051	TGGGATATGCAAAGACGCTTA	H	7

JOSD1	oligo 3	SI05098058	CAGCGTTGGGTGAGGAAAGTA	H	7
JOSD1	oligo 4	SI02640988	CAACCTCGACTCCAAACTCAA	H	7
JOSD2	oligo 1	SI03075541	CCAGGTGGACGGTGTCTACTA	H	8
JOSD2	oligo 2	SI00150528	CTGCCGCTGCTGCCTCAATAA	H	8
JOSD2	oligo 3	SI00150535	CTGGGAAAGGCCAGCACTTCA	H	8
JOSD2	oligo 4	SI02648009	ACCGGCAACTATGATGTCAAT	H	8
MPND	oligo 1	SI02779231	TCAGGTAATAAAGAAACGGAA	H	2
MPND	oligo 2	SI02779238	CCGGATGGGCTCAGGTAATAA	H	2
MPND	oligo 3	SI00144760	ACGGAGTGAGGTCGTGGGTTA	H	2
MPND	oligo 4	SI00144767	CACCTACCTCGACAAGCTTAA	H	2
MYSM1	oligo 1	SI04166358	TATAATCGAAATAATCCCTTA	H	4
MYSM1	oligo 2	SI04170803	AAGACCGGCCATAATCTTCAA	H	4
MYSM1	oligo 3	SI04332846	TGGGATGATTGTTAGTCCCTA	H	4
MYSM1	oligo 4	SI04371409	GAGGCGGATGTGGATATCGAA	H	4
OTUB1	oligo 1	SI00676039	CAGCAGGACCGAATTCAGCAA	F	3
OTUB1	oligo 2	SI00676053	CACTACGATATCCTCTACAAA	F	3
OTUB1	oligo 3	SI00676060	CTGCCAGGCGCTAGACATGTA	F	3
OTUB1	oligo 4	SI04168038	CTCCGACTACCTTGTGGTCTA	F	3
OTUB2	oligo 1	SI03246775	CAGGGAGATCTTCAAGTTCAA	F	4
OTUB2	oligo 2	SI05031740	CAGATGGCCTATTGAGGTCAA	F	4
OTUB2	oligo 3	SI00676074	CAGCCGATAAACATTGATTAA	F	4
OTUB2	oligo 4	SI04250064	AAGGTTCACCGCCATCCGCAA	F	4
OTUD1	oligo 1	SI00676109	AACGGACACTATGATGCTGTA	G	4
OTUD1	oligo 2	SI00676116	ACGAAGAACTTGCCAAATCTA	G	4
OTUD1	oligo 3	SI05150075	CACCCTGGGAATAATTGCATA	G	4
OTUD1	oligo 4	SI05150082	CTGGTGTACCTTCATCTATGA	G	4
OTUD3	oligo 1	SI00453838	CTGGGTCAGCATAGAATGCTA	F	8
OTUD3	oligo 2	SI00488299	TTGAATGTAGTGATTCATCAA	F	8
OTUD3	oligo 3	SI03215821	GACAGTGGACTACATGATAAA	F	8
OTUD3	oligo 4	SI04189934	CAGAAGCGAAGCAGAGGCGAA	F	8
OTUD4	oligo 1	SI00442785	CTGTATGAGAAGGTATTTAAA	F	7
OTUD4	oligo 2	SI05134976	TAGATGCATATTTGTAGAATA	F	7
OTUD4	oligo 3	SI05134983	GTGCCATACAAGGAAAGTTAA	F	7
OTUD4	oligo 4	SI04278610	CAGAGAGAAATTTGAAGCGTT	F	7
OTUD5	oligo 1	SI00368445	CAGGCCGGCTTGGACAATGAA	G	3
OTUD5	oligo 2	SI04153982	TACCACCTACATTAACAGGAA	G	3
OTUD5	oligo 3	SI04245283	TGCCGACTACTTCTCCAACTA	G	3
OTUD5	oligo 4	SI04303754	CCCATTCGTGTTAGCTACCAT	G	3
OTUD6A	oligo 1	SI00442792	CAAGACGACAGTAGCATTGAA	G	2
OTUD6A	oligo 2	SI04177866	CTACGACGACTTCATGATCTA	G	2
OTUD6A	oligo 3	SI04201785	AGGCCCAGATCCGGAGCTTAA	G	2
OTUD6A	oligo 4	SI04268285	AAGAGTGAACAGCAGCGCATA	G	2
OTUD6B	oligo 1	SI00344939	AGGGTCATTGATAGCAAGTAA	G	1
OTUD6B	oligo 2	SI04172420	TTCGGTTACACGGTTGGTAAA	G	1
OTUD6B	oligo 3	SI04185034	AAGGAGCGAGAAGAACGGATA	G	1
OTUD6B	oligo 4	SI04233915	CAGACCGCTGAGTATATGCAA	G	1
OTUD7A	oligo 1	SI04167408	CACGCCGTCGCCCACAGACAA	F	6
OTUD7A	oligo 2	SI04211242	CCACGTGGCAAGTGAATGCAA	F	6
OTUD7A	oligo 3	SI04298658	CGGGACCTGGTGTTACGGAAA	F	6
OTUD7A	oligo 4	SI04349338	CCGCGATTCGGTGTGCAGCAA	F	6
OTUD7B	oligo 1	SI04184383	AACCCATCCCTTGGAACGTAA	F	5
OTUD7B	oligo 2	SI04210850	ATCCGTTTGTTTAGATGGGAA	F	5
OTUD7B	oligo 3	SI04291308	ACCGAGTGGCTGATTCCTATA	F	5
OTUD7B	oligo 4	SI00764862	CAGGATGACATCGTTCAAGAA	F	5
PAN2	oligo 1	SI04987066	ACAGATGGTGCTATTAATTGA	E	10
PAN2	oligo 2	SI04987073	TAGAATTGACCCAGATGGAAA	E	10

PAN2	oligo 3	SI04192237	AAGGTGCTCAAGGGTCTTTAT	E	10
PAN2	oligo 4	SI04196101	AGCCGATATCTTTCATGTGAA	E	10
PRPF8	oligo 1	SI00088543	ACGGGCATGTATCGATACAAA	G	12
PRPF8	oligo 2	SI00088550	ATGGCTTGTCATCCTGAATAA	G	12
PRPF8	oligo 3	SI00088557	CAACGTCGTCATCAACTATAA	G	12
PRPF8	oligo 4	SI03089135	CTCATCGTGGACCACAACATA	G	12
PSMD14	oligo 1	SI00081396	CAGGCATTAATTCATGGACTA	G	11
PSMD14	oligo 2	SI05071101	AAGATCCCATTTAATATTTGA	G	11
PSMD14	oligo 3	SI00081410	TTGGATACTGTCGTATTTAAA	G	11
PSMD14	oligo 4	SI00081417	ACAGACATTATTACTCCATTA	G	11
PSMD7	oligo 1	SI00301483	AAGAATAGTTGGCTGGTACCA	G	10
PSMD7	oligo 2	SI00043596	CCGAATCGGCAAGGTTGGAAA	G	10
PSMD7	oligo 3	SI05062484	GTGGTGCTACGTGGAAGTGAA	G	10
PSMD7	oligo 4	SI05062491	CAGGCTTCAGATTGTATGAGA	G	10
STAMBP	oligo 1	SI05008465	CAGAAATTAAGTAGCTCAGAA	H	1
STAMBP	oligo 2	SI05008472	AGAAATTAAGTTACTCAGAAA	H	1
STAMBP	oligo 3	SI03034717	AAGGAGATTGCATTTCCCAAA	H	1
STAMBP	oligo 4	SI03037720	ACAGAGGGTAGCACAACAGAA	H	1
STAMBPL1	oligo 1	SI00127869	CAGGCTGTTCAGTATATGCAA	H	3
STAMBPL1	oligo 2	SI00127876	CCCAAATACTATGGCCAGATA	H	3
STAMBPL1	oligo 3	SI00127883	AACCATCGAGATTACCAGCAA	H	3
STAMBPL1	oligo 4	SI00127890	ACCGTCAACATCAGACACCTA	H	3
TNFAIP3	oligo 1	SI00086989	CCGAGCTGTTCCACTTGTTAA	F	12
TNFAIP3	oligo 2	SI05018608	CACGATGCTCAGGTTTGGTAA	F	12
TNFAIP3	oligo 3	SI00087003	CAGATGTATGGCTAACCGGAA	F	12
TNFAIP3	oligo 4	SI00087010	CTCGGCTATGACAGCCATCAT	F	12
UCHL1	oligo 1	SI00060648	CACGCAGTGGCCAATAATCAA	A	1
UCHL1	oligo 2	SI00060655	CTCCGCGAAGATGCAGCTCAA	A	1
UCHL1	oligo 3	SI00060669	CAGCCACACCCAGGCACTTAA	A	1
UCHL1	oligo 4	SI03030230	AACGTGGATGGCCACCTCTAT	A	1
UCHL3	oligo 1	SI00083545	CAGGGACAAGATGTTACATCA	A	2
UCHL3	oligo 2	SI00083552	TAGAAGTTTGCAAGAAGTTTA	A	2
UCHL3	oligo 3	SI00083559	CTGGCAATTCGTTGATGTATA	A	2
UCHL3	oligo 4	SI03077655	CCCGAGGTCACCAACCAGTTT	A	2
UCHL5	oligo 1	SI05707898	TGCAATCATGTTTGATGGTTA	A	3
UCHL5	oligo 2	SI05707905	TAGAGGATAGTATAACAGGAA	A	3
UCHL5	oligo 3	SI05707912	AACAGACAAACTGGATAGTTA	A	3
UCHL5	oligo 4	SI05707919	CAGAACTTCTCTAGTACTGAA	A	3
USP1	oligo 1	SI04346041	ACAGGCATTAATATTAGTGGA	A	5
USP1	oligo 2	SI04362631	AACCCTATGTATGAAGGATAT	A	5
USP1	oligo 3	SI05099507	CTGCACGATCTGTATATAGTA	A	5
USP1	oligo 4	SI05099514	AACTTAGAGGTGTGACCTTAA	A	5
USP10	oligo 1	SI00302113	AACACAGCTTCTGTTGACTCT	B	3
USP10	oligo 2	SI00072989	TCGCTTTGGATGGAAGTTCTA	B	3
USP10	oligo 3	SI00073003	AAGGGAACTGGTGCTACATTA	B	3
USP10	oligo 4	SI00073010	CAGCTTTGTTCGGCTAATGAA	B	3
USP11	oligo 1	SI02780813	CTGCGTCGGGTACGTGATGAA	B	4
USP11	oligo 2	SI02781156	ACCGATTCTATTGGCCTAGTA	B	4
USP11	oligo 3	SI04437573	AAGCGTTACTATGACGAGGTA	B	4
USP11	oligo 4	SI05127381	CCGCTTCTCTTATTCGTGTTA	B	4
USP12	oligo 1	SI02758224	CCGATCATGGTAGTTGATTTA	B	5
USP12	oligo 2	SI00162512	AAGAAGTTCATCACAAGATTA	B	5
USP12	oligo 3	SI00162526	ATGGATCAACTTCATCGATAT	B	5
USP12	oligo 4	SI00162533	TCACAAGATTACGGAAAGAAA	B	5
USP13	oligo 1	SI00058093	TCGCTTATGAACTAACGAGAA	B	6
USP13	oligo 2	SI05052250	AGACATGTGGATAACGTTATA	B	6

USP13	oligo 3	SI00058100	AGCGACGATTATGAATATGAA	B	6
USP13	oligo 4	SI03061968	CACTACGAGCAACGAATAATA	B	6
USP14	oligo 1	SI00072961	CAGAGTTGAAATGCCTTTCAA	B	7
USP14	oligo 2	SI00072968	CCCATCCTTTGCCTTATCTAA	B	7
USP14	oligo 3	SI00072975	CCGCTCTACTCCGTTACTGTA	B	7
USP14	oligo 4	SI00072982	TGGCTTCAGCGCAGTATATTA	B	7
USP15	oligo 1	SI00087353	ATGAATAATGTTGTAACTCGA	B	8
USP15	oligo 2	SI00087360	TATGTCGGAATTCTTAATTAA	B	8
USP15	oligo 3	SI00087367	AAGATGATACCAGGCATATAA	B	8
USP15	oligo 4	SI03072909	CAGTCGATACATGAGAGACAA	B	8
USP16	oligo 1	SI05021191	AATGGCTGAAATAACGATAAA	B	9
USP16	oligo 2	SI05021198	AACATTAAATACATGCCAGAA	B	9
USP16	oligo 3	SI04171412	CCAGTGCTTAGAGAACTACTA	B	9
USP16	oligo 4	SI00758135	CAAGGAGAAGTAAATATTAAA	B	9
USP17	oligo 1	SI04389847	TGGAAATTCCTTCAAGAGCAA	B	10
USP17	oligo 2	SI04389854	CCCGACGTACTTGTGATTCAT	B	10
USP17	oligo 3	SI04389861	ATGAAGAACCATCATCCTGAA	B	10
USP17	oligo 4	SI04389868	CACAGGCAACAAGATTGCCAA	B	10
USP17L2	oligo 1	SI04192174	AGCAGGTAGATCATCACTCTA	B	12
USP17L2	oligo 2	SI00374738	GACGTACTTGTGATTCATCAA	B	12
USP17L2	oligo 3	SI03130624	AAGCCTGAGTTCAACGTCAGA	B	12
USP17L2	oligo 4	SI04157237	CGCCGGCCTCCAAGACGTTAA	B	12
USP17L6P	oligo 1	SI03660657	GCCCTTGGCTCTGAAGACTAA	B	11
USP17L6P	oligo 2	SI03660664	AGCAGGTAGATCATCACTCTA	B	11
USP17L6P	oligo 3	SI03660671	TGGGAAATACCTGCTACGTGA	B	11
USP17L6P	oligo 4	SI03660678	CGCCGGCCTCCAAGACGTTAA	B	11
USP18	oligo 1	SI00118034	TAAGCGCTTCCTGGAAGTGAA	C	1
USP18	oligo 2	SI05112051	CAGGTCCTGATCAGTCAGAAT	C	1
USP18	oligo 3	SI00118041	AAGATGGAGTGCTAATGGAAA	C	1
USP18	oligo 4	SI03022915	TTCGCTTTCCATTCAGTGGAA	C	1
USP19	oligo 1	SI00758163	TTCAGTGGTGGTGCACGTGTA	C	2
USP19	oligo 2	SI00758170	AACGTGTTCTATCCTCTGGTA	C	2
USP19	oligo 3	SI00758177	CACGAGGACCTGAATCGCATT	C	2
USP19	oligo 4	SI00758184	CTGGCGTGACAAGATCAATGA	C	2
USP2	oligo 1	SI03246698	CAGATTGTGGTTACTGTTCTA	A	6
USP2	oligo 2	SI03247034	CAGGAGAATGGCACACTTTCA	A	6
USP2	oligo 3	SI05094292	ATGGAATTTAGTTGCCTCCAA	A	6
USP2	oligo 4	SI05094299	CTCCAAGAATTGTGCCTTATA	A	6
USP20	oligo 1	SI00090965	CCGGATGATGAAACAGGGATA	C	3
USP20	oligo 2	SI00090972	CAGGCTTGTTGAAACGACCAA	C	3
USP20	oligo 3	SI00090979	ACCGTCGTACGTGCTCAAGAA	C	3
USP20	oligo 4	SI00090986	TCGAGTGACACGGATGAGAAA	C	3
USP21	oligo 1	SI05043465	GAAGCCCTTTAAACACCCTTA	C	4
USP21	oligo 2	SI00100632	CAACCTAATGTGGAAACGTTA	C	4
USP21	oligo 3	SI00100639	GCGGCTACACCTTGAAATCAA	C	4
USP21	oligo 4	SI03072650	CAGTACAAAGATTCCCTCGAA	C	4
USP22	oligo 1	SI03246705	AAGGTGAATTTCATAAATGTA	C	5
USP22	oligo 2	SI03247041	CTGAGTTTATACAGAAATTTA	C	5
USP22	oligo 3	SI00758219	AAGAAGCATATTCACGAGCAT	C	5
USP22	oligo 4	SI00758226	CAGGACTACATCTATGACAAA	C	5
USP24	oligo 1	SI05013610	TGGGTCTAGATGAGAACCCTA	C	6
USP24	oligo 2	SI03031770	AAGAGCAATCAGGAAGCAGTA	C	6
USP24	oligo 3	SI03038399	ACCACAGAGTAATGTCTCTAA	C	6
USP24	oligo 4	SI03058790	CACCGTGTATATTATACGCTT	C	6
USP25	oligo 1	SI03246845	CAAGAGGAGTTTAATAAAGAA	C	7
USP25	oligo 2	SI05013995	CAGCACTGTGTACGATACATA	C	7

USP25	oligo 3	SI05014002	TTCCATGACTACAGCCATTTA	C	7
USP25	oligo 4	SI04156264	CTGGCAATGATAGATACATCA	C	7
USP26	oligo 1	SI04219453	TACGATGATATGCGGGTGTTA	C	8
USP26	oligo 2	SI04259962	CAGCTTAATAGCAAGGAGGTA	C	8
USP26	oligo 3	SI04346328	AAGATTATCAATAATCGGAGA	C	8
USP26	oligo 4	SI04358186	AACCGTTAGCTCACTTAATGA	C	8
USP27X	oligo 1	SI00528122	CAGAATGAATGGACAATTGCA	C	9
USP27X	oligo 2	SI00528129	CAGTCTGATGTCACCTGTCAA	C	9
USP27X	oligo 3	SI05147898	TACAACTGGCATCGAGATCTA	C	9
USP27X	oligo 4	SI05147905	CAGGCCTCAGCTAAGAGTATA	C	9
USP28	oligo 1	SI03246712	AAGGATTAGGTGGGCACATAA	C	10
USP28	oligo 2	SI03247048	CTACAAGAGATTAGAAATATA	C	10
USP28	oligo 3	SI04294759	GAGCGTTGGTTTACAAAGCTA	C	10
USP28	oligo 4	SI04149775	ATGAAGGTGGCTCAAGCGAAA	C	10
USP29	oligo 1	SI05115285	AGCAATCAGATGGAGATTCTA	C	11
USP29	oligo 2	SI04154633	AAGAATAACGAGCAAGTTTAT	C	11
USP29	oligo 3	SI04233131	CAGCTAGGGACTGATTAGAAA	C	11
USP29	oligo 4	SI04241503	CTCAAGGTAGAACCTAATAAT	C	11
USP3	oligo 1	SI00089432	AGCGCTCTAAGAATCAAGAAA	A	7
USP3	oligo 2	SI00089439	CTGGATCGGATAAACTTTAAT	A	7
USP3	oligo 3	SI00089446	CAGAAGTAAGCGCTCTAAGAA	A	7
USP3	oligo 4	SI03071432	CAGGGCGGTTTCAACGGTGTT	A	7
USP30	oligo 1	SI00758394	CACACCAGTATTTATCCTTAA	C	12
USP30	oligo 2	SI03122714	AACAAATTACCTGCCGCACAA	C	12
USP30	oligo 3	SI04286044	CTCCGATGACACTGTCCGCAA	C	12
USP30	oligo 4	SI04287920	CTCACGAATTATTCCATGTCA	C	12
USP31	oligo 1	SI00758415	CCCGAAATATTTAGGCCTGAA	D	1
USP31	oligo 2	SI00758422	CCGAGTTCATGAAGACCTCAA	D	1
USP31	oligo 3	SI00758429	GAGCGTCATCATCAGCCTCAA	D	1
USP31	oligo 4	SI03058272	CACCGAGCTCTTCGCCGAGTA	D	1
USP32	oligo 1	SI05015605	TACAAGCTCTCCGATAGAGAA	D	2
USP32	oligo 2	SI05015612	TAGAGTTTACCATAATCATAA	D	2
USP32	oligo 3	SI03021592	TTCACGAATATCTATCTCAAA	D	2
USP32	oligo 4	SI03023538	TTGAAGTTCGCAACAAAGATA	D	2
USP33	oligo 1	SI05031180	TTGATCTAGGATAAAGATGAA	D	3
USP33	oligo 2	SI05031187	CTGACAATTATCAGAGTTATA	D	3
USP33	oligo 3	SI00109130	CTGCAAGTAGTGGACACTATA	D	3
USP33	oligo 4	SI00109137	AAGAATTCCTTCGATGTTTAA	D	3
USP34	oligo 1	SI05022507	CTCTGCTTGAATGGCAAGATA	D	4
USP34	oligo 2	SI00758450	CTGGATTGAGTCAGATAACAA	D	4
USP34	oligo 3	SI00758464	AAGCCTAGATCTTGCATTTAA	D	4
USP34	oligo 4	SI03042795	AGCAGTGATAATAGCGATACA	D	4
USP35	oligo 1	SI05068924	CAGATATGGAAGTAAGACCTA	D	5
USP35	oligo 2	SI00758478	CCCTTCTAACTTCTAACCGAA	D	5
USP35	oligo 3	SI03022530	TTCCTTCGAATCTGTCAGCAA	D	5
USP35	oligo 4	SI03054373	CAAGGACTTGATGGAAGCCAT	D	5
USP36	oligo 1	SI00138068	TCCGTATATGTCCCAGAATAA	D	6
USP36	oligo 2	SI00138075	CCCGAGTGTGATTCCAGATCA	D	6
USP36	oligo 3	SI00138082	CAAGAGCGTCTCGGACACCTA	D	6
USP36	oligo 4	SI00138089	CCGCATCGAGATGCCATGCAT	D	6
USP37	oligo 1	SI05080026	AAGCAGCTTATGAAACCATAT	D	7
USP37	oligo 2	SI04191873	AAGGATTTACTCAAGAAGGTT	D	7
USP37	oligo 3	SI04196262	ATGGTCCTATCAGAATTCGAA	D	7
USP37	oligo 4	SI04337690	CTCGGACGATTCCTTCTTTGA	D	7
USP38	oligo 1	SI00143612	CAGCATAGTACTAATGGTTTA	D	8
USP38	oligo 2	SI00143619	CAGGAAGTAGCTAGTAAAGCA	D	8

USP38	oligo 3	SI00143626	ATGGGTAATTGCACTCCTGAA	D	8
USP38	oligo 4	SI00143633	CTGGTCTTATTAACCTAGGAA	D	8
USP39	oligo 1	SI04131869	ACCAAGTTGCCTCCATATCTA	D	9
USP39	oligo 2	SI04157615	CCCGTACCTGGACACCATTAA	D	9
USP39	oligo 3	SI04188513	CAGGCTCTATCTAATGTTCCT	D	9
USP39	oligo 4	SI04226278	CTGGAACCCTCGAAATTTCAA	D	9
USP4	oligo 1	SI00051247	ACCGAGGCGTGGAATAAACTA	A	8
USP4	oligo 2	SI05110952	CTCCGTTGAGTCATCTTGTAA	A	8
USP4	oligo 3	SI00051261	TAGATGAATTAAGACGGTTAA	A	8
USP4	oligo 4	SI02630964	CAGGCAGACCTTGCAGTCAAA	A	8
USP40	oligo 1	SI05100144	CTCAGCGTAATGAAATATTAA	D	10
USP40	oligo 2	SI04161717	AAGGTTCGAATCATCCCTTTA	D	10
USP40	oligo 3	SI04310152	ATGGTGTTTGATATTCGAATT	D	10
USP40	oligo 4	SI04328324	AAAGTCGGCCAAATTACGTAA	D	10
USP41	oligo 1	SI05646774	CAGCCAGATCCTTCCAATGAA	D	11
USP41	oligo 2	SI05646781	CCGGAGTGCTGTGGATGGAAA	D	11
USP41	oligo 3	SI05646788	GCCCAGGGAGTTATCAAGCAA	D	11
USP41	oligo 4	SI05646795	TACGTGCATCCTTGTGTACAT	D	11
USP42	oligo 1	SI05099976	CTGCGTGGTGCTTCTTTAGTA	D	12
USP42	oligo 2	SI05099983	TACCGTGTATATAAATCCCAT	D	12
USP42	oligo 3	SI00758618	TTGGAGGATACCTAAGATCTA	D	12
USP42	oligo 4	SI03048920	ATCTTGATATTCGGCCATATA	D	12
USP43	oligo 1	SI05100690	CCCAAGGTCCATATAACCCAA	E	1
USP43	oligo 2	SI05100697	CCCGTTGTCTTGTAATCTCTA	E	1
USP43	oligo 3	SI00758646	CACCTTTCAGAGAGTCAAATA	E	1
USP43	oligo 4	SI03041836	ACGGTGGAACCGCTTCGAGAA	E	1
USP44	oligo 1	SI05069393	TTGGTCACTAATAGTCTTTCA	E	2
USP44	oligo 2	SI00142268	TTGCATGTGACAACAAATCAA	E	2
USP44	oligo 3	SI00142275	ACGGCAGGAATTGGAGTATCA	E	2
USP44	oligo 4	SI03091473	CTCGCTCAGTCGACCATAATA	E	2
USP45	oligo 1	SI02779273	CAGGAAATTATCGGAACATAA	E	3
USP45	oligo 2	SI02779280	CGGGTGAAAGATCCAACTAAA	E	3
USP45	oligo 3	SI03067988	CAGCTAGTACTTACTTCTGAT	E	3
USP45	oligo 4	SI03071320	CAGGGCCATCTAGTGGTATAT	E	3
USP46	oligo 1	SI02778685	TAGGGAAATGTTTGTACTATA	E	4
USP46	oligo 2	SI04916660	CAGGTTGTCAATTACACGGAT	E	4
USP46	oligo 3	SI04934860	TCCATGAAACTTACGCAGTAA	E	4
USP46	oligo 4	SI00134729	CAGCACGGCATTGTTCCTTAT	E	4
USP47	oligo 1	SI00758716	CAGGATGCTCATAGCTTAATA	E	5
USP47	oligo 2	SI04203262	AGGATTAAACTGAATGATCGA	E	5
USP47	oligo 3	SI04322080	TGGCGTCAAGTCAACATATAT	E	5
USP47	oligo 4	SI04355183	TGGATCGGCATGCAAATACAA	E	5
USP48	oligo 1	SI02779091	ACCAGATGCGTTGGTCCATAA	E	6
USP48	oligo 2	SI04387257	AAGGAACTCATTGCTCTCGAA	E	6
USP48	oligo 3	SI04387264	AAGATCTAGCAGAACCTTCTA	E	6
USP48	oligo 4	SI05001381	CAACACGTAACCGAAGCAATA	E	6
USP49	oligo 1	SI00635068	TCCAGTCAATATCCCACTTAA	E	7
USP49	oligo 2	SI05071997	CAGGACCTAGGCCCTGTGCAA	E	7
USP49	oligo 3	SI05072004	TACCTAGAGGGAAATTACATA	E	7
USP49	oligo 4	SI04195821	CTGGAATTCCCTGAACGCTAT	E	7
USP5	oligo 1	SI00052416	ACCGACGATCCGGGTCCCTAA	A	9
USP5	oligo 2	SI00052423	TACGTCTGCCACATCAAGAAA	A	9
USP5	oligo 3	SI00052430	AGCGAGGAGAAGTTTGAATTA	A	9
USP5	oligo 4	SI03076717	CCCAGCGAGTTGACTACATCA	A	9
USP50	oligo 1	SI00758751	CAGCTCAATTATAGCATCGTA	E	8
USP50	oligo 2	SI05131546	CAGCATCTGGTGGTAGAGTTT	E	8

USP50	oligo 3	SI00758758	CCCGGAGAAGATCATATGAGA	E	8
USP50	oligo 4	SI03069038	CAGGAAGTGGATTACCACTGA	E	8
USP51	oligo 1	SI05065431	GACAGCTAGTATCTTGATATA	E	9
USP51	oligo 2	SI00758786	GAGGACTTACTCTACAGTGAA	E	9
USP51	oligo 3	SI00758793	CCAGAGACTAGGAAACGTAAA	E	9
USP51	oligo 4	SI00758800	AGGCCTGAGAGGGCTAATCAA	E	9
USP53	oligo 1	SI04133283	TTGTACTATGCTGGTAAACTA	E	11
USP53	oligo 2	SI04197487	CAGATTACGACAAGCAACCTA	E	11
USP53	oligo 3	SI04247614	ACCGAGGTTGGAAACCTATGA	E	11
USP53	oligo 4	SI04282103	CTTCGTCCTGTTAAAGATAAA	E	11
USP54	oligo 1	SI05088692	CTGGATACTAGCCATTCCTTA	E	12
USP54	oligo 2	SI00758870	CAGGGTGCAATCCTCAACTAA	E	12
USP54	oligo 3	SI04170460	CAGCAGAGCCCTAGTCGATAA	E	12
USP54	oligo 4	SI04198236	AAGGGATGTTTGCACCTCGAA	E	12
USP6	oligo 1	SI00064512	CCCAGGATCGTGATAACTGTA	A	10
USP6	oligo 2	SI00064519	TGCGGAGAGGTTCACAACAAA	A	10
USP6	oligo 3	SI02633442	GCGGAAGGACATACTTATGAA	A	10
USP6	oligo 4	SI03032715	AAGCACAGTAGCAAACTCATA	A	10
USP7	oligo 1	SI00052276	CGGGCCGACACCAGTACATAA	A	11
USP7	oligo 2	SI05082133	TAGAATTTCGTTAAAGTGGAA	A	11
USP7	oligo 3	SI00052283	ATGGAGTTGCGTGGGATTCAA	A	11
USP7	oligo 4	SI00052290	CCCAAATTATTCCGCGGCAAA	A	11
USP8	oligo 1	SI00073017	CAGGGTCAATTCAAATCTACA	A	12
USP8	oligo 2	SI00073024	AAGGCTCGTATTCATGCAGAA	A	12
USP8	oligo 3	SI00073031	CAGGTTCAGGCAAGCCATTTA	A	12
USP8	oligo 4	SI03103604	GAGGATACAGACGATACCGAA	A	12
USP9X	oligo 1	SI00066584	CCGCCAGATAGCACAACGATA	B	1
USP9X	oligo 2	SI00066598	CAGCTAGTATTTAGCCCAAAT	B	1
USP9X	oligo 3	SI00066605	CCGCCTGCAGTGGAAAGTGTA	B	1
USP9X	oligo 4	SI03101973	GACGATGTATTCTCAATCGTA	B	1
USP9Y	oligo 1	SI00066640	ATGACTGGTCCTAATCTGTAA	B	2
USP9Y	oligo 2	SI00066647	AACCGATTGCAATATAGTTTA	B	2
USP9Y	oligo 3	SI00066654	CACTAAGGTCTTATAGTCCAA	B	2
USP9Y	oligo 4	SI03067827	CAGCGTTGGATGCACTTAGTA	B	2
USPL1	oligo 1	SI03156776	CAAGACCAATTTGTGGACATA	F	2
USPL1	oligo 2	SI03181640	CCAGGGACTGATATAGGGATA	F	2
USPL1	oligo 3	SI04251058	AAGGTATAAACCAGAAGGCCA	F	2
USPL1	oligo 4	SI04342625	ATGCCTGCGTTAGAACATTAA	F	2
VCPIP1	oligo 1	SI00759521	CCCGATGATTATACTCCTGTA	F	10
VCPIP1	oligo 2	SI04141543	TACCAGAAGCTTTCCCTATTA	F	10
VCPIP1	oligo 3	SI04227510	CAGGGACAGACTTTAGTAATA	F	10
VCPIP1	oligo 4	SI04327190	CAGCTCCGGTAGAAACCATTA	F	10
YOD1	oligo 1	SI02809576	ATAAGCTATGGTAACCCTAAA	F	11
YOD1	oligo 2	SI02809590	GACCGTCAAATTAGAGCTTTA	F	11
YOD1	oligo 3	SI04270091	CAGCGTAACTTCCCTGATCCA	F	11
YOD1	oligo 4	SI04277420	AAACTGGTATAGGCTATGTAA	F	11
ZRANB1	oligo 1	SI00118846	CAGATCTGTAATGACCCTAAA	F	9
ZRANB1	oligo 2	SI00118853	CAAGGGTGAAATCTTCGTATA	F	9
ZRANB1	oligo 3	SI00118860	CACATATTCTTAGACGACCAA	F	9
ZRANB1	oligo 4	SI00118867	TAGGATAATTCAATGTCGAAA	F	9

DUB siRNA oligos were purchased from Qiagen. Four individual siRNA oligos were used to target each DUB. The row and column sections encode the coordinate of each of the DUB siRNA in a 96-well plate.

Supplementary videos are in the CD attached with this thesis.

Supplementary Video 1. Depletion of PINK1 protects Parkin-overexpressing cells from CCCP-induced cell death. hTERT-RPE1-YFP-Parkin cells were transfected for 72 hours with either non-targeting (NT1) or PINK1-targeting siRNA (40 nM). Cells were treated with CCCP (10μM) and imaged in the presence of the membrane impermeable dye DRAQ7 (pink. YFP-Parkin is shown in grey. Frames were collected every 30 min interval and saved for playback at 3 frames/sec.

Supplementary Video 2. Z-VAD-FMK treatment inhibits CCCP-induced cell death. hTERT-RPE1-YFP-Parkin cells were treated with CCCP (10μM) in the absence or presence of Z-VAD-FMK (20μM) and imaged in the presence of the membrane impermeable dye DRAQ7 (pink). YFP-Parkin is shown in grey. Frames were collected every 30 min interval and saved for playback at 3 frames/sec.

Supplementary Video 3. siRNA-mediated depletion of USP30 enhances CCCP-induced cell death. hTERT-RPE1-YFP-Parkin cells were transfected for 72 hrs with either non-targeting siRNA (NT1, see also Supplementary Movie 2) or USP30-targeting siRNA (D1 and D3, 40 nM). Cells were treated with CCCP (10μM) and imaged in the presence of the membrane impermeable dye DRAQ7 (pink). YFP-Parkin is shown in grey. Frames were collected every 30 min interval and saved for playback at 3 frames/sec.

Supplementary Video 4. USP30 depletion sensitizes Parkin-overexpressing cells to cell death induced by the BH3-mimetic ABT-263. hTERT-RPE1-YFP-Parkin cells were transfected for 72 hrs with either non-targeting siRNA (NT1) or USP30-targeting siRNA (D1 and D3, 40 nM). Cells were then treated with ABT-263 (10μM). Cells were imaged in the presence of the membrane impermeable dye DRAQ7 (pink). YFP-Parkin is shown in grey. Frames were collected every 30 min interval and saved for playback at 3 frames/sec.

Supplementary Video 5. USP30 depletion sensitizes Parkin-overexpressing cells to cell death induced by the BH3-mimetic ABT-737. hTERT-RPE1-YFP-Parkin cells were transfected for 72 hrs with either non-targeting siRNA (NT1) or USP30-targeting siRNA (D1 and D3, 40 nM). Cells were then treated with ABT-737 (10μM). Cells were imaged in the presence of the membrane impermeable dye DRAQ7 (pink). YFP-Parkin is shown in grey. Frames were collected every 30 min interval and saved for playback at 3 frames/sec.